Bioavailability and mechanisms of iron uptake from pea ferritin and ferric phosphate nanoparticles using cell culture models

Antonio P. Perfecto Jr.

A thesis submitted for the Degree of Doctor of Philosophy

University of East Anglia, Norwich, UK

Norwich Medical School

August 2017

Introduction

Iron deficiency is a global health burden. Despite sustained efforts to eradicate iron deficiency, it remains the number one nutritional deficiency in the world, affecting over two billion people [1]. One of the main causes of iron deficiency is insufficient dietary intake and/or low bioavailability. Public health approaches to eradicate iron deficiency include supplementation and food fortification. The aims of my PhD project were to investigate the bioavailability and mechanisms of apical uptake of novel iron forms using cell culture models and thereby provide insight toward improving iron deficiency.

Chapter 1 is an introduction to the importance of iron to human health, strategies to alleviate iron deficiency, our current understanding of dietary intestinal iron absorption, and methods for measuring iron bioavailability, with a particular emphasis on the *in vitro* digestion / Caco-2 cell model. Chapter 2 provides an outline of the basic methods used to study iron uptake in Caco-2 and Hutu-80 cells. Chapter 3 investigates the use of ferric phosphate nanoparticles (NP-$FePO_4$) as a source of iron fortification. NP-$FePO_4$ was kindly donated by Michael Zimmerman's group based at ETH Zurich. Chapter 4 focuses on the use of plant-derived ferritin (phytoferritin) as a potential iron supplement. Phytoferritin was extracted and purified from marrowfat peas by Janneke Balk's lab group, based at the John Innes Centre. Chapter 5 examines the use of the commercially available iron ingot, Lucky Iron Fish©, as a source of home iron fortification. Chapters 3, 4, and 5 are the basis of 3 separately submitted manuscripts; one of which has been accepted, and the other two currently under peer review. Lastly, a general discussion of the experiments undertaken and recommendations for future work are outlined in Chapter 6.

All three iron sources used in this thesis comprise the newest strategies for iron therapeutics. By assessing iron bioavailability, and more importantly the

mechanisms of iron uptake, it is hoped that the work will prove insightful and can be used in the design of future prospective human trials.

Declaration

No portion of the work referred to in this thesis has been submitted in support of an application for another degree or qualification at this or any other university or other institute of learning.

Statement of Originality

I certify that this thesis, and the research to which it refers, is my own work, and that any ideas or quotations from the work of other people, published or otherwise, are fully acknowledged.

List of Publications

Lead author publications

- Perfecto A, Elgy C, Valsami-Jones E, Sharp P, Hilty F, Fairweather-Tait S. Mechanisms of Iron Uptake from Ferric Phosphate Nanoparticles in Human Intestinal Caco-2 Cells. Nutrients. 2017;9:359. DOI:10.3390/nu9040359.
- Perfecto A, Rodriguez-Celma J, Rodriguez-Ramiro I, Sharp P, Balk J, Fairweather-Tait S. Native pea phytoferritin is taken up by intestinal Caco-2 cells via a non-DMT1 dependent mechanism. *Currently under peer review.*

Other publications:

- Rodriguez-Ramiro I, Brearley CA, Bruggraber SFA, Perfecto A, Shewry P, Fairweather-Tait S. Assessment of iron bioavailability from different bread making processes using an in vitro intestinal cell model. Food Chemistry. 2017;228:91-8. DOI:10.1016/j.foodchem.2017.01.130.

Table of Contents

List of Tables

List of Figures

Acknowledgments

Over 3 years ago, I left home for my PhD and moved over 5,000 miles away. Doubts, worries, and sense of loneliness surfaced during the 10 hr flight to London, 1 hr Underground, and 5.5 hr bus ride to Norwich. Adjustments to new culture and lifestyle were tremendously difficult.

As PhD students, we sacrifice a lot. On a personal level, anxieties over experiments, late hrs, deadline pressure, budgets, working environment, and uncertainty over career prospects, are all aspects of the PhD experience we all struggle with. The relationships and the support of others helped me persevere through some very difficult times.

Thanks to Sue for being a great mentor. She possesses a rare quality as an advisor that genuinely invests in her students' best interests. Thanks to all of my advisors and the collaborations with JIC and FENAC. Thanks to my roommates, my friends and colleagues at UEA, and the people of Norwich. These relationships were invaluable and continue far and beyond a PhD. It is amazing to think that Norwich has become a second home and welcomed me with open arms. I want to thank my mother for supporting me in this inherently transient scientific world. Always supportive, always enthusiastic, always showing me what is important in life. Most of all, thanks to my girlfriend, who stayed patient, supported me through each step, my confidant and best friend throughout all my bests and all my worsts. I could not be a luckier individual.

I come out of this PhD a more skilled, better researcher. My knowledge base has expanded several-fold. The opportunities that I have been given have been tremendous. I have learned so much and am very thankful.

List of Abbreviations

AA:	ascorbic acid
ANOVA:	analysis of variance
AP2:	adaptor complex protein 2
BCA:	bicinchoninic acid
BPDS:	bathophenanthroline disulfonic acid disodium salt hydrate
CME:	clathrin mediated endocytosis
CPZ:	chlorpromazine
DCS:	disc centrifugal sedimentation
DcytB:	duodenal cytochrome B
DMEM:	Dulbecco's modified eagle medium
DMT1:	divalent metal transporter 1
FAC:	ferric ammonium citrate
FPN:	ferroportin-1
FSP:	flame spray pyrolysis
HEPES:	4-(2-hydroxyethyl)-1-piperazineethanesulfonic acid
HCl:	hydrochloric acid
HCP1/PCFT:	haem carrier protein 1/proton coupled folate transporter
HEPH:	hephaestin
kDa:	kilodalton
MEM:	minimal essential media
$NaHCO_3$:	sodium bicarbonate
NP-$FePO_4$:	ferric phosphate nanoparticles
pFer:	phytoferritin
PIPES:	piperazine-N,N-bis(2-ethanesulfonic acid)
PVP:	polyvinylpyrroldione
RBV:	relative biological value
RNAi:	RNA interference
shRNA:	short hairpin RNA
SSA:	specific surface area
SDS-PAGE:	sodium dodecyl sulphate polyacrylamide gel electrophoresis
SEM:	standard error of the mean
TEM:	transmission electron microscopy

Chapter 1: Literature Review

1. Literature Review

1.1 Iron

Iron is an essential nutrient required by the human body to support life. Dietary iron is absorbed primarily in the upper gastrointestinal tract (duodenum and part of the upper jejunum), where approximately 1-3 mg iron is absorbed per day. The majority (80-90%) of absorbed iron is incorporated into haemoglobin (for oxygen transport to tissues and carbon dioxide removal) in red blood cells (RBC) or myoglobin (for oxygen binding in muscle tissue) [2]. The remainder of absorbed iron is incorporated into iron-sulfur clusters, as a substrate of the tricarboxylic acid cycle, cytochromes for oxidative phosphorylation, as a cofactor for various enzyme-catalyzed reactions, and stored in the liver as ferritin. Active excretory mechanisms for iron do not exist; only minor losses of iron occur through urine, sweat, and desquamation of intestinal cells, except in cases of blood loss, such as menstruation. Iron requirements are balanced by dietary iron absorption; iron-replete individuals absorb less iron and iron-deficient individuals absorb more iron. Within the body, iron is recycled in a state of constant turnover. Iron is transported from the intestine using transferrin and directed toward the bone marrow, where new synthesis of haemoglobin occurs. After approximately 120 days, senescent erythrocytes become degraded by macrophages of the reticuloendothelial system found in the liver and spleen. A diagram of iron turnover is depicted in Figure 1.1.

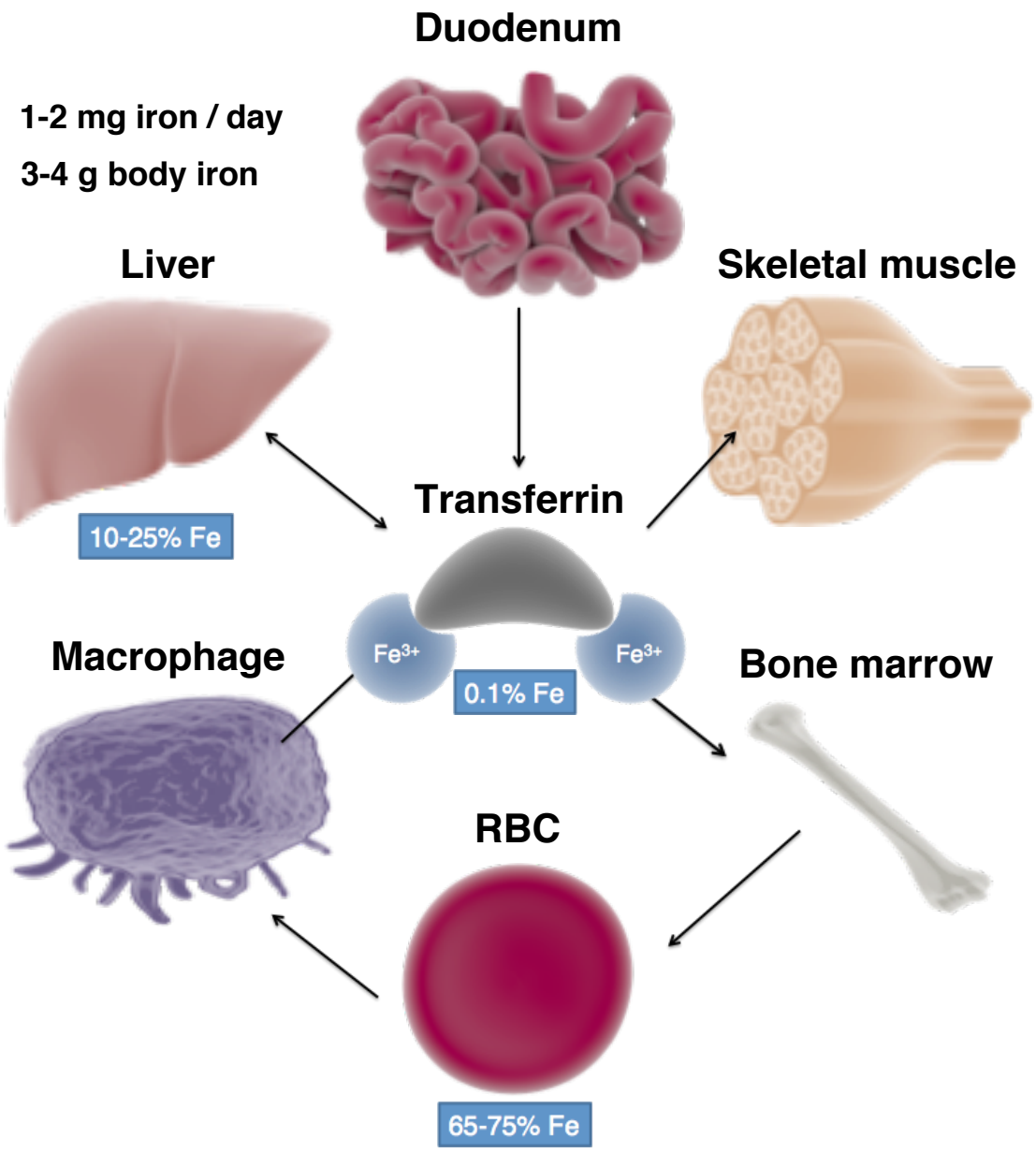

Figure 1.1 Iron circulation, transport, and percentage found in body tissues.

Dietary iron is absorbed in the duodenum and transported around the body by the protein, transferrin. Iron is stored within liver or skeletal muscle for physiological function or directed to bone marrow for synthesis of haemoglobin in RBC. Senescent RBC's are degraded by macrophages of the liver and exported out for circulation to synthesise new RBC's. For more detail, see Andrews et al 2000 [3].

1.2 Mechanisms of iron absorption

This literature review will be primarily focused on intestinal iron absorption. Dietary iron is categorised as either haem or non-haem. The mechanisms involved in intestinal non-haem iron absorption have been elucidated over the last 20 years, and forms the majority of this section. The mechanisms of haem iron absorption are distinct from non-haem iron, and while this distinction has been recognised for over half a century, little information exists on the mechanisms regulating its absorption. The uptake of haem will be discussed within this section, while a stand-alone section on ferritin structure/function and uptake will be presented in Chapter 4. All forms of iron, regardless of origin, absorbed in the intestine join the labile iron pool (LIP) within the enterocyte prior to export into the blood [4].

1.2.1 Important factors regulating iron absorption

The homeostatic mechanisms coordinating iron absorption are highly controlled, involving several levels of regulation. Central to iron absorption is the expression of the iron transport proteins in the intestine (DMT1, DcytB, ferritin, ferroportin, hephaestin) which facilitate iron entry, storage, and export to and from the enterocyte. Post-transcriptional regulation involving the iron response proteins (IRP) and their interaction with iron response elements (IRE), transcriptional regulation involving hypoxia-induced factor 2 alpha (HIF-2α), and systemic regulation through hepcidin expression all control the expression of the iron transport proteins of the intestinal cell, which are fundamental to iron absorption.

In general, under iron-deficient conditions, DMT1, Dcytb, and TfR1 protein expression is increased, and simultaneously, ferroportin, ferritin (H and L chain), and hepcidin expression is decreased. This results in increased cellular iron concentrations. The converse occurs when intestinal cells are iron-replete.

1.2.2 Iron response proteins (IRP): Post-transcriptional regulation

The two iron response proteins, IRP1 (*ACO1*) and IRP2 (*IREB2*), regulate the protein expression of several duodenal iron proteins [5-8]. Under low, or iron-deficient cytosolic conditions, IRP1 and IRP2 are expressed and bind to cis, regulatory hairpin untranslated regions (UTR) of mRNA found in several iron proteins (discussed below). The location of the binding determines whether the mRNA transcript is stabilised or degraded. IRP binding to the 5' UTR results in mRNA degradation by blocking transcriptional initiation while binding to the 3' UTR confers mRNA stability (and protein expression) by protecting the transcript from endonuclease activity.

In iron-replete or iron-overloaded enterocytes, both IRP1 and IRP2 are inactivated. The formation of a [4Fe- 4S] cluster induces a conformational change to IRP1, switching its function as a post-transcriptional iron regulator to a mitochondrial aconitase enzyme of the citric acid cycle. The conformational changes, in addition, inhibit IRP1-IRE binding.

IRP2 is also inactivated by iron using a different regulatory mechanism to IRP1. Iron (and oxygen) stabilises the expression of FBXL5 (F box and leucine-rich repeat protein 5). FBXL5 binds to IRP2 (and to some extent IRP1), leading to the active recruitment of SCF-type ubiquitin ligase (E3) to the complex [9, 10], and subsequent ubiquitination and proteasomal degradation of IRP2 [7, 9, 10]. In $FBXL5^{-/-}$ knockout mice, IRP2 over accumulates resulting in iron overload and embryonic lethality [11].

Interestingly, DMT1, Dcytb, and ferroportin mRNA and protein levels were unaltered in $IRP2^{-/-}$ knockout mice. Moreover, the mice display a mildly microcytic phenotype, indicating that IRP1 and IRP2 can functionally replace one another [12]. Double intestinal knockout $IRP1^{-/-}$ and $IRP2^{-/-}$ mice resulted in 10-fold decreased DMT1 expression, 4-fold increased ferroportin expression, and

significantly increased serum hepcidin. Mice body weights were half that of wild type and knockout mice survived less than 30 days. This model reflects the importance of the IRP system to intestinal iron absorption [13].

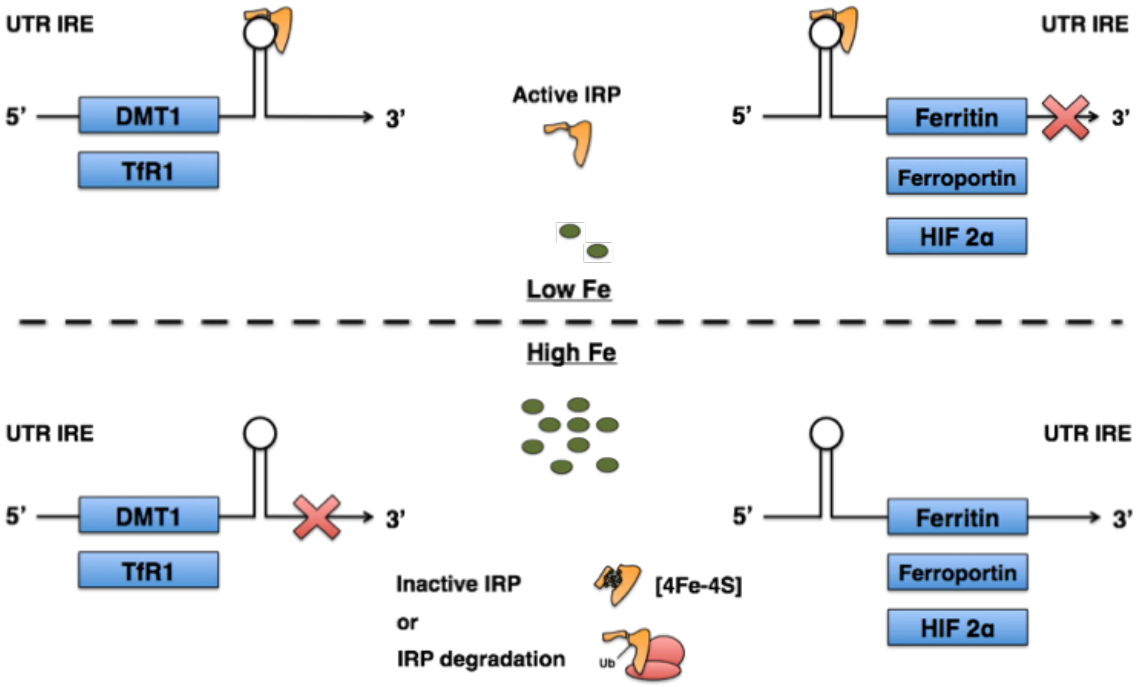

Figure 1.2 IRP-IRE system.

Iron response proteins are activated under iron-deficient conditions and bind to UTR IRE's of several iron proteins to drive increased cellular iron concentrations. Iron response proteins are inactivated under iron-replete conditions to decrease cellular iron concentrations.

1.2.3 HIF2α: Transcriptional regulation

The mechanisms involved in transcriptional regulation of duodenal iron proteins have recently become unraveled. HIF2α is a transcriptional factor of several duodenal iron proteins. Under iron-deficient cellular conditions, HIF2α binds directly to the DNA promoters of both DMT1 and DcytB to drive transcription [14] and protein expression. Iron-replete or oxygenated cellular

conditions increase VHL-E3-ligase complex expression, which leads to the ubiquitination of HIF2α and its degradation [15].

In an elegant example of this regulation, researchers showed that the expression of DMT1 and Dcytb in iron-replete $VHL^{-/-}$ knockout mice was similar to iron-deficient WT mice [16]. Conversely, $HIF^{-/-}$ knockout mice failed to express DMT1 or Dcytb during iron depletion. Both knockout models provided importance evidence that HIF2α is an important physiological regulator of iron absorption. Furthermore, intestine-specific $HIF2\alpha^{-/-}$ knockout mice resulted in decreased dietary iron uptake and iron status [16]. Interestingly, a feedback loop has been shown to exist between transcriptional and translational regulation of iron metabolism. Recently, it was discovered that HIF2α also contains an mRNA 5' UTR IRE and is also post-transcriptionally regulated by the IRP's [17]. It is important to note that HIF2α inhibitors are currently being investigated as a therapeutic target for clinical iron overload conditions.

1.2.4 DMT1

DMT1 (DCT1/NRAMP2/*SLC11A2*) is currently the only identified intestinal iron importer. DMT1 spans 12 transmembrane domains, is localised mainly in the brush border membranes, and is an exclusive transporter of ferrous iron (Fe^{2+}) into the enterocyte [18]. DMT1 functions as a proton-coupled (H^+) co-transporter and thereby functions optimally within more acidic conditions (proximal intestine) generated from the Na^+/H^+ exchanger [18, 19].

Alternative splicing of the DMT1 transcript results in 4 different isoforms; a 3'UTR IRE that is highly expressed in the duodenum (exon 1b, DMT1 +IRE) [18], a non-IRE isoform (exon 1b, DMT1 –IRE) [20], and two other (-/+) IRE transcripts containing conserved 21-23 amino acid sequences extended within the 5' open reading frame (exon 1a, ±IRE) [21, 22].

DMT1 is essential to intestinal non-haem iron absorption. It was discovered using extracted RNA and the generation of cDNA libraries from rat duodenal segments [18]. Cloning and expression of DMT1 in Xenopus oocytes resulted in a 200-fold increase in ferrous iron uptake [18]. Subsequent studies found that DMT1 was translocated to brush border microvillae and highly upregulated in iron-deficient rats [23, 24].

The *mk* mouse and the Belgrade rat are two murine models of iron deficiency that result from DMT1 abnormalities. Positional cloning techniques identified that iron deficiency in these models resulted from a missense gene mutation located at G185R in the DMT1 transcript of both the *mk* mouse [25] and Belgrade rat [26]. Transfection of the G185R mutant into HEK293 cells decreased non-haem uptake compared to WT due to the loss of function in the DMT1 protein [27]. *DMT1*$^{-/-}$ knockout was embryonically lethal to mice and intestine-specific *DMT1*$^{-/-}$ knockout resulted in severe iron deficiency, growth, loss of weight, and eventually lethality at 7 days [28].

The identification of patients exhibiting DMT1 mutations is a strong indicator of its physiological importance. Patients exhibiting DMT1 mutations displayed symptoms of both microcytic anaemia and liver iron overload [29, 30]. These symptoms resulted in iron loading anaemia, which is thought to be the result of increased iron absorption resulting from low plasma hepcidin levels [31]. In other cases of DMT1 mutations, severe anemia resulted without iron overload [31]. The differing phenotypes exhibiting several DMT1 mutations are probably reflective of differences in human duodenal iron absorption and erythroid iron utilization, unveiling unknown functional complexities of DMT1 [31].

1.2.5 IMP pathway

A mechanism of iron uptake has been proposed for ferric iron as well. Conrad and Umbreit, thorough a succession of several publications, has

proposed a model for ferric iron uptake existing separately from DMT1. This model was termed the integrin-mobilferrin-paraferritin (IMP) pathway, which is exclusive for ferric iron, and is not associated with other metals [32]. The group observed that mucins lining the gastrointestinal tract of mice had strong affinity for ferric iron at gastric pH and prevented the precipitation of iron to insoluble complexes at neutral pH [33]. They hypothesised that ferric iron binds to mucins and proceeds to bind with luminal surface β-3-integrins prior to enterocytic uptake [34]. Ferric iron is then proposed to bind to the cytosolic protein, mobilferrin [35, 36]. Whether mobilferrin binds exogenous ferric iron prior to cell entry is unknown. Intestinally absorbed ferric iron is reduced by the membrane bound, intracellular ferrireductase, paraferritin using NADPH [37]. The paraferritin complex (520 kDa) contains β-3-integrin, mobilferrin, and flavin monoxygenase [37] and DMT1 [38], which allows ferrous iron to be exported into the cytosol.

The physiological importance of the IMP pathway is currently unknown. Confocal studies revealed that the IMP pathway is upregulated in mucin secreting goblet cells and extracellularly with mucin during iron deficiency [39]. Knockdown of calreticulin, the homologue of paraferritin, in mice caused severe abnormalities in cardiac development [40-42] resulting in lethality.

Conrad et al [32] demonstrated that excess Mn^{2+} inhibited Fe^{2+} but not Fe^{3+}, suggesting that Mn^{2+} and Fe^{2+}, but not Fe^{3+}, both compete for DMT1 transport in K562 cells. They also demonstrated that antibodies targeting DMT1 blocked Fe^{2+}, but not Fe^{3+}, uptake. Furthermore, cDNA expression of DMT1 in HEK-293 cells resulted in the transport of Fe^{2+} but not Fe^{3+}. Given the identification and subsequent characterisation of DMT1 and ferrireductases such as Dcytb, the IMP pathway may contribute to, but is likely not essential, to iron absorption until proved otherwise.

1.2.6 Dcytb

Duodenal cytochrome B reductase (Dcytb/*Cybrd1*) is the only identified brush border membrane ferrireductase identified to date. The enzyme catalyses the reduction of Fe^{3+} to Fe^{2+} prior to DMT1 transport. McKie et al identified Dcytb from subtractive hybridisation using the hypotransferrinaemic *hpx/hpx* iron-deficient mouse model [43]. The method compares hypotransferrinaemic mice, which upregulates the expression of iron transporters, such as Dcytb, with wild type mice. In parallel with DMT1, Dcytb was upregulated during hypoxia and iron deficiency. Dcytb has been shown to increase iron absorption from Fe^{3+}. cRNA Dcytb injected into *Xenopus oocytes* resulted in a 6-fold increase in iron uptake from ^{59}Fe(III)-NTA [43]. Moreover, Caco-2 cells and MDCK cells transfected with Dcytb cDNA showed a 2.5-fold increase in iron uptake [44, 45]. In the haemochromatosis overload mouse model, $HFE^{-/-}$ knockout resulted in significantly upregulated levels of Dcytb [46].

Dcytb ferrireductase activity is likely driven by intracellular ascorbic acid. In either Caco-2 cells loaded with ascorbic acid [44] or iron-deficient mice stimulated to produce increased intracellular ascorbic acid levels Dcytb expression and reductase activity was upregulated [47]. These examples of Dcytb function in cellular and *in vivo* models are strongly suggestive of its physiological importance as an intestinal ferrireductase. However, in $Dcytb^{-/-}$ knockout mice fed either a normal or iron deficient diet short term (4 weeks) or long term (12 weeks) showed no differences in haemotological parameters, such as iron liver stores, compared to wild type [48], providing compelling evidence that Dcytb is not essential to iron absorption. The study indirectly implied the existence (and/or presence) of other reductases that functionally compensate for Dcytb. One major limitation of the study was that the mice were fed a normal chow (containing Fe^{2+} and Fe^{3+}); thus it is not possible to fully distinguish whether Dcytb is essential to intestinal iron uptake. Furthermore, mouse models

naturally synthesise endogenous ascorbic acid in the liver [49] which may compensate for the Dcytb$^{-/-}$ knockout. Further studies are required to determine the importance of Dcytb in intestinal iron absorption.

1.2.7 HCP1

The mechanisms of intestinal haem absorption still remain unresolved. HCP1 (*SLC46A1*) is the only identified candidate transporter to date. HCP1 has structural homology with the bacterial tetracycline transporters. Identified by Shayageshi et al [50] using suppression subtractive hybridisation (a technique to amplify differing cDNA fragments of the transcriptome), HCP1 protein expression in mice was induced in iron deficiency and hypoxia. Expression of HCP1 in *Xenopus oocytes* and HeLa cells increased haem transport 2.5 and 6-fold, respectively. HCP1 knockdown in Caco-2 cells also significantly reduced haem iron absorption (50%) in a time and concentration-dependent manner [51, 52].

A separate group disputed the importance of HCP1 as the haem transporter. Using data mining techniques, HCP1 was later identified as a candidate folate transporter (PCFT) [53]. In fact, PCFT was the same protein as HCP1 identified by the group of Shayageshi [50]. Folate incubated with *Xenopus oocyte* expressed PCFT generated K_m values of 1.3-6.0 μM [53], 20 to 100-fold higher binding affinities than haem (125 μM) [50]. Other researchers have validated these results. PCFT/HCP1 transiently expressed in HEK-293 cells resulted in K_m values of 1.76 μM from folate [54] and knockdown of PCFT/HCP1 in Caco-2 cells inhibited folate uptake two-fold greater than haem [51].

Furthermore, a PCFT1/HCP1 mutation was observed in siblings with hereditary folate malabsorption. Qiu et al [53] discovered that a single nucleotide polymorphism resulting in an in-frame deletion of 28 amino acids in PCFT1/HCP1 resulted in the disease. It is currently accepted that PCFT1/HCP1 is a folate transporter, and possibly a low affinity transporter for haem. Knockout mice

models of PCFT1/HCP1 are required distinguish whether PCFT1/HCP1 is indispensable for haem iron absorption. It is likely that other haem transport mechanisms exist.

1.2.6 Poly r(C)-Binding Protein 1

Once transported from the intestinal lumen into the cell, non-haem iron joins the labile iron pool (LIP) and is directed toward the physiologic requirements of the cell, stored within ferritin, or exported to the blood for body iron needs. Haem iron is also thought to join the LIP. Haem oxygenase-1 (HO-1) catalyses the rapid, oxidative degradation of haem to bilirubin, CO_2 and free iron [52, 55]. The mechanism behind iron shuttling to its various physiological functions in the cytosol, and whether it's mediated by protein chaperones, has recently been elucidated.

Poly r(C)-Binding Protein 1 (*PCBP1*) is a cytosolic iron chaperone recently identified by Shi et al [56]. Co-expression of ferritin and PCBP1 in yeast resulted in ferritin-PCB1 binding and ferritin-iron loading. Targeting of siRNA to PCBP1 increased the labile iron pool, suggesting that PCBP1 chaperones iron directly to ferritin. PCBP1 and PCBP2 also activated HIF-prolyl hydroxylase, an enzyme hydroxylating and mediating HIF degradation [57], providing evidence that that these iron chaperones are functionally important in intestinal iron absorption. However, more evidence is required to prove that PCBP1 is the iron chaperone involved in enterocytes and the existence of other functional analogues remains to be demonstrated.

1.2.7 Ferritin

Ferritin is a 24-mer globular protein that functions as an iron storage protein. The human protein consists of structurally homologous H and L subunits. The H subunit has ferrioxidase activity (initiating the oxidation of Fe^{2+} to Fe^{3+} for

storage), while the L subunit contributes to iron nucleation [58-60]. A detailed and comprehensive review of ferritin regarding its role in iron nutrition will be presented in section 1.8.

In the intestine, ferritin protein expression responds directly to labile iron pool concentrations. In order to regulate cell iron concentrations, ferritin is expressed highly in iron-replete conditions, functioning as an 'iron sink' while its expression is inhibited when cytosolic iron concentrations are low. This switching is regulated by iron and IRP's. In iron-deficient cells, ferritin protein expression is repressed by IRP binding to its mRNA 5' UTR IRE [61, 62]. Under these conditions, ferritin is also degraded after delivery to endosomes using the cargo receptor NCOA4 [63, 64]. This has the effect of increasing iron absorption/transport to systemic tissues.

Although ferritin was thought to play a 'passive' role in iron regulation, e.g. its expression responding only to cell iron concentration, recent evidence suggests that its function is much more complex than first thought. Intestine-specific knockout $Ftn^{-/-}$ mice exhibited severe inhibition of duodenal DMT1 expression [65] and iron overload, even in the presence of elevated serum hepcidin levels. These results demonstrate that ferritin may play other physiological roles other than iron storage.

1.2.8 Ferroportin

Ferroportin (FPN/MTP1/IREG1/*SLC40A1*) is the only identified iron exporter in the intestine. Ferroportin is localised exclusively in the basolateral membrane and exports ferrous iron for transferrin-iron loading prior to systemic iron circulation. Several researchers discovered Ferroportin independently [8, 66, 67]. The hypochromatic phenotype in the zebrafish mutant, *weissherbst*, is caused by a ferroportin mutation. Positional cloning comparing *weissherbst* to wild-type identified a defective mutation in the ferroportin gene (L167F), resulting

in reduced iron export to systemic tissues. Functioning wild-type ferroportin expressed in *weissherbst* reversed the hypochromatic phenotype [67]. Ferroportin was also identified in the mouse model. McKie et al [8] identified ferroportin using the same strategy as with Dcytb [43]. Ferroportin localised to the basolateral membrane when transfected into Caco-2 and MDCK cells, increased iron export when expressed in *Xenopus oocytes*, and was upregulated (2.5-fold) in iron deficiency.

Similar to ferritin, ferroportin expression is also regulated by a 5'IRE in its mRNA [66]. In contrast to ferritin, ferroportin expression is also inhibited by hepcidin [68], and therefore has a significant role in regulating systemic iron homeostasis. Donovan et al [69] demonstrated the essentiality of ferroportin to iron metabolism. Systemic $Fpn^{-/-}$ knockout was embryonically lethal to mice and intestinal-specific $Fpn^{-/-}$ knockout mice resulted in iron overload in duodenal tissues and severe hypochromic, microcytic anaemia.

1.2.9 Hephaestin

Transferrin-Fe loading after ferroportin driven iron export requires iron oxidation from Fe^{2+} to Fe^{3+}. The ceruloplasmin analogue, hephaestin (*Heph*), is an extracellular ferrioxidase that is a candidate for this role. Hephaestin was discovered in the *sla* (sex-linked anaemia) mouse, a model of iron deficiency, which is caused by enterocyte blockage of iron export. Using gene mapping techniques, Vulpe et al [70] discovered a mutation in the previously uncharacterised hephaestin, a multi-copper ferrioxidase that provides a novel interaction between iron absorption and copper. Hephaestin (and ferroportin) expression is iron regulated in animal models [71] and its overexpression in cells has shown to increase iron efflux [72]. Interestingly, while systemic and/or intestine-specific $Heph^{-/-}$ knockout mice were intestinally iron overloaded and suffered from hypochromic, microcytic anaemia, they still remained viable,

indicating that hephaestin is one of, but not the only functionally important ferrioxidase regulating intestinal iron efflux [73].

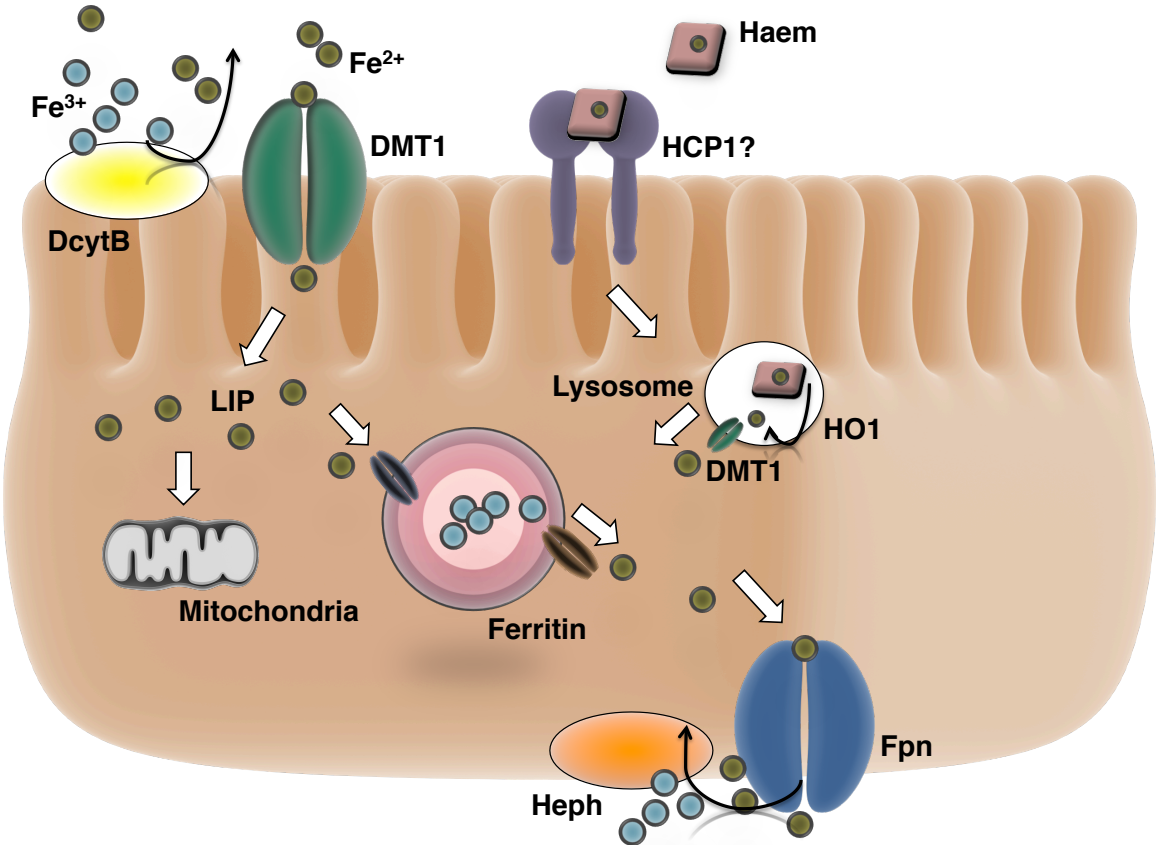

Figure 1.3 Cartoon illustration depicting the current mechanisms of iron absorption.

Non-haem iron uptake in intestinal cells is absorbed using Fe^{2+} mediated DMT1, with aid of the ferrireductase, DcytB. Iron absorbed in the cell joins the LIP and is directed, likely by a member of the PCBP family, to various organelles or stored as ferritin. During increased body iron needs, iron exported out of the cell to other tissues by Fpn and oxidized by the ferrioxidase, Heph prior to transferrin loading.

1.2.10 Hepcidin

Hepcidin (Hepc/LEAP1/*Hamp*) is a liver derived, cysteine-rich, 25 amino acid polypeptide [74] that regulates systemic iron homeostasis by inhibiting duodenal (and macrophage) iron export. The expression of hepcidin, a type-II acute phase protein, increases during iron overload, infection, or inflammatory disease [75-77]. As such, anaemia of chronic disease (ACD) is a result of hepcidin overproduction, which occurs in response to infections. This condition frequently arises in developing countries as well as in patients with chronic inflammation induced by cancer, diabetes, obesity, arthritis, and old age [78].

Hepcidin is considered the 'master controller' of iron absorption. It was first identified in blood and urine using mass spectrometry and first attributed with antimicrobial properties. Hepcidin inhibited the growth of pathogenic microbes such as *S. cerevisiae*, *S. aureus*, and *S. typhimurium* [74, 79]. The discovery of hepcidin as the key regulator of iron homeostasis was made rather serendipitously. Researchers investigating the mechanisms of glucose metabolism by the transcriptional regulator, USF2 using $USF2^{-/-}$ knockdown mice found that $USF2^{-/-}$ knockdown also resulted in severe iron overload [80]. By happenstance, USF2 is also a transcriptional regulator of hepcidin.

Hepcidin cDNA, separately identified using subtractive hybridisation from mice genomes, was significantly upregulated in mice fed a high iron diet [75]. Its effect on iron absorption has shown to be dose-dependent [81]. An inverse relationship was found between hepcidin and the protein expression of DMT1, DcytB, ferroportin, and transferrin when mice were switched from an iron-replete diet to an iron-deficient diet. In this same study, rats injected with synthetic hepcidin decreased intestinal iron uptake but iron liver stores or haemoglobin

levels remained unchanged, providing compelling evidence that the inhibitory effects of hepcidin on iron absorption are intestine-specific.

The inhibitory mechanism of iron absorption mediated by hepcidin was discovered by Nemeth et al [68]. Hepcidin binds directly to ferroportin dimers, resulting in subsequent JAK2-activated phosphorylation of ferroportin [82] and its subsequent internalisation and lysosomal degradation [68] thereby inhibiting duodenal iron export. In iron-replete or iron-overloaded intestinal cells, hepcidin expression is stimulated by the binding of bone morphogenic protein-6 (BMP6) to its co-receptor haemojuvelin in the liver, resulting in a cascade of phosphorylation of SMAD proteins that initiate *HAMP* transcription [83]. In iron-deficient intestinal cells, erythropoietin suppresses hepcidin expression through a pathway involving matripase-2 [84], resulting in the cleavage of haemojuvelin from the cell surface of liver cells [85]. This mechanism of hepcidin regulation is supported in several knockout mice models. In TMPRSS6$^{-/-}$ knockout mice, which inhibits the transcription of matripase-2, hepcidin was overproduced, ferroportin protein levels were decreased, and severe iron deficiency resulted [86]. In the *mask* mutant mouse model, microcytic anaemia is caused by the overproduction of hepcidin which is a result of defects in the TMPRSS6 gene [87]. TMPRSS6 gene mutations cause the clinical condition, iron refractory iron deficiency anaemia (IRIDA), which cannot be corrected by oral iron therapeutics [88]. Moreover, the importance of hepcidin in iron regulation is evident in cases of juvenile haemochromatosis. Gene mutation analysis of two separate families with haemochromatosis revealed separate point mutations on the exons of hepcidin cDNA [89], resulting in non-functional hepcidin and insufficient iron blockage. In summary, current knowledge strongly indicates that hepcidin is the most important factor regulating iron absorption.

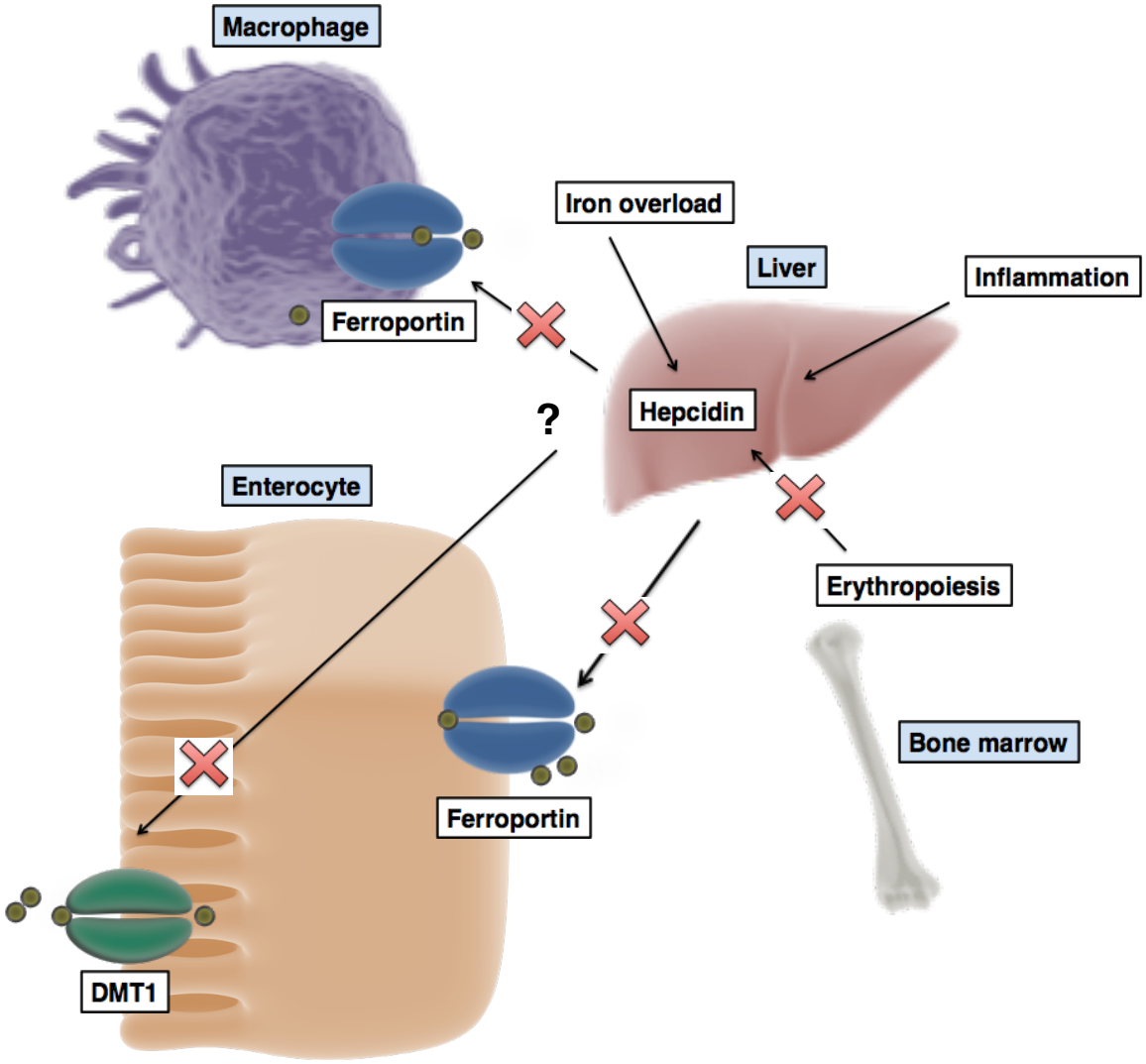

Figure 1.4 Hepcidin regulation on iron metabolism.

Hepcidin inhibits intestinal iron absorption and systematically regulates iron status by binding and inducing ferroportin degradation during iron-replete conditions. Under these conditions, BMP6 is activated and binds to its co-receptor HJV in the liver, resulting in the cascade of SMAD protein phosphorylation activating the transcription of hepcidin. Under iron-deficient conditions, erythropoiesis is increased and EPO is stimulated. EPO activates matripase-2, which actively degrades HJV, resulting in the inhibition of hepcidin.

1.3 Iron deficiency

As recent as 2010, the prevalence of anaemia was estimated to affect one-quarter to one-third of the world's population [90]. Half of the cases of anaemia is a result of iron deficiency [91]. Despite sustained efforts, iron deficiency remains the number one nutritional deficiency in the world, affecting over two billion people [1]. Improvements to alleviate iron deficiency over the last twenty years have been modest at best despite nutritional interventions and increased awareness [92]. Iron deficiency usually results when body iron physiological demands are not matched by dietary iron intake. This results in several conditions, such as decreased work productivity, poor pregnancy outcomes, decreased immune response, and cognitive developmental decline [93-95]. The economic burden of iron deficiency has been estimated to represent about 4% of the gross domestic product (GDP) in developing countries [96]. Inherently linked with either inadequate iron intake and/or diets that are predominately plant based [1], low-income and developing countries are especially prone to iron deficiency. The most vulnerable groups include women of childbearing age and children. These groups are predisposed and at risk for iron deficiency even in developed countries due to their increased iron demands. The WHO estimates that iron deficiency anaemia occurs in 40% of women of reproductive age and 50% of children (5-14 years old) in non-industrialised countries [97].

Contemporary dietary habits and viewpoints may have significant effects on iron status into the future. There is a growing societal effort to reduce meat consumption, based upon sustainability, ethics, and health effects [98-100]. This may have an impact on iron nutrition as meat is an important source of bioavailable iron and also increases the absorption of non-haem, an enhancing effect often referred to as the 'meat factor' [101-103].

While the scope of this thesis is to address iron deficiency from a dietary perspective, it is important to note a causal relationship between infection and iron deficiency. Iron deficiency is exacerbated in populations afflicted with chronic disease states, such as *H. pylori* infection or malaria. This form of iron deficiency, known as anaemia of chronic disease, has also been associated with cancer, obesity, inflammatory bowel disease, heart failure and kidney disease [104].

1.4 Iron bioavailability

Iron bioavailability is defined as the proportion of dietary iron that is absorbed and utilised for haemoglobin synthesis [103, 105]. Dietary iron is generally classified into two distinct categories; haem and non-haem. As briefly discussed previously, iron-containing foods of non-animal origin (in which the iron is free or chelated to proteins, organic acids, phytates, or polyphenols), soluble iron salts, and insoluble iron fortificants all are generally categorised as non-haem iron. Non-haem iron in foods exists in both the ferrous (Fe^{2+}) and ferric (Fe^{3+}) oxidation state, but the majority of iron is Fe^{3+} [106]. These foods include plants, cereals, and grains. Non-haem iron is the usual form of iron supplements and fortificants.

Haem iron, found almost exclusively in animal tissues, exists in the ferric state, centrally bound within the porphyrin ring of haemoglobin and myoglobin. Haem represents 10% percent of total iron intake, but despite the fact that plant foods can contribute equivalent amount of total iron as haem, absorption of haem iron is much more efficient [107]. Haem iron absorption in the diet is estimated to be 15-35% compared to 1-10% observed for non-haem iron [103]. The differences in iron absorption between haem and non-haem iron is attributed to the chemical species of iron, the divergent and discriminate routes of absorption into the intestinal epithelium [106], and the absence of effects of dietary inhibitors on haem iron [108].

Human trials measuring haemotological indices is the direct measurement of iron bioavailability. The gold standard measurement utilises radio or stable iron isotopes and measures its incorporation into haemoglobin. Other surrogate measurements of iron bioavailability include murine models (such as the haemoglobin repletion technique), cellular models (Caco-2 cells are the most extensively used), and measures of iron solubility and/or dialysability. These methods can be thought of as hierarchal, ranging from the most to the least predictive of human iron bioavailability.

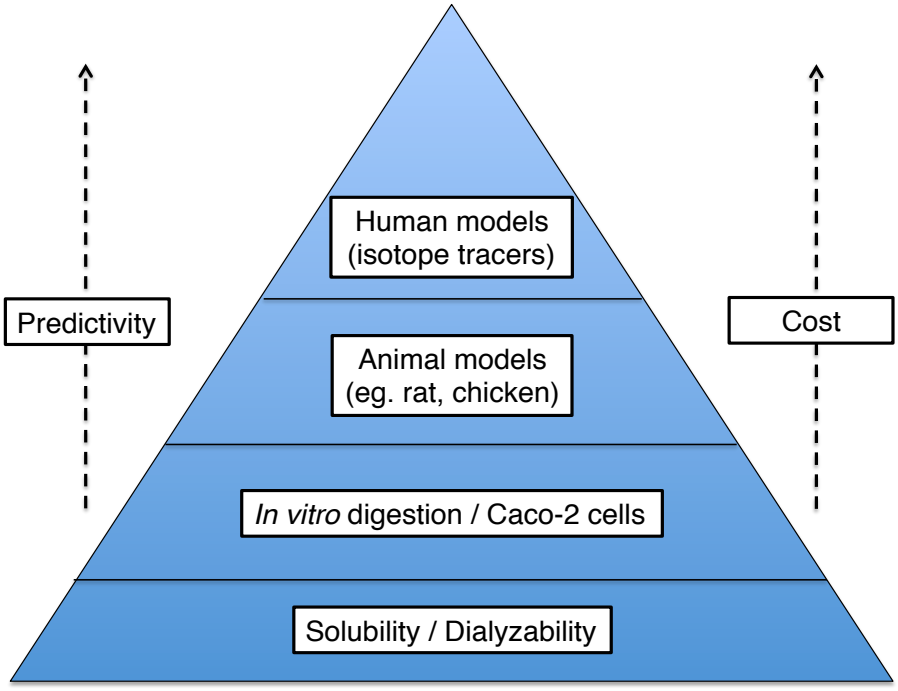

Figure 1.5 Hierarchical representation of the methods to assess iron bioavailability.

At the bottom of the pyramid, solubility is provides the lowest cost to measure iron bioavailability but is the least predictive. Meanwhile, human trials are the gold standard to measure iron bioavailability but costs are prohibitive. Animal models are shown as more predictive than *in vitro* digestion / Caco-2 cells

because they represent an *in vivo* response, but this is not true under all circumstances, such as the effect of enhancers and inhibitors on iron bioavailability.

While iron bioavailability is strictly defined as iron utilisation, it can also be described as a series of sequential stages [109].

(1) Availability: the effect of digestion on the release of iron from the food matrix, and the presence of soluble iron (sometimes referred to as bioaccessibility).

(2) Uptake: iron transport into the enterocyte.

(3) Absorption: basolateral transfer of iron into the blood.

(4) Utilisation: functional iron usage (e.g. RBC incorporation).

Although each step can be considered a proxy of bioavailability, the term bioavailability in the strictest sense refers to utilisation. In practical terms, each method has its merits depending on experimental objectives and, ultimately, cost. *In vitro* simulated digestion techniques can be used to measure the first stage, and Caco-2 cells the second and third stages.

Gastrointestinal transit contributes a minor role in iron bioavailability relative to the effects of digestion. Salivary enzymes such as amylase initiate the digestion of food. The low pH conditions (2-4) and the stimulated release of pepsin in the stomach result in protein degradation and the release of iron. In some individuals, achlorydia, a condition that leads to reduced or no hydrochloric acid production, results in iron deficiency [110, 111]. Once food is digested in the stomach, chyme is transported into the small intestine. The neutral pH (6.8-7.4) environment in the small intestine results in iron precipitation unless chelated to organic acids or other dietary components. The duodenum is the main site for iron absorption.

Iron status is one of the most important determinants of iron absorption. Iron-deficient individuals increase iron absorption and hence, measured dietary iron bioavailability is higher, even when the properties of the food are unchanged. This illustrates the difficulties of attempting to quantify dietary iron bioavailability. There is a need for reference materials to be used for comparison so that results from different experiments can be compared.

Since the thesis is based strictly upon *in vitro* cell culture techniques, a thorough and detailed review of the usefulness of Caco-2 cells to predict human iron bioavailability will be presented later in the chapter.

1.4.1 Ascorbic acid

Ascorbic acid (AA) is the most potent dietary enhancer of non-haem iron. AA has been shown to offset the inhibitory effects of dietary inhibitors, such as phytates [112, 113], polyphenols [112, 114] and calcium [115] in a dose-dependent manner. The use of AA is strongly recommended at 2:1 AA:Fe molar ratios in the presence of low to medium dietary inhibitors and 4:1 in the presence of high dietary inhibitors when introduced for food fortification [116, 117]. Other acids found in the diet, such as citric acid, also enhance iron absorption to some extent but to a lesser degree compared to AA. Gillooly et al [118] found that adding citric acid (1 g) and 3 mg Fe to vegetables increased iron absorption to the same degree as AA (15 mg), thus highlighting the potency of AA as an enhancer of non-haem iron absorption.

Single meal studies have consistently demonstrated the potent enhancing effects of AA on iron bioavailability, but mixed-meal and longer-term studies indicate that its enhancing effects are subtler. In a 10-week human trial, Hunt et al [119] found that the addition of 1500 mg AA / day had no effect on iron absorption in women with low iron stores. Similarly, only modest improvements in iron bioavailability (35% increase) were shown in a complete diet study over 5

days comparing low AA and high AA meals (51 vs. 247 mg / day), respectively [120]. Cook et al [120] hypothesised that a portion of undigested, luminal contents from successive meals, and/or the inherently varied composition of the diets between individuals may blunt the effects of AA long-term.

The mechanism underlying the interaction between AA and increased iron bioavailability is well understood. Conrad et al [121] demonstrated that AA is a strong chelator of Fe^{3+} at gastric (acidic) pH. The chelation of solubilised Fe^{3+} (and Fe^{2+}) to AA at gastric pH prevents the formation of insoluble ferric hydroxides [$Fe(OH)_3$] at intestinal pH [121-123]. Separately, AA also is a potent reductant that is able to catalyse the reduction of Fe^{3+} to Fe^{2+} [124], resulting in increased rates of DMT1 transport.

To a lesser degree, AA may also increase Fe bioavailability by an intracellular effect. Researchers using Hutu-80 cells demonstrated that AA donates electrons intracellularly to DcytB to drive ferrireductase activity [125]. Moreover, Scheers et al [126] was also able to demonstrate that short-term incubation of AA (16 hrs) increased protein expression of DMT1 and DcytB while long-term exposure (38 hrs) decreased its expression in Caco-2 cells, possibly providing a mechanistic explanation for the differences in AA-mediated iron bioavailability between single meal and multiple meal studies [119, 120]. Overall, it is generally well-accepted that AA increases non-haem iron bioavailability, but its added cost and instability in food matrices makes it less effective for improving iron bioavailability at the population level [127, 128]

1.4.2 Calcium

Calcium is the only iron inhibitor that has been shown to inhibit both haem and non-haem iron [129-131]. Given that calcium inhibits both forms of iron, it has been suggested that its mechanism of inhibition occurs during basolateral iron export [129].

The inhibitory effects of calcium on iron absorption have been demonstrated in single meal, short-term studies. The initial study by Hallberg et al [130] showed that its inhibitory effect is dose-dependent, with maximal inhibition of iron absorption (33-50%) at concentrations of 300 mg calcium (as $CaCl_2$) when introduced into bread rolls [130]. Similar to Hallberg, Dawson-Hughes et al [132] found that 500 mg calcium (as $CaCO_3$) introduced into a single meal inhibited iron absorption by 50%. Hallberg et al [129] also found that high doses of $CaCl_2$ (800 mg) were required to inhibit iron from $FeSO_4$ or haem when given as supplements without a food vehicle, suggesting that their initial study design may have overestimated the inhibitory effects of calcium on iron absorption. Cook et al [133] showed that a calcium supplement at 600 mg decreased iron absorption only when the supplement was taken with food. The form of calcium supplement (chloride, carbonate, etc) may also have an effect on iron absorption [133].

The long-term inhibitory effect of calcium on iron absorption has not been demonstrated. In a study examining the effect of high calcium supplementation on iron absorption over multiple meals (5 consecutive days) [134], no change in iron absorption was observed. Surprisingly, iron absorption with high calcium supplementation was similar to diets consumed ad libitum. In a study investigating calcium supplementation over 6 months (1200 mg / day), iron status was not different compared to participants without calcium supplementation [135].

The inhibitory effects of calcium on iron absorption may be relevant in cases of food fortification, in which populations are commonly deficient in both calcium and iron and thus given multiple mineral formulations. Similar to calcium supplementation, the effects of calcium fortification on iron absorption have been marginal. In one study, low (39 mg / serving) and high (156 mg / serving) calcium-fortified breakfast cereals (as $CaCO_3$) had no effect on the absorption of

7.5 mg iron [136]. In another study, an iron-fortified casein drink with added calcium (100 and 200 mg) modestly inhibited iron absorption, and the effect was reversed by low doses of AA at 2:1 and 4:1 AA:Fe molar ratios [115]. Calcium inhibition of iron absorption is hypothesised to be a result of high calcium dosage rather than high Ca:Fe molar ratios [131].

The differences between short-term and long-term effects of calcium on iron absorption may reflect individual adaptation to iron uptake after an initial, short-term high dose of calcium [137]. The mechanisms underlying how calcium inhibits iron absorption are mixed and remain inconclusive. Several studies have suggested that calcium inhibits iron absorption through DMT1. Calcium non-competitively inhibited non-haem iron transport through DMT1 in DMT1 RNA expressed *Xenopus* oocytes [138]. In Caco-2 cells, calcium inhibited iron uptake from ferric ammonium citrate (FAC) by decreasing DMT1 protein concentration at the apical surface [139]. Conversely, it has also been shown that 500:1 and 1000:1 Ca:Fe molar ratios increased iron uptake but decreased basolateral decrease in Caco-2 cells [140]. Differences in iron compound ($FeCl_3$ vs FAC), incubation time (1 hr vs 4 hr), and iron uptake measurements (radioisotope tracer vs ferritin formation) may explain the disagreement between results obtained by Thompson [43] and Gaitan [44]. In summary, while the inhibitory effects of calcium on iron absorption remain unresolved, calcium has only demonstrated a modest effect on iron absorption and iron status [141].

1.4.3 Phytic acid

Phytic acid (PA) is present in many staple foods and as such is the predominant inhibitor of non-haem iron in plant-based diets [142]. In cereals and legumes, the majority of phosphate (60-80%) constitutes PA [143]. PA concentrations in cereals and legumes vary depending on plant species, but range between approximately 0.5-2% of the total plant [144]. PA decreases iron

bioavailability in a dose-dependent manner. Hallberg et al [113] demonstrated that increasing PA concentrations from 2 to 250 mg in radioisotope iron-labeled bread rolls decreased iron absorption from 82% to 18%. In a separate study, increasing PA levels (14 mg to 58 mg) in a bread meal decreased iron absorption ratios (AR) from 1.21 to 0.54 [112].

The inhibitory effect of PA on iron bioavailability is not the result of the fibre content. Several studies have demonstrated that the PA content of wheat-bran, irrespective of fibre content [145, 146], is solely responsible for its low iron bioavailability [145, 147].

Many vegetables also contain high levels of PA, such as beans and lentils. In a human study using radiolabeled iron, the addition of exogenous $FeSO_4$ (3 mg) to beans and lentils did not improve iron absorption compared to beans and lentils alone [118], demonstrating the potent inhibitory effects of PA on non-haem iron.

Common names		***Taxonomic names***	**Phytic acid g/100g (DW)**
Cereals			
Maize		*Zea mays*	0.72 - 2.22
	germ		6.39
Wheat		*Triticum* spp.	0.39 - 1.35
	bran		2.1 - 7.3
	germ		1.14 - 3.91
Rice		*Oryza glaberrima/sativa*	0.06 - 1.08
	bran		2.56 - 8.7
Barley		*Hordeum vulgare*	0.38 - 1.16
Sorghum		*Sorghum* spp.	0.57 - 3.35
Oat		*Avena sativa*	0.42 - 1.16
Rye		*Secale cereale*	0.54 - 1.46
Millet		*Pennisetum* sp.	0.18 - 1.67
Triticale		*Triticale secale*	0.50 - 1.89
Wild rice		*Zizania* sp.	2.20
Legumes			
Kidney beans		*Phaseolus vulgaris*	0.61 - 2.38
Haricot beans			
Pinto beans			
Navy beans			
Blackeye beans			
Broad beans		*Vicia faba*	0.51 - 1.77
Peas		*Pis sativum*	0.22 - 1.22
Dry cowpeas		*Vigna unguiculata*	0.37 - 2.90
Black-eyed peas			
Chickpeas		*Cicer arietinum*	0.28 - 1.60
Lentils		*Lens culinaris*	0.27 - 1.51

Table 1.1 Phytic acid content of staple foods.

Table adapted from Frontela et al [148].

There are several strategies used to improve iron bioavailability from PA containing foods. Consuming cultivars of foods with lower PA concentrations is a relatively straightforward solution. Using Caco-2 cells, Eagling et al [149] compared iron bioavailability of white flour from two cultivars of wheat differing in iron content. Iron bioavailability was higher in the lower iron content cultivar despite having half the amount of endogenous iron. After measuring the PA

content, the higher PA concentration of the higher iron content cultivar inhibited non-haem iron to an extent that the lower iron content cultivar was more bioavailable.

Another strategy to improve iron bioavailability is the reduction of PA levels. The levels can be reduced or completely degraded using fermentation. In Caco-2 cells, sourdough (fermented) breads [148] and lacto-fermented vegetables [150] were more bioavailable compared to their non-fermented controls. Similar to these studies, our laboratory recently demonstrated that iron uptake in Caco-2 cells was higher in $FeSO_4$ supplemented sourdough bread compared to other bread making processes as a result of complete degradation of PA [151].

The use of exogenous phytase is another strategy to reduce PA levels. Phytase added to infant complementary foods and then exposed to an *in vitro* digestion at infant gastric conditions (pH 4) increased iron bioavailability in Caco-2 cells compared to foods without phytase [152]. In a human stable iron isotope study, phytase added to cereal porridges increased iron bioavailability 2-12 fold compared to control. In a similarly designed human trial using phytase, Davidsson et al [153] did not observe increases in iron bioavailability even with an 88% reduction in PA, demonstrating that PA is a potent inhibitor of iron bioavailability at even relatively low concentrations. In our study, only full degradation of PA increased iron bioavailability in Caco-2 cells. Given that low, basal levels of PA can exert potent inhibitory effects on iron absorption, current recommendations suggest that PA levels are reduced to below 1:1 Fe:PA molar ratios [142], considering that 1 mol of phytate can bind up to 6 mol of ferric iron [117].

PA inhibits non-haem iron bioavailability at the stage prior to apical uptake. At intestinal pH, PA is negatively charged, and its affinity for positively charged

Fe results in the formation of highly insoluble PA-Fe complexes. These insoluble complexes are unavailable for absorption as humans lack phytase specific enzymes that cleave PA-Fe complexes [154].

1.4.4 Polyphenols

Polyphenols (PP) are a group of compounds with variable hydroxyl groups bound to aromatic rings (phenolic structures). As a potent inhibitor of iron bioavailability, PP functions as secondary metabolites for host defense mechanisms [155]. Tea, coffee, and wine are among the most prevalent PP containing foods [118, 156]. Total PP content of foods was inversely correlated with iron bioavailability [118] and iron bioavailability was decreased dose-dependently with increasing PP [156]. In a human trial, Tuntawiroon et al [157] demonstrated that increasing the serving size of a native Southeast Asian vegetable high in PP from 0-20 g per meal (0-600 mg tannic acid (TA) equivalent) dose-dependently reduced iron absorption from 12.8 to 1.7%. Similarly, Siegenberg et al [112] found a dose-dependent relationship with increased TA (12-833 mg) and decreased iron absorption ratios AR (0.7 to 0.21).

Tea is one of the most well-known dietary iron inhibitors [158]. It contains the hydrolysable form of tannic acid (TA) containing multiple gallic acid subunits [155]. Among polyphenol beverages, Hurrell et al [156] observed that black tea was the most potent iron inhibitor at the lowest PP concentration, with 50 mg PP inhibiting up to 70% iron. Tea consumed with breakfast meals reduced iron absorption from ferrous ascorbate by 60% [159]. Coffee is also an inhibitor of iron bioavailability [160], albeit to a lesser extent than tea, and its mechanism of inhibition is thought to be due to either the presence of TA or chlorogenic acid, which constitutes the majority of PP in coffee. In a human study, iron absorption from semi-synthetic meals was reduced by 72% when consumed with a cup of

coffee [160]. TA is thought to inhibit iron bioavailability by forming non-absorbable complexes with iron prior to apical uptake [161].

Since PP constitutes hundreds of phenolic compounds, the inhibitory mechanism and potency of iron bioavailability from PP is likely type-specific. In Caco-2 cells, epigallocatechin gallate (ECGC) [found in green tea] and quercetin [the most abundant flavanol in the diet (apples, grapes, tea)], inhibited iron bioavailability at the step of basolateral export [162, 163]. Also in Caco-2 cells, quercetin inhibited miRNA regulation on the 5' UTR of ferroportin, resulting in its decreased protein expression [163]. The modulatory effect of quercetin on ferroportin may partially explain its effect on iron absorption.

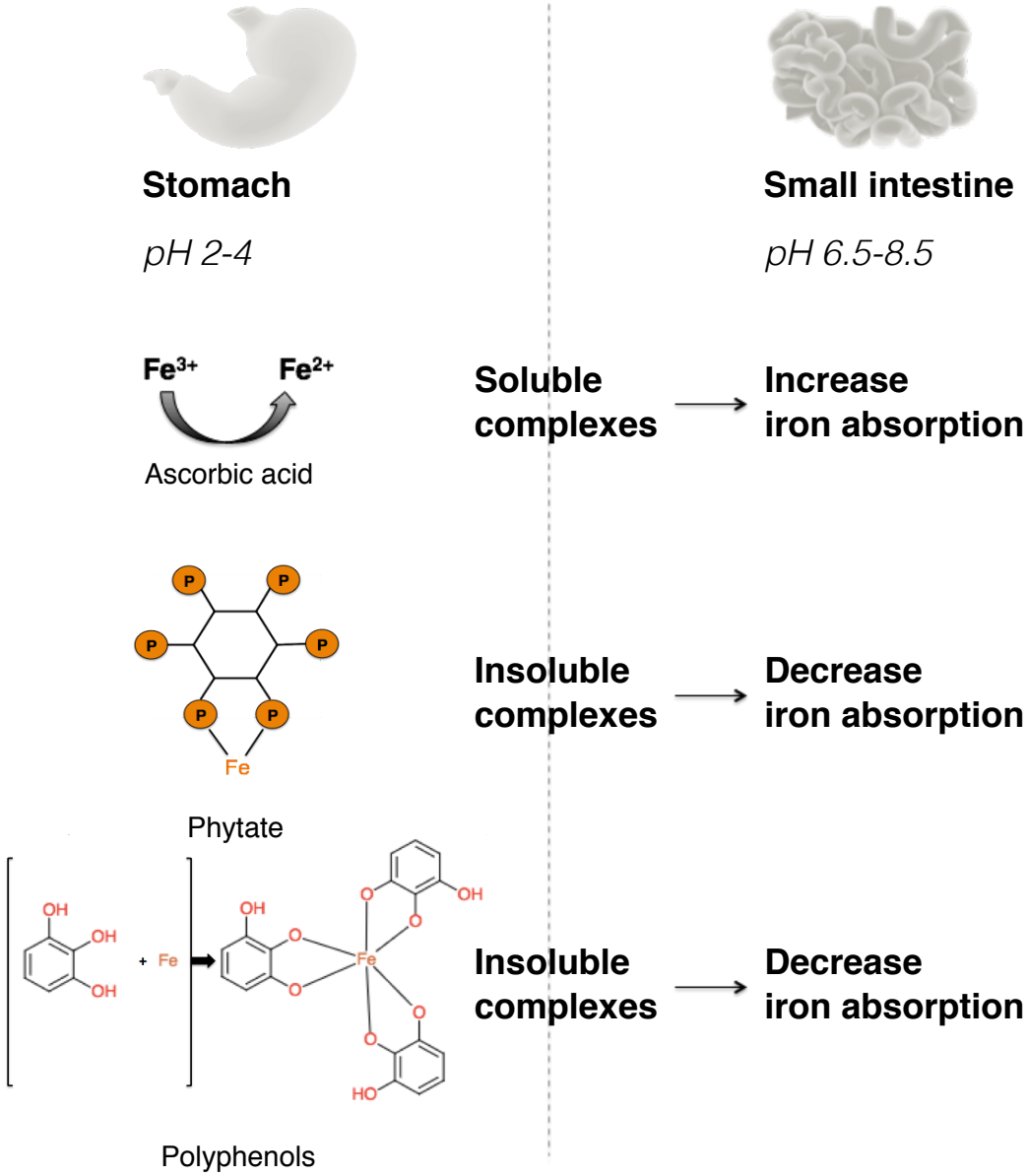

Figure 1.6 Schematic cartoon depicting the predominate enhancer and inhibitors of non-haem iron absorption found in the diet.

Ascorbic acid reduces ferric to ferrous iron and forms soluble complexes in the stomach to enhance iron absorption. Phytate and polyphenols bind iron in the stomach, which results in insoluble complex formation in the intestinal lumen, inhibiting iron absorption.

1.5 Strategies to reduce iron deficiency

1.5.1 Iron supplementation

Iron deficient individuals that cannot meet their iron requirements through dietary intervention are usually prescribed iron supplements. Soluble ferrous salts are the most commonly prescribed supplements. Ferrous sulfate, gluconate and fumurate, are inexpensive, well-absorbed and normally correct anaemia [164]. Intakes of 150-200 mg / day elemental iron are usually recommended (e.g. 300 mg $FeSO_4$ which is 60 mg elemental iron 3x per day) [165, 166].

Soluble ferrous salts may be cheap and well absorbed but recent evidence has highlighted several health concerns. Short-term supplementation trials have routinely demonstrated to correct anaemia and improve iron status, but the benefits of routine supplementation have not been demonstrated [107]. Routine supplementation is also not particularly useful or sustainable in many public health settings. Furthermore, routine supplementation can decrease the absorption of dietary non-haem iron [167], possibly through the mucosal block theory.

$FeSO_4$ is considered the 'gold standard' of iron supplementation. Testing of other iron compounds for iron bioavailability is measured relative to $FeSO_4$. Iron bioavailability of $FeSO_4$ is estimated to be between 10-15% [168], but depends greatly on the presence or absence of inflammation and iron status of the individual. In non-anaemic women, Lonnerdal et al [169] and Harrington et al [170] both reported ca. 20% bioavailability from $FeSO_4$. While highly bioavailable, $FeSO_4$ is not well-tolerated in individuals and can induce multiple, adverse gastrointestinal conditions such as nausea, diarrhoea, and constipation (see review by Cancelo-Hidalgo et al [171]). During these cases, lower or less frequent dosages are prescribed. For example, in one study, 20 mg / day decreased ID during pregnancy and post-partum without side effects [172].

Difficulties in poor palatability and digestibility caused by $FeSO_4$ supplementation are common, resulting in less than 50% compliance [173]. The adverse gastrointestinal conditions caused by $FeSO_4$ have been attributed to excess, unabsorbed iron in the lumen, which can participate in Fenton-based redox reactivity [174]. The effects of iron supplementation (and particularly $FeSO_4$) on health outcomes and clinical significance have so far not been fully evaluated. In animal models, $FeSO_4$ has been shown to induce and exacerbate carcinogenesis in patients with irritable bowel disease (IBD) [175]. Lund et al [174] found that routine iron supplementation for 2 weeks increased fecal free radical generation. Moreover, human supplementation trials have demonstrated that iron supplementation resulted in changes to gut microbial populations, favouring iron sequestering negative bacteria over positive bacteria such as lactobacilli [176, 177].

1.5.2 Iron biofortification

The WHO defines biofortification as 'the process by which the nutritional quality of food crops is improved through agronomic practices, conventional plant breeding, or modern biotechnology.' The three current methods for the biofortification of food crops in increasing iron concentrations are (a) agronomical (increasing soil iron content and / or foliar spray of plants), (b) selective breeding and (c) genetic engineering. HarvestPlus, an organisation that funds the majority of biofortification research, has set out specific guidelines for successful nutrient biofortification. These guidelines are termed: discovery, development, and delivery. In general, biofortification strategies to improve the iron content in plants are tested. If the first stage is successful, human bioavailability trials are conducted to assess efficacy. If the second stage is successful, scaled-up approaches to grow sufficient quantities for local communities are implemented [178].

The simplest biofortification approach is agronomic. Direct addition of iron to soil (fertilisation) or foliar application (spray) has been shown to increase the iron content of plants. Mixed results have been generated using this approach. Wheat fertilised with soluble iron resulted in the increase in iron concentration in the roots and shoots, but the rapid conversion to ferric unavailable forms blocked its transport to the edible grain [179]. Iron foliar application has resulted in either marginal increases [180] or no effect [181] on the iron content of wheat. In one study, similar to the fertiliser approach, foliar application did not result in increased iron transport to the endosperm of wheat [180], demonstrating the limitation of this technique on certain food crops. The effect of agronomic approaches on the iron content and bioavailability is likely crop dependent, as the difficulties in agronomic approaches to wheat may be due to its complicated genome. Foliar spray has been effective for *P. sativum* and *V. umculada* [182].

There are numerous concerns with agronomic approaches. Agronomic methods may be unsuitable in the long-term and/or sustainable due to the requirements for constant application. Furthermore, associated costs and environmental concerns may hinder its use in developing countries [178, 183].

Increasing the iron content in crops can also be accomplished using conventional breeding. Using this strategy, iron-biofortified rice contained 4-5 fold increases in iron content compared to conventional rice and improved iron status in non-anaemic Filipino women [184]. In another example of biofortified rice, co-overexpressed soybean ferritin and nicotiniamine synthase genes using transgenic approaches resulted in 5-fold increases in iron (15 µg/g vs 2 µg/g) in polished grains and when applied to the *in vitro* digestion / Caco-2 model, significantly increased iron bioavailability compared to wild-type rice [185].

Another iron biofortification strategy is cultivating crops low in PA. This approach has recently had some success, but these strains low in PA suffered

from low yield [186, 187], which greatly limits its potential. Moreover, iron bioavailability in low PA biofortified beans was higher than normal PA, low PP, and high PP beans in women with low iron status, suggesting that, at least in beans, PA is the more potent inhibitor of iron bioavailability [188]. Unfortunately, women on the low PA bean diet reported adverse gastrointestinal distress, which may severely limit its consumer acceptability and consumption [189]. Recent studies in both the short [189] and long-term (4 months) [190] have shown that iron-biofortified beans improved the iron status of iron-deficient women. These studies suggest, given the ability to grow sufficient quantities that the best strategy for biofortification is breeding for high iron, irrespective of antinutritional factors.

1.5.3 Iron fortification

Food fortification is the most effective strategy to alleviate iron deficiency for large-scale populations. Iron is added exogenously to various foodstuffs/matrices such as cereals, condiments (soy / fish sauce), meal replacements, infant foods, etc. Iron fortificants are categorised based upon their acid dissolution profile: (a) water-soluble, (b) water-insoluble, but soluble in dilute acid, and (c) insoluble. Choice of iron fortificant is a compromise between soluble iron fortificants that are well absorbed but are highly reactive, unstable, may cause organoleptic changes when introduced to foods, and insoluble iron fortificants which are unreactive and stable in food matrices, but have low iron bioavailability. Many iron formulations exist, but stability, foodstuff application, and ultimately costs are important drivers of its implementation.

Key characteristics of Fe compounds commonly used for food fortification		
Compound	Relative bioavailability[a]	Relative cost (per mg Fe)
Water soluble		
Ferrous sulfate 7•H_2O	100	1.0
Ferrous sulfate, dried	100	1.0
Ferrous gluconate	89	6.7
Ferrous lactate	67	7.5
Ferrous bisglycinate	>100[c]	17.6
Ferric ammonium citrate	51	4.4
Sodium iron EDTA	>100[c]	16.7
Poorly water soluble, soluble in dilute acid		
Ferrous fumarate	100	2.2
Ferrous succinate	92	9.7
Ferric saccharate	74	8.1
Water insoluble poorly soluble in dilute acid		
Ferric orthophosphate	25-32	4.0
Ferric pyrophosphate	21-74	4.7
Elemental iron:		
H-reduced	13-148[d]	0.5
Atomized	-24	0.4
CO-reduced	(12-32)	<1.0
Electrolytic	75	0.8
Carbonyl	5-20	2.2
Encapsulated forms		
Ferrous sulfate	100	10.8
Ferrous fumarate	100	17.4

Table 1.2 Iron compounds used for food fortification.

Reproduced using World Health Organisation, Iron deficiency anaemia: assessment, prevention, and control [116].

Iron fortificants, either soluble in water or dilute acid, enter the non-haem iron pool in the gastrointestinal tract and are absorbed to the same extent as native non-haem iron compounds in the meal. As previously described, insoluble iron fortificants, such as electrolytic iron and ferric pyrophosphate, are poorly

absorbed. Hurrell et al [117] suggested that these insoluble iron fortificants should be added to the food vehicle at twice the amount of iron as $FeSO_4$ since it is absorbed half as well as $FeSO_4$. Other insoluble iron fortificants such as atomised and hydrogen-reduced iron powders have been shown to have such poor iron bioavailability that they are not recommended at any level [191].

Particle size reduction of poorly soluble iron compounds is one strategy that has been shown to increase iron absorption [192-194]. Harrison et al [194] found that the relative biological value (RBV) increased by 2-3 fold and 5-fold when the particle size was reduced for electrolytic iron (27-40 micron to 7-10 micron) and $FePO_4$ (12-15 micron to 1 micron), respectively. RBV was positively correlated to iron solubility at 0.1 N HCl and human iron bioavailability. In another study, particle size reduction of ferric pyrophosphate (FePP) from 21 microns to 0.5 microns improved RBV from 59% to 95% compared to $FeSO_4$ in rats [195]. Recently, a dispersible micronised FePP (mean particle size 0.3 μM) has been developed (commercialised as SunActive®, Taiyo Japan) and in a human trial was as equally bioavailable as $FeSO_4$ when introduced in infant cereal and yoghurt food matrices [196]. Its addition in fortified salt and extruded rice has also been demonstrated to improve iron status and decrease iron deficiency in anaemic children [197].

NaFeEDTA (sodium iron ethylenediaminetetraacetic acid) is a well-absorbed iron compound and is recommended in the presence of high PA foods. Iron bioavailability of NaFeEDTA is 2-3x higher than $FeSO_4$ in high PA foods [116], likely because EDTA has a high affinity for iron and prevents its binding to PA [198, 199]. NaFeEDTA introduced into meals containing corn masa flour and black beans was 2x more bioavailable than $FeSO_4$ (9.0 vs 5.5%) in young girls [200]. In another study, sugar fortified with NaFeEDTA improved iron stores in community based trials in Guatemala [201]. One particular benefit of NaFeEDTA is its stability in liquids. It's introduction into sauces, such as soy and fish, is

advantageous for iron fortification. In a 6 month community trial, NaFeEDTA fortified soy sauce and fish sauce improved iron status and reduce iron deficiency by 50% in studies conducted in Vietnam [202]. In a separate clinical study, NaFeEDTA fortified soy sauce and fish sauce was as bioavailable as $FeSO_4$ fortified soy sauce (3.3 vs 3.1%) and fish sauce (6.1 vs 5.6%) given as rice-based meals [203]. Given these results, China and Vietnam have introduced NaFeEDTA fortified soy sauce and fish sauce into their national fortification programs [116].

Amino acid chelates (e.g. ferrous bisglycinate) are another promising form of iron but their bioavailability requires further investigation [204, 205]. Each molecule of amino acid chelate has Fe^{2+} forming heterocyclic ring structures with two glycines bound on each side. This theoretically protects Fe^{2+} from chelation with iron inhibitors. The iron bioavailability from ^{59}Fe-bisglycinate was 3-4 fold increased compared to $^{55}FeSO_4$ (10.8% vs 2.7%) in iron deficient men consuming high phytate whole-meal maize porridge [206]. Similarly, iron bioavailability from ferrous bisglycinate was 2-fold greater than $FeSO_4$ in meals containing corn flour, margarine, and cheese consumed by non-anaemic individuals [207].

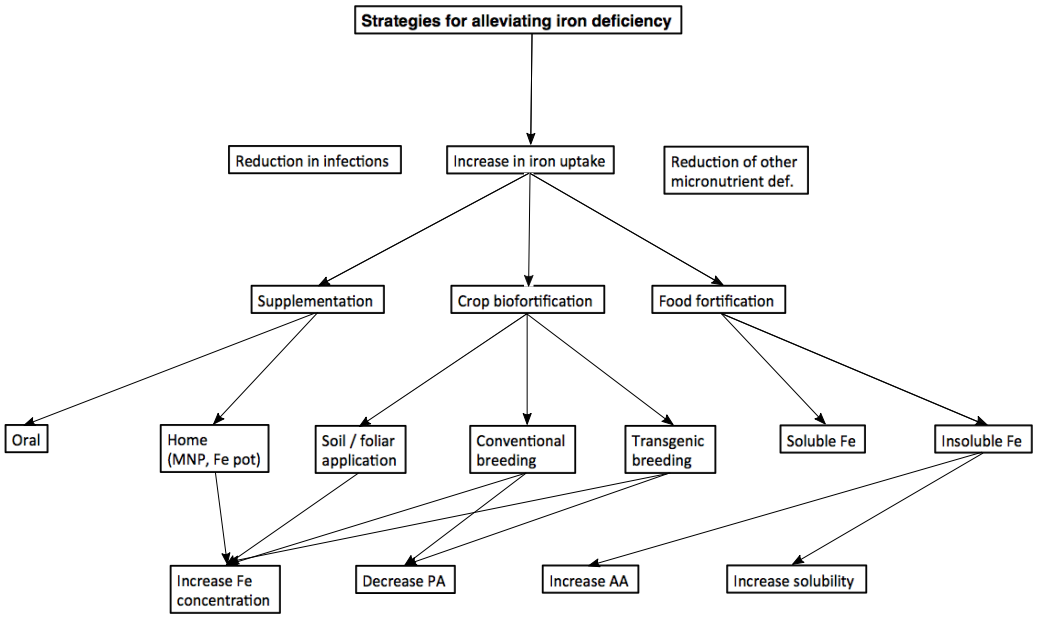

Figure 1.7 Flow chart representing the strategies for alleviating iron deficiency.

1.6 Methods to estimate iron bioavailability

1.6.1 *In vitro* techniques for estimating iron bioavailability

Much of our understanding in iron metabolism has been generated using *in vivo* rodent models. While an invaluable resource in investigating the mechanisms of iron metabolism, its ability to recapitulate human iron bioavailability has been questioned. For example, when identical test meals were given to human volunteer subjects (18-40 yr old) and rats and iron isotope incorporation was measured after 14 days, Reddy et al [208] showed that rats fed mixed diets containing various dietary factors (enhancers: AA and meat, inhibitors: tea and bran) had little to no effect on iron bioavailability. The iron absorption ratio (test: control) for rats was 1.23 and 0.92 for AA and tea, significantly less than the potent effects observed from volunteer subjects (3.77

and 0.17, respectively). The results of this study are in part due to differences in intestinal physiology between species. Rats endogenously synthesise AA [49], whereas humans must obtain AA from the diet. Moreover, rats upregulate the synthesis of AA under conditions of iron deficiency [47]. While dietary factors tend to underestimate their effects in rats, in general, iron bioavailability from whole meals in rats tends to overestimate that of humans [209]. These results have led to the suggestion that iron bioavailability as determined in animal models is 'of little to no use' in assessing dietary iron bioavailability in humans [209].

The majority of recent studies have used stable isotopes [210, 211], such as ^{57}Fe and ^{58}Fe, to simultaneously determine iron absorption from 2 test meals (or one test meal and one reference meal). Older methods, such as those of Hallberg [212], used radioisotopes to establish much of our understanding of iron bioavailability, but due to ethical constraints, its use of limited to cellular and animal models. Human trials are, however, time-consuming and expensive [213] and cannot be used to study the mechanisms of iron absorption at the cell or molecular level.

In vitro methods are relatively rapid, inexpensive and can provide surrogate measures of iron bioavailability. These methods utilise a simulated *in vitro* digestion with food components, single foods, or complex meal matrices to simulate human *in vivo* conditions. *In vitro* digestion is categorised as either static or dynamic; static models use fixed pH digestions with HCl, digestion enzymes, and incubation times. They are rapid, inexpensive, and easier to use than dynamic models but lack the comprehensiveness and refinement that occurs naturally in *in vivo* digestion. Dynamic models, such as the Dynamic Gastric Model (Institute of Food Research, Norwich) and TIM models (TNO, Netherlands) are more precise and refined. These models are based on data obtained from human *in vivo* digestion and offer a more representative model of *in vitro*

digestion compared to static models, but require more user-training, are difficult to replicate, and are not well adapted for high throughput comparison studies.

Most *in vitro* digestion models measuring iron bioavailability are based on variants of the established static procedure of Miller et al [214]. Iron-containing foods and/or components are exposed to a gastric digestion step at pH 2 with pepsin. After a period of time (normally 1 to 2 hr), the pH of the 'digest' is raised to intestinal conditions, followed by the addition of a pancreatin-bile solution. The 'digest' is then applied to a molecular weight cut off (MWCO) dialysis membrane to screen for soluble, dialysable iron, and fractional iron 'availability' is quantified. The digestion enzymes concentrations were calculated from data obtained from prior human studies.

The model is relatively quick, simple, and straightforward but has several drawbacks. For example, it does not fully replicate the dynamic changes in pH, rates of gastric emptying, and peristaltic movements naturally occurring *in vivo*. The method also assumes that either all insoluble or soluble large molecular weight complexes (such as NaFeEDTA) are unavailable, and that all soluble iron is bioavailable [213]. Pynaert et al [215] found that processed complementary foods, containing more soluble iron than the unprocessed variety, did not improve iron status in field trials. Subsequently, they showed in Caco-2 cells that the processed food contained less bioavailable iron than the unprocessed food.

In an improvement over the solubility/dialysability technique, Garcia et al [216] demonstrated that Caco-2 cells could be used to predict iron bioavailability from foods. The group observed that iron absorption from foods increased in the presence of AA or meat using extrinsic isotope tagging methods. Garcia relied solely on pH changes and omitted the pancreatin-bile enzymes and the dialysis membranes of Miller et al [214], likely because these enzymes are damaging to cell monolayers. The lab of Ray Glahn developed the widely accepted technique

for iron bioavailability used currently. His lab adapted the *in vitro* digestion methods of Miller et al [214] coupled to Caco-2 cells. The iron bioavailability from *in vitro* digested foods either radiolabeled with iron [217] or more commonly unlabeled using cell ferritin formation as a proxy for iron bioavailability [218] is measured in Caco-2 cells.

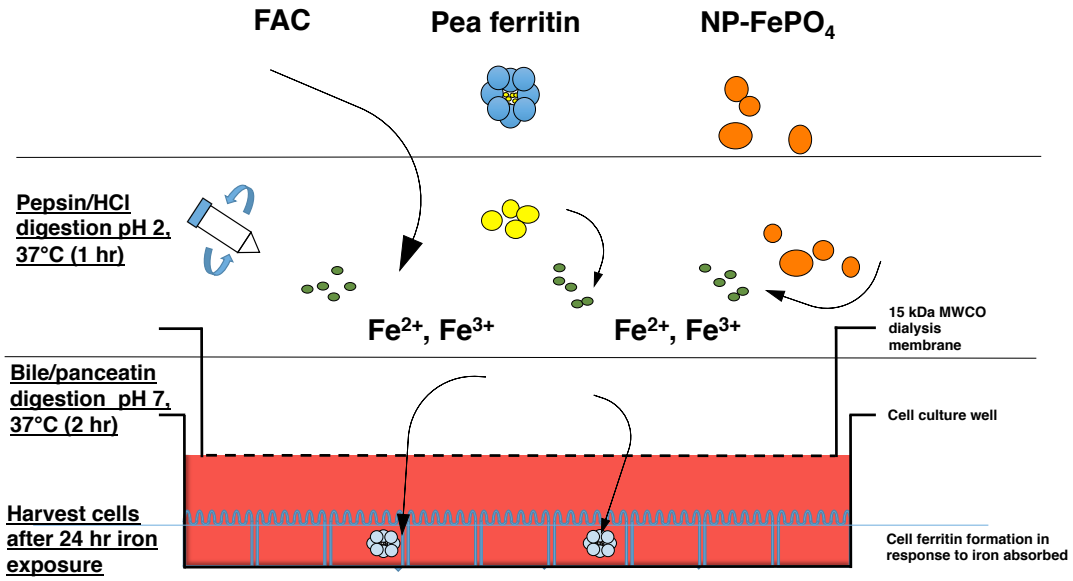

Figure 1.8 Representative schematic diagram of the *in vitro* digestion / Caco-2 cell model to assess iron bioavailability of iron containing foods and compounds developed by the Glahn lab [218].

The *in vitro* digestion protocol was essentially adapted from Miller et al [214]. FAC, pea ferritin, and NP-$FePO_4$ are examples of iron compounds that can be used with this technique. Iron compounds are exposed to gastric digestion (with 0.1 M HCl) at pH 2 for 1 hr. After 1 hr, the pH is increased to pH 5.5-6.0 (with 0.1 M $NaHCO_3$) and digestive enzymes added. Finally, the pH of the digests are increased to pH 7.0 and placed on top of cells, which are protected by a 15 kDa MWCO dialysis membrane. Cell ferritin formation, a surrogate marker of iron uptake, is measured after 24 hrs post cellular exposure.

1.6.2 Caco-2 cell line

The Caco-2 (Colon Adenocarcinoma) cell line is the most extensively used cellular model for investigating dietary iron absorption and bioavailability. Caco-2 cells were originally cultured from a cancer patient in the 1970's [219]. They form polarised monolayers [220] resulting in its spontaneous differentiation into a heterogeneous cell line [221, 222] and morphological features representative of the mature intestinal epithelium. These features include the formation of tight junctions, brush-border microvilli, enzymes, and differentiation markers [220, 222-224]. The rate of Caco-2 cell differentiation is highly dependent on culturing conditions, such as time and passage number [225], which is why strict adherence to passage number between experiments is usually advised.

1.6.2.1 Caco-2 cells and iron absorption

Many of the features of human iron absorption and bioavailability are similarly replicated in Caco-2 cells. For example, Caco-2 cells regulate iron absorption in response to cell iron stores. Researchers observed that Caco-2 cells doubled their rate of non-haem iron absorption when incubated in iron-deficient compared to iron-replete media [223, 226]. Moreover, Caco-2 cells preferentially absorb Fe^{2+} compared to Fe^{3+}. Cells incubated in Fe^{2+}-ascorbate increased iron uptake 100 to 200-fold compared to Fe^{3+}-NTA [226, 227]. Subsequent studies revealed that Caco-2 cells could also import Fe^{2+} iron, not Fe^{2+}. It was speculated that Fe^{3+} was reduced to Fe^{2+} by AA [124, 228] and/or a putative surface bound ferric reductase [228], offering a mechanistic hypothesis regarding the reduced rates of iron uptake observed for Fe^{3+} compared to Fe^{2+}.

The identification of the iron transporter DMT1 by Gunshin et al [18] and recently discovered insights on the mechanisms of iron absorption have validated the use of Caco-2 cells for iron bioavailability studies. Han et al [229] first reported the presence of DMT1 on the apical surface of Caco-2 cells. They found

that DMT1 mRNA expression increased with cell differentiation time and when grown in low-iron medium. In another study, DMT1 mRNA and protein expression increased as a function of differentiation time (7-21 days) in the subclone Caco-2 TC7 cell line [230]. Moreover, DMT1 protein expression is also regulated in response to cell iron concentrations. It was reduced in cells incubated in high-iron medium (100 - 200 μM Fe) for 24 – 72 hrs [230, 231]. Incubation of 100 μM FAC with cell surface biotinylated DMT1 cells resulted in DMT1 internalisation and lysosomal degradation without affecting total DMT1 protein levels [232].

Non-haem iron absorption in Caco-2 cells and pH are also inversely correlated. Tandy et al [233] and Bannon et al [234] demonstrated that rates of iron uptake of ferrous ascorbate were 1.5-fold and 3-fold higher at pH 5.5 compared to pH 6.5 and 7.5 respectively, consistent with the function of DMT1 as a proton coupled transporter functioning best at lower pH [18, 230]. Short hairpin RNA (shRNA) knockdown of DMT1 in Caco-2 cells decreased $^{55}FeCl_3$ (solubilised in 4-fold NTA and 10-fold AA) uptake by more than 50% [235], suggesting that similar to rat and human studies, DMT1 is the major transporter of non-haem iron absorption in the cell line.

Caco-2 cells also express other important iron transport proteins essential for iron absorption. Confocal imaging and GFP tagging of ferroportin in Caco-2 cells demonstrated that ferroportin is also expressed and is colocalised with hephaestin at the basolateral surface [236]. Furthermore, mRNA expression of ferroportin was also down regulated by 50% after 72 hrs in iron-replete (200 μM Fe^{3+}-NTA) compared to control (without iron) cells [231].

In comparison to *in vivo* [237, 238], hepcidin also inhibits iron absorption in Caco-2 cells but uses different mechanisms compared to current knowledge. Caco-2 cells incubated with hepcidin for 24 hrs had no effect on ferroportin protein expression [237, 239-241]. Interestingly, hepcidin decreased iron

absorption by inhibiting DMT1 mRNA [237] and protein [232, 240, 241] expression. Brasse-Lagnel et al [241] demonstrated that hepcidin mediates the ubiquitin-conjugated proteasome degradation of DMT1 in Caco-2 cells using the ubiquitin inhibitors MG132 and PYR41. Whether hepcidin also inhibits iron absorption through DMT1 *in vivo* remains to be answered. Regardless, the Caco-2 response reveals another inhibitory and regulatory mechanism of iron absorption by hepcidin.

While the IRP system has been shown to actively regulate the expression of iron proteins in Caco-2 cells, evidence also supports HIF2α is a transcriptional regulator. Investigators used luciferase reporter constructs tagged to the promoter of DMT1 to show that HIF2α directly activates DMT1 in the Caco-2/TC7 line [16]. Thus, similar to *in vivo*, HIF-2α appears to be a transcriptional regulator of iron absorption in Caco-2 cells. Overall, the Caco-2 cell line recapitulates all of the identified iron regulatory proteins and responds accordingly to external stimuli (iron status, pH, hepcidin, etc) in a similar fashion to *in vivo*.

1.6.2.2 Caco-2 cells and iron bioavailability

There are a large number of studies using the *in vitro* digestion / Caco-2 model to investigate iron bioavailability. A recent PubMed search (1.3.2017) with the keywords ‘iron bioavailability’ and ‘Caco-2’ revealed 175 journal citations. Three general themes emerge using these keywords; (a) the effect of dietary promoters and inhibitors on iron bioavailability (b) iron bioavailability of staple food crops, and (c) comparison of iron bioavailability between different iron species as either supplements or fortificants.

The response of Caco-2 cells to the effects of dietary promoters and inhibitors of iron bioavailability are similar to those published in human studies [242]. Animal proteins have an enhancing effect on non-haem iron bioavailability, but specific proteins such milk and eggs have not been demonstrated as

enhancers in iron bioavailability in human models [243, 244]. Similarly, Glahn et al [245] reported that beef, chicken, and fish all enhanced the iron bioavailability of $^{59}FeCl_3$ 4-5 fold relative to casein, which did not show any enhancing effects. The 'meat factor' enhancing effect in animal proteins may be related to its amino acid composition. Using Caco-2 cells, the amino acids cysteine and cysteine-glycine promoted non-haem iron solubility and increased non-haem iron uptake from $FeCl_3$ and Fe^{3+}-NTA [246]. In another study, low molecular weight meat fractions containing a large percentage of histidine content [247] also promoted non-haem iron bioavailability in Caco-2 cells.

Phytic acid and polyphenols are potent inhibitors of non-haem iron absorption in Caco-2 cells. The response in Caco-2 cells appears to be more sensitive to the inhibitory effects of tannic acid compared to phytic acid. In one study, the maximum inhibition of $FeCl_3$ absorption occurred at 1:1 Fe:TA molar ratios (up to 95% inhibited) compared to 1:10 Fe:PA (up to 70% inhibited) [248]; only with phytic acid was this inhibitory effect offset by 1:10 and 1:20 Fe:AA molar ratios [249]. In another study comparing the relative iron bioavailability among fruit juice beverages, red grape and prune juice, beverages with the highest polyphenol content among those tested, had the highest inhibitory effects whereas the other beverages (apple, orange, and pear) had no effect on iron bioavailability despite similar amounts of endogenous AA [250].

The specific polyphenol structures responsible for inhibiting iron bioavailability have also been investigated using Caco-2 cells. Certain classes of polyphenols found in black beans have shown to be either inhibitory (myricetin, quercetin) or enhancing (epichatechin, gallic acid) [251]. Within the seed coat of red beans, kaempferol also had a strong inhibitory effect on iron bioavailability [252]. Using Caco-2 cells in order to identify and screen for particular inhibitors of iron bioavailability within certain polyphenols classes has the potential to inform the future direction of plant iron biofortification.

The *in vitro* digestion / Caco-2 cell model is routinely used as a screening tool to determine which genotypes of staple crops have the highest iron bioavailability. This shows the power of the model, as similar studies *in vivo* would be expensive. The model can identify and predict the most promising genotypes suitable for eventual human trials. For example, 15 rice varieties grown at the International Rice Research Institute were tested for relative iron bioavailability compared to control rice varietal. The results showed that all rice varieties had similar iron bioavailability despite 2-fold differences in iron content [253]. In another example, 15 maize varieties were identified as having significantly higher iron bioavailability (up to 1.4-fold) compared to a commercially available control variety despite similar iron content [254]. In examining the iron bioavailability from beans, white beans were more bioavailable than red beans with similar iron content and the investigators concluded that red bean genotypes were in general poorly bioavailable; only two of the eight red bean genotypes examined had iron bioavailability above blank controls [255, 256]. Polyphenol concentration localised in the seed coat was considered the dietary factor most responsible for affecting iron bioavailability in all investigated staple crops (rice, maize, and beans).

While iron biofortification can result in increased iron concentration of staple crops, the *in vitro* digestion Caco-2 cell model is able to determine whether the increase in iron content also results in a concomitant increase in iron bioavailability. In one example, the model predicted that phytase-expressed maize was 3-fold more bioavailable than control maize [257]. In newly developed biofortified beans, the model predicted that iron biofortified beans (71 µg/g) were 4-fold more bioavailable than control beans (49 µg/g) [258]. The *in vitro* model's prediction was validated in *in vivo* models (chicken [258] and human [189, 190]).

The model also measures iron bioavailability from supplements and fortificants. In a study comparing the relative bioavailability from Fe^{2+}

supplements, ferrous sulphate, ferrous fumurate, and ferrous gluconate had similar iron bioavailability, which was 3-fold higher than a polysaccharide-iron complex [259]. NaFeEDTA, in the presence of non-haem inhibitors, is well absorbed in humans, which has led to the speculation whether its uptake is different than for other non-haem iron forms. Using the model, iron bioavailability of NaFeEDTA was similar to $FeSO_4$ and $FeCl_3$ and its absorption was inhibited by ferrozine, a Fe^{2+} chelator. It was concluded that NaFeEDTA was absorbed similarly to other soluble iron compounds, using Fe^{2+} mediated DMT1, in Caco-2 cells [260].

The method is not always predictive of human bioavailability. Specifically, several studies have suggested that certain iron compounds are not well predicted by *in vitro* digestion Caco-2 cell model. In one study, iron bioavailability of NaFeEDTA was significantly less than electrolytic iron [261], even though NaFeEDTA has consistently been shown to be well-absorbed and electrolytic iron poorly absorbed in humans. In screening to identify the most bioavailable iron fortificants, iron bioavailability from bread [262] and cereal [263] fortified foods were generally not informative. Iron bioavailability from these studies was not correlated to iron form, iron content, or phytic acid concentration. Lynch et al [264] concluded that the Caco-2 response to elemental iron powders is not an accurate predictor of human iron absorption. Currently, the only validated *in vitro* model for iron powders as a predictor of human iron absorption is iron dissolution at pH 1 [127, 194, 264], which correlates well with rat and human models [265]. It is important to note, however, that Caco-2 cells were able to accurately predict the increased iron bioavailability from small particle powders compared to larger powders [266, 267], thus may be able to distinguish iron bioavailability from nano-sized compounds.

1.6.2.3 Usefulness of Caco-2 cells and iron bioavailability

Researchers have examined whether the *in vitro* digestion Caco-2 cell model is an accurate predictor of iron bioavailability in humans. Caco-2 cells were exposed to matching meal compositions as previous human trials and its iron bioavailability was compared with prior absorption data. Au et al [268] measured the ferritin response of Caco-2 cells to the effects of dietary enhancers and inhibitors on semi-purified meals [269]. Phytates, bran, and tea responded similarly in the Caco-2 model as previous published human absorption data; iron absorption ratios in Caco-2 cells correlated well with human iron absorption ratios ($r=0.97$, $p < 0.0001$). In a similar study, Caco-2 absorption ratios generated from a dose-response of AA and TA added to meals also correlated well ($r=0.986$ and 0.927) with human iron absorption. Both studies validate the use of Caco-2 cells to predict human iron absorption [242].

In other studies, the response of Caco-2 cells to accurately predict iron bioavailability of staple food crops in comparison to human absorption data has also been examined. The absorption ratio generated from maize in Caco-2 cells was similar to the results of women volunteers consuming the same diets. The ability of Caco-2 cells to accurately predict human bioavailability may be crop or genotype dependent. Caco-2 cells predicted the iron bioavailability from Great Northern (white) beans, but overestimated human absorption data from pinto (red) beans [270].

Certainly more studies are required to characterise the response of Caco-2 cells to different forms of iron and iron-containing foods and examine if the estimated iron bioavailability is an accurate predictor of human iron absorption. The precision of the model could be optimised in several ways. Standardised digestion protocols between labs, such as the protocol proposed by the COST framework [271], and standardised culturing conditions would help to alleviate

some of the inconsistencies in Caco-2 cell data found among labs. Moreover, since the intestinal epithelium is representative of many cell types, co-cultures of Caco-2 cells (which includes mucin-secreting cells) may be better predictors of iron bioavailability [272]. Further research is required to develop a reproducible and robust co-culture model. Furthermore, comparisons with *in vivo* data could be strengthened with careful recapitulation of the diets used in prior *in vivo* trials. Overall, the *in vitro* digestion Caco-2 cell model is predictive but tends to overestimate iron bioavailability relative to human trials [273]. It is accepted that Caco-2 cells are able to predict the direction [109] but not necessarily the magnitude of iron bioavailability. As such, the data provided by Caco-2 cells provides data generating hypothesis, which requires follow-up in human trials. More importantly, they can be used for mechanistic research (at the cellular and molecular level), which is not possible *in vivo*. Caco-2 cells provide an invaluable resource for improving our understanding of human iron absorption and iron bioavailability.

1.7 Nanoparticles

1.7.1 Nanoparticles and cellular routes of gastrointestinal uptake

Nanoparticles (NP) are broadly classified as particles between 1 to 100 nm in size with altered and unique physio-chemical properties that differ from their larger or bulk constituents [274]. Iron NP's have been synthesised physically [275, 276], chemically [277, 278], or are naturally occurring in nature [58]. For an in-depth review, see Hilty and Zimmerman [279]. The unique property of iron NP's is that they may be absorbed more efficiently than their larger counterparts because the uptake of particles, in general, has been shown to be inversely proportional to particle size [280]. The important characteristics of nanoparticles are their synthesis / characterisation and behavior in biological systems; usually the former informs the latter. Particle behavior of ingested nanoparticles in

physiological fluids and alterations in the gastrointestinal tract are important features of the nanoparticle–intestinal dynamic, and likely determine whether particles can be internalised in tissues. Four possible mechanisms of absorption have been proposed for nanoparticles in the gastrointestinal tract [281]:

a. Transcytosis in the M-cell layer of Peyer's Patches within the gut associated lymphoid tissue (GALT)

b. Enterocyte absorption through endocytosis

c. Enterocyte absorption through persorption

d. Paracellular uptake

Transcytosis uptake of nanoparticles in the lymphatic system is the most widely understood route. Nanoparticles have been found to be highly concentrated in Peyer's Patches [282] and interestingly in one study, have been shown to disrupt iron bioavailability [283]. The evidence for enterocytic translocation of nanoparticles in the GALT emerges from previous work using Caco-2 cells differentiated to an M cell-like phenotype (co-culture with Raji B-lymphocyte cells). Des Rieux et al [284] observed increased rates of translocation from latex nanoparticles 200 nm and 500 nm in size. In comparison, Caco-2 monocultures were not able to translocate these same particles. In a separate study, they also found that Caco-2 co-cultures increased the transport of 50 nm polystyrene particles by 1.25-fold and increased the transport of 200 nm particles by 8-fold compared to monocultures [283].

1.7.2 Evidence of iron nanoparticles and absorption / bioavailability

Non-haem iron absorption has predominately focused on Fe^{2+} uptake using the DMT1 transporter, the only identified intestinal iron importer to date. As previously discussed, a Fe^{3+} uptake mechanism has been proposed by Conrad

and Umbreit [35-37] but has yet to be confirmed and fully characterised. For iron nanoparticles, an endocytosis uptake pathway distinct from DMT1 may exist. Several studies have showed evidence of the process in Caco-2 cells.

Iron oxide NP's solubilised in negatively-charged carbohydrate shells (gluconic acid, sucrose, polyacrylic acid) [285], iron oxide NP's coupled to hemin [277] or iron hydroxide adipate tartrate (IHAT) NP's [286] are all examples of chemically synthesised iron nanoparticles that have been shown to be transported and visually detected in the cytosol of Caco-2 cell monolayers using TEM. In the case of IHAT, researchers exploring it's uptake in Caco-2 cells more in-depth showed that its absorption followed an endocytosis-like pathway [286]. The possibility that iron from IHAT can be transported *in vivo* using endocytosis still remains to be demonstrated but in iron deficient women, IHAT showed good iron bioavailability (80%) compared to $FeSO_4$ [287]. Currently, iron supplementation trials in the MRC Gambia using IHAT are being conducted (personal correspondence with Dr. Pereira)

Novel iron phosphate and iron oxide nanoparticles for use as iron fortificants have recently been developed using flame spray pyrolysis (FSP) [275, 276]. For these particles, there has not been evidence to suggest that they are translocated in the intestine in rat studies. In fact, the evidence from *in vitro* solubility tests suggests that these nanoparticles are absorbed more efficiently as a result of its improved solubility at gastric pH. The exact mechanism of absorption has not been fully characterised, but its enhanced solubility compared to larger precursors suggests that the mechanism of iron uptake is mediated by DMT1. Irrespective of the mechanism uptake, these nanoparticles have similar relative bioavailability (RBV) as $FeSO_4$ in rats without any indication of mucosal toxicity [288, 289].

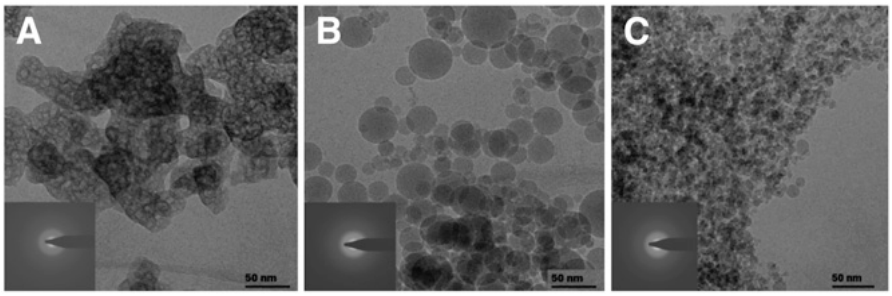

TEM and SAED images. (a) $FePO_4$ large particle, (b) $FePO_4$ medium particle, and (c) $FePO_4$ small particle.

The SAED insets reflect non-crystalline amorphous structures. Image obtained from Rohner et al [288] with permission from the American Society for Nutrition.

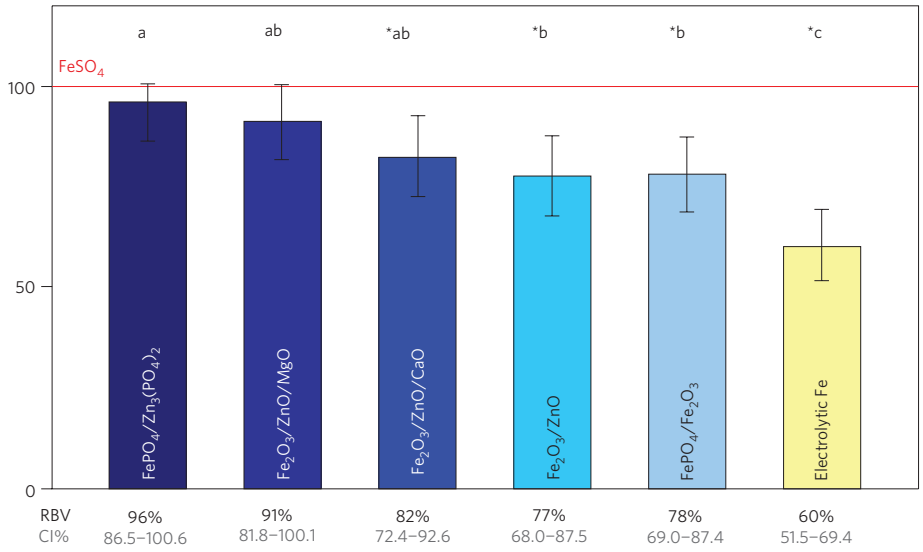

Figure 1.10 Relative biological value (RBV) of different iron nanoparticles compared to $FeSO_4$.

Bar graph obtained from Hilty et al [289] with permission from the Nature Publishing Group.

1.8 Ferritin

1.8.1 Ferritin structure and content

Ferritin is ubiquitously conserved in animals, plants, and bacteria. Serving as an iron storage protein, it consists of 24 protein subunits arranged into a spherical shell surrounding a ferrihydrite (ferric oxyhydroxide, $(Fe^{3+})_2O_3$)-like mineral core [58, 290, 291]. As stated earlier, ferritin synthesis is regulated by labile iron concentrations in the cytosol. Specifically, ferritin is expressed in response to high levels of cellular iron to balance cellular iron requirements and sequester labile free iron; this prevents the formation of reactive oxygen species (ROS) [292] and cellular iron toxicity.

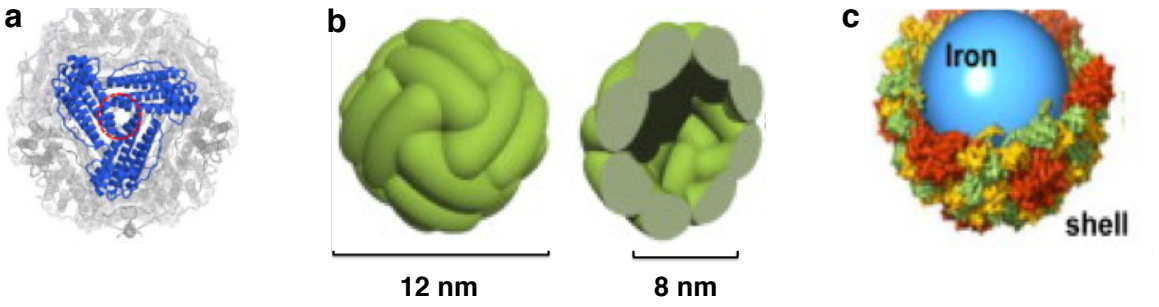

Figure 1.11 Graphical representation of the ferritin structure.

(a) X-ray crystallography of soybean ferritin viewed axially (top down) (b) Outer and inner diameter of the ferritin shell. (c) Iron core (blue) housed within ferritin shell. Images were obtained from Yang et al [293] with permission from Elsevier.

1.8.2 Plant ferritins

Plant ferritin (phytoferritin) is localised within the plastids of leaves and the amyloplasts of tubers and seeds [294]. The legume family, such as beans, peas, and lentils are considered rich sources of phytoferritin. Concentrations and iron-sequestration into phytoferritin differs widely among several legumes [295]. Ambe

et al [296] estimated that 90% of the iron in soybeans is mineralised within ferritin iron core using Mossbaüer spectroscopy. Similarly, semi-quantitative Western blotting of phytoferritin from peas suggests that 92% of its iron is mineralised within its core [297]. These results differ greatly from more recent studies. Newer estimates quantifying the amount of iron-sequestered ferritin in plants, using isotope dilution mass spectrometry (ID-MS) and a recombinant ferritin spike, showed that only 10-40% of iron in various legumes was found stored within ferritin [298, 299]. The highest percentage of iron-sequestered ferritin (40%) was found in dried peas. The disparity in estimates of iron-sequestered ferritin among studies is most likely related to differences in analytical technique.

1.8.3 Iron bioavailability of ferritin

Phytoferritin is currently being investigated for its possible use as a source of bioavailable iron [300, 301]. Theoretically, ferritin can sequester up to 4500 iron atoms in its iron core [60] but generally plants contain between 2000-2500. Insights into the bioavailability of phytoferritin are particularly relevant given that it is concentrated source of iron and naturally-derived. With ongoing efforts to promote plant-based diets, phytoferritin could be promoted as a well-accepted form of iron to consumers. Developments in biofortification, such as breeding for high ferritin crops [302, 303], have recently have come into view. Given all these information, the bioavailability and mechanisms of absorption from ferritin-iron still remains controversial.

Several recent human trials have suggested that ferritin is a highly bioavailable source of iron. Soybeans labeled with ^{59}Fe, consumed as either muffins or soup [296], were well-absorbed (27%) and comparable to $FeSO_4$ in marginally anaemic women as measured by whole body counting techniques after 14 days [304]. Given the estimation that the majority of iron in soybeans is sequestered in ferritin [296], these researchers concluded that phytoferritin was

bioavailable. In a subsequent trial to show that ferritin was indeed bioavailable, purified (animal) ferritin fed to non-anemic women was similarly bioavailable and as well absorbed (21.9%, 21.4%) as $FeSO_4$ [169], showing that ferritin was bioavailable regardless of animal or plant origin. The same researchers showed that reconstituted soybean ferritin fed to non-anaemic women also had similar iron bioavailability as measured by RBC incorporation (29.9%, 34.3%) or whole body counting techniques (33.0%, 35.3%) as $FeSO_4$ [305].

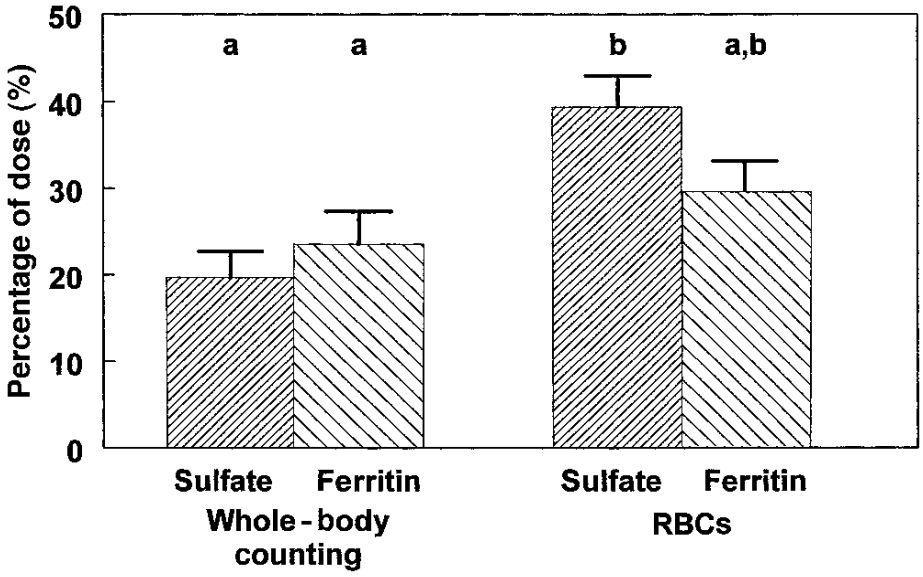

Figure 1.12 Comparison of iron absorption from soybean ferritin and $FeSO_4$ in iron-deficient women.

Soybean ferritin has similar iron bioavailability as $FeSO_4$ as measured by whole-body counting techniques and incorporation into red blood cells. Bar graph obtained from Davila-Hicks et al [169] with permission from the American Society for Nutrition.

Human trials investigating ferritin-iron bioavailability from this group is contradictory to the results of many earlier studies. These earlier studies, in fact, have shown that ferritin has low bioavailability. In one study, Fe-ascorbate was 4-fold more bioavailable than ferritin (rabbit) [44.2 vs. 11.5 %] when a 2.5 mg ^{59}Fe

dose was fed to iron-deficient subjects [306]. In a follow-up study, 10-fold differences in iron bioavailability were found (21.1 vs. 1.9%) between Fe-ascorbate and ferritin, which has been attributed to differences in the food vehicles from the previous study [307]. Similarly, 3 mg of ferritin given to healthy or iron-deficient individuals resulted in low iron bioavailability (0.9-1.1%) [308]. In another study, iron bioavailability from ferritin was 3.8% compared with 24.1% from $FeSO_4$ [309] in healthy volunteers.

The contrasting results for ferritin iron bioavailability have been attributed to the differences in iron labeling techniques [294, 305] and the source of ferritin i.e. animal or plant. In earlier studies, iron labeled ferritin was generated using Fe radioisotope injections into animals. This procedure has been criticized as not appropriately labeling the iron core in ferritin, and causing inflammatory/stress responses that result in changes to the ferritin protein structure. In newer studies, iron purified from ferritin was removed using thioglycolic acid and a radioisotope iron tracer was reincorporated to label the iron core. According to these researchers, this method of radio labeled Fe-ferritin is indistinguishable from non-labeled ferritin [169].

1.8.4 Non-haem uptake of iron absorption from ferritin

The mechanism of iron absorption from ferritin is also controversial. The traditional viewpoint is that ferritin is digested and that iron joins the non-haem iron pool; thus this viewpoint assumes that ferritin-Fe is absorbed using similar mechanisms of non-haem iron absorption. In support of this viewpoint, iron bioavailability in subjects consuming vegetables with purified phytoferritin was reduced by one-third [310], suggesting that the presence of non-haem iron inhibitors in vegetables inhibit the iron from ferritin. In another study, iron absorption increased from 0.7 to 12.1% when 100 mg AA was added to 3 mg ferritin in human volunteers [308]. Both studies strongly indicate ferritin is

degraded, the iron released, and likely to join the non-haem iron pool prior to absorption.

In vitro studies are in agreement with this hypothesis. *In vitro* gastric conditions at pH 2 resulted in the rapid and complete degradation of the ferritin protein over 1 hr as measured by SDS-PAGE, Western blot [311-313] and gel filtration [298]. The rate of degradation occurred as fast as 15 min at pH 2 solution [298].

In Caco-2 cells, iron bioavailability of digested ferritin was enhanced by AA 3-10-fold compared to controls [311, 312] and inhibited by PA, TA and calcium, suggesting that the ferritin protein shell and its protection from non-haem dietary inhibitors is lost [311, 312]. The effect of enhancing and inhibiting dietary factors on *in vitro* digested ferritin indicates that its iron is likely mediated by DMT1. From a practical perspective, ferritin has also been shown to be temperature-sensitive. Ferritin is degraded in foods using normal cooking methods [298, 314].

Given these data, it still remains unclear and difficult to prove whether ferritin can survive gastric digestion. One hypothesis is that the ferritin protein coat remains stable and is resistant to digestive enzymes and pH changes [60]. In previous studies, ferritin protein degradation was more influenced by pH than time. This was most evident at pH 4, which reflects the stomach pH of infants [298, 313]. Intact ferritin was detectable at pH 4 after 1 hr digestion (50-80%) [311, 313, 315] and was found to be stable at pH 3.5 to 7 after 2 hrs [298]. This would indicate the possibility that ferritin can survive gastric conditions depending on infant pH, the consumption of a mixed-meal (where ferritin can be protected by the bolus), or differing rates of gastric emptying.

1.8.5 Endocytosis uptake of ferritin-iron

The main reason why ferritin resistance to degradation is important is because an independent route of iron absorption for ferritin has been hypothesised. Three possible states of ferritin are thought to exist in the intestinal lumen prior to absorption [294]:

a. Intact ferritin resistant to low pH and proteolytic digestive enzymes.

b. Ferrihydrite iron-core released after ferritin dissociation.

c. Ferrihydrite iron-core hydrolysed to Fe^{3+} and Fe^{2+}.

Depending on the final ferritin state after digestion, iron absorption pathways likely differ.

Several studies have strongly suggested that the absorption of intact ferritin is not influenced by dietary inhibitors of non-haem iron [60, 313]. This provides a basis for which a route of ferritin absorption distinct from non-haem iron may exist and also helps to explain its high bioavailability relative to $FeSO_4$ in human trials. The intestinal uptake of ferritin is thought to occur using an endocytosis-like mechanism. Soybean ferritin incubated with Caco-2 cells (1 μM ^{59}Fe as the mineralised core) showed saturable kinetics and temperature-dependency [316], properties which are indicative of receptor-mediated uptake. In this same study, Mas-7, a stimulator of endocytosis, increased iron uptake whereas hypertonic sucrose, an inhibitor of endocytosis, decreased iron uptake. An endocytosis pathway for soybean ferritin was further validated in Caco-2 cells by San Martin et al [317]. They demonstrated that soybean ferritin was internalised in Caco-2 cells as evidenced by confocal microscopy, and its uptake was inhibited with hypertonic sucrose and cytosol acidification, two chemical methods that inhibit endocytosis. Further characterisation of an endocytosis pathway using shRNA gene knockdown suggested that adaptor protein 2 (AP2),

which mediates the formation of clathrin-coated vesicles [318], is involved in the uptake of soybean ferritin. In a later study, ferritin endocytosis in Caco-2 cells was confirmed using confocal microscopy. The internalisation and colocalisation of horse spleen ferritin was tracked with the endocytosis antigen markers: clathrin, early endosome antigen 1 (EEA1) and lysosome marker lysosomal-associated membrane protein 2 (LAMP2) [319]. This study also provided evidence that exogenous, internalised ferritin likely uses the same pathway for lysosomal degradation as endogenous ferritin [63, 64, 320].

Competitive studies in human volunteers demonstrated that a 9-fold excess of $FeSO_4$ or haem did not inhibit the absorption of iron from ferritin, providing indirect *in vivo* evidence of a separate iron uptake pathway for ferritin [321]. These findings warrant further investigation on ferritin bioavailability and the importance of DMT1 on its absorption.

1.9 Aims

The purpose of this thesis is to investigate the potential of NP-$FePO_4$, pea ferritin, and the Lucky Iron Fish™ to deliver bioavailable forms of iron and the optimal conditions for this to occur. The three main themes of this thesis will be (1) the extent of *in vitro* digestion on the state of iron, (2) iron bioavailability, and its modulation with non-haem iron promoters and inhibitors, as assessed in Caco-2 cells, and (3) mechanisms of iron absorption [specifically the physiological importance of the iron transporter, DMT1] in Caco-2 cells. This information will hopefully be informative for the future direction of these novel iron forms.

Chapter 2: Methods

2. Methods

2.1 General methods

2.1.1 Colorimetric iron assays

(a) Ferene-S

Ferene-S [3-(2-Pyridyl)-5,6-bis(5-sulfo-2-furyl)-1,2,4-triazine disodium salt hydrate] was used to determine the total iron content of samples. Ferene-S binds ferrous iron, forming a deep blue complex, which can be measured using spectrometry. Samples (100 µL) were digested in 100 µL 1% HCl for 10 min (*300 rpm*, 80°C). Once cooled, the following reagents were added sequentially and mixed after each addition: 500 µL 7.5% ammonium acetate, 100 µL AA, 100 µL 2.5% sodium dodecylsulphate (SDS), and 100 µL 1.5% ferene. Samples were centrifuged for 5 min (*12,000 rpm*). The absorbance of samples was measured at 593 nm against an iron standard curve (0-20 nmol Fe as ammonium iron (II) sulfate).

(b) Bathophenanthroline

Bathophenanthroline (4,7-diphenyl-1,10-phenanthroline), BPDS, was also used to determine the total iron content of samples. BPDS binds to ferrous iron, forming a red complex, which can be measured using spectrometry. Iron samples (380 µL) were digested in 20 µL hydroxylamine hydrochloride (HH) solution (0.1 g/mL dissolved in 10 M HCl). 100 µL aliquots of the digested sample were pipetted into 96-well microplates. 50 µL BPDS solution (15.64 mg bathophenanthroline disulfonic acid disodium salt in 50 mL 2 M sodium acetate) was added and the plate was incubated on a microplate shaker for 10 min (*500 rpm*). The absorbance of samples was measured at 535 nm using an iron standard curve (0-1.6 µg Fe as pure ferrous iron [High-Purity Standards, USA]).

Iron chelator	MW (kDa)	Product
Ferene-S	494.37	Sigma (P4272)
BPDS	536.49	Sigma (B1375)

Table 2.1 Iron chelators used for iron quantification

2.1.2 Simulated digestion

The simulated gastrointestinal digestion followed the methods of Glahn et al [218] with modifications. The method has been widely used to determine the bioavailability of iron samples. For each digestion, digestion enzymes were removed of contaminant iron using Chelex-100 (Bio-Rad, USA)*. All solutions were made fresh on the day of the experiment. Ferric ammonium citrate (FAC) diluted in H_2O was included in each experiment as a positive control. FAC is a well-absorbed form of iron in Caco-2 cells and used as the reference for DMT1 uptake [139, 322, 323]. Reference blanks (cells not treated with iron) were included in each experiment to ensure low baseline levels of cell ferritin. Using 50 mL-sized polypropylene tubes, 10 mL 140 mM NaCl, 5 mM KCl (pH 2) solution was added to samples (collectively referred to as 'digests') to initiate the gastric digestion phase. Digests were vortexed, readjusted to pH 2 with 0.1 M HCl, and 0.5 mL pepsin solution was added. The digests were placed onto a rotating table (100 rpm) and incubated for 1 hr at 37°C. After 1 hr, the digests were readjusted to pH 5.5-6.0 with 1 M $NaHCO_3$ and 2.5 mL pancreatin-bile solution was added to the digests.

Reagent	Concentration	Product
Pepsin	20 mg/mL	Sigma (P-7000)
Pancreatin	1.4 mg/mL	Sigma (P-1750)
Bile	8.6 mg/mL	Sigma (B-8631)

Table 2.2 Enzymes used for *in vitro* digestion

The pH of the digests were further readjusted to 6.9-7.0 with 1 M $NaHCO_3$, placed onto a rotating table (100 rpm), and incubated for 30 min at 37°C (intestinal digestion phase). The digests were readjusted to normalise for equal volumes (15 mL) with 140 mM NaCl, 5 mM KCl pH 7.0 solution. 1.5 mL of the digest was applied to each well, affixed with a 15 kDa molecular weight cut off (MWCO) dialysis membrane** (Spectrum Labs, USA) fitted to a Transwell upper chamber. The digests were incubated for 2 hrs at 37°C, carefully removed from the plates, and 1 mL additional MEM was added to each well. The plates were incubated for a further 22 hrs to allow for cell ferritin formation.

- Pepsin solution: 0.8 g pepsin was diluted in 20 mL 0.1 M HCl. 10 g of Chelex-100 was added and mixed for 30 min. The mixture was placed in a flex column (VWR, UK) and an additional 20 mL 0.1 M HCl was added.
- Pancreatin-bile solution: .25 g pancreatin and 1.5 g bile extract were diluted in 125 mL 0.1 M $NaHCO_3$. 62.5 g of Chelex-100 was added and mixed for 30 min. The mixture was placed in a flex column and an additional 50 mL 0.1 M $NaHCO_3$ was added. The filtered enzymes were stored at RT prior to use.

** Dialysis membranes were prepared the day before iron treatments. The membranes (tubular) were cut into approximately 5 cm in size and rinsed 3x with milli-Q H_2O. The membranes were fastened onto modified Transwells using silicone O-rings, and stored in milli-Q H_2O overnight (4°C). On the day of experiment, the milli-Q H_2O was replaced with 0.5 M HCl for 30 min. The membranes were removed of 0.5 M HCl and washed 3x with sterilized milli-Q H_2O prior to fitting on top of the cells.

The simulated digestion was primarily used for experiments carried out using LIF. In experiments for NP-$FePO_4$ and phytoferritin, simulated *in vitro*

digestions were carried out without digestion enzymes or dialysis membranes. The methodology (incubation solutions, times, pH changes, etc) of these "mock" *in vitro* digestions, collectively referred to in this thesis as pH treatments, were the same as stated above aside from these omissions.

2.1.3 Cell culture

Caco-2 cells (HTB-37® VA) were obtained from American Type Culture Collection at passage 20 and stored in liquid nitrogen or -80°C. Cells were grown in Dulbecco's Modified Eagle Medium (DMEM) containing 25 mM HEPES (Gibco, UK) supplemented with 10% foetal bovine serum, 1% MEM non-essential amino acid solution (Sigma, UK), 1% penicillin/streptomycin, and 1% L-glutamine. Cells were grown in 75 cm^2 cell culture flasks (Greiner, UK) and maintained at 5% carbon dioxide/95% air atmosphere at constant humidity. The media was replaced every 2-3 days. Hutu-80 cells (HTB-40 ® VA), obtained at passage 41, were kindly donated by Dora Pereira, PhD (Medical Research Council, Human Nutrition Research, Cambridge UK). These cells were cultured using the same growth media, and under the same conditions, as stated for Caco-2 cells.

(a) Subculturing

Both cell lines were cultured until 70-80% subconfluent (approx. 3-4 days). T-75 flasks were washed 1x with PBS and 1 mL trypsin-EDTA 10x (Sigma, UK) was added. Cells were placed in the incubator for 3-5 min until detached from the plastic substrate. Detached cells were diluted in DMEM and counted using the trypan blue exclusion method [324]. Cells were seeded at a density of $3x10^4$ cells/cm^2 in new 75cm^2 cell culture flasks.

Prior to seeding for cell culture experiments, cell culture plates (Greiner, UK) were coated with type 1 collagen [rat tail] (Gibco, UK). 50 µg/mL collagen solution diluted in 20 mM acetic acid was placed in each well and incubated for 1

hr. Plates were washed 3x with PBS and cells were immediately seeded onto the substrate or plates were stored at 4°C for up to 1 week. Plates using Hutu-80 cells were left uncoated.

Plate format	Cell density	Media volume (mL)
6 well	475,000	2
12 well	200,000*	1
24 well	100,000	0.5
96 well	25,000	0.1

*Hutu-80 cells were seeded at 100,000 cells/well

Table 2.3 Cell seeding densities

Caco-2 cells were grown for 12 days post-seeding for monolayer formation and used at passages 25-40. Hutu-80 cells were grown at 70% subconfluent (approx. 2-3 days) and used at passages 45-50.

(b) Serum starvation of cells

24 hrs prior to iron treatments, cells were removed of DMEM, washed 1x in PBS, and replaced with serum-free MEM (Gibco, UK) supplemented with 19.4 mM D-glucose, 26.2 mM $NaHCO_3$, 10 mM PIPES (piperazine-*N*,*N*-bis-[2-ethanesulfonic acid]), 1% antibiotic-antimycotic solution, 4 mg/L hydrocortisone, 5 mg/L insulin, 0.02 µM Na_2SeO_3, 0.05 µM triiodothyronine and 0.2 mg epidermal growth factor.

Reagent	Product
MEM powder	Gibco (41500-067)
D-gluose	Sigma (G-7528)
PIPES	Sigma P-3768
$NaHCO_3$	Sigma (S-6014)
Hydrocortisone	Sigma (H-00395)
Antimicrobial / Antibiotic	Gibco (15240-062)
Insulin	Sigma (I-1882)
Na_2SeO_3	Sigma (S-5261)
Tri-iodothyronine	Sigma (T-6397)
Epidermal growth factor	Sigma (E-4127)

Table 2.4 MEM formulation

2.1.4 Protein isolation

After iron treatments, CelLytic® M protein extraction buffer (Sigma, UK) containing cOmplete mini protease inhibitor cocktail (Roche, UK) was added (200 µL per 6 well plate). Plates were placed onto a rocking chamber (20 rpm/min) for 15 min (4°C). Monolayers were scraped from the plastic substrate using inverted 200 µL pipette tips. Cell lysates were collected into 1 mL microcentrifuge tubes, stored at -20 ^{o}C, thawed on ice, and centrifuged for 15 min (*14,000 x g*, 4°C). Supernatants were collected and analysed.

2.1.5 BCA protein

Cellular supernatants were quantified for total protein using the bicinchoninic (BCA) protein assay kit (Pierce, UK) following manufacturer's instructions. 10 µL samples were pipetted into a 96-well microplate followed by 200 µL BCA working solution. The plate was mixed for 1 min (*250 rpm*) and incubated for 30 min (37°C). The absorbance was measured at 562 nm against the bovine serum albumin protein standard (0-2000 µg/mL).

2.1.6 Ferritin ELISA

Cellular supernatants were quantified for cell ferritin using the Spectoferritin ELISA kit (Ramco, USA) following manufacturer's instructions. 10 µL of samples were pipetted into a 96-well microplate pre-coated with rabbit anti-human spleen ferritin. 200 µL conjugated anti-human ferritin was added to each well and incubated on a microplate shaker for 2 hrs (*250 rpm*). After 2 hrs, the plate was washed 3x with milliQ H_2O. 100 µL substrate solution was added to each well, and the plate was incubated for 30 min. 100 µL potassium ferricyanide was placed in each well, and the plate was mixed for 1 min (*250 rpm*). The absorbance was measured at 490 nm (using a subtraction correction of 630 nm) against pre-calibrated human ferritin standards (6-2000 ng/mL).

2.1.7 Chemical targeting iron uptake

For digestion experiments, AA (1:20 Fe:AA molar ratio, 600 µM), an enhancer of non-haem iron bioavailability, was added at the beginning of the gastric phase. 2.5 mM $CaCl_2$ (final concentration in MEM after dilution with digests) was used as an inhibitor of non-haem iron bioavailability. Stock solutions for AA and $CaCl_2$ were made fresh the day of. Stock solutions of AA were diluted in milliQ H_2O and $CaCl_2$ in 0.1 M HCl. When AA and $CaCl_2$ were used, treatments were incubated with cells for 24 hrs.

Inhibitor	Stock solution	Working solution	Product
Chlorpromazine hydrochloride	0.5 M in DMSO	100 µM	Sigma (C8138)
Sucrose	10 M in H_2O (fresh)	0.45 M	Fisher Scientific (S5)
Filipin III	500 mg/L in DMSO	5 mg/L	Sigma (F4767)
5-(*N*,*N*-Dimethyl) amiloride hydrochloride	0.5 M in DMSO	200 µM	Sigma (A4562)
Calcium chloride dihydrate	1 M in HCl (fresh)	2.5 mM	Fisher Scientific (C79)

Table 2.5 Endocytosis inhibitors used in Caco-2 cells

Uptake

Stock solutions were diluted in MEM (containing iron treatments) to working solutions and incubated on Caco-2 cells for 1 hr. After 1 hr, endocytosis – iron treatments were removed and cells were washed 3x with PBS. Cells were incubated in MEM for a further 23 hrs.

pH treated

The methods were similar to uptake experiments, except that stock solutions were diluted in MEM to 2x working solutions. pH treated iron compounds were diluted 1:1 in MEM to achieve 1x working solutions of endocytosis inhibitors.

2.1.8 Short interfering RNA (siRNA) transient knockdown

Caco-2

Cells were seeded in collagen coated 12-well plates (200,000 cells/well) for 10 days. Cell monolayers were transfected according to the manufacturer's protocol for 24 hrs. On the day of transfection, cells were washed 1x with PBS. 1 mL Opti-MEM™ (Gibco) was added to each well and plates were placed into the incubator. Silencer® Select siRNA targeting *SLC11A2* or Negative control no. 1 was diluted in Opti-MEM. Separately, Lipofectamine® 3000 transfection reagent (Invitrogen) was diluted in Opti-MEM. The siRNA dilution was added to the transfection reagent dilution and the siRNA/transfection mixture was incubated for 10 min to allow for complex formation. 100 µL siRNA/transfection mix was added drop wise to each well and the plates were incubated for 24 hrs. Each well contained a final concentration of 200 nM siRNA and 6 µL transfection reagent. After 24 hrs, cells were washed 1x PBS, and incubated for 24 hrs in MEM (and iron treatments for 2 hrs). Cells were analysed for gene knockdown efficiency by RTPCR 48 hrs post-transfection.

Hutu-80

Cells were seeded in 12-well plates (100,000 cells/well) for 24-48 hrs. Cells (50-70% confluent) were transfected similarly to Caco-2 cells, except that each well contained a final concentration of 10 nM siRNA and 3 µL transfection reagent.

Silencer® Select siRNA			
		SLC11A2	**Negative control #1**
	Catalogue	4390825	4390844
	ID	s9708	-
Sequence	Sense	GGAUUUAAGUUGCUCUGGAtt	-
5' → 3'	Antisense	UCCAGAGCAACUUAAAUCCag	-

Table 2.6 siRNA sequences

2.1.9 RTPCR

(a) RNA extraction

RNA was extracted from cells using the RNeasy Mini Kit (Qiagen) according to manufacturer's suggestions. Cells were washed 1x with PBS and lysed in 350 µL Buffer RLT per well. 350 µL 70% EtOH was added and lysates were transferred to silica spin columns fitted onto collection tubes for sequential centrifugation steps. The columns were centrifuged for 15 sec (*10,000 x g*). The flow through was discarded and 700 µL Buffer RW1 was added. The columns were centrifuged for 15 sec (*10,000 x g*). The flow through was discarded, 500 µL Buffer RPE was added, and centrifuged for 15 sec (*10,000 x g*). The flow through was discarded, 500 µL Buffer RPE was added, and centrifuged for 2 min (*10,000 x g*). The spin columns were placed into new collection tubes and centrifuged for 15 sec (*16,000 x g*) to remove traces of remaining EtOH. Spin columns were placed into new 1.5 mL collection tubes and 30 µL RNase free H_2O was added. Spin columns were centrifuged for 1 min (*10,000 x g*) to elute the RNA. The

process was repeated with a further 30 µL RNase free H_2O and the RNA was stored at -80°C. RNA concentrations were determined using the UV-Vis NanoDrop 2000 spectrophotometer. 1 µL samples were analysed for RNA using H_2O as the reference blank. RNA quality was determined using the $A_{260/280}$ ratio for protein contamination and $A_{230/260}$ ratio for solvent (EtOH) contamination.

(b) cDNA synthesis

Complementary DNA (cDNA) was synthesized using the qPCRBIO cDNA Synthesis Kit (PCR Biosystems, UK). A master mix was generated containing 2 µL 5x cDNA synthesis mix, 0.5 µL 20x Rtase, and 6.5 µL PCR grade water per reaction. 1 µL RNA was added into each PCR microtube (Bio-Rad) and 9 µL master mix added for a total well volume of 10 µL. Samples were vortexed, briefly centrifuged, and placed into a PCR Thermocycler (BioRad T100) using the following settings:

cDNA settings		
Application	Temperature	Time
Incubation	42°C	30 min
Denaturation	85°C	10 min
Cooling	4°C	-

Table 2.7 Settings used for cDNA synthesis using the Bio-Rad thermocycler.

The newly reverse transcribed cDNA was diluted 1:5 in nuclease-free H_2O.

(c) Instrumentation

A master mix was generated using 4 µL 2x SYBR Green Mix Lo-ROX (PCR Biosystems), 1 µL (forward and reverse primers), and 1 µL nuclease-free

H_2O. 4 µL cDNA was added to each well of a polymerase chain reaction (PCR) microplate (Roche), followed by 6 µL master mix.

KiCqStart® SYBR® Green Predesigned Primers		
Gene	Forward (5' → 3')	Reverse (5' → 3')
SLC11A2	GAGTATGTTACAGTGAAACCC	GACTTGACTAAGGCAGAATG
18S	ATCGGGGATTGCAATTATTC	CTCACTAAACCATCCAATCG

Table 2.8 DNA primers used for RTPCR.

Samples were briefly vortexed, centrifuged and placed into the RTPCR instrument (Roche LightCycler 480). The settings for each real time PCR reaction were as follows:

RTPCR Settings		
Application	Cycles	Temperature
Pre-incubation	1	95°C
Amplification	45	95°C (denature), 58°C (annealing), 72°C (extension)
Melt curve	1	95°C, 65°C, 97°C
Cooling	1	40°C

Table 2.9 RTPCR settings

DMT1 was normalised to the housekeeping gene, 18S. Relative gene expression was assessed using the ΔΔCt method [325].

2.1.10 Cell proliferation assay

Cell proliferation in Caco-2 cells was measured using the CellTiter 96® Aqueous One Solution Cell Proliferation Assay (MTS) (Promega). Cells metabolize MTS (3-(4,5-dimethylthiazol-2-yl)-5-(3-carboxymethoxyphenyl)-2-(4-sulfophenyl)-2H-tetrazolium) in the presence of the electron-coupling reagent, phenazine ethosulfate (PES), to a formazan product using NADP or NADPH. The blue formazan product is detected using an absorbance maximum at

490 nm. The assay was conducted according to manufacturer's instructions. Cells were washed 1x with PBS and replaced with fresh MEM. 20 µL CellTiter reagent was added to each well (96-well plate) containing 100 µL cell culture medium and incubated for 3 hrs (37°C). Sample absorbance was recorded at 490 nm relative to positive (1% Triton X-100) and negative (no treatment) controls.

2.2 Ferric phosphate nanoparticle methods

Ferric phosphate nanoparticles (NP-$FePO_4$) were donated by Florentine Hilty, PhD (Laboratory of Human Nutrition, ETH Zürich). Their synthesis, chemical composition, and physicochemical properties have been previously described [288, 289].

2.2.1 Dispersion

NP-$FePO_4$ suspensions were prepared in MEM. When diluted in MEM, NP-$FePO_4$ rapidly agglomerated and sedimented in solution. This necessitated using probe sonication, which uses ultrasonic cavitation, for proper dispersion. 1 mg/mL NP-$FePO_4$ was diluted in MEM and placed in 15 mL centrifuge tubes. Tubes were placed on ice and samples were probe sonicated (MSE Soniprep 150, UK) for 15 min (amplitude: 16.1 A, 150 W). Immediately after sonication, NP-$FePO_4$ was either characterised (see below) or further diluted in MEM to achieve working iron concentrations for cell culture.

2.2.2 Dynamic light scattering

Dynamic light scattering (DLS) is a widely used technique for the characterisation of nanoparticles in solution. The rate of particle diffusion in the medium as a result of Brownian motion is measured by the scattering of laser light. Smaller particles tend to move faster in solution, and scatter more light relative to larger particles. The hydrodynamic diameter (based on a sphere) of nanoparticles can be determined using the Stokes-Einstein equation:

$d(H) = \kappa T / 3\pi\eta D$, where κ is Boltzmann's constant, T is the absolute temperature, η is the viscosity of the dispersant, and D is the translational diffusion coefficient.

This method was used to measure the particle size distribution of sonicated NP-$FePO_4$ in MEM. Measurements were taken 3 times, on 3 separate days. The refractive index of NP-$FePO_4$ relative to the sodium d line (589 nm) was estimated as 1.680 using the Becke line test. The viscosity of the medium was considered 0.890 cP at 25°C. The refractive index of the dispersant was 1.330. Particles were measured after a 30 sec equilibration time over 10 cycles.

2.2.3 Transmission electron microscopy

Transmission electron microscopy (TEM), a high-resolution (limit of detection 0.2 nm) imaging technique, is also used routinely to characterise the size of nanoparticles. The technique uses a beam source of high velocity electrons that are accelerated under vacuum. The electrons are focused directly onto the nanoparticle using condenser lenses. As the electron beam collides with particles, they scatter (or reflect) the electrons more frequently. The electrons are 'transmitted' and detected as darker areas in a CCD camera in contrast to the bright background (TEM grids absorb electrons from the beam).

10 µL NP-$FePO_4$ samples were deposited onto TEM copper grid supports (Electron Microscopy Sciences, USA). The grids were covered to protect the sample from environmental contamination, and incubated for 1 hr to allow for evaporation. Grids were rinsed in milli-Q H_2O 5 consecutive times (10 sec each), and dried overnight (covered). Deposited particles were imaged using a Jeol 1200EX fitted with a LaB6 filament and a Gatan Orius charged-coupled device (CCD) camera.

2.2.4 Disc centrifugation sedimentation

Differential centrifugal sedimentation (DCS) is a sensitive, high-resolution analytical technique for analysing the size distribution of particles in solution. The wide dynamic range (10 nm to 50 microns) makes it particularly useful for determining the size distribution of polydispersed particles (such as those found in aggregates and agglomerates).

DCS works on the principle of particle sedimentation. Particles injected into the instrument sediment at different rates depending on their size. The rate of sedimentation is accelerated using centrifugation to create higher g-force. Particle sedimentation time (detected by a laser) is converted to particle size using a modification of Stokes' law:

$D = [(18\eta * \ln(R_f/R_0)) / ((\rho_p - \rho_f)\omega^2 t)]^{0.5,}$ where D = particle diameter, η is the fluid viscosity, R_f is the final radius of rotation, R_0 is the initial radius of rotation, ρ_p is the particle density, ρ_f is the fluid density, ω is the rotational velocity, and t is the time required to sediment from R_0 to R_f. The particle density was considered 2.87 g/cm^3 and the fluid density was 1 g/cm^3.

The CPS disc centrifuge 2400 (CPS Instruments, UK) was run at *5000 rpm* (20°C). After a 10 min warm-up period, a sucrose gradient was established. Two separate sucrose solutions (24% and 8% w/v) were prepared and injected into the system. 100 µL dodecane was added to prevent gradient evaporation. Once the gradient was set, the instrument was calibrated using 100 µL polystyrene standard (0.239 µM) followed by 100 µL of the sample. The settings for size detection were 50 nm to 10 µM. A typical run time lasted approximately 30 min.

2.2.5 Atomic force microscopy

Atomic force microscopy (AFM) is another nanoparticle characterisation technique determining particle size. Complementary to TEM data, AFM measures nanoparticle size relative to x, y and z axis, essentially providing an added dimension for 3-D topology of the nanoparticles. After depositing nanoparticles on a substrate, a cantilever is scanned over the surface of the substrate. As the cantilever approaches the surface of the substrate, the force between the cantilever and the nanoparticles can be detected from deflection. In essence, the larger the size of the nanoparticle, the greater the deflection of the cantilever. The force is translated into size determinations.

NP-$FePO_4$ samples for AFM were prepared in parallel with TEM experiments. The protocol for AFM preparation was also similar to TEM. 10 µL NP-$FePO_4$ was spotted onto freshly cleaved AFM grade mica (Agar Scientific), covered, and incubated for 1 hr to allow for evaporation. Micas were rinsed in milli-Q H_2O 5 consecutive times (10 sec each), and dried overnight (covered). Micas were fixed onto stainless-steel metal specimen discs and examined using AFM (XE-100, Park instruments) in non-contact mode.

2.2.6 Supernatant iron during *in vitro* gastric digestion

Supernatant iron from NP-$FePO_4$ was determined using established methods [265, 326] with minor adaptations. Supernatant iron was determined after sonication and after pH treatment. For pH treatment, 40 mM NaCl, 5 mM KCl solution was titrated to either pH 1, 2, or 4 using 1 M HCl. 4 mg NP-$FePO_4$ was diluted in 50 ml pH solution, placed onto a rotating table (100 rpm), and incubated (37°C). At 15 min intervals, sample aliquots were removed (1 mL) and centrifuged for 5 min (*10,000 x g*). After centrifugation, 500 µL supernatant aliquots were collected and analysed for iron content using colorimetric reagents.

The iron content of the supernatant was compared to the total iron content of the sample.

2.2.7 Phase distribution of iron during *in vitro* gastric and intestinal digestion.

The phase distribution of iron was determined using a modification of the method from Pereira et al [286]. Similar to 2.2.6, the supernatant iron was obtained during *in vitro* digestion. The supernatant iron was further distinguished from soluble and nanoparticulate iron using 3 kDa MWCO ultrafiltration columns (Vivaspin, UK). The supernatant iron was placed in a column and centrifuged for 10 min (*10,000 x g).* Iron in the supernatant and in the ultrafiltrate was determined. The calculation to determine iron fractions as microparticulate (agglomerate fractions and ferric hydroxides), nanoparticulate (< 100nm), and soluble iron (< 1 nm) was as follows:

% Soluble = [(Fe ultrafiltrate / total Fe)] x 100

% Nanoparticulate = [(Fe supernatant – Fe ultrafiltrate) / total Fe] x 100

% Microparticulate = [Total Fe – Fe supernatant / Total Fe] x 100

These are expressed in bar graphs as a percentage of total Fe.

2.2.8 Confocal reflectance microscopy

Caco-2 cells were grown on coverslip embedded 35 mm glass bottom dishes (Mattek, USA). Cells were treated with sonicated NP-$FePO_4$ (200) [30 µg/mL] for 1 hr. After 1 hr, cells were washed 3x with PBS and fixed in 4% paraformaldehyde (PFA) for 15 min. After removal of PFA, cells were washed 1x with PBS, washed 1x in ddH_2O, counterstained with DAPI (Vector Laboratories, USA) and stored at 4°C until analysis. NP-$FePO_4$ (200) was visualised in Caco-2 cells using a Nikon A1R laser scanning confocal microscope equipped with a Ti

inverted microscope and a wide field detector in reflectance mode. 3-D projections were generated with 2 µM optical slices on the z-axis courtesy of Dr. Christine Elgy.

2.2.9 TEM for Caco-2 cell uptake

Cells were grown on Thermanox coverslips (Nunc) placed in 12 well plates. Caco-2 cell monolayers were treated with iron for 2 hrs and washed 3x with PBS. Cells were fixed and embedded by Kim Findlay at the John Innes Centre Bioimaging facility. Cells were washed 2x in 0.05 M sodium cacodylate (2 min), and primary fixed in 2.5% glutaraldehyde in 0.05 M sodium cacodylate for 20 min. Cells were washed 3x in 0.05 M sodium cacodylate (10 min) and post fixed in 1% osmium tetroxide (OsO4) for 20 min. Cells were washed 3x in ddH_2O (10 min) and placed at 4°C overnight. 2% uranyl acetate in ddH_2O was added to the cells (20 min). Cells were washed 3x in ddH_2O (10 min) and dehydrated in increasing EtOH concentrations; 70%, 80%, 90%, 95%, 100% for 10 min each. Cells were replaced with fresh 100% EtOH for 30 min, and replaced with fresh 100% EtOH for a further 10 min. Coverslips were transferred into polythene cups and embedded in 1:1 (EtOH:LR white resin) for 2 hrs on a rocking platform. Cells were replaced with 100% LR White for 90 min followed by fresh 100% LR White for 3.5 hrs. Finally, cells were replaced with fresh 100% LR White overnight at 60°C. Samples were removed and left at RT overnight to harden. Cells were removed from the polythene cups and left at RT (> 12hrs) for the final cure prior to sectioning.

Cells were sectioned and mounted by Paul Stanley, University of Birmingham. Approx. 100 µM sections were cut using a Diatome diamond knife (EMS, PA, USA) and collected onto 200 mesh copper grids prior to analysis. Sections were analysed using a Jeol 2100 electron microscope at 200 kV.

2.3 Pea ferritin

2.3.1 Pea ferritin purification

Dry marrowfat peas (*Pisum sativum cv Sakura*) were obtained from Wherry and Sons (Lincolnshire, UK). Phytoferritin (pFer) was extracted and purified from the peas according to the methods of Laulhere et al [327] with slight modifications. 200 g dry marrowfat peas were coarsely ground using a coffee grinder. The coarsely ground peas were diluted in 680 mL of cold phosphate buffer (50 mM, 1% polyvinylpyrroldione [PVP], pH 7) and finely ground into a slurry using a Polytron® probe homogenizer (Kinematica, Switzerland). The slurry was centrifuged for 10 min (*10,000 rpm*, 4°C). The supernatant was collected, 50 mM $MgCl_2$ was added, and the solution was immediately centrifuged for 5 min (*5,000 rpm*, 4°C). The supernatant was collected, 70 mM trisodium citrate was added, followed by 40 mg RNase A. This solution was incubated for 2 hrs (4°C). After 2 hrs, the solution was centrifuged for 40 min (*13,000 rpm*, 4°C). The pellet, containing the crude ferritin fraction, was removed and centrifuged for 2 min (*14,000 rpm*, 4°C). 2 mL milliQ water was added to the pelleted ferritin and the solution was centrifuged for another 2 min (*14,000 rpm*, 4°C).

Phytoferritin was further purified using size-exclusion chromatography. Phytoferritin was separated using a Superose 12 10/300 GL column (GE Healthcare) with PBS as the running buffer, which eluted in the void volume. Purity of phytoferritin was confirmed using Coomasie stained gels. Polyclonal antibodies were generated in rabbits (Agrisera, Sweden). Phytoferritin was stored at -20°C until use.

2.3.2 pH treatment

100 µL purified phytoferritin was diluted in 1 mL 140 mM NaCl, 5 mM KCl salt solution and titrated to pH 2, 4 or 7 using 0.1 M HCl (*100 rpm, 37°C*). At 15 min intervals, 100 µL aliquots were removed and/or:

(a) Immediately spin-filtered

(b) Snap-frozen in liquid nitrogen and stored at -20°C prior to analysis by Western blot.

2.3.3 Ultrafiltration

The effect of pH treatment on the soluble iron released from phytoferritin was determined using ultracentrifugation. Phytoferritin was ultracentrifuged using 3 kDa MWCO spin filters (Vivaspin®, GE Healthcare). The iron in the filtrate represents the soluble iron released from phytoferritin. By calculation, the difference between total iron and soluble iron in the filtrate equals the iron in the retentate (ferritin iron core). Phytoferritin digests were placed in spin filters and centrifuged for 5 min (*15,000 x g*). The iron content of the filtrate was measured using the Ferene-S colorimetric assay and expressed relative to total iron content.

2.3.4 SDS-PAGE

Sodium dodecyl sulfate-polyacrylamide gel electrophoresis (SDS-PAGE) was used to separate proteins based upon charge to mass ratio. 15% separating gels were used to identify ferritin monomers (23 kDa). Samples were diluted in 4x SDS loading buffer containing β–mercaptoethanol (BME), denatured for 5 min (95°C), and loaded onto 10 well gels, including 3 µL PageRuler™ Prestained Protein Ladder (ThermoFisher Scientific) in the first well. 100 ng of protein was loaded into each well for pure phytoferritin for experiments determining its degradation when exposed to pH treatment. 40 µg of protein were loaded into

each well in experiments using Caco-2 cell lysates. Samples were run at 100 V for 15 min and 200 V for 45 min, or until the loading buffer migrated to the bottom of the gel.

SDS-PAGE formulation

15% Resolving gel		5% Stacking gel	
Reagent	per gel	Reagent	per gel
30% Acrylamide (w/v) 37.5:1 (mL)	2.5	30% Acrylamide (w/v) 37.5:1 (mL)	0.53
1.5 M Tris-HCl, pH 8.8 (mL)	2.5	1.5 M Tris-HCl, pH 6.8 (mL)	1
ddH_2O (mL)	2.45	ddH_2O (mL)	2.47
10% APS (µL)	50	10% APS (µL)	25
TEMED (µL)	5	TEMED (µL)	2.5

Table 2.10 Reagents used to generate SDS-PAGE gels

2.3.5 Native-PAGE

The protocol for Native-PAGE was similar to SDS-PAGE, but proteins were electrophoresed under non-reducing and non-denaturing conditions (no BME or SDS) to preserve its secondary and tertiary structures. 6% gels were used to visualise native ferritin (552 kDa) exposed to pH treatment. Samples, buffers, and electrophoresis were used at 4°C. 100 ng samples, diluted in 4x native loading buffer (containing only bromophenol blue), were loaded into 10 well gels, including horse-spleen ferritin (Sigma, F4503) in the first well for comparison. Samples were run at 100 V for 3-4 hrs, or until the loading buffer migrated to the bottom of the gel.

Native-PAGE formulation

6% Resolving gel		4% Stacking gel	
Reagent	per gel	Reagent	per gel
30% Acrylamide (w/v) 37.5:1 (mL)	1.2	30% Acrylamide (w/v) 37.5:1 (mL)	0.25
1.5 M Tris-HCl, pH 8.8 (mL)	1.5	1.5 M Tris-HCl, pH 6.8 (mL)	0.5
ddH_2O (mL)	3.265	ddH_2O (mL)	1.23
10% APS (µL)	25	10% APS (µL)	15
TEMED (µL)	10	TEMED (µL)	6

Table 2.11 Reagents used to generate NATIVE-PAGE gels

2.3.6 Western blot

Proteins were transferred from gels to nitrocellulose membranes (GE Healthcare) using a semi-dry transfer system. Gels were washed with ddH_2O to remove detergent, placed on top of the nitrocellulose membrane, sandwiched in between 4 layers of presoaked filter paper (in transfer buffer). Protein transfer was set for 30 min (200 mA). Protein transfer efficiency was visualised using Ponceau-S solution.

Membranes were placed in blocking solution (tris-buffered saline [TBS] containing 0.1% [v/v] Tween 20 and 5% [w/v] dried skimmed milk) for 1 hr (*20 rpm*). After 1 hr, the blocking solution was removed and membranes were incubated with primary antibodies diluted in blocking solution overnight (*20 rpm*, 4°C). The membrane was washed 3x with blocking solution (5 min each) then incubated with horseradish peroxidase HRP-conjugated anti-rabbit IgG secondary antibodies (Abcam) for 40 min (*20 rpm, rocking*). Proteins were washed 2x with blocking solution (5 min) and 2x with TBS-tween before protein visualisation.

	Antibody	MW (kDa)	Dilution	Product
1°	Pea ferritin	23	1:5000	Agrisera (AS15 2898)
1°	β-actin	42	1:1000	Sigma (A2066)
2°	Goat Anti-Rabbit IgG (HRP)		1:5000	Abcam (ab6721)

Table 2.12 Western blot antibodies

Immunolabeled proteins were detected using enhanced chemiluminescent reagents. Equal volumes solution 1 (1 mL) and solution 2 (1 mL) were mixed together, added to the membrane, and incubated for 1 min. The membrane was

briefly dried using filter paper, then scanned using the ImageQuant™ LAS 500 CCD imaging system (GE Healthcare).

ECL solutions	Reagents
Solution 1	88.5 mL ddH_2O 10 mL 1 M Tris-HCl pH 8.5 1 mL luminol stock 0.44 mL coumarate stock
Solution 2	89 mL ddH_2O 10 mL 1 M Tris-HCl pH 8.5 0.06 mL 30% H_2O_2

Table 2.13 Enhanced chemiluminescence reagents

2.3.7 Confocal fluorescence microscopy

Caco-2 cells were grown on coverslip embedded 35 mm glass bottom dishes (Mattek, USA). Cells were treated with 20 nmol/L phytoferritin in MEM for 1 hr. After 1 hr, cells were washed 3x with PBS and fixed in 4% paraformaldehyde (PFA) for 15 min. After removal of PFA, cells were permeabilised in 0.2% Triton X-100 for 10 min, washed 1x with PBS, and blocked in 1% BSA for 30 min. After 30 min, cells were incubated in primary antibodies against phytoferritin (1:1000) overnight (4°C). Cells were washed 3x with PBS (5 min each), and incubated with Alexa Fluor™ 488-conjugated anti-rabbit IgG secondary antibodies (1:1000) (ThermoFisher Scientific) for 30 min. Cells were washed in ddH_2O, counterstained with DAPI (Vector Laboratories, USA) and stored at 4°C until analysis. Pea ferritin was visualised in Caco-2 cells using the Nikon A1R laser scanning confocal microscope equipped with a Ti inverted microscope and a wide field detector with DIC for simultaneous detection of confocal and transmitted light images. 3-D projections generated with 2 µM optical slices on the z-axis were generated by Dr. Christine Elgy.

2.4 Work attributions

The multi-disciplinary work presented in this thesis could not have been conducted without the expertise of many individuals.

In Chapter 3, nanoparticle characterisation by TEM, AFM, DCS, and confocal microscopy was conducted at the University of Birmingham under the supervision of Dr. Christine Elgy.

In Chapter 4, phytoferritin purification, protein/iron quantification, and synthesis of pea ferritin polyclonal antibodies from marrowfat peas were conducted by Dr. Jorge Celma-Rodriguez at the John Innes Centre. Western blots quantifying holo-ferritin, monomers, iron stain and *in vitro* digestion of marrowfat peas after boiling and microwaving were conducted by Dr. Emily Jones at the John Innes Centre. The *in vitro* digestion of marrowfat peas and ROS generation was conducted by Dr. Ildefonso Ramiro-Rodriguez at UEA. Confocal microscopy was conducted under the supervision of Dr. Elgy.

In Chapter 5, iron concentrations determined by ICP-OES in Caco-2 cells and ROS generation were conducted by Dr. Ramiro-Rodriguez.

In Appendix B, Caco-2 cells monolayers were treated for TEM analysis by Dr. Kim Findlay at the John Innes Centre. TEM micrographs were conducted under the supervision of Dr. Elgy.

I would like to personally thank Dr. Anna Wawer for training in the *in vitro* digestion Caco-2 cell culture technique, Dr. Florentine Hilty for providing the NP-$FePO_4$, Dr. Janneke Balk for providing technical expertise and lab space for Western blots, Dr. Dora Pereira for her technical advice in nanoparticle characterisation and donation of Hutu-80 cells, Dr. Mohamad Aslam for siRNA training, Dr. Stuart Rushworth and Ms. Amina Abdul-Aziz in RT-PCR training, and Dr. Paul Sharp for PhD mentorship.

Chapter 3: Ferric phosphate nanoparticles

3. Ferric phosphate nanoparticles

This chapter is based upon the manuscript entitled 'Mechanisms of iron uptake from ferric phosphate nanoparticles in human intestinal Caco-2 cells; submitted and accepted in the journal, *Nutrients* (DOI: 10.3390/nu9040359) [328].

3.1 Introduction

Decreasing particles to the nano scale has recently gained attention as a technique to improve iron absorption. Chemically synthesised 5 nm iron hydroxide nanoparticles (named IHAT) have been recently developed by the Powell lab at MRC Cambridge. These nanoparticles were well absorbed (80%) in animal and human subjects [287] relative to $FeSO_4$. They also provided compelling evidence in cell culture models that their nanoparticles were absorbed independently from DMT1 [329] using an endocytosis like pathway [286]. A separate group provided evidence for the presence of hemin-coupled iron nanoparticles internalised in Caco-2 monolayers [277], which also indicates the presence of an endocytosis pathway. In these prior studies, the effect of gastrointestinal digestion was not measured. Whether dietary iron nanoparticles are absorbed using clathrin-mediated endocytosis pathways after exposure to *in vitro* digestion has not been demonstrated.

Previous studies examining the bioavailability of elemental iron powders have shown an inverse relationship between particle size and iron absorption. Harrison et al [194] found that decreasing the particle size of $FePO_4$ from 12-15 µm to 1 µm increased iron solubility and improved RBV 5-fold. Decreasing particle size to the nano scale could be a strategy to improve iron bioavailability. Recently, $FePO_4$ synthesised to the nano scale (NP-$FePO_4$) by flame spray pyrolysis (FSP) was reported to have similar iron bioavailability to $FeSO_4$ in rat models [288], and it was proposed that this was a function of higher surface area

and increased solubility relative to its larger precursors. However, further studies are required to confirm that these findings in rats can be extrapolated to humans [209] given that rodents endogenously synthesise AA [49] and are less affected by dietary inhibitors of iron absorption than humans [208].

In this study, the effects of *in vitro* simulated gastrointestinal digestion on the size distribution of NP-$FePO_4$, iron solubility, iron uptake into Caco-2 cells, and mechanisms of iron absorption were examined. The overall aim of this chapter is to understand how iron is absorbed from NP-$FePO_4$ in Caco-2 cells after exposure to pH treatment.

3.2 Materials and Methods

Samples of NP-$FePO_4$, previously characterised for crystalline structure, phase distribution, chemical composition, and specific surface areas (SSA, 100 and 200 m^2/g) [288, 289], were kindly donated by ETH Zurich.

3.2.1 Sonication

NP-$FePO_4$ was diluted to a concentration of 1 mg/mL in water or minimum essential media (MEM) and was sonicated for size characterisation and cell culture studies. For detailed methodology, see section 2.2.1.

3.2.2 *In vitro* simulated gastrointestinal (GI) digestion

NP-$FePO_4$ was exposed to *in vitro* simulated gastrointestinal digestion (GI) [149, 218, 248]. Briefly, 10 mL of 40 mM NaCl and 5 mM KCl pH 2 solution containing 0.4% pepsin was added to NP-$FePO_4$ in a 50 mL polypropylene tube. The mixture was placed on a rotating table (100 rpm) and incubated for 1 hr at 37°C. After 1 hr, the pH of the digests was readjusted to 5.5-6.0 and a pancreatin-bile solution (0.25%) added. The pH was further adjusted to 6.9-7.0 with 1 M $NaHCO_3$ and incubated for a further 30 minutes at 37°C.

3.2.3 Transmission electron microscopy (TEM)

TEM micrographs were generated for visualisation of NP-$FePO_4$ (200) during GI digestion. For detailed methodology, see section 2.2.3.

3.2.4 Disc centrifugal sedimentation (DCS)

The CPS disc centrifuge model 2400 (CPS Instruments, UK) was used to measure the total particle distribution given the heterogeneity, polydispersity, and aggregated/agglomerated particle dispersions during GI digestion. For detailed methodology, see section 2.2.4.

3.2.5 Dynamic light scattering (DLS)

The hydrodynamic particle size of NP-$FePO_4$ in cell culture media was measured using dynamic light scattering (DLS) with the Zetasizer Nano-ZS (Malvern Instruments, UK). For detailed methodology, see section 2.2.2.

3.2.6 Caco-2 cell culture

Caco-2 cells (HTB-37® VA) from American Type Culture Collection were used as the representative model of iron uptake. For detailed methodology, see section 2.1.3.

3.2.7 Supernatant iron during gastric pH treatment

Supernatant iron from NP-$FePO_4$ (soluble and < 100 nm fractions) was quantified using similar methods [265, 289] for iron dissolution at low pH. For detailed methodology, see section 2.2.6.

3.2.8 Phase distribution of iron during gastric and intestinal pH treatment

The phase distribution of iron was determined using a modification of the method from Pereira et al [286]. For detailed methodology, see section 2.2.7.

3.2.9 Measurement of iron uptake into Caco-2 cells

Iron uptake into Caco-2 monolayers was determined using the surrogate marker, cell ferritin formation (ng cell ferritin / mg cell protein). The effects of pH, time, and dietary factors on iron uptake were measured. For detailed methodology, see sections 2.1.5 and 2.1.6.

3.2.10 Chemical inhibitors targeting iron uptake

All chemicals, unless otherwise stated, were from Sigma. For pH treatment experiments, ascorbic acid (1:20 Fe:AA molar ratio, 600 μM) was added at the beginning of the gastric phase and 2.5 mM $CaCl_2$ was added directly to MEM (final concentration in MEM after dilution with digests). For sonicated NP-$FePO_4$ (200), chlorpromazine hydrochloride (CPZ, 100 μM), sucrose (0.5 M), filipin (5 mg/L), and dimethyl amiloride (DMA, 200 μM) were used to inhibit endocytosis [286, 316, 317, 330-332]. Caco-2 cells were co-incubated with iron treatment and endocytosis inhibitors for 1 hr, removed from cells, and incubated for a further 23 hrs in MEM. For detailed methodology, see section 2.1.7.

3.2.11 siRNA knockdown of DMT1 in Caco-2 and Hutu-80 cells

For Caco-2 cells, cell monolayers were transfected with Silencer® Select siRNA targeting *SLC11A2* (the gene encoding DMT1) or Negative control no. 1 (200 nM, Life Technologies) using Lipofectamine 3000 in Opti-MEM (Gibco) for 48 hrs. Pre-confluent Hutu-80 cells were transfected following similar methods as for Caco-2 cells. For detailed methodology, see section 2.1.8.

3.2.12 RT-PCR

RNeasy Mini Kit (Qiagen) was used for RNA extraction. Complementary DNA (cDNA) was synthesised using the qPCRBIO cDNA Synthesis Kit (PCR

Biosystems). Real time PCR (RTPCR) was conducted using the Roche LightCycler 480. Relative expression of *SLC11A2* (DMT1) was normalised to the housekeeping gene, 18S and assessed using the ΔΔCt method [333]. For detailed methodology, see section 2.1.9.

3.2.13. Statistical analysis

Statistical analysis was performed using GraphPad Prism v.6.0 (San Diego, CA). Particle size was calculated using Feret's diameter and particle size distributions expressed using the median particle size (d50) with d10 and d90 representing 10% and 90% of the particle sizes, respectively. One-way repeated measures ANOVA with Tukey's multiple comparisons test was used to compare differences in iron uptake or one-way repeated measures ANOVA with Dunnett's test were used to compare differences between NP-$FePO_4$ (200) and NP-$FePO_4$ (200) treated with chemical inhibitors. Cell culture experiments were repeated 2-3 times, with n = 3 per experiment. Differences were considered significant at $p < 0.05$.

3.3 Results

3.3.1 Characterisation of sonicated and *in vitro* digested NP-$FePO_4$

Particles synthesised to the nano-scale are novel technologies. While iron nanoparticles have been shown to be absorbed directly into enterocytes, these studies have used stabilised particles in solution with defined particle sizes, which may not be physiologically representative in humans. Our aim, therefore, was to characterise its exposure to gastrointestinal digestion. Furthermore, nanoparticle agglomeration is a well-described phenomena occurring in cell culture media [334-336]. To prevent large agglomerates, ultrasonic cavitation was used as it produces sufficient energy to stabilise particles in solution as demonstrated below.

a

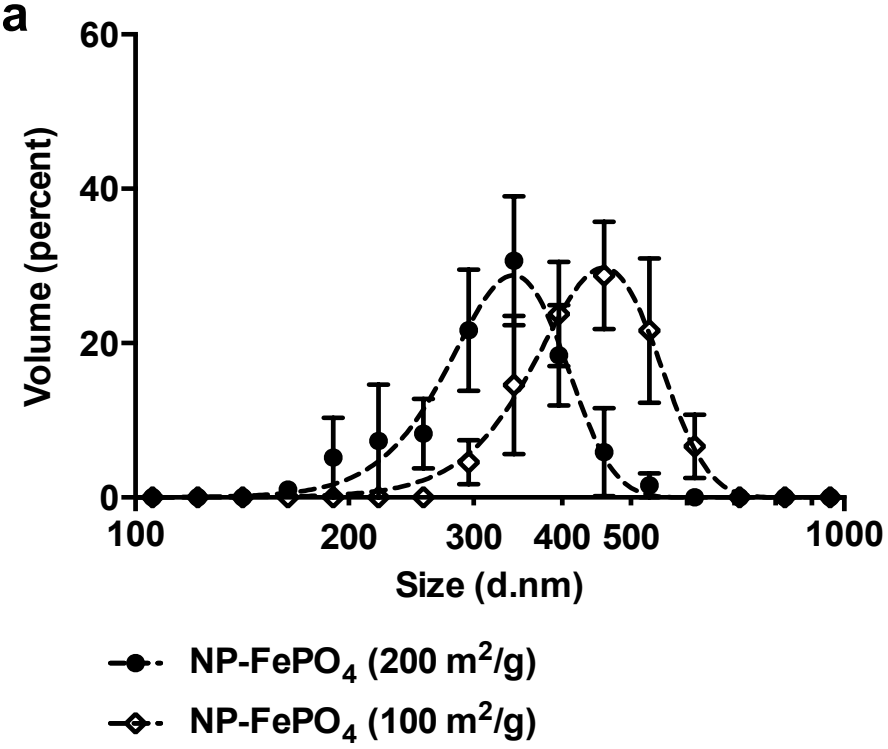

b

Particle	SSA (m2/g)	Estimated MPS (nm)	Hydrodynamic diameter (nm)	dv10	dv50	dv90
NP-$FePO_4$ (200)	200	10	341	220	342	396
NP-$FePO_4$ (100)	100	20	458	342	459	531

Figure 3.1 (a) Size determination of sonicated NP-$FePO_4$ as measured by dynamic light scattering (DLS) and (b) Particle-size distribution assessed using DLS.

1 mg/mL NP-$FePO_4$ dispersions in MEM were measured using probe sonication (MSE Soniprep 150, UK) for 15 min (amplitude: 16.1 A, 150 W). 3 independent determinations were taken on separate days.

Particle size characterisation using DLS was conducted with NP-$FePO_4$ (200) and NP-$FePO_4$ (100) in MEM (Figure 3.1). Although the mean particle size (MPS) of the dried precursor NP-$FePO_4$ was 10 and 20 nm respectively, in MEM

the MPS was in the 300-500 nm size range. The mean particle size generated with sonicated NP-$FePO_4$ (200) was less than sonicated NP-$FePO_4$ (100). Sonicated NP-$FePO_4$ (200) hydrodynamic diameter averaged 341 nm (d10, d90: 190, 459) and NP-$FePO_4$ (100), 458 nm (d10, d90: 342, 532).

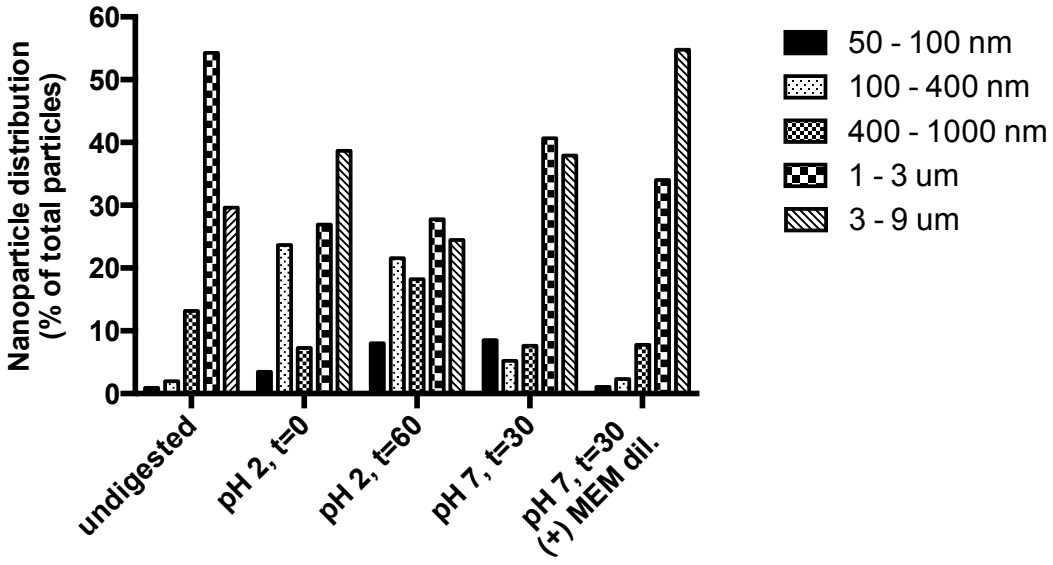

Figure 3.2 Histogram representing the particle distribution based upon total particle population during stages of GI digestion as measured by DCS.

Particle size distributions investigating the total particle population during GI digestion were conducted using CPS (Figure 3.2). After 60 min digestion at pH 2, 50% of the particles were ≤1000 nm, and 30% of the particles were ≤ 400 nm. At pH 7, rapid agglomeration of the particles led to an 80% increase in micron-sized fractions, and the proportions of the 100-400 nm and 400-1000 nm fractions were reduced to < 10%. Overall, about 15% of the particles were ≤ 400 nm after digestion. Dilution 1:1 in MEM caused further agglomerate formation, resulting in < 5% of the particles in the ≤ 400 nm range.

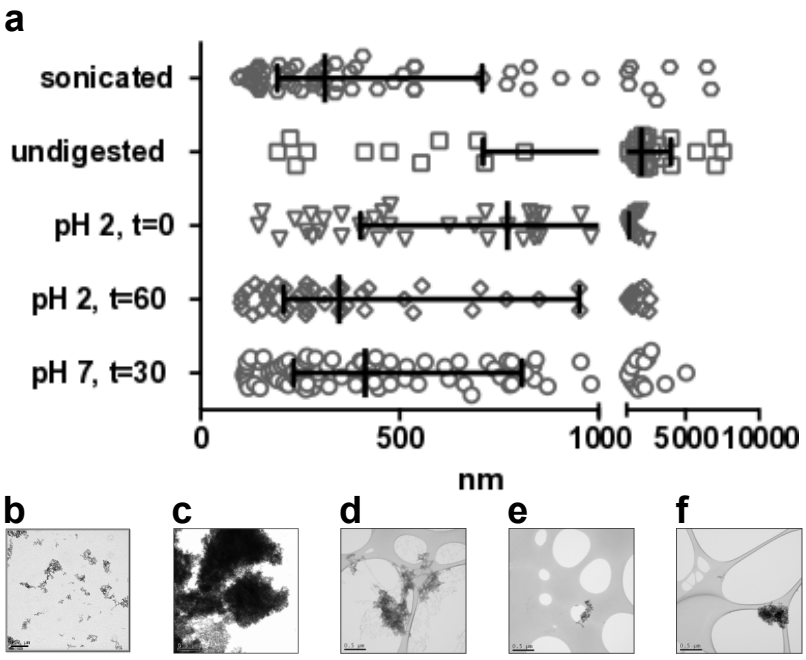

Figure 3.3 Size determination of NP-$FePO_4$ (200) during different stages of GI digestion using TEM.

(a) Scatter bar plot of NP-$FePO_4$ (200) sizes (in nm), measured using Feret's diameter, and calculated using ImageJ software analysis. Representative TEM micrographs used in the analysis of size and size distributions at (b) sonicated, (c) unsonicated, (d) pH 2, t = 0 min, (e) pH 2, t = 60 min, and (f) pH 7, t = 30 min with scale bar set at 0.5 µM.

Treatment	Measured particle sizes (nm)			
	dv10	dv50	dv90	Particle count
Sonicated	138	312	1264	59
Undigested	264	1996	10354	38
pH 2, t=0	260	771	1606	47
pH 2, t=60	135	348	1602	55
pH 7, t=30	142	413	1694	48

Table 3.1 Particle-size distribution analysis of NP-$FePO_4$ (200) during different stages of GI digestion from TEM analysis.

Particle size of NP-$FePO_4$ (200) during GI digestion was visualised using TEM and particles analysed for size with ImageJ software. First, the size distribution of non-sonicated NP-$FePO_4$ (200) was compared with sonicated NP-$FePO_4$ (200) in milliQ H_2O. Large, agglomerated, electron dense particles formed without sonication in the micron range (Figure 3.3c) with d50 = 1996 nm (Table 3.1). Sonication of NP-$FePO_4$ (200) resulted in particle dispersal of similar size range to the DLS data, d50 = 312 nm. After exposure initially to gastric digestion (pH 2), the large, agglomerated particles shifted to a reduced size (d50 = 771 nm). Longer exposure time in pH 2 (60 min) caused further reduction of particle size to d50 = 348 nm. After the GI digest was neutralized to intestinal conditions (pH 7, t = 30) with 0.1 M $NaHCO_3$, the particle size slightly agglomerated to d50 = 413 nm (Table 3.1).

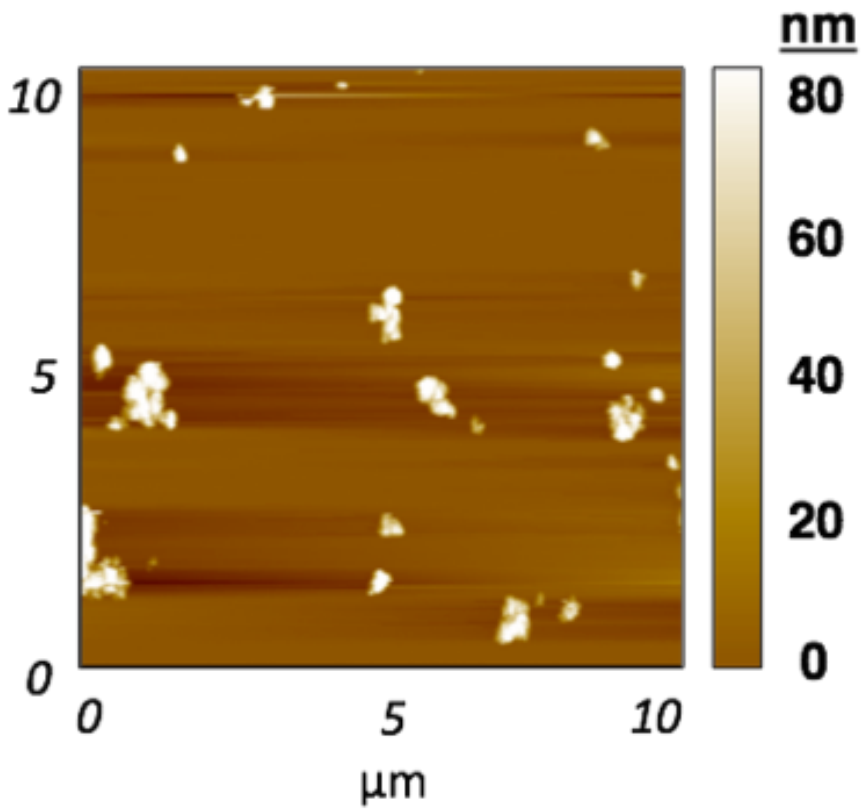

Figure 3.4 Representative AFM micrograph depicting sizes of NP-$FePO_4$.

The x and y-axis represent the scan size used for each micrograph examined. The scale bar (right) represents the size of NP-$FePO_4$ as measured in the z-axis.

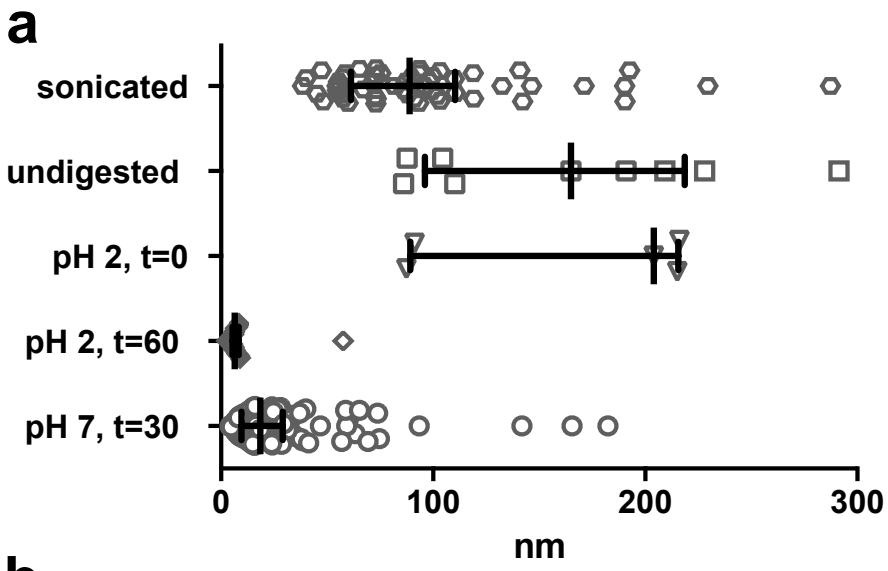

b

Treatment	Measured particle sizes (nm)			
	dv10	dv50	dv90	Particle count
Sonicated	50	98	184.5	52
Undigested	86	164	291	9
pH 2, t=0	87	163	216	5
pH 2, t=60	4	9	13	18
pH 7, t=30	7	25	58	125

Figure 3.5 Size determination of NP-$FePO_4$ (200) during different stages of GI digestion using AFM.

(a) Scatter bar plot of NP-$FePO_4$ (200) sizes (in nm) using XEI software (Park Systems) and (b) Particle-size distribution analysis of NP-$FePO_4$ (200) during different stages of GI digestion using AFM data.

Similar to the TEM data, particle size was significantly larger in undigested NP-$FePO_4$ (200) compared to sonicated NP-$FePO_4$ (200). Particle sizes were not altered at pH 2 (t=0) but after 30 min were greatly reduced (d50 = 9). Mean particle size was 2x larger when the digest was neutralised at pH 7, t=30 (d50 = 25). Overall, particle sizes determined by AFM were less than for TEM.

3.3.2 Effect of gastric time and pH on supernatant iron, soluble iron, and uptake into Caco-2 cells

These sets of experiments determined how factors of gastric digestion affect iron solubility and bioavailability from NP-$FePO_4$ in comparison with fully soluble, FAC. The effects of exposure time and pH on supernatant iron concentration and Caco-2 cell uptake were examined. At pH 2, NP-$FePO_4$ (100 and 200) was digested for 30, 60, and 120 min and aliquots were taken to determine supernatant iron. The remaining digestion solution was neutralised at pH 7 and incubated for a further 30 min for cellular iron uptake.

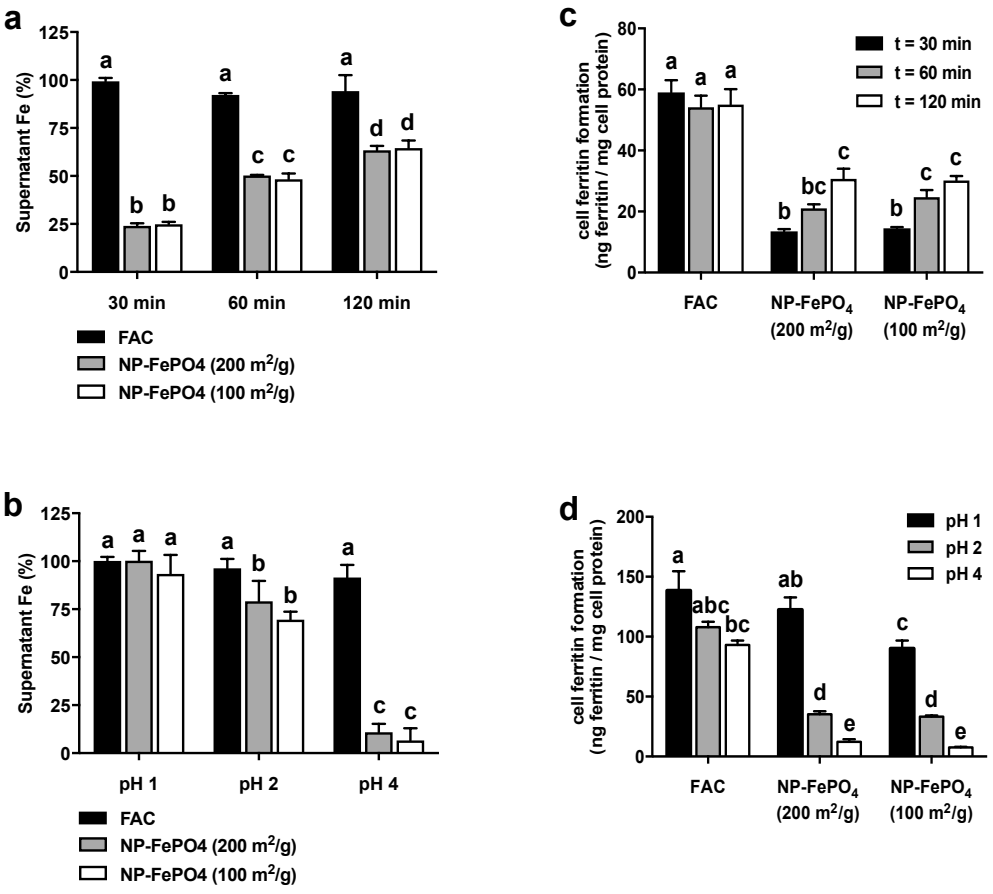

Figure 3.6 Effect of gastric digestion on supernatant iron and iron uptake in Caco-2 cells.

FAC or NP-$FePO_4$ were (a) digested at pH 2 for varying times [30, 60, 120 min] or (b) varying pH [1, 2, 4] for 1 hr and supernatant iron determined at the end of gastric digestion. Iron treatments were also exposed to Caco-2 cells and measured for cell ferritin formation (c, d). Data are expressed as the means of two independent experiments (n = 3 per experiment, ± SEM).

Supernatant iron was increased with longer gastric digestion times, but no significant difference was observed between the two particle sizes. Compared to FAC, supernatant iron of NP-$FePO_4$ reached 70% after 2 hrs digestion. In contrast, the pH of the gastric digest had a large effect on supernatant iron from NP-$FePO_4$. The entire iron fraction was exclusively found in the supernatant fraction when NP-$FePO_4$ was digested at pH 1 for 1 hr, whereas only 5-10 % of iron was in the supernatant at pH 4 for both particles.

Iron uptake was significantly increased 2-fold when NP-$FePO_4$ was digested for 120 min compared to 30 min for both particle sizes. Iron uptake between two particle sizes evaluated over 30, 60, and 120 min was not different. In comparison to FAC, in which the ferritin formation was not affected by time, the two particle sizes were only half as absorbed. Iron uptake of FAC was significantly greater at pH 1 than pH 4. NP-$FePO_4$ was not taken up (compared to controls not containing iron) after digesting both particles at pH 4 for 1 hr. While iron uptake of both particles was not different when digested at pH 2 or 4, a significant increase was found in NP-$FePO_4$ (200) compared to NP-$FePO_4$ (100) when digested at pH 1. At pH 1, iron uptake of NP-$FePO_4$ (200) was similar to FAC digested at every pH.

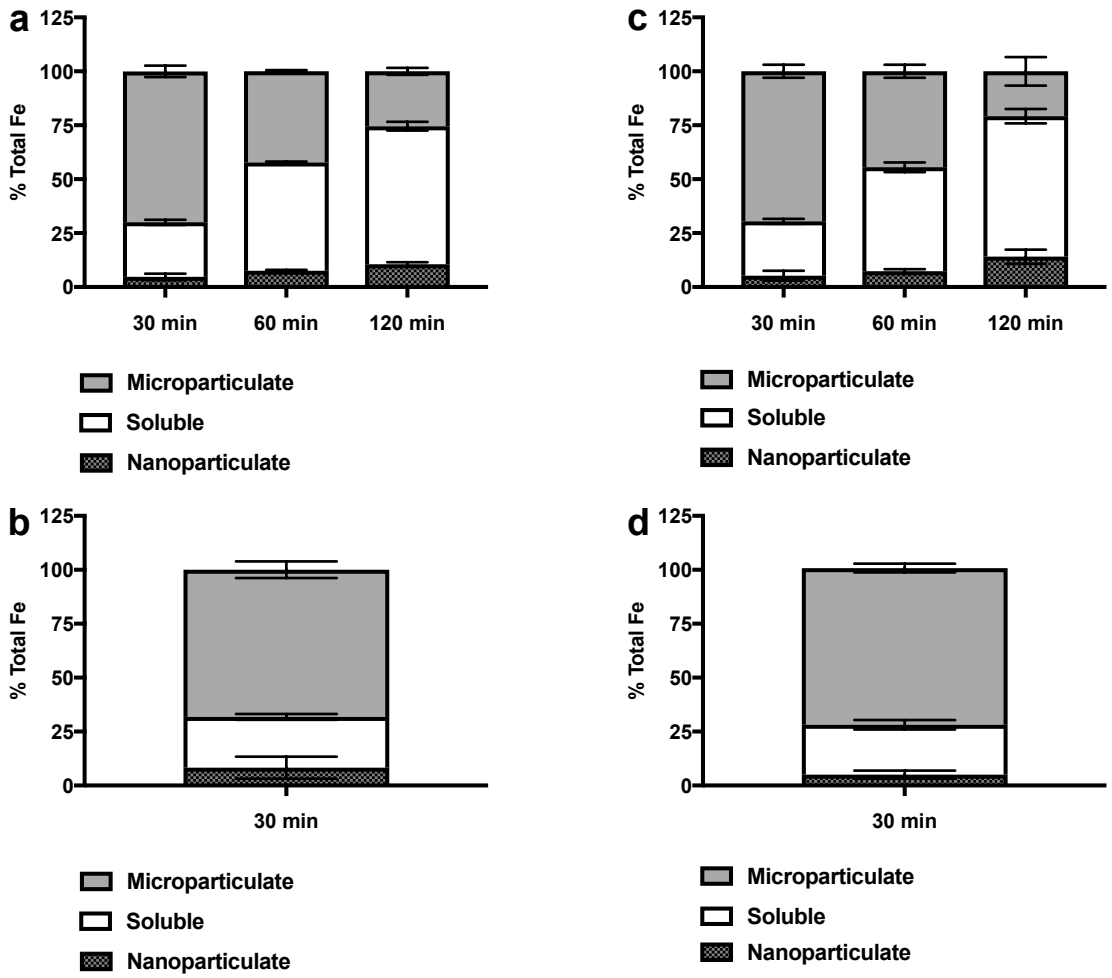

Figure 3.7 Total iron determination of NP-$FePO_4$ after pH gastric digestion (pH 2) and intestinal digestion (pH 7).

NP-$FePO_4$ was digested at pH 2 for varying times and: (a) NP-$FePO_4$ (200) or (c) NP-$FePO_4$ (100) phase distribution determined. NP-$FePO_4$ was digested for 1 hr, neutralised to pH 7 with 1 M $NaHCO_3$, incubated for 30 min and: (b) NP-$FePO_4$ (200) or (d) NP-$FePO_4$ (100) phase distribution determined. Data are expressed as the means of two independent experiments (n = 2 per experiment, ± SD).

Soluble iron was distinguished from nanoparticulate iron within the supernatant fraction. As the supernatant increased during gastric digestion, the

soluble fraction also increased concurrently from both NP-$FePO_4$. The nanoparticulate iron percentage from NP-$FePO_4$ (200) increased from 4.7% to 10.6% and NP-$FePO_4$ (100) from 5.3% to 14.1% when the gastric digestion was extended from 30 min to 120 min.

Phase distributions were also determined after pH treatment when NP-$FePO_4$ was neutralised to pH 7, t=30. The percentage of nanoparticulate iron was not significantly altered in NP-$FePO_4$ when the digest was neutralised from gastric to intestinal digestion. The percentage of microparticulate iron increased from 42.3% and 44.5% in the gastric digestion after pH 2, t=60 to 68.2% and 72.6% at pH 7, t=30 min for NP-$FePO_4$ (200) and NP-$FePO_4$ (100), respectively.

3.3.3 Effect of AA and calcium on supernatant iron and iron uptake in Caco-2 cells

Supernatant iron at gastric pH is an important determinant of iron bioavailability; AA is a potent enhancer of non-haem iron bioavailability, and calcium is an inhibitor of non-haem iron bioavailability. We wanted to assess whether these dietary components had an effect on iron solubility and bioavailability from NP-$FePO_4$. We also measured supernatant iron at neutral pH to understand whether iron from NP-$FePO_4$ precipitated out of solution to iron-hydroxides similar to other insoluble iron fortificants.

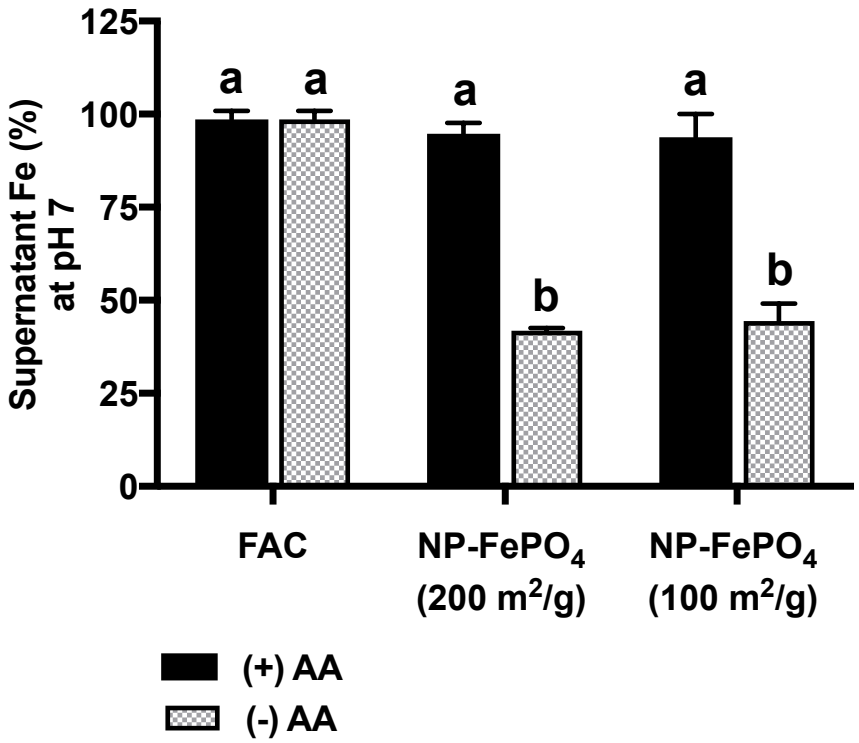

Figure 3.8 Supernatant iron of digested NP-$FePO_4$ after pH treatment.

NP-$FePO_4$ was digested at pH 2 for 1 hr, neutralised to pH 7 with 1 M $NaHCO_3$, incubated for 30 min and supernatant iron measured relative to total iron. Data are expressed as the n = 3 ± SD.

Supernatant iron at neutral pH (pH 7) was similar among FAC, NP-$FePO_4$ (200) and NP-$FePO_4$ (100) when AA (1:20 Fe:AA) was added to the gastric step of each digest. In the absence of AA, supernatant iron from FAC was not different from with AA. In contrast, supernatant iron from NP-$FePO_4$ without AA was reduced by 50% at pH 7 in comparison with AA. No differences in supernatant iron was found between NP-$FePO_4$ (200) ad NP-$FePO_4$ (100) at neutral pH.

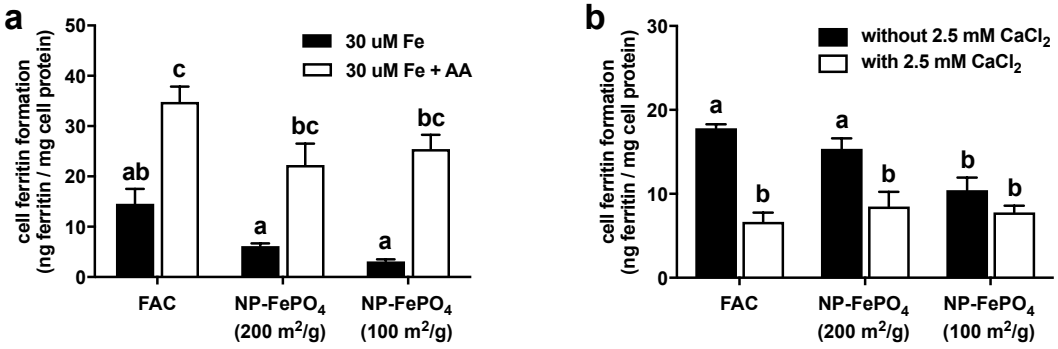

Figure 3.9 Effect of AA and $CaCl_2$ on iron uptake from pH treated FAC or NP-$FePO_4$

Iron uptake of pH treated FAC or NP-$FePO_4$ after incubation with (a) AA (1:20 AA molar ratio, 600 µM) or (b) $CaCl_2$ (2.5 mM, final volume in MEM after dilution) in Caco-2 cells after 24 hrs. Data are expressed as the means of two independent experiments (n = 3 per experiment, ± SD).

AA added to the digest (1:20 AA molar ratio) during the gastric phase increased iron uptake from FAC 2-fold and both forms of NP-$FePO_4$ 3-4 fold. The increase in iron uptake from NP-$FePO_4$ with added AA was similar to FAC and FAC with AA, which correlates well with the increased supernatant iron from NP-$FePO_4$ with AA at neutral pH.

NP-$FePO_4$ was digested and added to MEM containing a final concentration of 2.5 mM $CaCl_2$ after dilution (Figure 3.9). Calcium (as $CaCl_2$) inhibited iron uptake from FAC and NP-$FePO_4$ (200) by 50%. Iron uptake from NP-$FePO_4$ (100) was marginally decreased with $CaCl_2$ but the effect was not statistically significant. This might be due to the low basal levels of iron uptake observed from NP-$FePO_4$ (100) without $CaCl_2$.

3.3.4 Mechanisms of iron uptake from sonicated NP-$FePO_4$ (200)

To provide evidence that NP-$FePO_4$ is directly translocated into Caco-2 cells, particles were visually detected using confocal techniques. Using RCM and enhanced contrast to remove spurious NP detection [337], high intensity reflection spots were detected (Figure 3.10, top panel, 3rd column), indicating NP-$FePO_4$ internalisation in Caco-2 cells. Z-stack projection of Caco-2 cell monolayers confirmed that NP-$FePO_4$ was, in fact, internalised and not simply representative of cell surface interaction with NP-$FePO_4$, as this phenomena occurs with NP-$FePO_4$ (Florentine Hilty, personal communication). The green fluorescence, indicative of NP-$FePO_4$, was clearly evident on the cell surface (Figure 3.11, 1st panel) and on the z-axis (Figure 3.11, 4th panel).

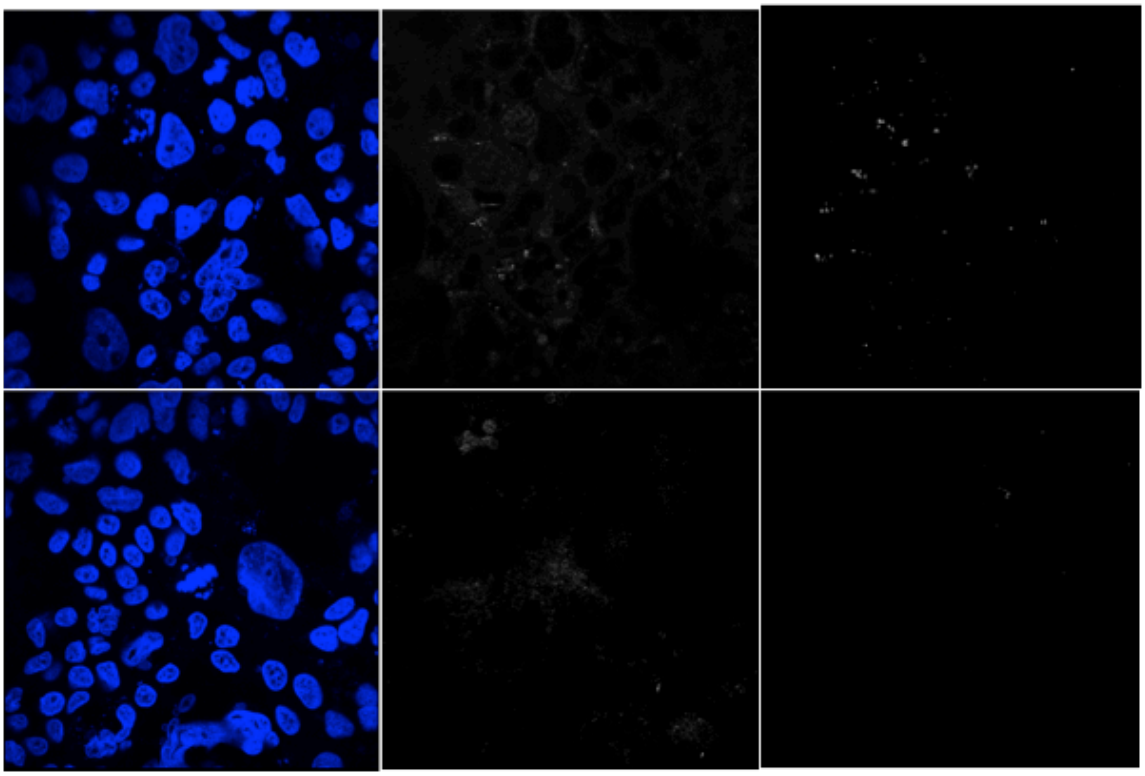

Figure 3.10 RCM images representing the interaction of NP-$FePO_4$ (200) with Caco-2 cells.

Caco-2 cells were treated with sonicated NP-$FePO_4$ (200) [top panel] or control (blank) sample [bottom panel]. Left panels depict cells stained with nucleus stain (DAPI). Middle panels depict unaltered (raw) reflection images. Right panels depict edited reflection images, with high contrast to distinguish particles (top) from artifacts (bottom).

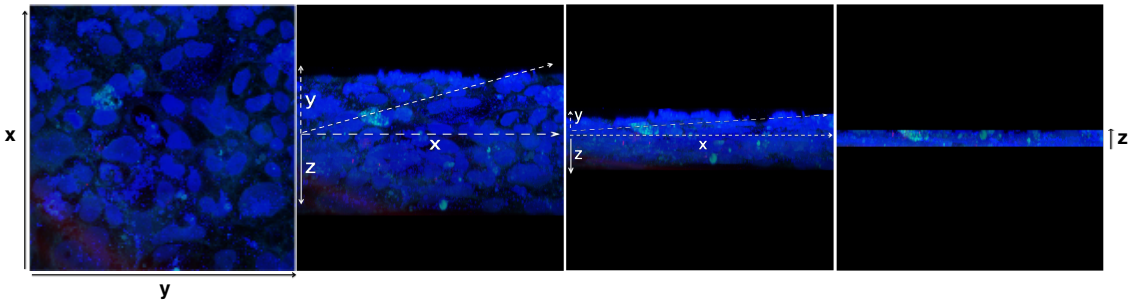

Figure 3.11 RCM images and z-stack projection of Caco-2 cells and internalised NP-$FePO_4$ (200).

Caco-2 cells were treated with sonicated NP-$FePO_4$ (200) and images were at different rotations on the z-axis. The first image depicts NP-$FePO_4$ (200) on the cell surface (particles are in light blue [aqua] against the DAPI background). The final image depicts internalisation of NP-$FePO_4$ (200) into cells.

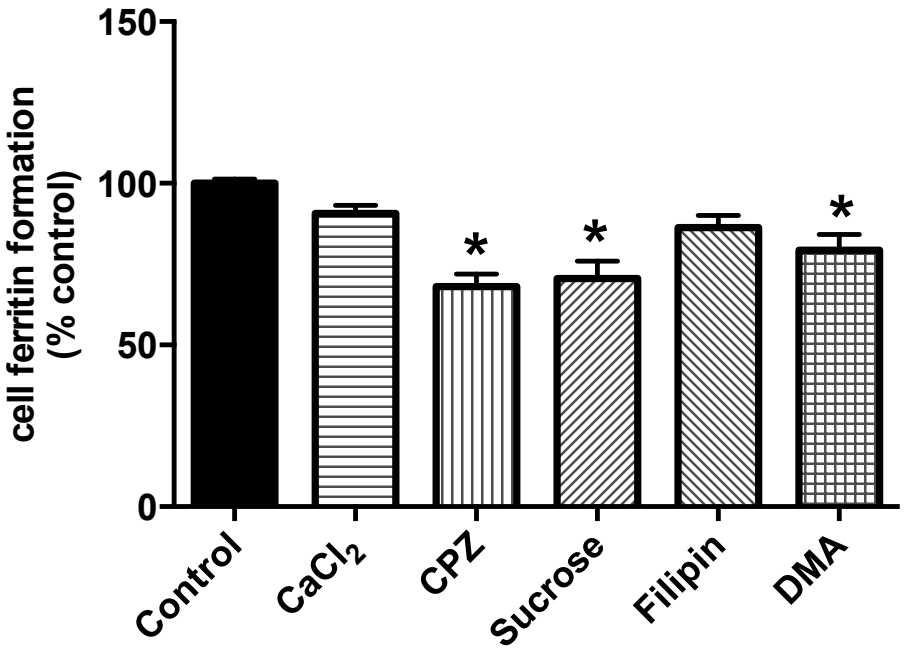

Figure 3.12 Iron uptake of sonicated NP-$FePO_4$ (200) co-incubated with chemical inhibitors targeting endocytosis uptake pathways in Caco-2 cells.

Data are expressed as the means of two independent experiments (n = 3 per experiment, ± SEM). Asterisks denote significant differences compared to control at $p < 0.05$.

Using sonicated NP-$FePO_4$ (200), $CaCl_2$ did not inhibit iron uptake, suggesting that DMT1 is not required for uptake of sonicated NP-$FePO_4$ (200). However, iron uptake was reduced by 30% compared to control when sonicated NP-$FePO_4$ (200) was incubated in the presence of CPZ and sucrose, both clathrin-mediated endocytosis inhibitors. Sonicated NP-$FePO_4$ (200) with DMA, an inhibitor of macropinocytosis, also resulted in reduction of iron uptake by 20%.

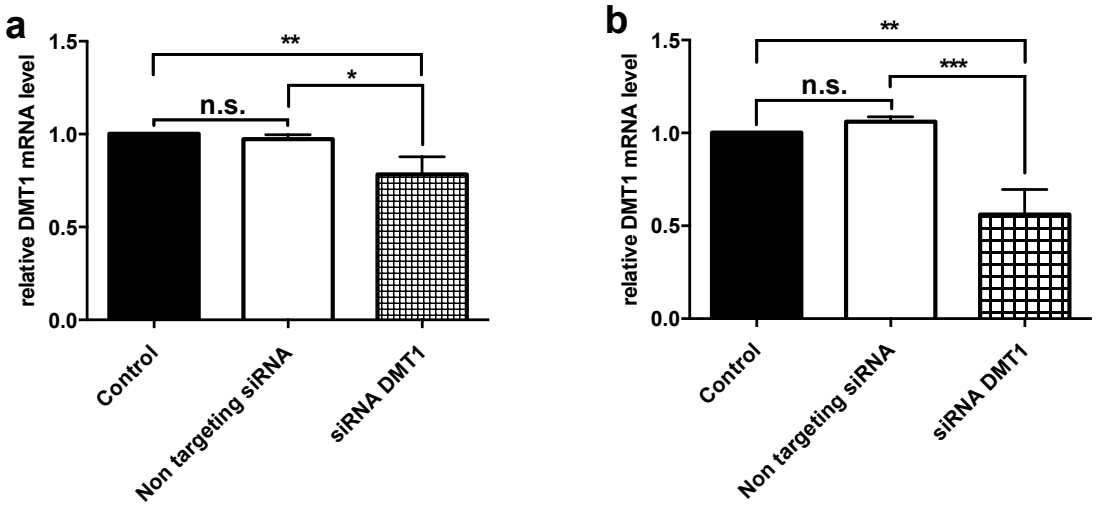

Figure 3.13 RTPCR measuring the effect of siRNA knockdown of DMT1 in Caco-2 and Hutu-80 cells.

DMT1 expression levels in (a) Caco-2 or (b) Hutu-80 cells determined in control (non-transfected cells), non-targeting siRNA (negative control cells) and *SLC11A2* siRNA treated cells as measured by RT-PCR and normalised to 18S housekeeping gene after 72 hrs. Data are expressed as the means of three independent experiments (n = 3 per experiment, ± SEM). Differences indicated

with one, two, or three asterisks are considered significant at $p < 0.05$, 0.01, and 0.001 levels, respectively.

Under experimental conditions, DMT1 gene expression was reduced by 20% in Caco-2 cells following exposure to *SLC11A2* siRNA. DMT1 gene expression of siRNA non-targeting (Negative control 1) cells was not different than control cells (cells with transfection reagent but without siRNA) [shown in Figure 3.13]. Transfection of Hutu-80 cells with DMT1 siRNA resulted in a 50% decrease in DMT1 gene expression compared to control and siRNA non-targeting siRNA cells. The transfection efficiency of Hutu-80 cells was greater than for Caco-2 cells (20%).

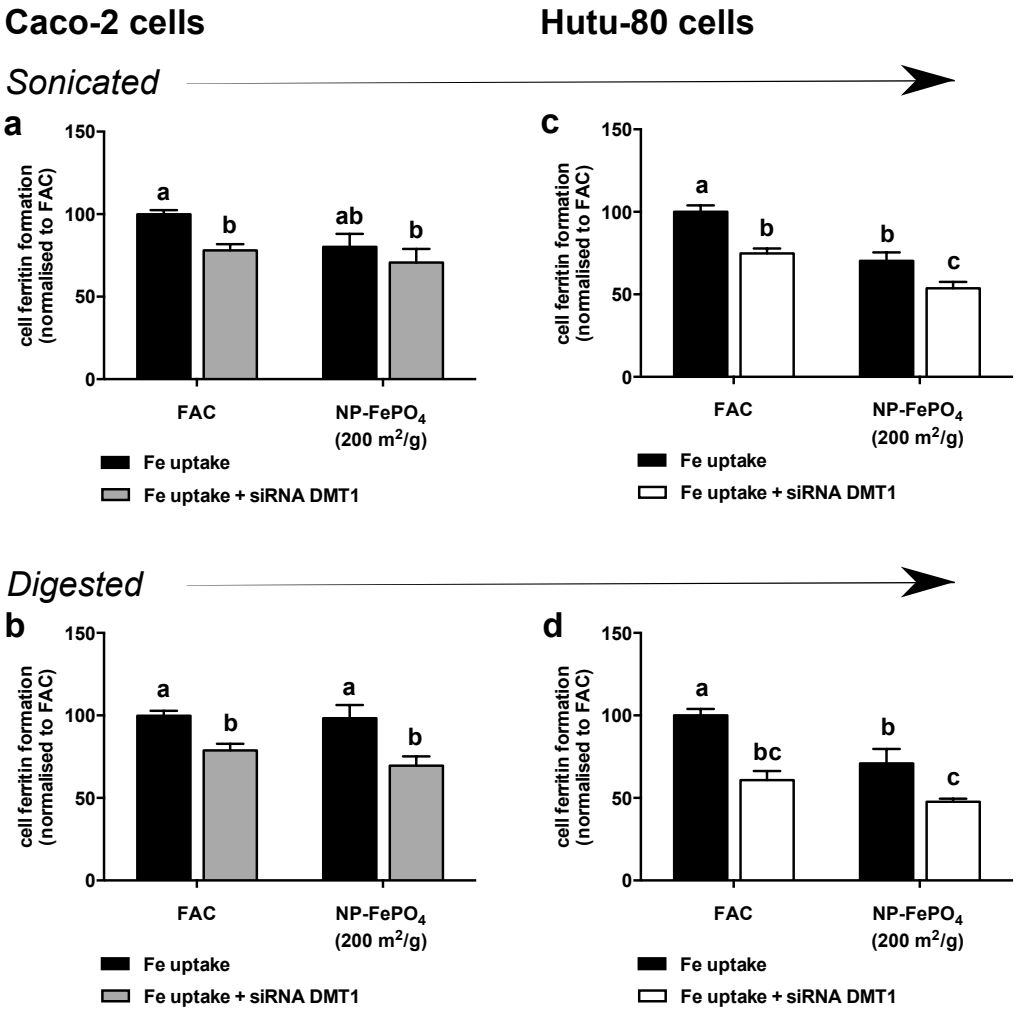

Figure 3.14 Effect of siRNA targeting DMT1 on iron uptake in Caco-2 and Hutu-80 cells.

Iron uptake of (a, c) sonicated NP-$FePO_4$ (200) and FAC or (b, d) pH treated NP-$FePO_4$ (200) and FAC in non-targeting siRNA or *SLC11A2* siRNA treated Caco-2 and Hutu-80 cells after 2 hr exposure followed by incubation in MEM for a further 22 hrs. Data are expressed as the means of three independent experiments (n = 3 per experiment, ± SEM). Different letters indicate statistically significant differences ($p < 0.05$).

Iron uptake from FAC was significantly reduced by 20% in cells treated with siRNA DMT1 compared to cells treated with non-targeting siRNA. Iron

uptake from sonicated NP-$FePO_4$ (200) was slightly reduced but not significantly different in cells treated with siRNA DMT1 relative to cells treated with non-targeting siRNA. In contrast to sonicated NP-$FePO_4$ (200), iron uptake from pH treated NP-$FePO_4$ (200) was significantly reduced (30%) in cells treated with siRNA DMT1 compared to cells treated with non-targeting siRNA. Iron uptake from pH treated FAC was reduced by 20% in cells treated with siRNA DMT1 compared to cells with non-targeting siRNA, similar to FAC without pH treatment.

Iron uptake of sonicated NP-$FePO_4$ (200) was significantly inhibited in cells treated with siRNA DMT1 compared to non-targeting cells (24%), which was similar to the inhibitory effect of iron uptake in FAC (25%). Iron uptake was 30% lower from sonicated NP-$FePO_4$ (200) compared to FAC. Similar to sonicated NP-$FePO_4$ (200), iron uptake from pH treated NP-$FePO_4$ (200) was significantly decreased in cells treated with siRNA DMT1 compared to cells treated with non-targeting siRNA (33%). pH treated FAC was also significantly decreased in cells treated with siRNA DMT1 compared to cells treated with non-targeting siRNA (40%). Overall, while inhibitory effects of iron uptake were observed for both sonicated and pH treated NP-$FePO_4$ (200) in siRNA DMT1 cells, the effect was larger when NP-$FePO_4$ (200) was pH treated compared to sonicated.

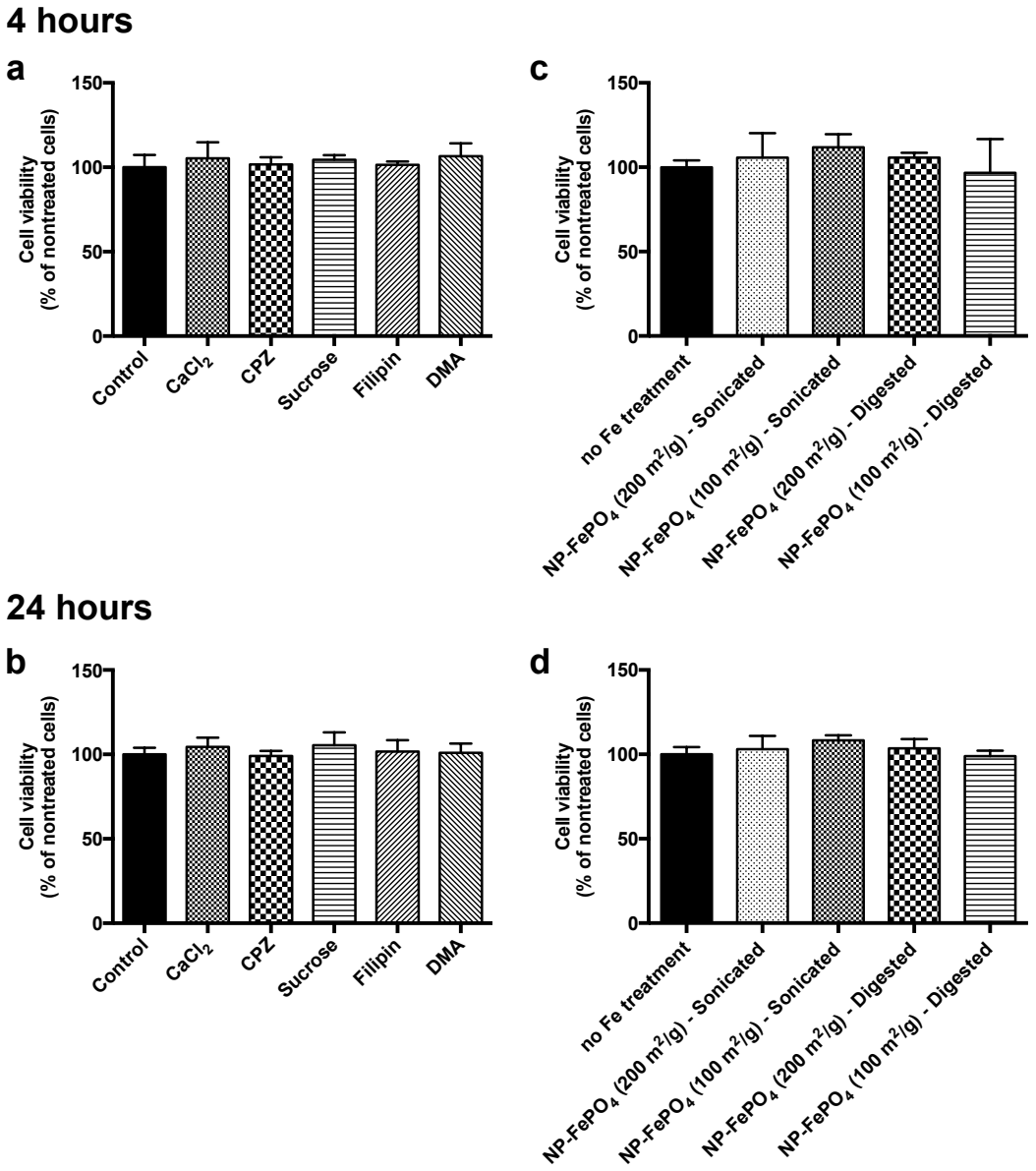

Figure 3.15 Viability of Caco-2 cells measured 4 and 24 hrs after incubation with chemical inhibitors or NP-$FePO_4$ treatments.

Chemical inhibitors with concentrations used in the experiments described were incubated with Caco-2 cells for 1 hr and cells were measured for viability after (a) 1 hr or (b) 24 hrs. Iron compounds were incubated with Caco-2 cells for either (c) 1 hr (100 µM Fe) or (d) 24 hrs (30 µM Fe). 1% Triton X-100 was used as the positive control; 10-40% cell viability was assessed between experiments.

Data values are expressed as the n = 3 ± SD. One-way ANOVA with Dunnett's multiple comparison test was used to distinguish differences between untreated cells with chemical inhibitor or iron compound. Different letters indicate statistically significant differences ($p < 0.05$).

Cell viability was unaffected by either NP-$FePO_4$ dose or chemical inhibitors, suggesting that ferritin formation is due to iron uptake and not a response to cell damage or inflammation.

3.4 Discussion

The bioavailability of NP-$FePO_4$ has been shown to be similar to $FeSO_4$ in rats using the haemoglobin repletion assay [288, 289]. Rohner and Hilty suggested that increased iron solubility of the particles at low pH was responsible for increased iron absorption, indicating that iron uptake in the intestine is facilitated through gastric dissolution, hydrolysis of Fe^{3+} from the particle, reduction to Fe^{2+}, and absorption via the DMT1 transporter. The present study aimed to elucidate the mechanisms involved in iron uptake from NP-$FePO_4$ using cellular models.

Characterisation of particle size and the size distribution of nanoparticles are very important determinants for understanding the mechanisms of iron uptake in the duodenum and also given the growing concern over nanoparticle toxicity. Along with surface characteristics, charge, and cell type interactions, particle size directly correlates with whether nanoparticles are able to be absorbed directly into tissues [284, 338-340].

In terms of duodenal iron absorption, gastrointestinal digestion strongly influences iron bioavailability and nanoparticle translocation [341]. In this chapter, a validated *in vitro* digestion technique was used that mimics *in vivo* conditions [218, 342] in order to understand the changes in NP-$FePO_4$ size and size

distribution. The analysis was conducted to determine whether direct transcytosis of particles is physiologically relevant. Although many versions of simulated *in vitro* digestion exist, this particular method was selected as it estimates iron bioavailability when coupled to the Caco-2 cell model and has been shown to correlate well with data from human trials [242, 268].

The nanoparticle characterisation described in the chapter is complimentary and includes DLS and DCS, which measures the particles in solution, and TEM and AFM, which measure the non-aquated particle core.

DLS is one of the most widely used techniques to characterise nanoparticles due to its ease of use. The hydrodynamic sizes of sonicated NP-$FePO_4$ were 341 and 458 nm, which were 30x and 20x larger in magnitude than its dried precursors. Unsonicated NP-$FePO_4$, and the effects of *in vitro* digestion on the size of particles cannot be used with DLS because the technique is unable to cope with rapidly sedimenting particles in solution. In addition, because DLS calculates particle sizes to the 6^{th} power, larger particles tend to mask smaller particles within solution.

To address the size heterogeneity of NP-$FePO_4$ in solution, we used DCS to model particle behavior of NP-$FePO_4$ during *in vitro* GI digestion. Particle sizes decreased with time during gastric digestion. At pH 2, t=60, 50% of the particles were < 400 nm but at pH 7, t=30 min, only 15% of the particles were < 400 nm. This indicated that the majority of NP-$FePO_4$ (200) agglomerated (75% particles > 1 μM) when exposed to GI digestion. The agglomerated particle fractions also suggest that NP-$FePO_4$ (200) is likely non-toxic to the intestinal epithelium as its size is probably not predictive of uncontrolled absorption [11, 21, 27]. Nonetheless, 15% of the total particle distribution < 400 nm was still a significant amount and warranted further investigation whether these sized particles undergo transcytosis. It is important to note that the DCS data indicated that the

dilution of the *in vitro* digest with MEM resulted in very few particles < 400 nm (< 5%). This suggests that the *in vitro* digestion method cannot measure particle transcytosis and sonication would be required.

Similarly to DCS, the TEM data indicated that particle size of NP-$FePO_4$ decreased with respect to time at gastric pH. Neutralisation of the digest to pH 7 resulted in d50 = 413 nm with 10% of the particle distribution less than 142 nm. Unlike DCS, particle agglomeration was not observed using TEM, which is likely due to technical differences in microscopy and laser diffraction [28].

It is important to note several important points about using TEM for nanoparticle characterisation. Systematic selection bias of the images is always a concern with this technique. To address this issue, at least 15 separate images (and grid areas) were calculated for each treatment and particles less than 50 nm were excluded from analysis to avoid any artifacts. One major disadvantage of using TEM to characterise nanoparticles is that drying effects tend to increase particle agglomeration [343]. If this were the case, the measurements obtained most likely overestimated the size of particles.

The AFM technique uses a cantilever and its displacement after particle contact results in a measurement of force that is converted and calculated to particle size on the z-axis (top of the particle, as opposed to x and y). The AFM data was less conclusive regarding the size of NP-$FePO_4$. Likely this resulted because it was not possible to obtain a sufficient quantity of particles for proper analysis due to time constraints and the length of instrumentation time required per run. Particles counted were overall < 200 nm in size, not unsurprising as and the drying of particles on the mica substrate most likely leads to spreading of the particles. The general size patterns GI digested NP-$FePO_4$ (200) as measured by AFM was qualitatively similar to that of DCS and TEM. Using AFM, the size of NP-$FePO_4$ (200) decreased with time, and slightly agglomerated at neutral pH.

Given these data on the size of NP-$FePO_4$ (200) during GI digestion, two separate mechanisms of iron uptake from NP-$FePO_4$ into Caco-2 cells were investigated. These were (a) iron uptake via DMT1 as a result of higher supernatant iron of NP-$FePO_4$ at low gastric pH, and (b) uptake of non-hydrolysed NP-$FePO_4$ via endocytosis.

To measure iron uptake of NP-$FePO_4$ via DMT1, the effect of pH treatment on iron uptake of NP-$FePO_4$ in Caco-2 cells was examined. The term supernatant iron is used in the majority of these experiments, rather than soluble iron, as it more accurately describes the aqueous layer, which contains the combination of soluble iron and nanoparticles < 100 nm [286, 341]. Gastric digestion at pH 1 (1 hr) significantly increased supernatant iron and iron uptake compared to pH 2 and pH 4. Gastric digestion at pH 2 for 30 min, 60 min, and 120 min led to increases in supernatant iron and uptake with time, but the effect of time was much less pronounced than pH. Coupling gastric digestion at pH 1 to Caco-2 cells resulted in increased iron uptake from NP-$FePO_4$ (200) compared to NP-$FePO_4$ (100). Iron uptake of NP-$FePO_4$ (200) was similar to FAC. Rohner et al [6] and Hilty et al [7] observed similar iron uptake of NP-$FePO_4$ (200) compared to $FeSO_4$ in rats and suggested that its high iron uptake is a result of increased iron particle dissolution compared to $FePO_4$. We found similar results in Caco-2 cells.

To ensure that iron uptake at low pH was a function of increased soluble iron, the supernatant iron obtained was fractionated further using 3 kDa spin filters to distinguish soluble iron from nanoparticulate iron. As a control, this technique was used on undigested NP-$FePO_4$ in water; as expected, all the iron was in the microparticulate fraction as these particles free agglomerate in solution. Nanoparticulate iron (from 5 to 10-15%) increased as a function of time at pH 2, but the rate was less than the increase in soluble iron. After the digest was neutralised to pH 7, t=30, the phase distribution was also examined. While the amount of soluble iron decreased to 25% total iron, most likely due to the

formation of ferric hydroxides, the amount of nanoparticulate iron was slightly reduced to the same amounts found at pH 2, t=30 (~5%). It is likely that NP-$FePO_4$ < 100 nm was a minor contribution to iron uptake in these experiments.

The iron bioavailability of foods and the effects of dietary factors using the *in vitro* digestion / Caco-2 cell model has been shown to correlate well with human absorption data [242, 268]. However, the usefulness of the *in vitro* digestion / Caco-2 cell model for elemental iron powders as a predictor for human bioavailability has been questioned [127, 264]. In Caco-2 cells, breads fortified with H-reduced iron had improved iron bioavailability with particle size of 8 micron compared to 45, and a linear relationship was found between solubility and iron bioavailability [266]. Similarly, 40-60 nm H-reduced iron particles had improved iron bioavailability compared to its larger precursors [267]. Others found that the Caco-2 cell model could not consistently predict iron bioavailability of iron fortificants in different food matrices that were observed in humans [262, 263]. The current recommended *in vitro* test for iron bioavailability of iron fortificants is iron dissolution at pH 1 [4,39]. This low pH is not physiological, as it does not represent the pH found within the stomach, but has been shown to be a predictive model of human iron bioavailability [326]. It was observed in these experiments that the supernatant iron concentration from NP-$FePO_4$ at pH 1 was equal to that of FAC, and that there was a positive correlation with Caco-2 cell ferritin concentration. Iron uptake of NP-$FePO_4$ (200) was equal to that of FAC at pH 1. Thus, NP (and other insoluble fortificants) exposed to in vitro digestion at pH 1 and coupled to Caco-2 cells may better predict human bioavailability.

The role of DMT1 transport in iron uptake from pH treated NP-$FePO_4$ in Caco-2 cells was examined. Two to 4-fold increases in ferritin formation were observed when AA was added to the gastric digest with NP-$FePO_4$, similar to FAC. AA is a potent enhancer of non-haem iron absorption which is thought to occur via reduction of Fe^{3+} to Fe^{2+} and the prevention of insoluble iron hydroxides

[49, 344]. The data suggests that AA increases iron uptake of NP-$FePO_4$, similar to FAC and FAC + AA in Caco-2 cells, by facilitating Fe^{2+} DMT1 mediated uptake. It was further confirmed that iron uptake from NP-$FePO_4$ occurred via DMT1 by incubating Caco-2 cells with 2.5 mM $CaCl_2$. Calcium has been shown to inhibit non-haem iron uptake in Caco-2 cells by decreasing apical protein expression of DMT1 [139]. Iron uptake from pH treated FAC and NP-$FePO_4$ was reduced when incubated with $CaCl_2$, providing evidence that DMT1 is required for iron uptake. Similarly, using siRNA targeting DMT1 in both Caco-2 and Hutu-80 cell lines, it was demonstrated that iron uptake was decreased in DMT1 knockdown cells compared to negative control cells in both cell lines, thereby confirming the role of DMT1 in iron uptake from NP-$FePO_4$.

It is important to note that a significant difference was observed in iron uptake when Caco-2 cells were treated with DMT1 siRNA even though only a 20% knockdown in gene expression was observed using RTPCR. It is acknowledged that several other housekeeping genes should have been run simultaneously to verify whether the knockdown measured was underestimated. 18S rRNA was used as our housekeeping gene but is usually highly expressed in tissues. Its Ct values are much higher relative to DMT1, thus actual differences in gene expression between siRNA treated cells may be difficult to distinguish.

The effects of long-term exposure and potential toxicity of NP-$FePO_4$ requires further investigation. Health concerns have been raised about the toxicological effects of daily consumption of nanoparticles found in various consumer products (see review by Nel et al [338]). NP-$FePO_4$ was non-toxic to Caco-2 cells when incubated for 24 hrs, but recent studies have shown that chronic exposure of Caco-2 / HT-29 MTX co-cultures to polystyrene or TiO_2 nanoparticles can markedly remodel the intestinal epithelium and affect iron absorption [272, 283]. This requires further investigation.

DMT1 transport is most likely the predominant mechanism of iron uptake, but an alternative route of iron uptake may also be operational, since ~15% of the particles were between 50 and 400 nm. Gastric pH in rats is considerably higher than pH 1 [345, 346] and the experiments showed that a large amount of iron (25-50%) from NP-$FePO_4$ remained insoluble at pH 2, with very little iron in the supernatant fraction at pH 4. This suggests that a significant fraction of iron bound to NP-$FePO_4$ could be directly transported into the epithelium by endocytosis, given particle translocation of 200 and 500 nm particles seen in Caco-2 cells co-cultured with M-cell like phenotype [284, 347]. Sonicated NP-$FePO_4$ was used to investigate this possibility. The particle size range of sonicated NP-$FePO_4$ (200) was similar to the range expected for the non-agglomerated fraction of GI digested NP-$FePO_4$ (200). Iron uptake from sonicated NP-$FePO_4$ (200) was inhibited with CPZ and sucrose, and to a lesser extent DMA. The chemical inhibitors used have been shown to be successful in inhibiting endocytic pathways in Caco-2 cells [286, 331, 332]. Since the size distribution of sonicated NP-$FePO_4$ (200) was unimodal, consisting of non-uniform particles with a wide range (150 – 500 nm), it is possible that the smaller sized particles may be absorbed using clathrin-mediated endocytosis and the larger sized particles by macropinocytosis.

Evidence of particle transcytosis by NP-$FePO_4$ is not unsurprising as recent reports have shown nanoparticle uptake for iron compounds 10–100 nm size in Caco-2 cell TEM micrographs [285, 286, 319]. Moreover, in support of our findings, a number of previous studies have also shown that nano-sized iron compounds are absorbed using endocytic pathways in Caco-2 cells [286, 316, 317]. In comparison to these other studies, the chemical inhibitors used did not inhibit iron uptake to the same extent. This is most likely due to decreased particle transport of NP-$FePO_4$ given the relatively large particle sizes in solution. Regardless, the siRNA data provided compelling evidence that DMT1 is not a

requirement for iron uptake from sonicated NP-$FePO_4$ (200). It was surprising to observe that DMT1 knockdown in Hutu-80 cells also decreased iron uptake from sonicated NP-$FePO_4$ (200). The reason for the effect might be due to differences in cell physiology between polarised Caco-2 cells and non-polarised Hutu-80 cells.

The future use of NP-$FePO_4$ as an iron fortificant is to some extent dependent on factors other than nutritional considerations. Food fortification for large-scale populations requires that the iron compound is cost-effective and scalable. Although inherent disadvantages exist in the use of $FeSO_4$ as a fortificant, namely its rancidity / instability during storage and colour induced changes to the matrix [127, 194], its use meets the criteria described above compared to other iron compounds, such as NaFeEDTA and FePP [116]. Advances in nanotechnology necessitate decreasing the cost and increasing the scalability of production for NP-$FePO_4$ prior to its use as an iron fortificant.

3.5 Conclusions

The experiments in the Caco-2 model system described in this chapter show that iron uptake from NP-$FePO_4$ occurred predominately through iron solublisation and entry via the DMT1 transporter. Some NP-$FePO_4$ (200) may be absorbed intact into Caco-2 cells, independently from DMT1, but most likely this mechanism contributes a minor role in iron uptake. This conclusion is based on the fact that the digestion experiments showed that less than 15% of NP-$FePO_4$ (200) remained as particles < 400 nm, and with sonicated NP-$FePO_4$ (200), CPZ and siRNA DMT1 treated cells inhibited 20% of iron uptake. These results suggest that NP-$FePO_4$ (200) endocytosis in Caco-2 cells is dependent on particle size, with clathrin-mediated endocytosis (CME) as the predominant mechanism of particle internalisation. This is the first paper to suggest a mechanism of particle transcytosis for iron compounds that could be used for

food fortification. However, one of the assumptions made in these experiments is that sonicated particles were similar to the nanoparticle fractions after GI digestion, which illustrates the difficulties in translating the relatively novel field of nanotechnology to biological systems. Nevertheless, the results demonstrate that iron uptake from NP-$FePO_4$ (200) results from both DMT1 transport and particle transcytosis, which should be taken into consideration when assessing the potential of iron nanoparticles for food fortification.

Chapter 4: Phytoferritin

4. Phytoferritin

This chapter is based upon the manuscript entitled 'Native pea phytoferritin is taken up by intestinal Caco-2 cells via a non-DMT1 dependent mechanism.' The manuscript has been submitted and is currently under peer review.

4.1 Introduction

The majority of the world's population depends on plant-based foods as the main source of dietary iron despite the fact that iron absorption from plants is generally considered low (1-10%) [103, 348]. Given the importance of decreasing meat consumption due to concerns over health, sustainability, and global warming [98-100], investigating plant foods and novel dietary forms of iron that are potential sources of bioavailable iron is of particular importance. Peas, beans, soybeans and other pulses are rich sources of plant ferritin (phytoferritin) [58, 305]. Recent studies have suggested that soybean phytoferritin is as bioavailable as $FeSO_4$ [169, 304]. One reason for its bioavailability is that it may be absorbed separately from non-haem iron using endocytosis [316, 317], yet the role of the non-haem iron transporter, DMT1, in phytoferritin-iron uptake remains unclear. This chapter's aim is to investigate the bioavailability of iron and mechanisms of absorption from phytoferritin extracted from marrowfat peas.

4.2 Materials and Methods

4.2.1 Phytoferritin purification

Pisum sativum cv Sakura, sold as 'marrowfat' peas in the UK, was donated by Wherry and Sons (Rippingale, UK). Phytoferritin extraction and purification were according to the methods of Laulhere et al [327]. For detailed methodology, see section 2.3.1. The enriched ferritin fractions were further purified by gel filtration using a Superose 12 10/300 GL column (GE Healthcare)

using PBS as the running buffer. Proteins were quantified using the Bradford method (BioRad); iron was quantified using the colorimetric iron chelator, Ferene-S. The iron content averaged 2360 ± 20 Fe atoms (n = 3 purification extracts) based on a calculated molecular mass of 552 kDa from the 24-mer protein. Purified phytoferritin was used to generate rabbit polyclonal antibodies (Covalab, Cambridge, UK). This work was conducted by Dr. Jorge Celma-Rodriguez under the JIC Innovation grant entitled “Pea ferritin as a nutritional iron supplement” within the Balk lab.

4.2.2 Caco-2 cell culture

Caco-2 cells (HTB-37® VA) were grown and cultured as described previously. For detailed methodology, see section 2.1.3.

4.2.3 Phytoferritin treatments on differentiated Caco-2 cell monolayers

Uptake by DMT1

The extent of DMT1 mediated iron uptake from phytoferritin was determined using (a) chemical enhancement/inhibition of the DMT1 pathway and (b) small-interfering RNA (siRNA) targeting of *SLC11A2*, the gene encoding DMT1. FAC was used in parallel as a positive control of DMT1 uptake. Phytoferritin (30 µM Fe) was co-incubated with AA, an enhancer of non-haem iron uptake, BPDS, an Fe^{2+} chelator [260], or calcium (as $CaCl_2$), an inhibitor of DMT1 protein expression [139] in MEM for 24 hrs. The concentrations of AA, $CaCl_2$, and BPDS were 600 µM, 2.5 mM, and 50 µM, respectively. Liposomal transfections with siRNA, targeting the knockdown of DMT1 gene expression in the Caco-2 and Hutu-80 cell lines, were carried out as previously published [328]. For detailed methodology, see section 2.1.8.

Uptake by endocytosis

Chemical inhibitors were used at previously described concentrations [286, 316, 328, 332] that were found to disrupt endocytosis in Caco-2 cells. To investigate clathrin-mediated endocytosis (CME), cells were pre-incubated with 100 µM CPZ, washed 3x with PBS, and incubated with phytoferritin (30 µM Fe) for 24 hrs. To probe for specificity of CME, phytoferritin was co-incubated with an array of endocytosis inhibitors targeting various pathways. CPZ (100 µM), sucrose (0.5 M), filipin (5 mg/L), or DMA (200 µM), were each co-incubated with phytoferritin (100 µM Fe) for 1 hr, washed 3x with PBS, and cellular proteins harvested immediately or after 23 hrs incubation.

4.2.4 Measurement of iron uptake in Caco-2 cells

Cells were lysed, centrifuged, and the supernatants collected. Supernatants were analysed for cell ferritin and total protein. For detailed methodology, see sections 2.1.5 and 2.1.6.

4.2.5 Western blotting

Western blots were used for several determinations. They were used to (a) measure the integrity of phytoferritin in peas after cooking and *in vitro* gastrointestinal digestion, (b) measure the integrity of purified phytoferritin after pH treatment and (c) identify phytoferritin in Caco-2 cell monolayers. The amounts loaded onto gels were 10-20 µg of pea protein, 0.1 µg of purified phytoferritin, and 40 µg of Caco-2 cell protein. SDS-PAGE, NATIVE-PAGE, and Western blot methodologies were described in sections 2.3.4-2.3.6.

4.2.6 Reactive oxygen species

Cellular free radical generation in Caco-2 cells was determined using the 2′,7′-dichlorofluorescein (DCFH) assay as previously described [349] with minor modifications. 5 µM DCFH was added to each well for 30 min (37°C). Cells were washed with 1x PBS. Phytoferritin or $FeSO_4$ (100 µM Fe) was added and free

radical generation measured over time (up to 2 hrs) using an excitation of 485 nm and an emission of 530 nm.

4.2.7 pH treatment

The pH treatment protocol was similar to that of Glahn et al [218, 248] except that the digestive enzymes and MWCO membranes were omitted to allow for passage of soluble and nanoparticulate iron. For detailed methodology, see section 2.3.2. Digested phytoferritin was diluted 1:1 in MEM prior to cell incubation.

4.2.8 Soluble iron determination

The percentage of iron released from the iron core during pH treatment was quantified. For detailed methodology, see section 2.3.3.

4.2.9 Statistical analysis

Statistical analysis was performed using GraphPad Prism v.6.0 (San Diego, CA). Data are presented as mean values with standard error (SEM). Two-way repeated measures ANOVA with Tukey's multiple comparisons test was used to evaluate differences in iron uptake between phytoferritin and FAC when pH and time variables were studied together. One-way repeated measures ANOVA with Tukey's multiple comparisons test was used to compare differences in iron uptake between phytoferritin and FAC. One-way repeated measures ANOVA with Dunnett's test were used to compare differences between phytoferritin and phytoferritin treated with chemical inhibitors. Differences were considered significant at $p < 0.05$.

4.3 Results

4.3.1 Phytoferritin purification, antibody cross-reactivity, and ELISA cross-reactivity

Marrowfat peas were used as the source of phytoferritin because of its naturally high ferritin concentration and low-cost/economical price per kg. Combined with the low cost of phytoferritin extraction (per communication with Dr. Balk), if scaled-up approaches are used, the use of pea ferritin as a nutritional iron supplement is feasible.

Extracted phytoferritin from dried marrowfat peas as the crude fraction (CF) and its subsequent purification using gel filtration is shown below (Figure 4.1). Phytoferritin is a large protein (552 kDa) and does not interact with the packed column; thus it elutes at the beginning in the void volume. Fractions of purified phytoferritin (F1-F5) are also shown and the majority eluted at F2 and F3. All fractions were pooled together for *in vitro* digestibility and cell culture studies. The purified phytoferritin contained ca. 2360 ± 20 Fe atoms per protein shell.

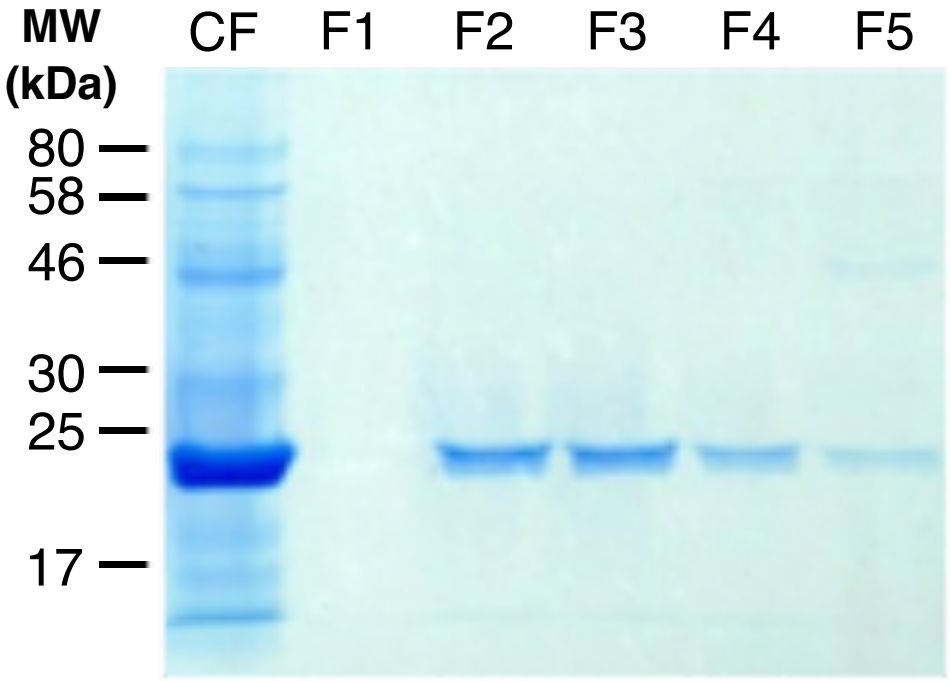

Figure 4.1 SDS-PAGE of purified phytoferritin from peas (*Pisum sativum*).

The gel was stained with Coomassie blue to detect total proteins. Lane 1 represents the crude fraction (CF). After gel filtration, purified phytoferritin was collected in the flow through (F1-F5) found within the void volume.

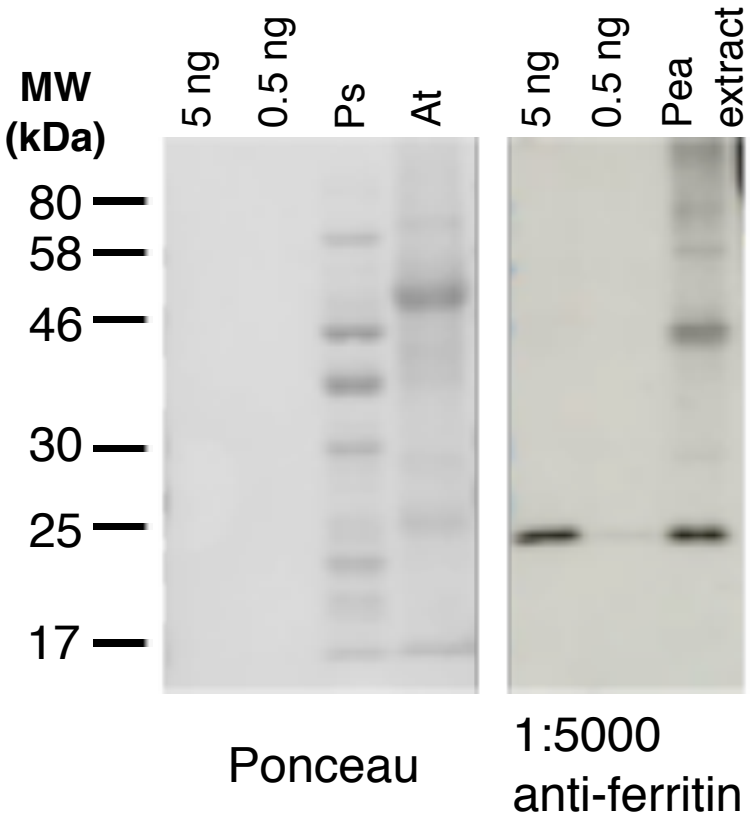

Figure 4.2 Western blot of purified phytoferritin from peas (*Pisum sativum*).

The immunoblot was stained with Ponceau-S for total protein (left panel) and labeled with anti-pea ferritin antibodies (right panel). The immunosignal from 5 and 0.5 ng of purified pea ferritin was compared to the signal in the total pea extract.

Antibodies (Ab) raised against pea ferritin showed high specificity. As shown in Figure 4.2 (right panel), Ab was also sensitive and could detect 0.5 ng pea ferritin. Gel and blot are courtesy of Dr. Jorge Celma-Rodriguez.

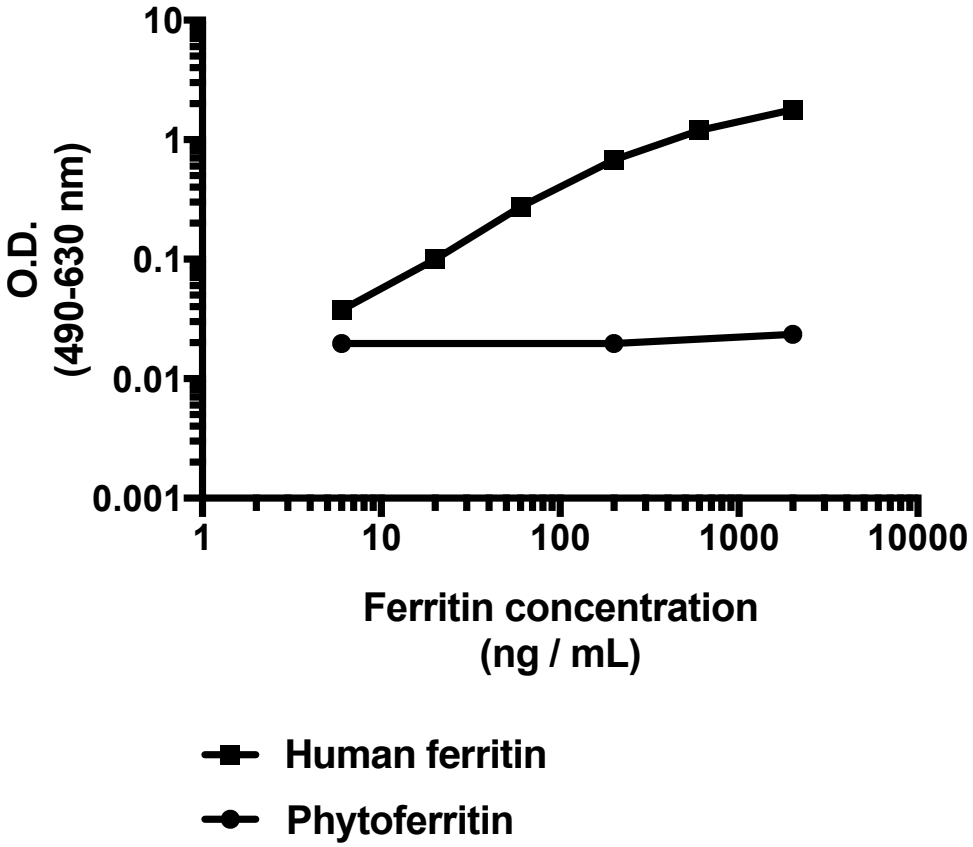

Figure 4.3 Cross-reactivity of the human ferritin ELISA kit (Ramco) with purified phytoferritin from *P. sativum*.

A standard curve was generated with pre-calibrated human ferritin standards (6, 20, 200, 600, 2000 ng/mL) provided by the manufacturer. Separate wells were incubated with 20, 200, and 2000 ng/mL phytoferritin.

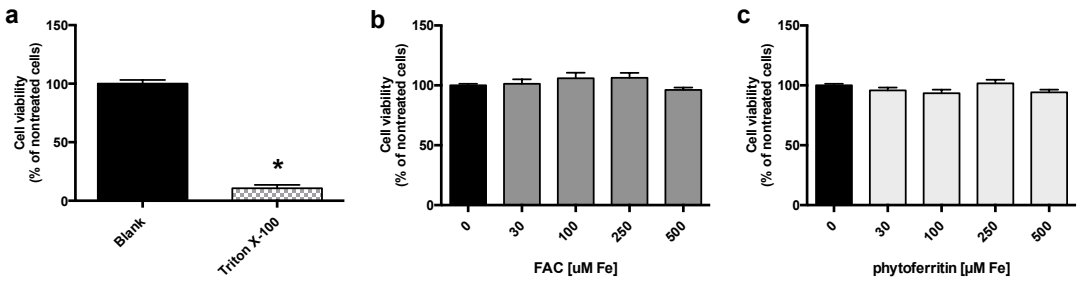

Figure 4.4 Viability of Caco-2 cells exposed to increasing concentrations of FAC and phytoferritin.

Cells were treated (a) 1% Triton X-100 (positive control), (b) FAC, and (c) phytoferritin at increasing dose concentrations for 24 hrs. After 24 hrs, cell viability was assessed using the MTS cell proliferation assay (CellTiter® 96 MTS, Promega) using manufacturers instructions.

The commercial human ferritin ELISA kit was tested for cross-reactivity with phytoferritin. This experiment was conducted to address concerns that measuring cell ferritin formation would underestimate iron uptake if phytoferritin were in fact absorbed intact in cells and not lysosomally degraded by the time of measurement. A signal was not detected for phytoferritin at low, medium, or high protein concentrations of the standard curve. The maintenance of healthy cells after phytoferritin and FAC treatments was also measured. Using the MTS cell proliferation assay (CellTiter® 96 MTS, Promega), cell viability compared to non-treated cells was the same across increasing iron concentrations (30, 100, 250, and 500 μM Fe) for phytoferritin and FAC.

4.3.2 An endocytosis pathway is involved in iron uptake from phytoferritin

Confocal images were generated to provide evidence that phytoferritin is directly absorbed in Caco-2 cells. In Figure 4.5, green fluorescence, indicative of phytoferritin, was associated with the cell monolayer after 1 hr incubation. Further detailed analysis using optical slices generated across the z-axis (Figure 4.5) revealed that phytoferritin is localised intracellularly (bottom panel, green fluorescence).

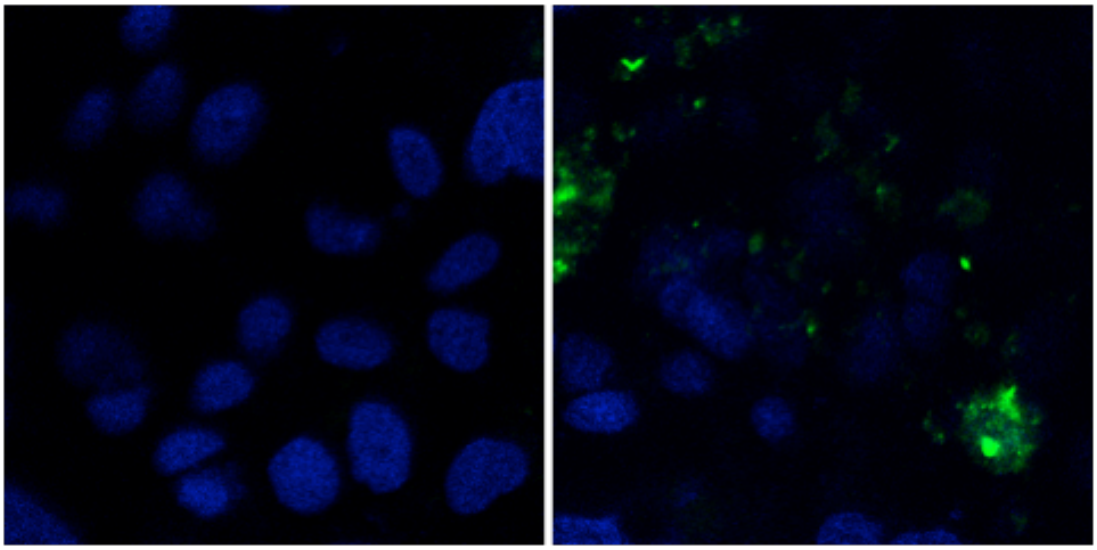

Figure 4.5 Confocal microscopy of phytoferritin interaction with Caco-2 cells at the cell surface.

The left panel depicts untreated cells and the right panel depicts phytoferritin-treated cells. Cell fixation, permeabilization, and staining were identical for both images. Blue signifies the DAPI nuclear stain; green for phytoferritin.

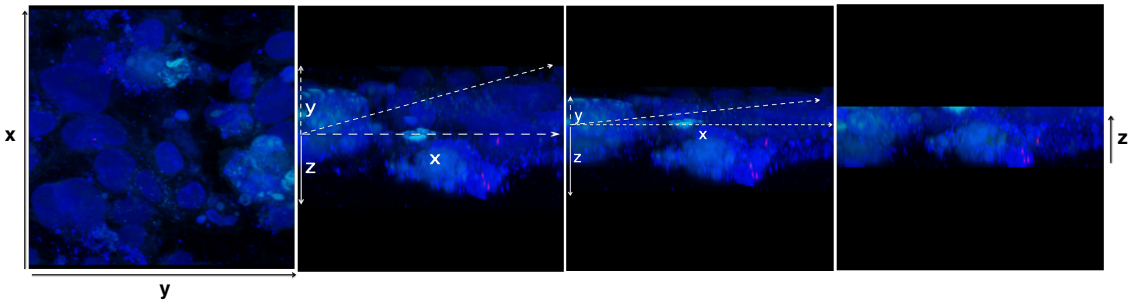

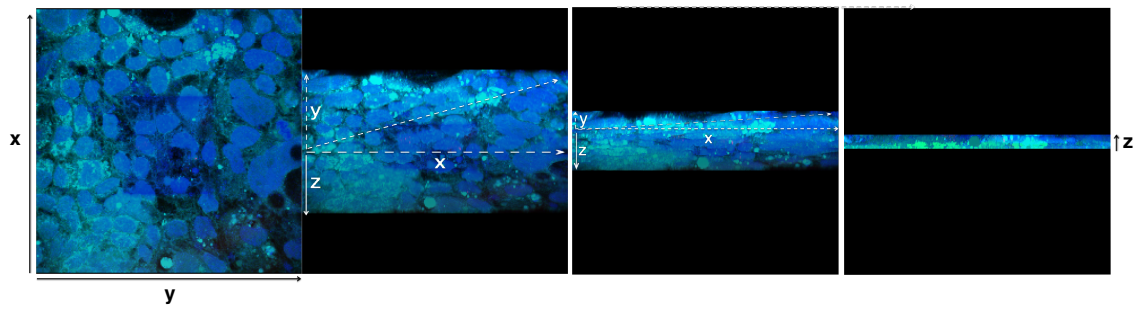

Figure 4.6 Z-axis projection of internalised pea ferritin in Caco-2 cells.

Caco-2 cells were untreated (top panel) or phytoferritin-treated (bottom panel) and images from left to right were derived from rotation on the z-axis. The first column depicts Caco-2 cells on the x and y axis; bottom image contains green fluorescence- associated cells. The last column depicts the z-projection of Caco-2 cells; the bottom image displays green fluorescence indicative of phytoferritin internalisation.

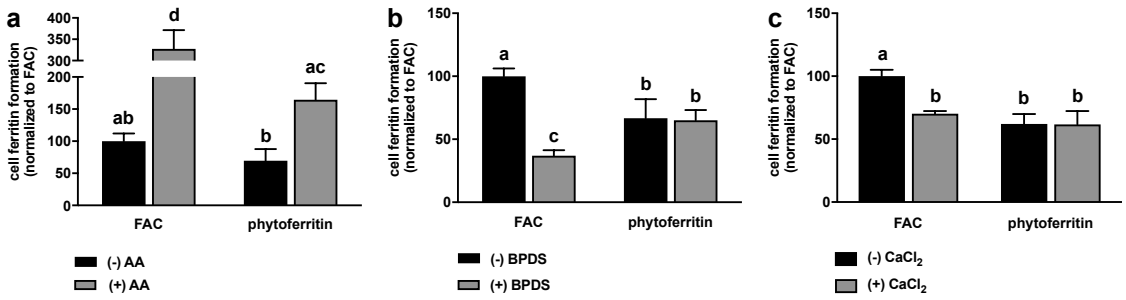

Figure 4.7 Iron uptake of phytoferritin after incubation with Fe^{2+} enhancer or inhibitors after 24 hrs.

Caco-2 cells were incubated with phytoferritin or FAC (30 µM Fe) and (a) AA (in the digest), (b) BPDS (in MEM), or (c) $CaCl_2$ (in MEM) for 24 hrs. Cell ferritin formation was normalized relative to FAC treatments. Data are expressed as the means ± SEM of two independent experiments (n = 3 per experiment). Different letters indicate statistically significant differences ($p < 0.05$).

To further verify if native phytoferritin is absorbed intact and whether DMT1 is required for uptake, enhancers and inhibitors of non-haem iron

absorption were used. AA catalyses the reduction of Fe^{3+} to Fe^{2+}, BPDS is a chelator of Fe^{2+}, the iron oxidation state required for DMT1, and calcium inhibits iron uptake by removing DMT1 cell surface receptors. Iron uptake from phytoferritin with AA was increased 2-fold compared to control when incubated for 24 hrs (1:20 Fe:AA molar ratio). This increase in iron was less than for FAC, which had a 3-fold increase in iron uptake in the presence of AA.

Incubation of phytoferritin with BPDS for 24 hrs did not affect iron uptake compared to phytoferritin alone, which contrasts with FAC. Iron uptake from FAC was significantly reduced in the presence of BPDS (60%). Iron uptake from phytoferritin incubated with BPDS was significantly greater than FAC incubated with BPDS (50%).

Similar to BPDS, $CaCl_2$ (2.5 mM) co-incubated with native phytoferritin for 24 hrs did not affect iron uptake compared to phytoferritin alone. In contrast, iron uptake from FAC incubated with $CaCl_2$ was reduced by 40%. Although iron uptake as phytoferritin was significantly less than FAC, when both iron treatments were incubated with $CaCl_2$, iron uptake was similar.

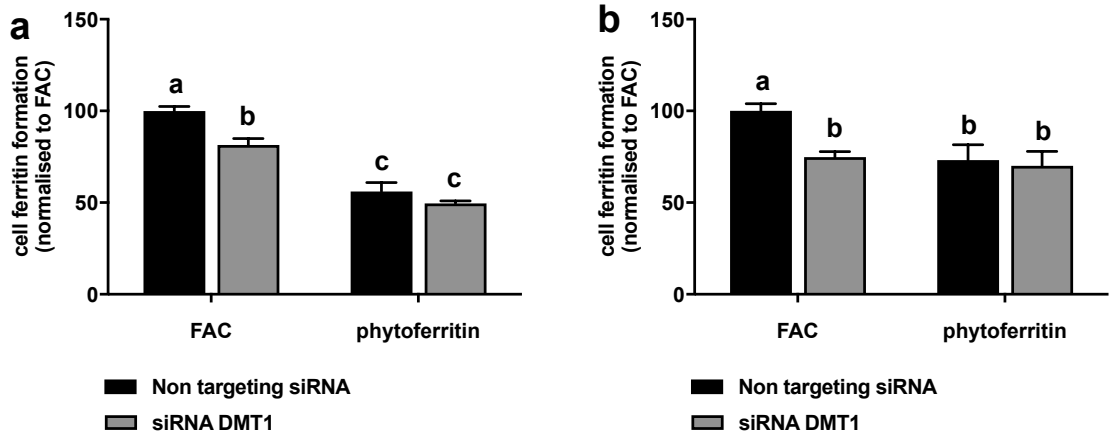

Figure 4.8 Iron uptake of phytoferritin after cellular transfection with siRNA targeting DMT1 or Negative control 1.

Cells were treated with phytoferritin or FAC for 1 hr (100 µM Fe). Knockdown of the DMT1 transcript was conducted in (a) Caco-2 or (b) Hutu-80 cells. Cell ferritin formation was normalised relative to FAC treatments. Data are expressed as the means ± SEM of three independent experiments (n = 3 per experiment).

BPDS and $CaCl_2$ co-incubation with phytoferritin demonstrated that DMT1 was not required for the uptake of phytoferritin-Fe. To verify this observation, siRNA silencing of the DMT1 transcript was used. Caco-2 and Hutu-80 cells In Caco-2 cells, siRNA transfection resulted in 20% knockdown of *DMT1* gene expression and a 20% decrease in iron uptake from FAC. Iron uptake from phytoferritin was not inhibited when incubated in knockdown DMT1 Caco-2 cells compared to phytoferritin in non-targeting siRNA cells.

Hutu-80 cell transfection with siRNA resulted in the reduction of *DMT1* gene expression by 50%. Similar to Caco-2 cells, siRNA targeting *DMT1* did not have an effect on iron uptake from phytoferritin, but did reduce iron uptake from FAC. Surprisingly, we found that phytoferritin uptake relative to FAC was more efficient in transfected Hutu-80 cells compared to Caco-2 cells.

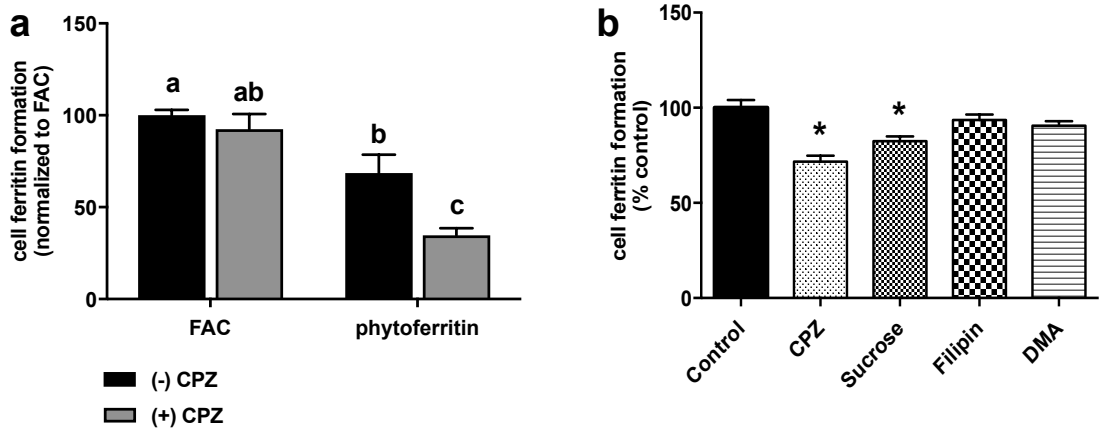

Figure 4.9 Iron uptake of phytoferritin in Caco-2 cells with endocytosis inhibitors.

Caco-2 cells were either (a) pre-incubated with CPZ for 1 hr, which was replaced with phytoferritin (100 μM Fe) for 1 hr or (b) co-incubated with phytoferritin (100 μM Fe) and endocytosis inhibitors for 1 hr. Cell ferritin formation was normalized relative to (a) FAC treatments or (b) control (cells treated without inhibitors). Data are expressed as the mean ± SEM of two independent experiments (n = 3 per experiment). Different letters indicate statistically significant differences ($p < 0.05$).

To investigate alternative pathways of iron uptake that are distinct from DMT1, Caco-2 cells were pretreated with CPZ, an inhibitor of clathrin-mediated endocytosis. Cells treated afterwards with phytoferritin (30 μM Fe) for 24 hrs resulted in a 50% decrease in iron uptake. Conversely, cell pretreatment with CPZ had no effect on iron uptake from FAC.

Chemical inhibitors targeting specific endocytosis pathways were also used to explore mechanisms of iron uptake from phytoferritin. Similar to the previous result, clathrin endocytosis inhibitors, CPZ and sucrose, decreased iron uptake from native phytoferritin by 25 and 20 percent, respectively. In contrast, incubating Caco-2 cells with clathrin-independent endocytosis inhibitors, filipin or DMA, did not affect iron uptake from phytoferritin.

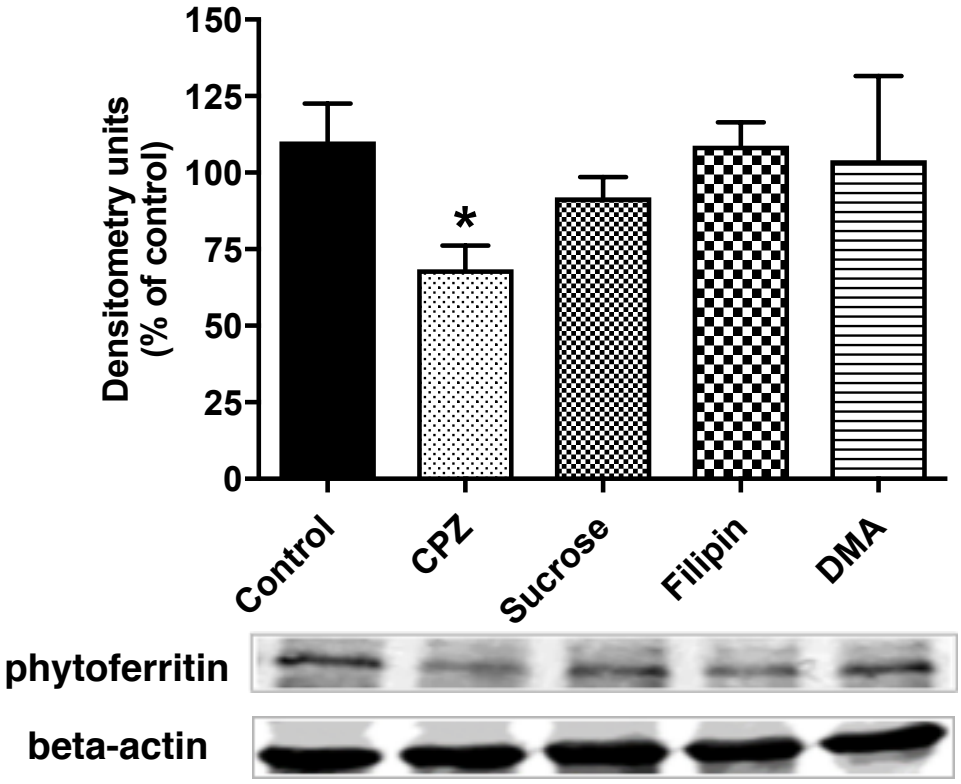

Figure 4.10 Western blot detection of phytoferritin associated with Caco-2 cells.

Phytoferritin (100 µM Fe) was co-incubated with endocytosis inhibitors in MEM for 1 hr and cells were immediately lysed for protein extraction. Phytoferritin was detected in cell lysates using Western blot analysis. Data are expressed as the means ± SEM of two independent experiments (n = 2 or 3 per experiment). Differences indicated with an asterisk are considered significant at $p < 0.05$.

Cell extracts were analysed by Western blot analysis for direct detection of phytoferritin uptake. Using the same conditions as for Figure 4.9, CPZ significantly inhibited phytoferritin uptake. To a lesser degree, sucrose inhibited phytoferritin uptake but the difference was not statistically significant. Similar to Figure 4.8, filipin and DMA did not inhibit phytoferritin uptake.

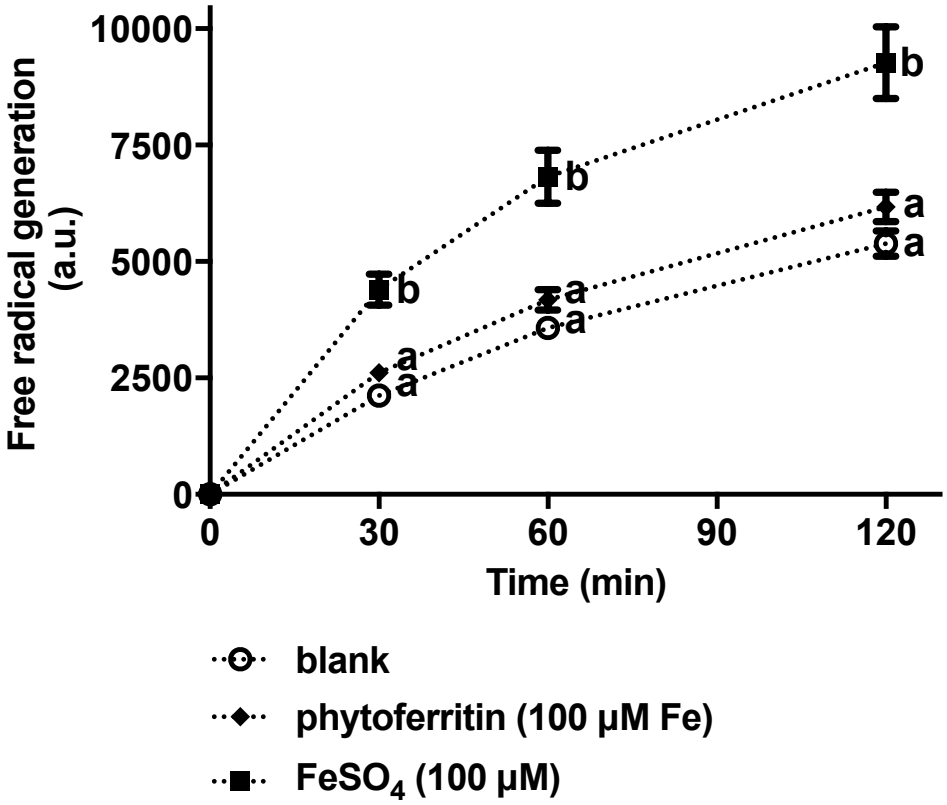

Figure 4.11 Free radical generation from phytoferritin in Caco-2 cells.

Cells were treated with 100 µM Fe as phytoferritin or $FeSO_4$ (combined with bovine serum albumin [BSA] to normalise protein concentrations) for 0, 30, 60 and 120 min and measured for free radical generation. Data are expressed as the means ± SEM of two independent experiments (n = 4 per experiment). Different letters indicate statistically significant differences at each time point ($p < 0.05$). Experiments were conducted by Dr. Ildefonso Rodriguez-Ramiro, Fairweather-Tait lab.

To evaluate phytoferritin as a supplemental iron source, it was tested for its ability to generate reactive oxygen species, relative to $FeSO_4$, in Caco-2 cells. After 30 min, free radical generation was 60% higher in $FeSO_4$ compared to phytoferritin treated cells. The differences in free radical generation between the 2 iron sources were sustained over time. Free radical generation in phytoferritin treated cells was not significantly different from control cells.

4.3.3 Phytoferritin, either from whole foods or purified, is not resistant to cooking and/or gastric digestion, and its iron uptake occurs through DMT1.

Phytoferritin has been suggested to be a target for crop biofortification. In this study, it was examined whether the protein, as the whole food, is resistant to breakdown when subjected to different states representative of a consumed food, such as cooking or gastric digestion.

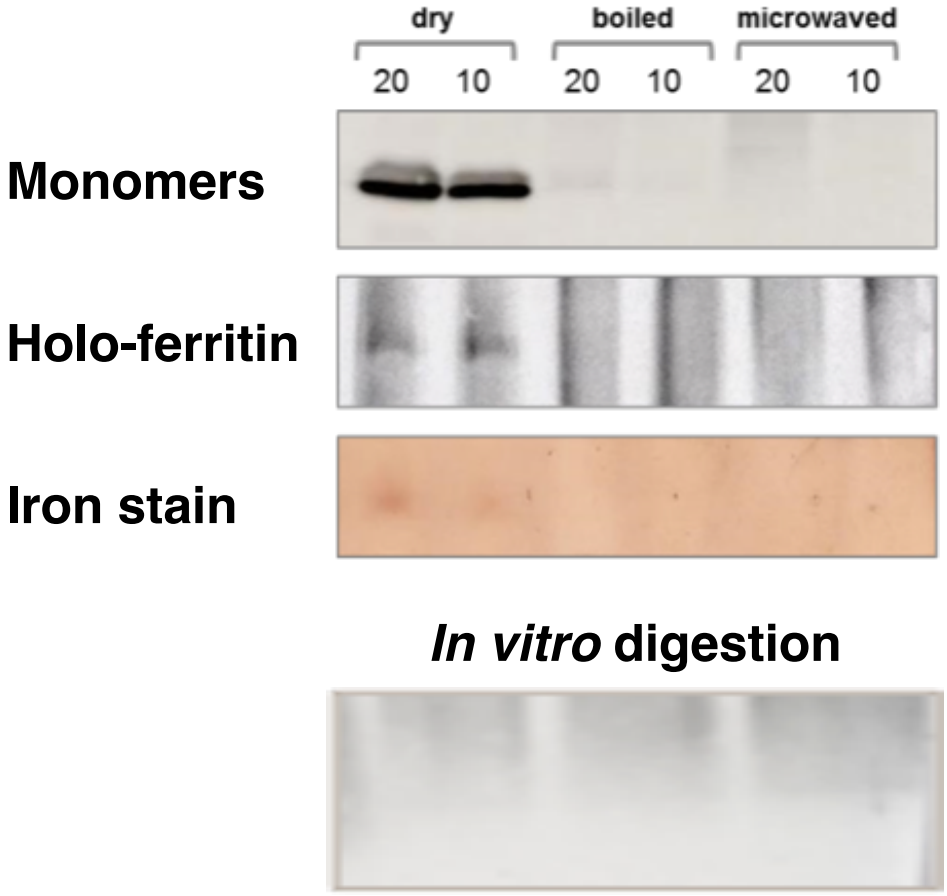

Figure 4.12 Western blots displaying the effect of cooking and *in vitro* digestion on phytoferritin monomers, holo-ferritin, and iron-sequestered ferritin in marrowfat peas.

Phytoferritin protein from dry marrowfat peas was determined after 1 hr boiling, 5 min microwaving, or *in vitro* digested. The protein load was 10 or 20 mg. Images courtesy of Dr. Emily Jones, Balk lab.

Phytoferritin extracted from dried marrowfat peas were intact and detected in the monomers (23 kDa) and holo-ferritin (552 kDa). Staining of iron in the protein was clear when 10 and 20 mg of protein were loaded onto gels using the modified Perls' reaction. In contrast, boiling, microwaving, and *in vitro* digestion resulted in the degradation of the monomers, holo-ferritin, and release of iron-sequestered ferritin.

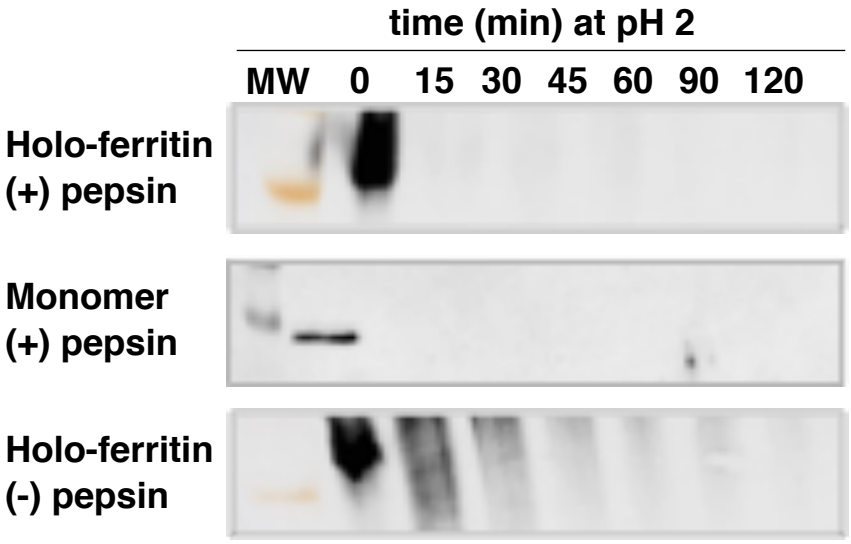

Figure 4.13 Western blots of phytoferritin digested at pH 2 ± pepsin with time.

Phytoferritin was digested for up to 120 min. The MW marker used for reference in the NATIVE gels (and WB) was horse-spleen ferritin, which stains at 440 kDa.

The degradation of phytoferritin was evident using time-course gastric digestion. Both holo-ferritin and the ferritin monomers degraded rapidly when pepsin was added at pH 2. Phytoferritin was not detected in either blot after 15

min. The rate of holo-ferritin degradation was reduced without pepsin, but after 45 min, the majority was completely degraded.

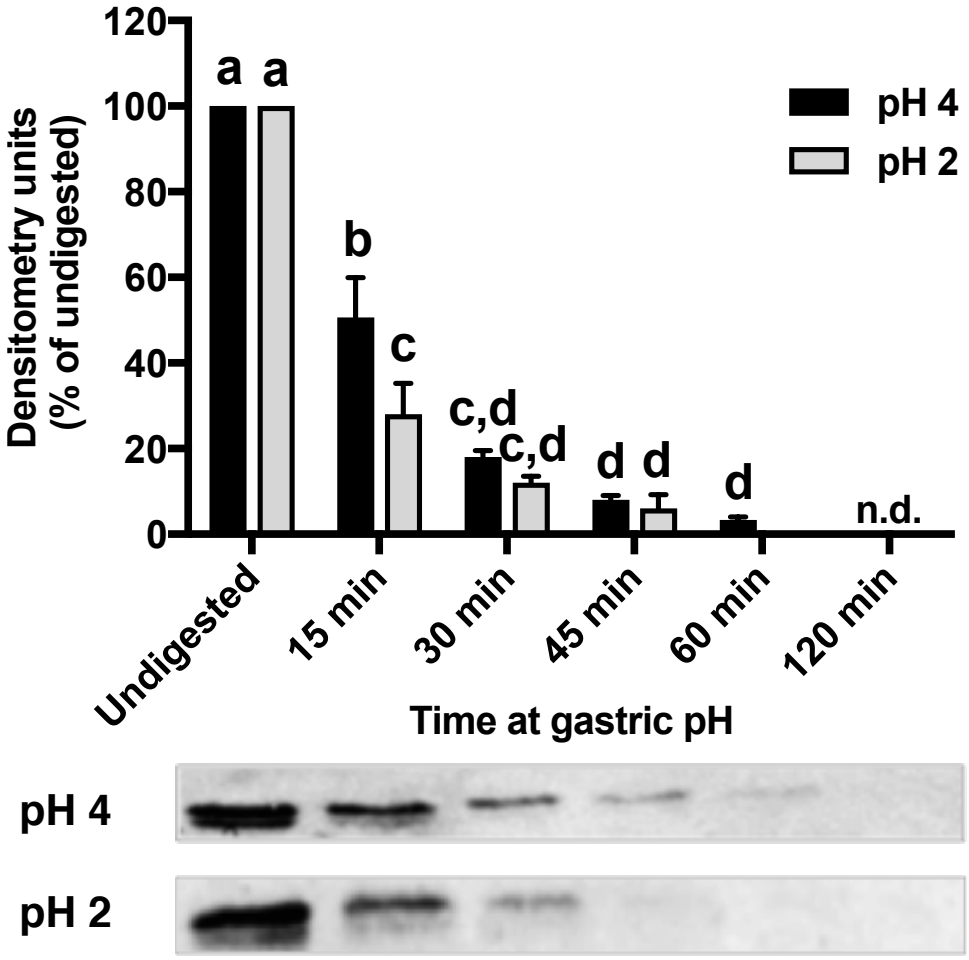

Figure 4.14 Time-course degradation of phytoferritin exposed to pH 2 and 4.

Phytoferritin was incubated at pH 2 or pH 4 (37°C) and analysed using Western blots at 15, 30, 45, 60, and 120 min. Data are expressed as the means ± SEM of three independent experiments (n = 3**).** Different letters indicate statistically significant differences ($p < 0.05$).

The effect of gastric pH on phytoferritin protein stability was examined to understand whether the protein is broken down in the stomach. Furthermore, because 3 states of phytoferritin are thought to exist in the intestinal lumen, the

fraction of soluble iron, and indirectly the iron core was also measured. Phytoferritin was incubated at low (pH 2) and less acidic (pH 4) conditions and its protein levels semi quantified. Comparatively, the rate of phytoferritin degradation was faster at pH 2 compared to pH 4. After 15 min at pH 2, 70% of phytoferritin was degraded, compared to 50% at pH 4. At 60 min, the levels of phytoferritin incubated at pH 2 were below the limit of detection.

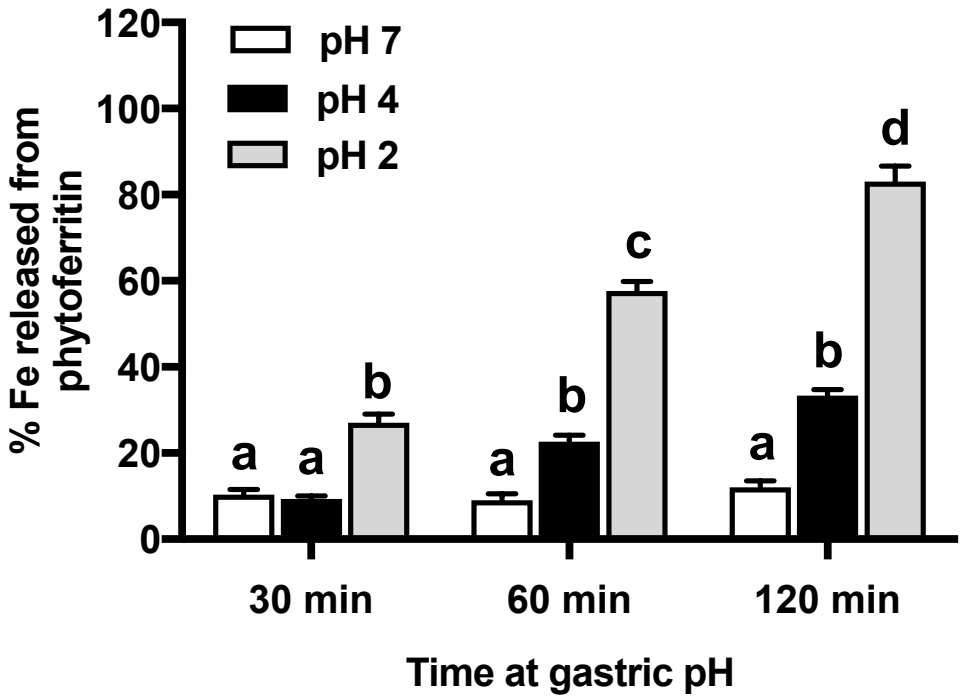

Figure 4.15 Time-course release of iron from phytoferritin exposed to pH 2 and 4.

Phytoferritin was incubated at pH 2 or pH 4 (37°C) and analysed for soluble iron at 30, 60, and 120 min. Data are expressed as the means ± SEM of three independent experiments (n = 3**).** Different letters indicate statistically significant differences ($p < 0.05$).

The effect of gastric pH on soluble iron (released iron), hydrolysed from the phytoferritin iron core, was assessed. Soluble iron increased over time as a

result of lower pH. At pH 2, 80% of the iron was solubilised after 120 min compared to 25% at pH 4. As a control, phytoferritin was also assessed for soluble iron at pH 7. This resulted in ca. 10% soluble iron independent of time.

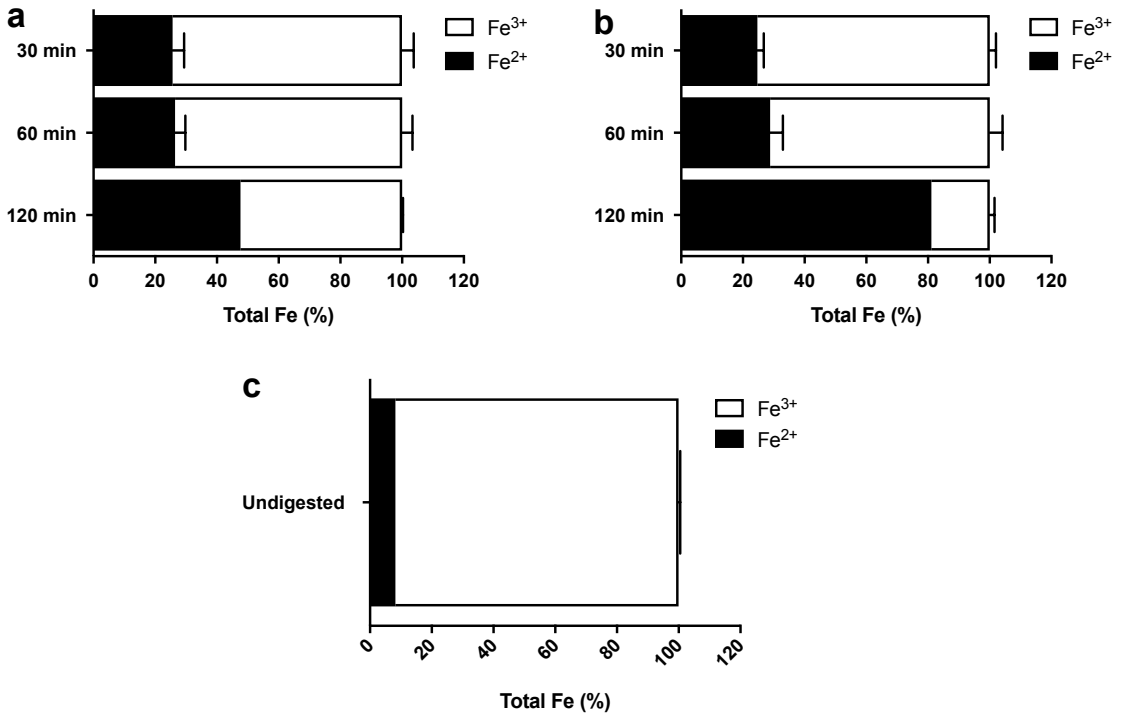

Figure 4.16 Time-course determining the Fe^{3+}/Fe^{2+} ratio during gastric pH treatment.

Phytoferritin was pH treated at (a) pH 4 or (b) pH 2 and the iron determined using the Ferene assay with and w/o AA. These values were used to calculate Fe^{3+}/Fe^{2+} ratios. The Fe^{3+}/Fe^{2+} ratio was also determined in (c) undigested phytoferritin. Data are expressed as the means ± SD of two independent experiments (n = 2**).**

Fe^{2+} and Fe^{3+} iron species were measured during gastric pH treatment at pH 2 and pH 4. Undigested phytoferritin (diluted in PBS) contained the majority of its iron as Fe^{3+}, consistent with its ferric oxyhydroxide core. After 30 and 60 min of pH treatment, the percentage of iron as Fe^{2+} increased to 25-30% of the total iron at pH 2 and pH 4. Differences in iron species between pH digestions and

different pH values were evident with longer digestion times. At 120 min, 80% of the total iron at pH 2 was Fe^{2+} while only 50% was Fe^{2+} at pH 4.

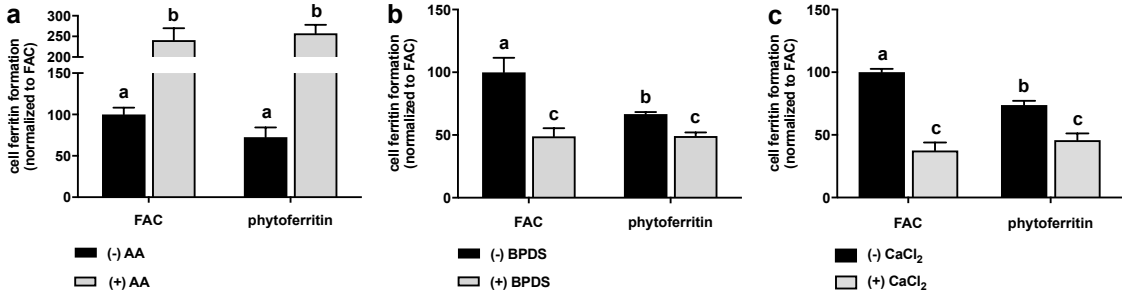

Figure 4.17 Iron uptake of pH treated phytoferritin with Fe^{2+} enhancer or inhibitors in Caco-2 cells.

Caco-2 cells were incubated with pH treated phytoferritin or FAC (30 μM Fe) and (a) AA (in the digest), (b) BPDS [in MEM], or (c) $CaCl_2$ [in MEM] for 24 hrs. Cell ferritin formation was normalised relative to FAC treatments. Data are expressed as the means ± SEM of two independent experiments (n = 3 per experiment). Different letters indicate statistically significant differences ($p < 0.05$).

We found that BPDS and $CaCl_2$ had no effect on iron uptake from native phytoferritin. Thus, we also investigated whether these non-haem iron inhibitors would affect gastric pH treated phytoferritin. Iron uptake from pH treated phytoferritin was increased over 2-fold in the presence of AA. This increase was similar to the increase observed with pH treated FAC with AA. In contrast with undigested phytoferritin (Figure 4.7), where iron uptake was less responsive to incubation with AA, iron uptake was higher in pH treated phytoferritin with AA.

The iron uptake of pH treated phytoferritin was inhibited when was incubated with BPDS. This inhibition was not to the same extent as pH treated FAC (50%). For both undigested and pH treated FAC, BPDS inhibited iron

uptake. These results are in contrast to undigested phytoferritin, where BPDS had no effect on iron uptake.

Similar to BPDS, $CaCl_2$ incubated with pH treated phytoferritin inhibited iron uptake after 24 hrs. The effect of $CaCl_2$ on iron uptake from pH treated phytoferritin differed from undigested phytoferritin, in which iron uptake was not inhibited. In both pH treated and undigested FAC, $CaCl_2$ significantly inhibited iron uptake.

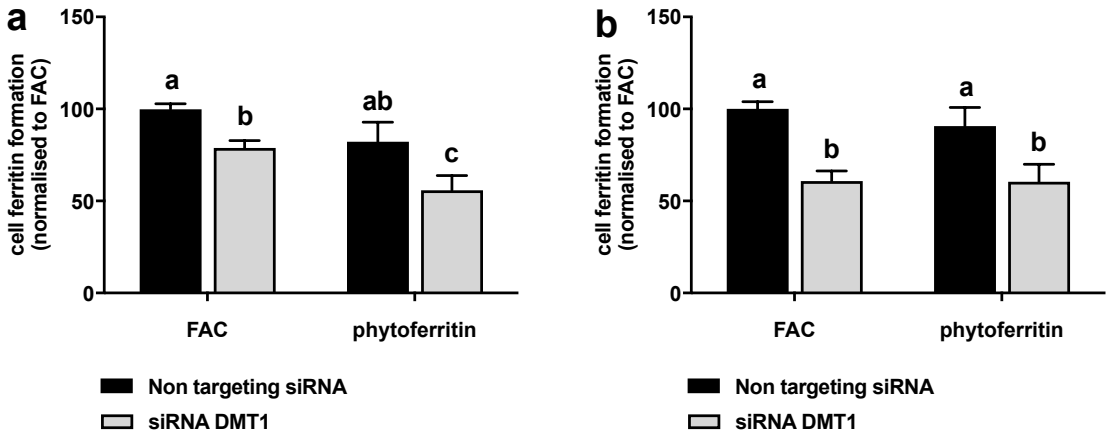

Figure 4.18 Iron uptake of pH treated phytoferritin after celluar transfection with siRNA targeting DMT1 or Negative control 1.

Cells were treated with pH treated phytoferritin or FAC for 1 hr (100 µM Fe). Knockdown of the DMT1 transcript was conducted in (a) Caco-2 or (b) Hutu-80 cells. Cell ferritin formation was normalised relative to FAC treatments. Data are expressed as the means ± SEM of three independent experiments (n = 3 per experiment).

To confirm that gastric pH treatment of phytoferritin would result in iron uptake using DMT1, Caco-2 and Hutu-80 cells were also transfected with siRNA. Iron uptake from pH treated phytoferritin in Caco-2 cells transfected with siRNA targeting DMT1 was significantly decreased (40%) compared to non-targeting siRNA controls. A decrease in iron uptake for pH treated FAC was also observed.

These data are in contrast to undigested phytoferritin. While iron uptake from pH treated and undigested FAC were equally inhibited in DMT1 siRNA treated cells, no effect was seen in undigested phytoferritin.

Similar to the Caco-2 cell data, iron uptake from pH treated phytoferritin was significantly inhibited in Hutu-80 cells treated with siRNA DMT1. This inhibition did not occur when cells were incubated with undigested phytoferritin. Iron uptake was inhibited to a great extent in Hutu-80 cells treated with siRNA DMT1 (40%) compared to Caco-2 cells treated with siRNA DMT1 (20%), likely due to differences in siRNA transfection efficiency.

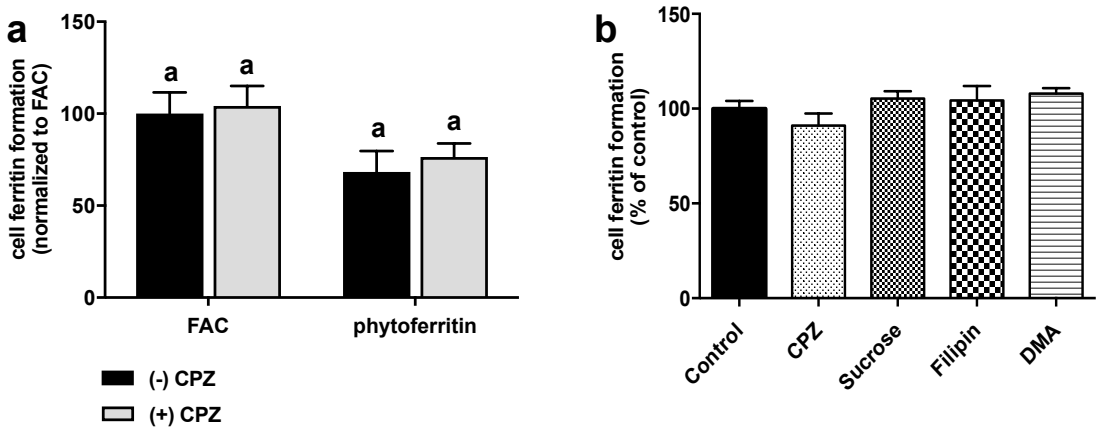

Figure 4.19 Iron uptake of pH treated phytoferritin in Caco-2 cells with endocytosis inhibitors.

Caco-2 cells were either (a) pre-incubated with CPZ for 1 hr and replaced with pH treated phytoferritin (100 µM Fe) for 1 hr or (b) co-incubated with pH treated phytoferritin (100 µM Fe) and endocytosis inhibitors for 1 hr. Cell ferritin formation was normalised relative to (a) FAC treatments or (b) control (cells treated without inhibitors). Data are expressed as the mean ± SEM of two independent experiments (n = 3 per experiment). Different letters indicate statistically significant differences ($p < 0.05$).

CPZ pretreatment of Caco-2 cells had no effect on iron uptake from pH treated phytoferritin, whereas CPZ had a large inhibitory effect (50%) on iron uptake from native phytoferritin. The other endocytosis inhibitors did not effect iron uptake from either phytoferritin or FAC.

4.4 Discussion

Findings of studies reporting iron bioavailability from phytoferritin using animal models have been mixed [307-310]. This is likely because different methods were used to label the iron core of phytoferritin between studies [169, 305]. In these current experiments, cell ferritin formation in Caco-2 cells was measured as a surrogate marker of iron absorption [31] to eliminate the requirement for isotopic labeling. Despite the variability of phytoferritin-iron uptake in Caco-2 cells, on average iron uptake was 70% of FAC, suggesting that its potential bioavailability is comparable.

To investigate the mechanisms underlying iron uptake of phytoferritin, chemicals targeting either DMT1 transport or endocytosis pathways were used. An increase in iron uptake from phytoferritin with AA was observed, which has been shown to induce iron mobilisation from phytoferritin via its strong reducing properties [350-352]. Incubation of phytoferritin with BPDS, an inhibitor of DMT1-mediated Fe^{2+} transport in Caco-2 cells [46], had no effect on iron uptake. These results concur with Kalgaonkar et al [353], who reported that phytates (1:10 Fe:PA) and tannins (1:50 Fe:TA), potent inhibitors of non-haem iron absorption, had no effect on iron uptake from soybean ferritin in Caco-2 cells.

Additionally, $CaCl_2$, an inhibitor of non-haem iron uptake [47-49], was used to further investigate Fe^{2+} dependent-mechanisms. Thompson et al [25] demonstrated that incubation of Caco-2 cells with $CaCl_2$ resulted in the internalisation of DMT1 from brush border microvilli, thereby inhibiting FAC uptake. Similar to this study, incubation of FAC with $CaCl_2$ in these experiments

inhibited iron uptake by 50%. $CaCl_2$ did not affect iron uptake from phytoferritin. To firmly establish the role of DMT1 on iron uptake from phytoferritin, siRNA was used to knockdown gene expression in Caco-2 and Hutu-80 cells. Hutu-80 cells were used in addition to Caco-2 cells for further validation; they also express DMT1 and its transfection efficiency is much higher [125, 329, 354]. There was no effect of DMT1 siRNA treatment on iron uptake from phytoferritin in either cell line, suggesting that DMT1 is dispensable for phytoferritin-iron uptake.

Confocal microscopy was used and provided evidence for the presence of intact phytoferritin in Caco-2 cells. Cells were labeled with primary antibodies against pea ferritin and secondary Alexa-Fluor 488 conjugated antibodies showed green fluorescent patches indicative of phytoferritin uptake.

In previous studies, soybean phytoferritin uptake in Caco-2 cells has been shown to occur via endocytosis [316, 317, 319]. In this study, iron uptake from phytoferritin was inhibited in cells treated with CPZ [286, 331, 332]; iron was not inhibited with filipin or DMA treatment. Pretreatment of cells with CPZ had a greater inhibitory effect on iron uptake than CPZ and phytoferritin co-treatment, which could reflect the slow absorption profile of phytoferritin [316]. To validate the effects of CPZ inhibition on both iron uptake and phytoferritin uptake, phytoferritin in cell lysates were detected using the same chemical endocytosis inhibitors listed previously. Bands detecting phytoferritin in Western blots were significantly decreased compared to control. The data generated strongly indicates that intact native phytoferritin is taken up by Caco-2 cells via clathrin-mediated endocytosis, which is in agreement with previous findings [317].

The benefits of phytoferritin as an iron supplement are three-fold; a sustainable iron source, well absorbed comparatively to soluble iron salts, and an inability to be affected by dietary inhibitors of non-haem iron absorption such as phytates and tannins. Biofortification of staple crops to increase phytoferritin

concentrations has been suggested as a strategy to increase bioavailable iron in large-scale populations [294, 300]. The data suggests that phytoferritin biofortification is unnecessary. In agreement with Hoppler et al [298], the Western blots indicated that cooking processes would likely degrade phytoferritin prior to consumption. Moreover, any remaining phytoferritin in the food will likely be degraded by digestion. In turn, dietary iron inhibitors, such as polyphenols in marrowfat peas, will likely prevent the absorption of released iron from phytoferritin. Thus, as suggested by Hoppler et al [299], crop breeding for improvement in total iron may be a better strategy than breeding for high ferritin crops, per se.

We investigated the effect of gastric digestion in greater detail. Chenyan et al [315] recently reported that more than 40% of phytoferritin protein derived from soybeans remained intact 45 min after *in vitro* digestion. In the present study, the degradation of phytoferritin at pH 2 and pH 4 was monitored using antibodies specific for phytoferritin; about 90% of phytoferritin was degraded after 45 min. The addition of pepsin (0.4% w/v) at pH 2 fully degraded phytoferritin after 15 min, similar to the results of Hoppler et al [298]. While the absolute rates of phytoferritin protein digestion have been shown to be variable at differing pH levels [298, 311, 312, 315, 353], significant degradation occurred at pH 2 in this study and suggests that phytoferritin is broken down under gastric conditions.

In addition, dissolution to Fe^{2+} and Fe^{3+} was investigated in pH treated phytoferritin. Ultrafiltration [286] was used to partition soluble iron (containing Fe^{2+} and Fe^{3+} species) from the phytoferritin core and protein at low pH. More soluble iron was released at pH 2 compared to pH 4, and a time dependent effect was observed. Moreover, in comparison to the phytoferritin control, Fe^{2+} formation increased significantly at both pH 2 and 4. These experiments suggest that phytoferritin exposure to gastric pH solubilises a large percentage of iron to Fe^{2+} or Fe^{3+}.

Similar cell culture experiments and conditions were undertaken for pH treated phytoferritin for comparison to undigested phytoferritin. The Caco-2 cell model to assess iron bioavailability from phytoferritin under *in vitro* conditions [218, 342] was used except that dialysis membranes were omitted. This was a requirement as it screens for soluble iron and thereby would theoretically inhibit phytoferritin uptake [213]. The removal of dialysis membranes necessitated the use of pH treatments, as pancreatic/bile enzymes are destructive to the unprotected cell monolayer. The cell culture experiments showed that iron uptake from pH treated phytoferritin followed the same pathway as FAC. Thus, these comprehensive studies examining the effects pH treatment on iron uptake from phytoferritin are strongly suggestive that its exposure to gastric pH not only solubilises a large percentage of its iron to either Fe^{2+} or Fe^{3+}, but also that its iron is absorbed using the DMT1 transporter.

4.5 Conclusion

Phytoferritin is a promising, alternative source of supplemental iron. Protection of phytoferritin from gastric pH exposure to maintain its stability is important if consumed with non-haem iron inhibitors. Phytoferritin generated less free radicals than $FeSO_4$ when co-incubated with Caco-2 cells, suggesting that not is it bioavailable and likely to cause less toxicity compared to commonly prescribed $FeSO_4$ (which typically causes gastrointestinal distress). Encapsulation to enhance phytoferritin stability and human absorption studies are required to validate our findings.

Chapter 5: Lucky Iron Fish

5. Lucky iron fish

This chapter is based upon the manuscript entitled 'Iron bioavailability of the Lucky Fish iron ingot determined in Caco-2 cells.' The manuscript is currently in preparation.

5.1 Introduction

Global iron deficiency continues to be a public health burden, affecting over 2 billion people [91]. The highest incidences of iron deficiency occur in predominately low-income communities within developing countries [355], where largely plant-based diets lacking bioavailable iron are consumed [107]. Iron deficiency in these vulnerable groups is largely targeted using one or more strategies: iron supplementation, fortification of staple foods, and/or home fortification with micronutrient powders (MNP) [97, 117, 356, 357]. However, these approaches, while efficacious in many situations, suffer from problems associated with cost, bureaucracy, and distribution. For these reasons, simple, practical, and sustainable approaches to obtain iron without reliance on external factors would be particularly useful in remote communities with a high prevalence of iron deficiency.

Cooking in iron pots and its consequent leaching of iron is a sustainable strategy to increase the iron content of cooked foods [358-362]. The quantity of iron leached from pots has shown to be largely dependent on the pH and organic acid content of the cooked food [363]. There is evidence to suggest from several studies that cooking in iron pots results in improved iron status. Haemoglobin status of iron-deficient Wistar rats fed low-iron meals cooked in iron pots were greatly improved; these levels were similar to iron-deficient and iron-replete rats fed high-iron meals [364]. In several human intervention trials, the use of iron pots was efficacious in improving the iron status in adults [365], children [366], and infants [367]. Despite its benefits, the adoption and implementation of iron

pots in these communities is difficult. They are expensive, heavy, and vulnerable to rusting. Often this rusting leads to unacceptable discoloration of the food. All these factors diminish its acceptability, compliance and ultimately its usefulness for their intended communities [368, 369].

The Lucky Iron Fish™ (LIF), an iron ingot placed in a cooking vessel during the cooking process, has recently been commercialised and marketed as a small and affordable alternative iron source that is similar in principle to iron pots. A rather simple solution, results from clinical trials based in Cambodia investigating the efficacy of LIF to improve iron status in women have been mixed, which may, in part, be due to study design [370, 371]. Discrepancies in these trials necessitate further investigation into the determinants of iron bioavailability from LIF.

The aims of the present study were to characterise the potential bioavailability of iron from LIF in order to evaluate its utility as an alternative source of iron for human nutrition. Iron bioavailability was assessed using the Caco-2 cell model, a representative model of the intestinal epithelium [218] that correlates well with human absorption data [242, 268]. We examined oxidative stress to the cell monolayer, the optimal levels of AA required to increase iron solubility and iron uptake from LIF, and the effects of a food source and dietary iron inhibitors on iron bioavailability.

5.2 Methods and Materials

5.2.1 Samples and reagents

The LIF was purchased from its e-commerce online shop (www.luckyironfish.com/shop). After each iron extraction, the LIF was rinsed with copious amounts of milliQ H_2O, dried using paper towels and stored covered at room temperature. Frozen mangetout peas were purchased from a nearby

supermarket (Sainsbury, UK). These were used for inclusion in the food matrix because of their high iron content. 100 g peas were microwaved in an acid washed beaker with 9.5 mL milliQ H_2O for 2.5 min at 900 watts. The peas were removed from the water, frozen and lyophilised before use. Prior to digestion experiments, its iron concentration was determined using ICP-OES according to the methods of Rodriguez-Ramiro et al [151].

All chemical reagents were purchased from Sigma unless otherwise stated. Stock solutions of ascorbic acid (AA), phytic acid (PA), and tannic acid (TA) were diluted in H_2O and freshly made prior to each experiment.

- In the first set of experiments, AA, a potent enhancer of non-haem iron uptake [122, 128], was used to determine the concentrations required to increase iron uptake from LIF-extracted iron. AA was added at the gastric step (pH 2) and molar ratios were relative to iron concentrations leached from LIF (ca. 1 mM Fe); AA was added at 1 and 10 mM to achieve a molar ratio of Fe:AA 1:0, 1:1, and 1:10, respectively.
- In the second set of experiments, PA and TA were added after AA at the gastric step [249]. AA, PA and TA molar ratios were relative to the iron concentration of $FeSO_4$ or peas (50 µM Fe); AA was added at 500 µM to achieve a molar ratio of Fe:AA 1:10, PA was added at 50, 250, 500, and 1000 µM to achieve molar ratios of Fe:PA 1:1, 1:5, 1:10, and 1:20, and TA was added at 5, 25, 50, and 500 µM to achieve molar ratios of Fe:TA 1:0.1, 1:0.5, 1:1, and 1:10.

5.2.2 LIF iron release

Depending on the experiment, 1 L of milliQ H_2O or 40 mM NaCl, 5 mM KCl solution (acidified to pH 2 with HCl) was heated in an acid-washed beaker to a rapid boil. The LIF ingot was placed in the boiling solution for 10 min and then removed, closely approximating the manufacturer's instructions. Aliquots of 25

mL were removed and allowed to cool at room temperature. AA was added, and the pH of the LIF solution was gradually increased to 7 with 0.1 M $NaHCO_3$. Samples were diluted 1:10, 1:3, or 1:1 in MEM depending on the experiment undertaken.

5.2.3 MTS Cell Proliferation

Differentiated Caco-2 cells were grown in 96-well plates. Cells were incubated with LIF for 24 hrs. After 24 hrs, the MTS cell proliferation assay (CellTiter® 96 MTS, Promega) was used according to manufacturer's instructions. For detailed methodology, see section 2.1.10.

5.2.4 Reactive Oxygen Species

Cellular free radical generation in Caco-2 cells was determined using the 2′,7′-dichlorofluorescein (DCFH) assay as previously described [349] with minor modifications. For detailed methodology, see section 4.2.6.

5.2.5 Iron solubility

Iron solubility was determined using similar methods to Swain et al [265]. For detailed methodology, see section 2.2.6.

5.2.6 Iron bioavailability in Caco-2 cells

Caco-2 cells (HTB-37), used at passages 30-40, were cultured as described for iron bioavailability assays. For detailed methodology, see section 2.1.3.

10 mL aliquots of LIF solution (with added AA) were placed either alone or in combination with 1 g dried mangetout peas and/or dietary inhibitors (see section 5.2.1), mixed and readjusted to pH 2. Pepsin (0.04 g/ml) was added to the samples and incubated for 1 hr at 37 °C to simulate gastric conditions. After

completion of the gastric phase, samples were gradually adjusted to pH 5.5-6.0 with 1 M $NaHCO_3$. Chelex-treated bile (0.007 g/ml) and pancreatin (0.001 g/ml) digestive enzymes were added to the samples, the pH was further adjusted to 7 with 0.1 M $NaHCO_3$, and LIF 'digestates' incubated for 30 min at 37 °C. 1.5 ml of the digestate was placed on top of a Transwell insert fitted with a 15 KDa molecular weight cut-off dialysis membrane (Spectra/Por 7 dialysis tubing, Spectrum laboratories, Europe) suspended over Caco-2 cells. The digestate was incubated with the cells for 2 hrs at 37 °C (5% CO_2 and 95% air). After 2 hrs, the inserts were removed, an additional 1 ml of supplemented MEM was added to each well, and cells were incubated for a further 22 hrs.

After 24 hrs post-treatment, cells were extracted and analysed for ferritin and total protein concentrations. For detailed methodology, see sections 2.1.5 and 2.1.6.

5.2.7 Statistical analysis

Statistical analysis was performed using GraphPad Prism v.6.0 (San Diego, CA). Data are presented as mean values with standard error (SEM). One-way ANOVA with Tukey's multiple comparisons test on log-transformed data was used to evaluate differences in iron uptake from LIF. Differences were considered significant at $p < 0.05$.

5.3 Results

The variability in iron extraction from LIF was tested to see whether the amount of leached iron was consistent from experiment to experiment, since the same LIF was used for every experiment. Any large differences in the amount of iron leached during each extraction may also explain some of the inconsistent data observed in previous human trials. Minor variability in iron extraction was observed after each use (Figure 5.1). As shown in the figure, the average iron

concentration per extraction was 946 ± 60 nmol/mL (SEM). AA concentrations were added to LIF solutions assuming ca. 1000 nmol/mL Fe.

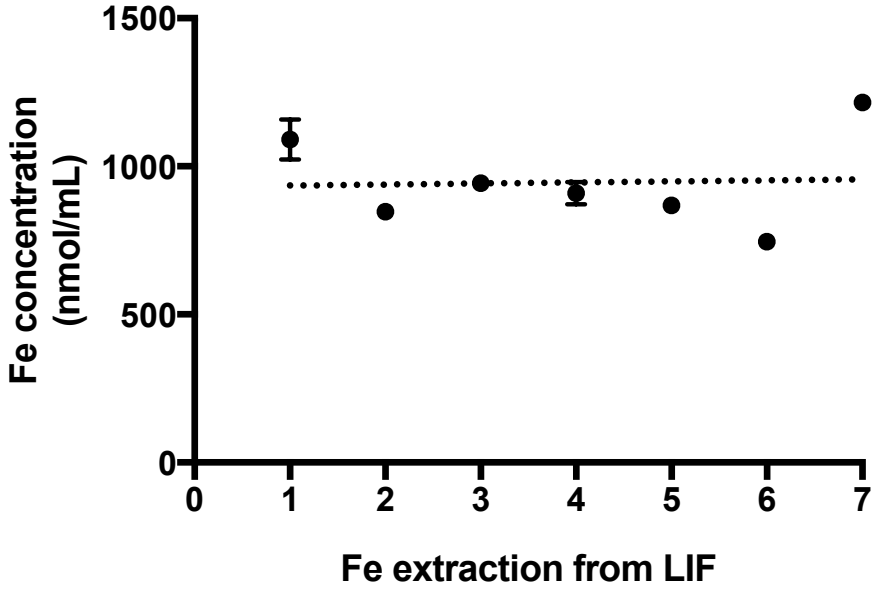

Figure 5.1 Total iron concentration in LIF solution at pH 7 with 1000 μM AA.

Iron concentrations from 7 separate LIF extractions were determined to assess iron variability during each usage. The dotted regression line is for reference (r = 0.002), showing that the iron concentration did not vary significantly over extraction number.

5.3.1 ROS generation in Caco-2 cells from LIF is similar to $FeSO_4$ at equimolar iron concentrations.

$FeSO_4$ is known to cause gastrointestinal distress and one reason may be its ability to generate reactive oxygen species (ROS) through the Fenton reaction. We compared the generation of ROS from $FeSO_4$ to LIF. The ability of LIF to induce reactive oxygen species when incubated on Caco-2 cells was thus measured. Compared to the blank (cells without iron treatment), LIF or $FeSO_4$ treated cells generated significantly more ROS. The increase in ROS generation

from LIF (1:10) was equivalent to the ROS generation from $FeSO_4$ at the same iron concentration (100 μM Fe). This relationship held at each time point (30, 60, and 120 min).

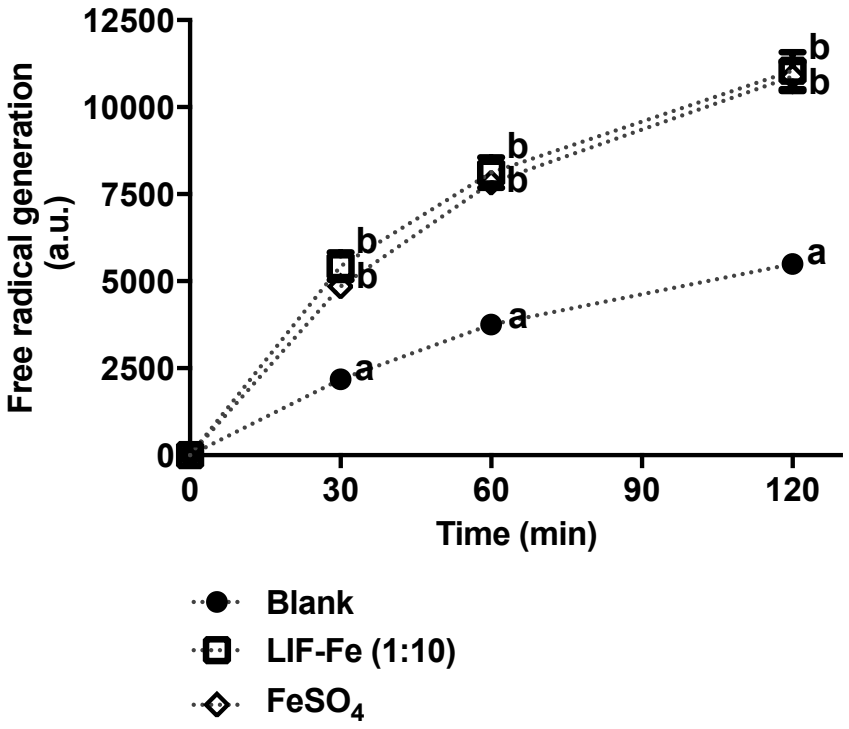

Figure 5.2 Free radical generation from LIF and $FeSO_4$ in Caco-2 cells.

Caco-2 cells were treated with LIF 1:10 (100 μM Fe) or $FeSO_4$ (100 μM Fe) for up to 2 hrs. Free radical generation was evaluated at 0, 30, 60 and 120 min. Data are expressed as the means ± of three independent experiments (n = 16). One-way repeated measures ANOVA with Bonferroni's test was used to compare differences in iron treatments at each time point. Different letters indicate statistically significant differences at each time point ($p < 0.05$). Experiments were conducted by Dr. Ildefonso Rodriguez-Ramiro, Fairweather-Tait lab.

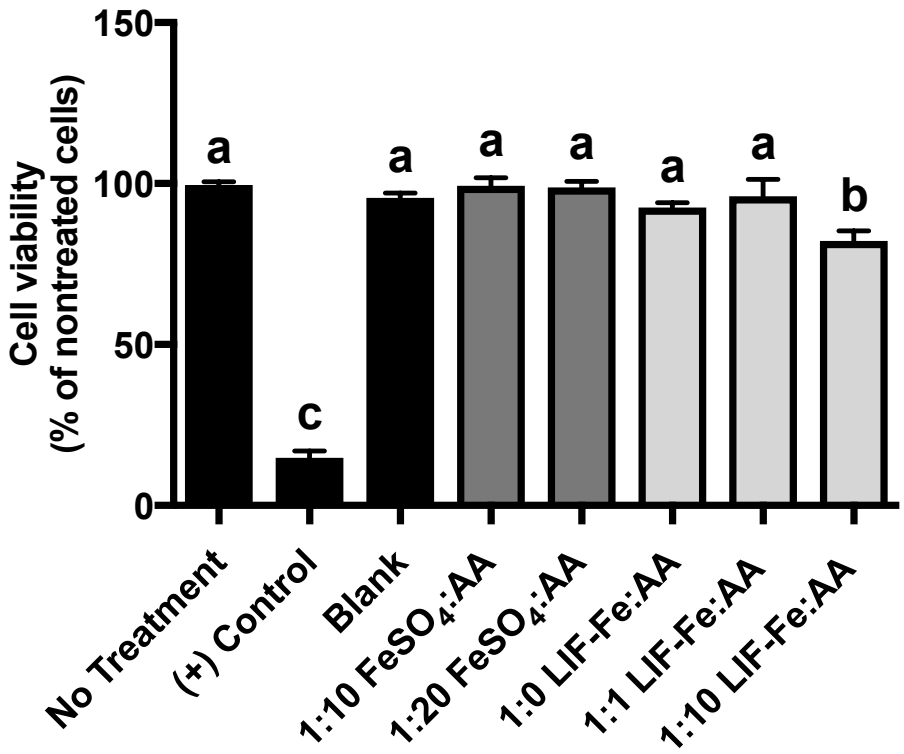

Figure 5.3 Viability of Caco-2 cells incubated with $FeSO_4$ + AA or LIF + AA over 24 hrs.

Cell viability was measured using the MTS assay. $FeSO_4$ concentrations were 50 µM Fe. LIF concentrations were 500 µM Fe (1:1 dilution with MEM). 1% Triton-X 100 was used as the positive control. Data are expressed as the means ± of two independent experiments (n = 3). Different letters indicate statistically significant differences ($p < 0.05$).

Cell viability was measured to ensure that the resulting iron bioavailability data occurred in healthy cells. A reduction in cell viability, especially at high LIF:AA concentrations, could indicate a stress response. As an acute phase protein, stress responses may result in falsely elevated levels of cell ferritin formation. Amongst all treatments, cell viability was significantly decreased (20%) by LIF (1:10 Fe:AA molar ratio) at a 1:1 dilution in MEM (Figure 5.3). Except for very high iron concentrations (~ 500 µM Fe), in general, LIF concentrations had

no effect on cell viability at the concentrations of iron and AA used. Similar experiments using 1:10 dilutions of LIF in MEM with varying AA concentrations were also measured for cell viability (data not shown). There was not any significant difference in cell viability from each treatment compared to baseline (no treatment).

5.3.2 Iron solubility and cellular uptake is highest at 1:10 LIF-Fe:AA molar ratios

Iron solubility is a general indicator of iron bioavailability; therefore we decided to test the concentrations of AA required to fully solubilise LIF. The iron from LIF extraction was fully solubilised at pH 2, irrespective of AA concentration (Figure 5.5). As the pH of the solution increased to pH 7, mimicking intestinal pH conditions, the majority of the iron precipitated out of solution (> 90%) unless AA was added. Iron solubility of LIF was dose-dependent on increasing AA concentrations; at 1:10 LIF-Fe:AA molar ratios, iron was nearly completely solubilised.

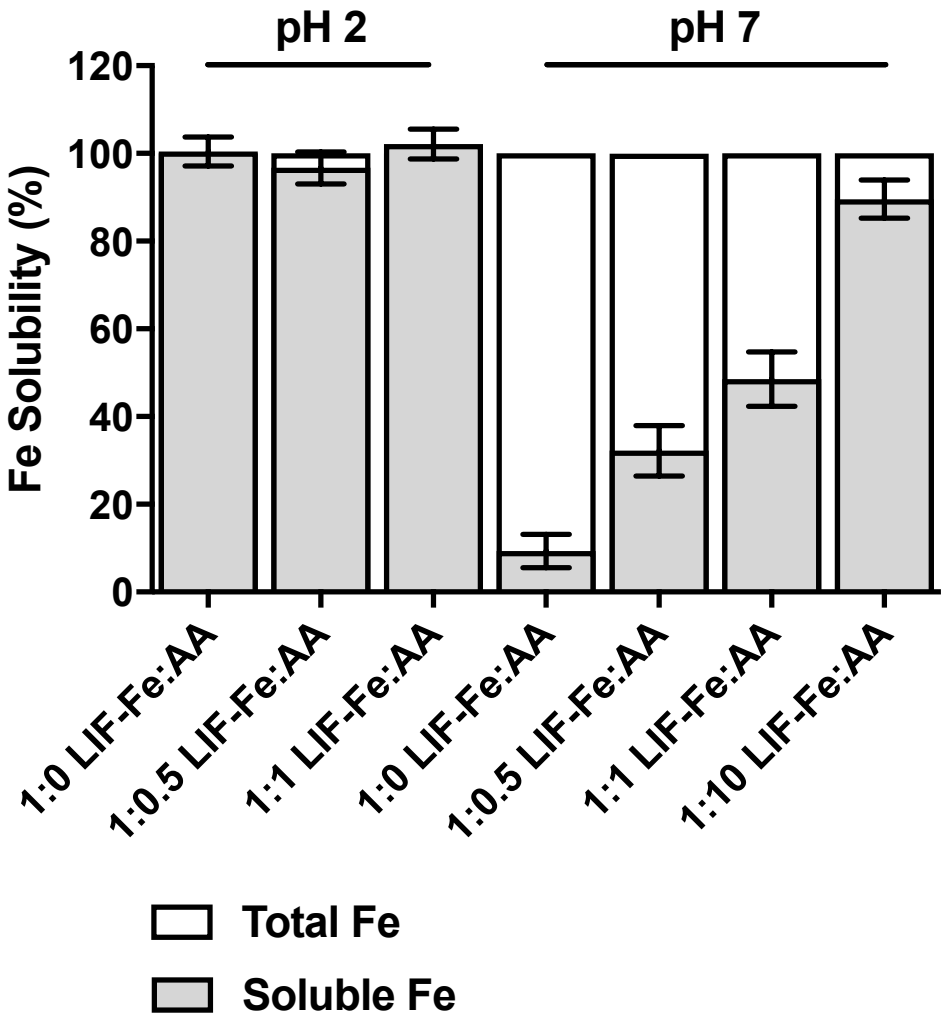

Figure 5.4 Solubility of released iron from LIF with AA.

LIF at pH 2 released about 1 mM Fe in the experimental conditions. AA was added at increasing AA concentrations (0, 1, and 10 mM) to achieve the indicated Fe:AA molar ratios and diluted 1:10 in MEM. Data are expressed as the means of three independent experiments (n = 7, ± SEM).

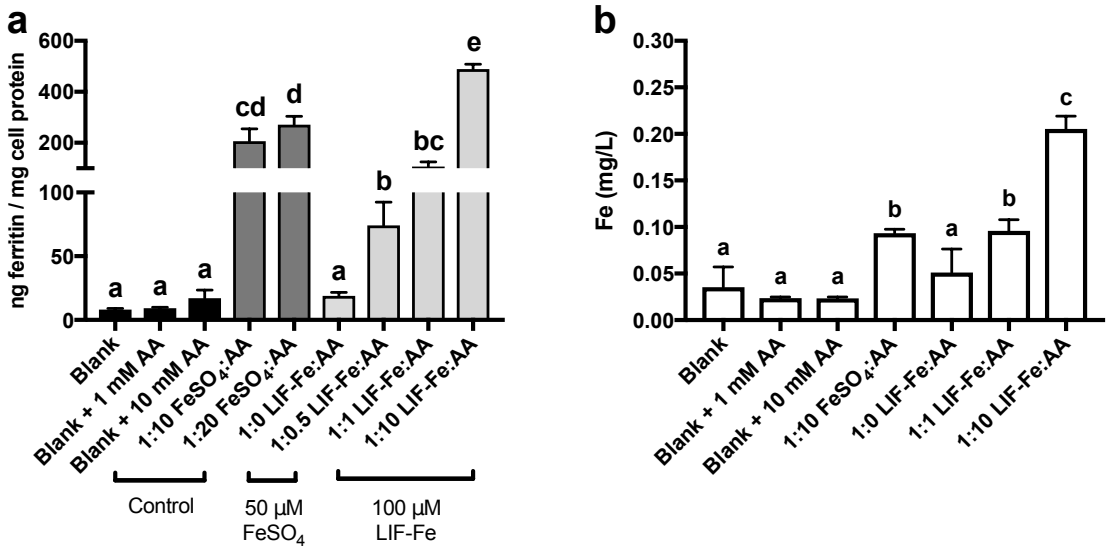

Figure 5.5 AA on iron bioavailability from $FeSO_4$ and LIF-Fe.

Caco-2 cells were treated with $FeSO_4$ or LIF-Fe for 24 hrs and measured for (a) iron uptake or (b) total iron. Data for ferritin formation are expressed as the means of 3-5 independent experiments (n = 6-18, ± SEM). Data for total iron are expressed as the means of n = 3 or 4. One-way repeated measures ANOVA with Tukey's multiple comparisons test was used to compare differences in iron uptake between treatments. ICP-OES determinations were conducted by Dr. Ildefonso Rodriguez-Ramiro, Fairweather-Tait lab.

A positive correlation was found between iron solubility and ferritin formation in Caco-2 cells with increasing AA concentrations; thus solubility is a very good indicator of iron bioavailability for LIF. The addition of increasing AA concentrations had a dose-response effect on iron uptake from LIF, with the highest uptake of iron observed at 1:10 LIF:AA molar ratio. Compared to the blanks (no iron added), iron from LIF was not bioavailable unless additional AA was added. Iron bioavailability at 1:1 LIF-Fe:AA molar ratios was similar to 1:10 and 1:20 $FeSO_4$:AA molar ratios despite the treatment having a significantly higher iron concentration (20x). Ferritin formation in Caco-2 cells was validated by directly measuring iron uptake (Figure 5.6b). Similar to ferritin formation,

increasing AA concentrations to LIF-Fe significantly increased iron uptake in Caco-2 cells.

5.3.3 Peas increased iron bioavailability from LIF-Fe

Peas were added to the digests with LIF + AA to mimic a food matrix that is more representative of LIF consumption. Although stated on the instructions that LIF in water could be consumed, it is more likely that LIF would be consumed in combination with other food components as part of a meal. Despite over a 10-fold increase in iron content in the digest (667 vs 50 µm Fe), iron bioavailability from LIF was the same as $FeSO_4$ and pea when AA concentrations were normalised among iron treatments (Figure 5.6). When estimating 30% iron solubility from 1:0.5 LIF-Fe:AA molar ratio (Figure 5.4), 200 µm Fe is soluble. Nonetheless, 4x more soluble iron provided by LIF resulted in similar bioavailability as $FeSO_4$. Unexpectedly, pea and LIF digested together with AA resulted in a 10-fold increase in iron bioavailability compared to pea or LIF alone. The large increase in iron bioavailability from 1:10 Pea-Fe:AA + LIF was validated by measuring the iron content of the cell lysates by ICP-OES. The results of ICP-OES were qualitatively similar to ferritin formation; the iron content of 1:10 Pea-Fe:AA + LIF was the highest among all treatments, and 5x more than either pea or LIF alone.

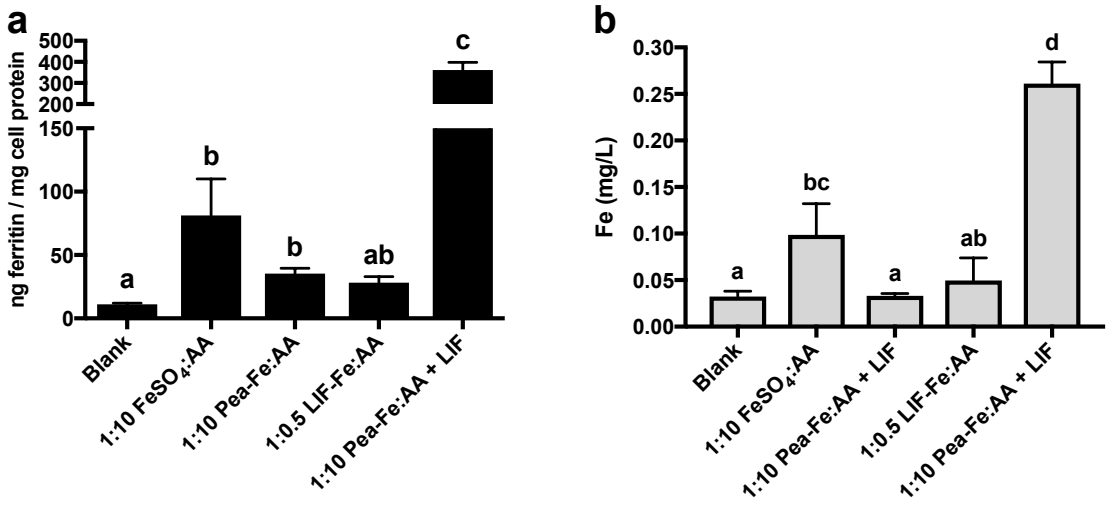

Figure 5.6 Pea food matrix increased iron bioavailability from LIF.

(a) The combination of pea and LIF (50 + 1000 µM Fe) resulted in a 10-fold increase in iron bioavailability compared to pea (50 µM Fe) or LIF (1000 µM Fe) alone. $FeSO_4$ (50 µM Fe) was used as the positive control, blank was used as the negative control (digests without iron), and AA (500 µM) was added to each iron-containing digest. (b) Cellular iron concentration (using ICP-OES) was determined and is positively correlated with cellular ferritin formation.

Data are expressed as the means of 3-5 independent experiments (n = 12-19, ± SEM). One-way repeated measures ANOVA with Tukey's multiple comparisons test was used to compare differences in iron uptake between treatments.

5.3.4 Tannic acid is a potent inhibitor of iron bioavailability from LIF

Staple foods, containing high amounts of non-haem dietary inhibitors such as phytates and tannins, represent a large portion of the daily diet in developing countries. Thus, it was important to investigate whether these inhibitors had an effect on iron bioavailability from LIF. An experiment was initially conducted to understand the inhibitory effects of TA and PA on iron bioavailability from $FeSO_4$, pea, and LIF. The concentrations of TA and PA chosen were based on previously published data [249]. TA, at 5x lower concentrations than PA, significantly

inhibited iron bioavailability from all 3 iron sources in the presence of AA. PA had no significant effect on iron uptake from all 3 sources, although it appears that it may have an effect on $FeSO_4$. The largest inhibitory effect of TA was with LIF-Fe; despite a relatively high ratio of iron to TA (1:0.05), a 6-fold decrease in iron bioavailability was observed (to baseline levels) compared to LIF-Fe without TA.

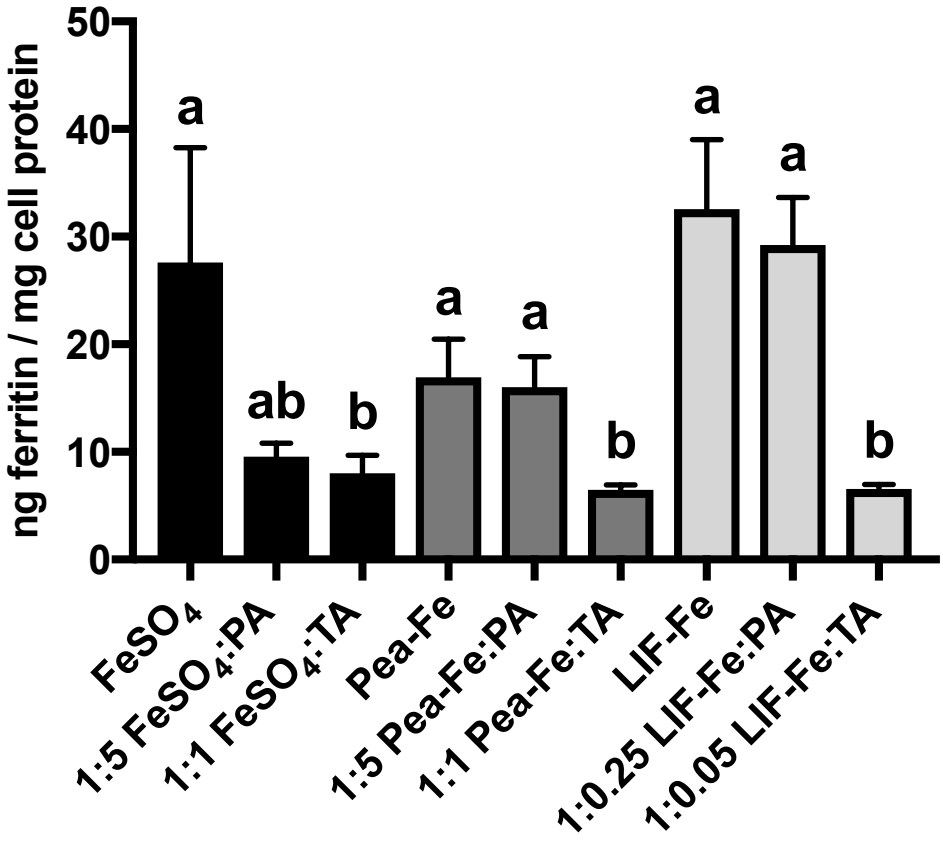

Figure 5.7 PA and TA on iron bioavailability from $FeSO_4$ + AA, pea + AA, and LIF + AA.

$FeSO_4$ (50 µM Fe) + AA (500 µM), pea (50 µM Fe) + AA (500 µM), and LIF (1000 µM Fe) + AA (500 µM) were *in vitro* digested with PA and TA and iron bioavailability measured in Caco-2 cells. PA was added at 50, 250, 500, and 1000 µM to achieve molar ratios of Fe:PA 1:1, 1:5, 1:10, and 1:20, and TA was added at 5, 25, 50, and 500 µM to achieve molar ratios of Fe:TA 1:0.1, 1:0.5, 1:1, and 1:10. Data are expressed as means (n = 3, ± SD). One-way ANOVA with

Tukey's multiple comparisons test was used to compare differences in iron uptake between treatments.

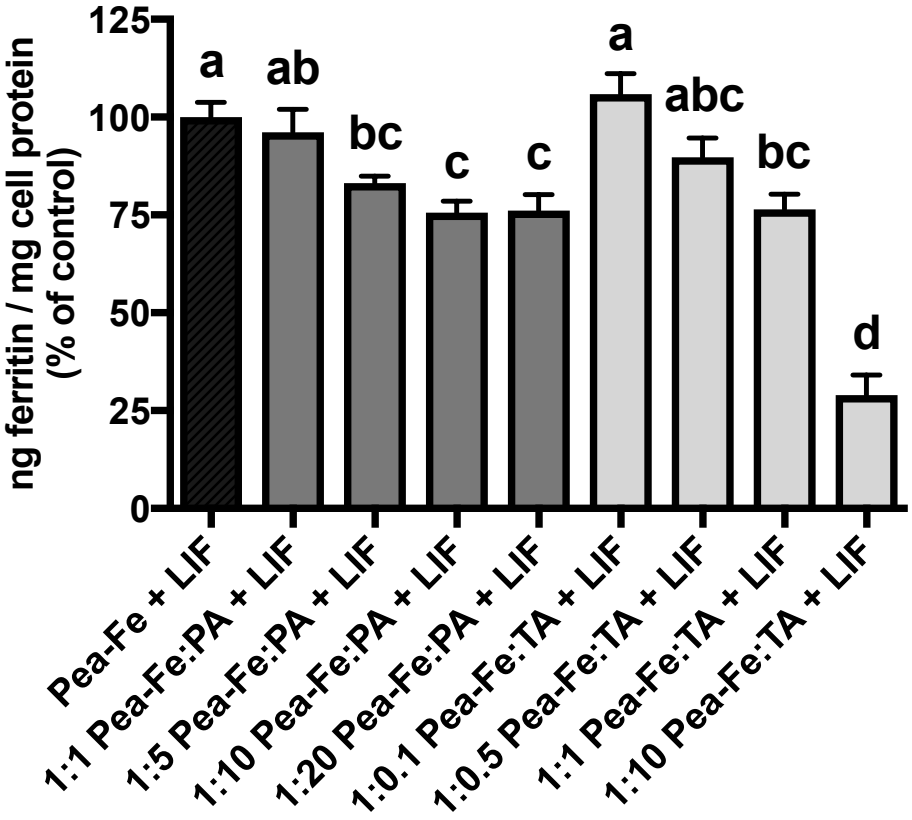

Figure 5.8 Effect of PA and TA on iron uptake from pea + LIF + AA.

Pea (50 µM Fe) + LIF (1000 µM Fe) were *in vitro* digested with increasing concentrations of PA and TA and iron bioavailability measured in Caco-2 cells. PA was added at 50, 250, 500, and 1000 µM to achieve molar ratios of Fe:PA 1:1, 1:5, 1:10, and 1:20, and TA was added at 5, 25, 50, and 500 µM to achieve molar ratios of Fe:TA 1:0.1, 1:0.5, 1:1, and 1:10. AA was added to each digest at 500 µM. Data are expressed as the means of 3 independent experiments (n = 3 per experiment, ± SEM). One-way repeated measures ANOVA with Tukey's multiple comparisons test was used to compare differences in iron uptake between treatments.

PA at 1:5, 1:10, and 1:20 significantly decreased iron bioavailability (~ 15-25%) in Caco-2 cells compared to Pea-Fe + LIF without PA. Similar to what was observed for LIF (Figure 5.7), TA was a more potent inhibitor of Pea-Fe + LIF in comparison to PA. Iron bioavailability at 1:10 and 1:20 Pea-Fe:PA + LIF was similar to 1:1 Pea-Fe:TA + LIF. At 1:10 Pea-Fe:TA + LIF, iron bioavailability was decreased by 70%.

5.4 Discussion

The LIF ingot is marketed as a simple home strategy to address iron deficiency based on the principle of cooking in iron pots, but with the added benefit of smaller size, ease of use, and maintenance. Charles et al [370, 371] carried out two studies in Cambodia investigating whether the effects of using the LIF ingot in food and drinking water could improve iron status. In both studies of similar methodology, the efficacy of the LIF ingot was assessed using haemoglobin as the primary biomarker of iron status in a cohort of Cambodian women over 3 month intervals. The results of the trials differed. In the first trial, the use of LIF improved haemoglobin concentration after 3 months, but reverted back to baseline after 6 months. In the follow-up trial, haemoglobin and serum ferritin were both measured. LIF improved haemoglobin (120 vs 130 g/L) and serum ferritin (66 vs 102 ng/mL) stores after 12 months, despite the fact that the prevalence of iron deficiency was only 11%. A complicating factor in both studies is the high prevalence beta-thalassemia in this population.

In order to understand whether LIF could improve iron status, the amount of LIF iron contributing to daily intake and the estimated increase in iron intake resulting from using LIF could have been measured. Taking into account both of these measurements may partially explain the differences in iron status from both studies, but still would not explain iron bioavailability from LIF.

The aims of the work described in this chapter were (a) to examine the effect of AA and pH on solublisation of iron from the LIF ingot in order to generate information that could be incorporated into guidance for users of the LIF ingot, and (b) to determine the effect of dietary inhibitors of iron absorption (phytic and tannin acids) on iron uptake by Caco-2 cells from digestates of LIF ingot boiled in water +/- AA in the absence and presence of a food (cooked peas).

The first experiments measured the quantity of iron released from LIF. We chose to extract LIF-Fe at pH 2 in order limit dilution effects when lowering to gastric pH and to maximise iron solubility (Figure 5.4). While this pH is much lower than manufacturer's instructions, the efficiency of iron extraction has been shown not to vary from pH 6.5 and below [372]. We then investigated the optimal levels of AA required to increase solubility and iron uptake from LIF at pH 7.

LIF is reported to be mainly composed of elemental iron; the majority of the interior of the ingot is in the ferrous state but the proportion of Fe^{3+} to Fe^{2+} is higher on the surface, likely due to oxidation [372]. Elemental iron is generally regarded as having low bioavailability [326, 373, 374], which can be increased with the addition of AA, a potent enhancer of iron absorption [49, 120]. High AA concentrations (1:10 Fe:AA molar ratio) were required to maintain iron solubility and increase iron uptake into Caco-2 cells from LIF. Moreover, despite 4x more soluble iron in the digest (Figure 5.6), LIF had similar bioavailability compared with $FeSO_4$; LIF-Fe has poor bioavailability when consumed without a food matrix. In a review on iron fortification, Hurrell [127] noted that at least 1:4-1:6 Fe:AA molar ratios were required to increase the absorption of insoluble iron food fortificants with low bioavailability. Insufficient addition of AA (in the form of lemon juice) to counteract the low bioavailability of LIF may partially explain why improved haemoglobin status was not maintained in the first clinical trial.

Iron bioavailability from LIF combined with a food matrix was also examined as this closely reflects its real world application. Peas were chosen as an appropriate dietary iron source because of their relatively high iron concentration. Despite the high content, iron in the legume family is not very bioavailable (reported as low as 1-2% [375]), which has been mostly attributed to the phytic acid content [144, 376, 377].

A large (and unexpected) increase (10-fold) in ferritin formation was observed when pea and LIF were digested together in the presence of AA. One hypothesis is that the response was due to added endogenous AA provided in the peas [118, 378], resulting in a more favorable Fe:AA molar ratio. Using values generated from the USDA National Nutrient Database and Widdowson & McCance food composition tables, frozen, boiled peas contain ca. 10 mg AA per 100 g. Converted to the concentration of dry material in our studies, these calculated levels of AA only contribute 0.01% of the total AA added exogenously. It is therefore unlikely that endogenous AA in the pea explains the synergistic effect of peas and LIF.

An alternative hypothesis is that mono/disaccharides in the peas promoted the increase in iron bioavailability from LIF. Mangetout (immature) peas have a high sugar content (4.4 g sugar per 100 g), which is converted to starch during its maturation [379]. Pollack et al [380] found that rats fed fructose with $FeCl_3$ increased iron absorption 1.5-fold more than $FeCl_3$ alone (10.1% vs 15.7%). Fructose is thought to increase non-haem iron absorption by forming soluble complexes with iron at neutral pH [381] and/or promoting iron reduction to Fe^{2+} [382] for increased DMT1 transport [18]. In Caco-2 cells, fructose promoted ferrous iron formation and increased uptake non-haem iron [383]. While sugars in the pea may explain the enhancing effect, the estimated sugar content in our digestates was 10 µM, 100-fold less than that used by Christides and Sharp [383]. It is possible that the combination of AA and sucrose was sufficient to

promote iron bioavailability from LIF. Considering the high levels of iron from LIF in our digests (1 mM Fe), with a small effect of promoters it is theoretically possible in enhanced iron uptake.

The *in vitro* digestion / Caco-2 cell model is a validated assay for measuring the effect of the non-haem iron inhibitors, PA and TA [118, 142, 156], on iron bioavailability from foods. Yun et al [242] found that the Caco-2 response correlated well with *in vivo* human iron absorption data using the same diets with increasing AA and TA levels. In these experiments, both PA and TA significantly reduced iron bioavailability from LIF digestates. Similar to previous findings using the Caco-2 bioassay [248-250], it was observed that TA was a more potent inhibitor of non-haem iron than PA in the presence of AA. PA is found in relatively high amounts in staple foods such as cereals and legumes [144] and TA is present in tea, coffee, fruit [157, 384]. It would appear from the *in vitro* data that the large quantities of iron provided by the LIF ingot are able to mitigate (to some extent) the negative effects on bioavailability from non-haem iron inhibitors; this is likely dependent on the concentration range of enhancers and inhibitors found in a typical meal. This may be one reason why LIF has been shown to be efficacious in improving the iron status of Cambodian women in the latter trial [371].

In the Charles et al [371] study, they calculated that the daily use of LIF in slightly acidified water would provide nearly 75% of the daily iron requirements for women aged 10-49 years. They concluded that safety concerns were negligible when compared to oral iron supplements, which is supported by the results of the cell proliferation assays in which LIF had no effects on cell viability except at very high AA concentrations, and the pro-oxidative capacity of LIF was similar to $FeSO_4$.

5.5 Conclusion

The LIF ingot can be a potentially bioavailable source of iron under certain conditions. The addition of AA to foods (peas) cooked with LIF increased iron bioavailability and mostly prevented the inhibitory effect from food matrix iron inhibitors such as PA and TA. However, consumption of foods high in polyphenols, such as red beans [252, 256], may need to be avoided when using LIF. Overall, the results provided by this chapter could be used as a guideline to improve LIF efficacy.

Chapter 6: Final discussion, main conclusions, and future research

6. Final discussion and main conclusions

6.1 Final discussion

Three of the most common strategies to alleviate iron deficiency and iron deficiency anaemia include iron fortification of staple foods, iron supplementation, and home iron fortification. The thesis' aims were to understand the mechanisms of iron absorption and bioavailability from novel sources of iron using the Caco-2 cell model. These novel sources of iron include: (a) NP-$FePO_4$, intended for use in the fortification of staple goods; (b) phytoferritin, a form of iron supplementation; and (c) LIF, a simple device for use as a home iron fortificant. From a biochemical perspective, the better we understand how iron from these sources are absorbed in the intestine, the more informed we will be regarding its implementation in human efficacy trials.

In Chapter 3, iron uptake from NP-$FePO_4$ in Caco-2 cells was investigated. The results overall strongly suggest that its high absorption profile, comparable to $FeSO_4$, observed in rat models is due to increased solubilisation at low pH and iron uptake via DMT1. Using sonicated NP-$FePO_4$, a method to disperse particles in solution, it was found that particles ~ 400 nm could be absorbed using an independent pathway of DMT1, possibly through clathrin-mediated endocytosis. This pathway was verified as physiologically relevant by exposing NP-$FePO_4$ to an *in vitro* gastrointestinal digest and determining the size distribution of particles during each stage. A small percentage of the particles were within the nano-size range for particle uptake and thus may contribute, to some extent, in the high bioavailability of NP-$FePO_4$ seen in previous studies.

Conducting cell culture experiments with nanoparticles was a challenging process. The major difficulty is that using nanoparticles does not necessarily translate well with the classical *in vitro* digestion / Caco-2 cell model. For

instance, we excluded the use of dialysis membranes in our experiments because they prevent the exposure of nanoparticles to cells. For this reason, we also omitted digestion enzymes in our digests, which may modulate NP dispersion (formation of protein corona) and uptake in cells. Moreover, 'nano' sized NP-$FePO_4$ digested fractions agglomerated when incubated with MEM; therefore its exposure to cells would not be a true NP exposure. While it is apparent that sonicated particles are not representative of true physiological exposure, and may not be the most accurate representation of digested particles, this was one of the unavoidable limitations encountered when combining very different disciplines (i.e. nanotechnology and nutrition).

In hindsight, because particle transcytosis has been hypothesized to occur in Peyer's patches, the use of Caco-2 / HT-29 MTX co-cultures may have been preferable to monocultures. In previous studies, co-cultures were more sensitive to transporting large size particles (200-500 nm) [284, 347]. The primary aim of this study was to determine whether DMT1 was required for iron uptake from NP-$FePO_4$; for this reason, monocultures were chosen, as it is the validated model for iron bioavailability studies. Co-cultures require further development before they can be considered useful for iron bioavailability studies. Mahler et al [272] found that the *in vitro* digestion cell ferritin response in Caco-2 / HT-29 MTX co-cultures did not correlate with the Caco-2 monoculture response, and in fact its responses were dampened significantly.

Iron homeostasis is a tightly regulated process. Given the concerns over nanoparticle toxicity, a process that may circumvent iron homeostatic mechanisms, baseline experiments in Caco-2 cells were conducted to measure the effect of NP-$FePO_4$ on cell viability. These experiments validated (a) the use of healthy cells and (b) that cell ferritin responded to iron uptake, rather than a by-product of toxicity/inflammation (ferritin is an acute phase protein). Using similar methods, Von Moos et al [385] also did not find any evidence of

cytotoxicity when Caco-2 cells were incubated with NP-$FePO_4$ at increasing particle concentrations and time (24-72 hrs). While NP-$FePO_4$ is a promising novel iron fortificant, cost and consumer acceptance will be difficult obstacles to overcome for its implementation.

In Chapter 4, the feasibility of using pea ferritin (phytoferritin) as a nutritional iron supplement was explored. The absorption of iron from phytoferritin still remains controversial; therefore experiments undertaken were aimed to investigate these mechanisms more in-depth. The results of this chapter strongly suggest that phytoferritin from marrowfat peas, either bound within peas or extracted, will likely degrade under gastrointestinal conditions. Similar to previous studies using undigested, native phytoferritin, its uptake appears to involve a clathrin-mediated endocytosis pathway that is independent of DMT1. Protection of phytoferritin from gastric digestion is ultimately the key to its bioavailability, as dietary non-haem iron inhibitors have no effect on iron uptake.

While the phytoferritin experiments indicated that a clathrin-mediated endocytosis pathway exists for phytoferritin, time restrictions prevented the exploration of these mechanisms further. Toward the end of the project, preliminary investigations were conducted to identify possible phytoferritin receptors in Caco-2 cells using co-immunoprecipitation and mass spectrometry; this was not completed due to time constraints. The identification/characterisation of receptors on the surface of enterocytes would definitively prove the existence of an alternative pathway for phytoferritin. Gene knockdown studies in mice would determine whether this pathway is physiologically important in iron nutrition. For the project at hand, the next experiments could examine different strategies to protect phytoferritin from gastric digestion. In addition, pilot studies should be conducted to determine its bioavailability relative to $FeSO_4$.

For Chapters 3 and 4, the data obtained provide strong evidence that an iron uptake route independent of DMT1 exists for both iron forms. In the near future, intestinal *DMT1*$^{-/-}$ knockout mouse models should be used to provide *in vivo* evidence whether this is indeed the case.

In Chapter 5, the dietary factors regulating iron uptake from LIF were examined. While some *in vitro* work has been conducted with LIF, there are no studies to date that have investigated iron bioavailability from LIF using the Caco-2 cell model. 1:10 Fe:AA ratios were required to optimally increase the solubility and iron bioavailability from LIF. The large quantity of AA required should be highlighted, as small doses of AA did not increase iron bioavailability from LIF despite high quantities of LIF-Fe released; this is one plausible explanation why LIF might have been ineffective in improving haemoglobin status of women in Cambodia in recent trials. The effect of food and dietary inhibitors on LIF iron uptake was also investigated. LIF was able to significantly increase iron uptake in the presence of peas; this effect is likely food matrix dependent, and its bioavailability was inhibited greatly in the presence of tannic acid. While it seems that LIF is a promising and sustainable iron source, understanding the factors that enhance and limit its bioavailability are essential to its effectiveness.

In the current chapter, peas were used to give an approximation of the synergistic effect LIF-Fe would have on iron bioavailability. The effect of LIF-Fe on whole-meal bioavailability would be more representative of the *in vivo* condition. The next set of experiments could address this. Carefully reproduction of representative meals used in prior clinical trials and its iron bioavailability with and without LIF using Caco-2 cells might explain some of the previous results. The meal compositions cited by previous studies include the use of fish, a protein that has shown to improve iron bioavailability. Subsequent experiments could also examine the *in vivo* relevance of the pro-oxidative capacity observed for LIF.

6.2 Main conclusions

Chapter 3

- NP-$FePO_4$ has comparable bioavailability to FAC.
- The majority of iron from NP-$FePO_4$ is absorbed using DMT1.
- Solubility at pH 1 increases iron bioavailability of NP-$FePO_4$ to the same levels as FAC, which validates results from *in vivo* rat studies.

Chapter 4

- Phytoferritin is easily broken down at low pH conditions of the stomach.
- Native phytoferritin is absorbed using clathrin-mediate endocytosis; pH treated phytoferritin is absorbed using DMT1.
- Phytoferritin may be a well-tolerated form of oral iron supplementation in comparison to $FeSO_4$.

Chapter 5

- LIF-Fe is generally not bioavailable unless large concentrations of AA are added.
- Certain foods (e.g. peas) may also improve iron bioavailability from LIF.
- TA is a potent inhibitor of LIF-Fe at low concentration; limiting TA (and polyphenol) concentrations, such as coloured beans, during its use may improve its efficacy.

6.3 Future research

While the *in vitro* data presented in this thesis shows the promise of novel iron supplements and fortificants to reduce the burden of iron deficiency, human

studies are needed to confirm whether NP-$FePO_4$ and phytoferritin are well absorbed in humans relative to $FeSO_4$. Concerns over the use of nanoparticles will be a difficult regulatory hurdle to overcome with regards to its safety. Currently, the use of IHAT as a nanoparticulate iron supplement is undergoing clinical trials in the Gambia. Depending on the outcome of these trials, other iron nanoparticles, such as NP-$FePO_4$, could be employed. Given external funding, conducting human trials for phytoferritin as a nutritional supplement should be much easier as it is naturally occurring in peas. Delivery systems, such as enteric coating and targeted release in the intestine, are being discussed.

In Chapters 3 and 4, we provide evidence that NP-$FePO_4$ and phytoferritin can both undergo direct uptake via endocytosis in Caco-2 cells. This uptake mechanism is dependent on the extent of gastrointestinal digestion, which is very difficult to recreate under *in vitro* conditions. Furthermore, while Caco-2 cells display a duodenal-like phenotype, they are originally of colonic origin, and are not completely representative of the many subtypes of cells found in the intestine. To investigate and confirm an endocytic pathway, $DMT1^{-/-}$ intestinal knockout mice are required to determine whether nanoparticles are translocated into the intestine independent of DMT1.

In Chapter 5, we found that the addition of peas with LIF greatly enhanced iron bioavailability from LIF alone and conversely, the addition of TA markedly reduced its bioavailability. These results strongly suggest that iron bioavailability from LIF is inherently dependent on the food matrix. Thus, in order to understand whether the LIF can improve iron status, the meal composition of a potential clinical trial could be replicated and its bioavailability determined with LIF. For example, replicating the traditional diets that were consumed in the previous two Cambodian trials and measuring bioavailability from meals with and without LIF using Caco-2 cells might help to explain the results of these trials.

7. References

[1] Zimmermann MB, Hurrell RF. Nutritional iron deficiency. Lancet. 2007;370:511-20.

[2] Beard JL, Dawson H, Piñero DJ. Iron metabolism: a comprehensive review. Nutrition Reviews. 1996;54:295-317.

[3] Andrews NC. Iron homeostasis: insights from genetics and animal models. Nature Reviews Genetics. 2000;1:208-17.

[4] Richardson DR, Ponka P, Vyoral D. Distribution of iron in reticulocytes after inhibition of heme synthesis with succinylacetone: examination of the intermediates involved in iron metabolism. Blood. 1996;87:3477-88.

[5] Klausner RD, Rouault TA, Harford JB. Regulating the fate of mRNA: the control of cellular iron metabolism. Cell. 1993;72:19-28.

[6] Hentze MW, Kühn LC. Molecular control of vertebrate iron metabolism: mRNA-based regulatory circuits operated by iron, nitric oxide, and oxidative stress. Proceedings of the National Academy of Sciences. 1996;93:8175-82.

[7] Iwai K, Drake SK, Wehr NB, Weissman AM, LaVaute T, Minato N, et al. Iron-dependent oxidation, ubiquitination, and degradation of iron regulatory protein 2: implications for degradation of oxidized proteins. Proceedings of the National Academy of Sciences. 1998;95:4924-8.

[8] McKie AT, Marciani P, Rolfs A, Brennan K, Wehr K, Barrow D, et al. A novel duodenal iron-regulated transporter, IREG1, implicated in the basolateral transfer of iron to the circulation. Molecular Cell. 2000;5:299-309.

[9] Salahudeen AA, Thompson JW, Ruiz JC, Ma H-W, Kinch LN, Li Q, et al. An E3 ligase possessing an iron-responsive hemerythrin domain is a regulator of iron homeostasis. Science. 2009;326:722-6.

[10] Vashisht AA, Zumbrennen KB, Huang X, Powers DN, Durazo A, Sun D, et al. Control of iron homeostasis by an iron-regulated ubiquitin ligase. Science. 2009;326:718-21.

[11] Moroishi T, Nishiyama M, Takeda Y, Iwai K, Nakayama KI. The FBXL5-IRP2 axis is integral to control of iron metabolism in vivo. Cell Metabolism. 2011;14:339-51.

[12] Galy B, Ferring D, Minana B, Bell O, Janser HG, Muckenthaler M, et al. Altered body iron distribution and microcytosis in mice deficient in iron regulatory protein 2 (IRP2). Blood. 2005;106:2580-9.

[13] Galy B, Ferring-Appel D, Kaden S, Gröne H-J, Hentze MW. Iron regulatory proteins are essential for intestinal function and control key iron absorption molecules in the duodenum. Cell Metabolism. 2008;7:79-85.

[14] Shah YM, Matsubara T, Ito S, Yim S-H, Gonzalez FJ. Intestinal hypoxia-inducible transcription factors are essential for iron absorption following iron deficiency. Cell Metabolism. 2009;9:152-64.

[15] Jaakkola P, Mole DR, Tian Y-M, Wilson MI, Gielbert J, Gaskell SJ, et al. Targeting of HIF-α to the von Hippel-Lindau ubiquitylation complex by O2-regulated prolyl hydroxylation. Science. 2001;292:468-72.

[16] Mastrogiannaki M, Matak P, Keith B, Simon MC, Vaulont S, Peyssonnaux C. HIF-2α, but not HIF-1α, promotes iron absorption in mice. The Journal of Clinical Investigation. 2009;119:1159-66.

[17] Sanchez M, Galy B, Muckenthaler MU, Hentze MW. Iron-regulatory proteins limit hypoxia-inducible factor-2α expression in iron deficiency. Nature Structural & Molecular Biology. 2007;14:420-6.

[18] Gunshin H, Mackenzie B, Berger UV, Gunshin Y, Romero MF, Boron WF, et al. Cloning and characterization of a mammalian proton-coupled metal-ion transporter. Nature. 1997;388:482-8.

[19] Mackenzie B, Ujwal M, Chang M-H, Romero MF, Hediger MA. Divalent metal-ion transporter DMT1 mediates both H+-coupled Fe2+ transport and uncoupled fluxes. Pflügers Archiv. 2006;451:544-58.

[20] Lee PL, Gelbart T, West C, Halloran C, Beutler E. The Human Nramp2 gene: Characterization of the Gene Structure, Alternative Splicing, Promoter Region and Polymorphisms. Blood Cells, Molecules, and Diseases. 1998;24:199-215.

[21] Hubert N, Hentze MW. Previously uncharacterized isoforms of divalent metal transporter (DMT)-1: Implications for regulation and cellular function. Proceedings of the National Academy of Sciences. 2002;99:12345-50.

[22] Tchernitchko D, Bourgeois M, Martin M-E, Beaumont C. Expression of the two mRNA isoforms of the iron transporter Nrmap2/DMTI in mice and function of the iron responsive element. Biochemical Journal. 2002;363:449-55.

[23] Canonne-Hergaux F, Gruenheid S, Ponka P, Gros P. Cellular and subcellular localization of the Nramp2 iron transporter in the intestinal brush border and regulation by dietary iron. Blood. 1999;93:4406-17.

[24] Trinder D, Oates P, Thomas C, Sadleir J, Morgan E. Localisation of divalent metal transporter 1 (DMT1) to the microvillus membrane of rat duodenal enterocytes in iron deficiency, but to hepatocytes in iron overload. Gut. 2000;46:270-6.

[25] Fleming MD, Trenor CC, Su MA, Foernzler D, Beier DR, Dietrich WF, et al. Microcytic anaemia mice have a mutation in Nramp2, a candidate iron transporter gene. Nature Genetics. 1997;16:383-6.

[26] Fleming MD, Romano MA, Su MA, Garrick LM, Garrick MD, Andrews NC. Nramp2 is mutated in the anemic Belgrade (b) rat: evidence of a role for Nramp2 in endosomal iron transport. Proceedings of the National Academy of Sciences. 1998;95:1148-53.

[27] Su MA, Trenor CC, Fleming JC, Fleming MD, Andrews NC. The G185R mutation disrupts function of the iron transporter Nramp2. Blood. 1998;92:2157-63.

[28] Gunshin H, Fujiwara Y, Custodio AO, DiRenzo C, Robine S, Andrews NC. Slc11a2 is required for intestinal iron absorption and erythropoiesis but dispensable in placenta and liver. The Journal of Clinical Investigation. 2005;115:1258-66.

[29] Mims MP, Guan Y, Pospisilova D, Priwitzerova M, Indrak K, Ponka P, et al. Identification of a human mutation of DMT1 in a patient with microcytic anemia and iron overload. Blood. 2005;105:1337-42.

[30] Iolascon A, d'Apolito M, Servedio V, Cimmino F, Piga A, Camaschella C. Microcytic anemia and hepatic iron overload in a child with compound heterozygous mutations in DMT1 (SCL11A2). Blood. 2006;107:349-54.

[31] Blanco E, Kannengiesser C, Grandchamp B, Tasso M, Beaumont C. Not all DMT1 mutations lead to iron overload. Blood Cells, Molecules, and Diseases. 2009;43:199-201.

[32] Conrad ME, Umbreit JN, Moore EG, Hainsworth LN, Porubcin M, Simovich MJ, et al. Separate pathways for cellular uptake of ferric and ferrous iron. American Journal of Physiology-Gastrointestinal and Liver Physiology. 2000;279:G767-G74.

[33] Conrad ME, Umbreit JN, Moore EG. A role for mucin in the absorption of inorganic iron and other metal cations: a study in rats. Gastroenterology. 1991;100:129-36.

[34] Conrad M, Umbreit J, Peterson R, Moore E, Harper K. Function of integrin in duodenal mucosal uptake of iron. Blood. 1993;81:517-21.

[35] Conrad ME, Umbreit JN, Moore EG, Peterson R, Jones MB. A newly identified iron binding protein in duodenal mucosa of rats. Purification and characterization of mobilferrin. Journal of Biological Chemistry. 1990;265:5273-9.

[36] Conrad M, Umbreit J, Moore E, Rodning C. Newly identified iron-binding protein in human duodenal mucosa. Blood. 1992;79:244-7.

[37] Umbreit JN, Conrad ME, Moore EG, Desai MP, Turrens J. Paraferritin: a protein complex with ferrireductase activity is associated with iron absorption in rats. Biochemistry. 1996;35:6460-9.

[38] Umbreit JN, Conrad ME, Hainsworth LN, Simovich M. The ferrireductase paraferritin contains divalent metal transporter as well as mobilferrin. American Journal of Physiology-Gastrointestinal and Liver Physiology. 2002;282:G534-G9.

[39] Simovich M, Hainsworth LN, Fields P, Umbreit JN, Conrad ME. Localization of the iron transport proteins mobilferrin and DMT-1 in the duodenum: The surprising role of mucin. American Journal of Hematology. 2003;74:32-45.

[40] Mesaeli N, Nakamura K, Zvaritch E, Dickie P, Dziak E, Krause K-H, et al. Calreticulin is essential for cardiac development. The Journal of Cell Biology. 1999;144:857-68.

[41] Rauch F, Prud'homme J, Arabian A, Dedhar S, St-Arnaud R. Heart, brain, and body wall defects in mice lacking calreticulin. Experimental Cell Research. 2000;256:105-11.

[42] Nakamura K, Robertson M, Liu G, Dickie P, Nakamura K, Guo JQ, et al. Complete heart block and sudden death in mice overexpressing calreticulin. The Journal of Clinical Investigation. 2001;107:1245-53.

[43] McKie AT, Barrow D, Latunde-Dada GO, Rolfs A, Sager G, Mudaly E, et al. An iron-regulated ferric reductase associated with the absorption of dietary iron. Science. 2001;291:1755-9.

[44] Latunde-Dada GO, Simpson RJ, McKie AT. Duodenal cytochrome B expression stimulates iron uptake by human intestinal epithelial cells. The Journal of Nutrition. 2008;138:991-5.

[45] Wyman S, Simpson RJ, McKie AT, Sharp PA. Dcytb (Cybrd1) functions as both a ferric and a cupric reductase in vitro. FEBS letters. 2008;582:1901-6.

[46] Muckenthaler M, Roy CN, Custodio ÁO, Minana B, Montross LK, Andrews NC, et al. Regulatory defects in liver and intestine implicate abnormal hepcidin and Cybrd1 expression in mouse hemochromatosis. Nature Genetics. 2003;34:102-7.

[47] Atanasova B, Mudway IS, Laftah AH, Latunde-Dada GO, McKie AT, Peters TJ, et al. Duodenal ascorbate levels are changed in mice with altered iron metabolism. The Journal of Nutrition. 2004;134:501-5.

[48] Gunshin H, Starr CN, DiRenzo C, Fleming MD, Jin J, Greer EL, et al. Cybrd1 (duodenal cytochrome b) is not necessary for dietary iron absorption in mice. Blood. 2005;106:2879-83.

[49] Sharp P, Srai SK. Molecular mechanisms involved in intestinal iron absorption. World Journal of Gastroenterology. 2007;13:4716-24.

[50] Shayeghi M, Latunde-Dada GO, Oakhill JS, Laftah AH, Takeuchi K, Halliday N, et al. Identification of an intestinal heme transporter. Cell. 2005;122:789-801.

[51] Laftah AH, Latunde-Dada GO, Fakih S, Hider RC, Simpson RJ, McKie AT. Haem and folate transport by proton-coupled folate transporter/haem carrier protein 1 (SLC46A1). British Journal of Nutrition. 2009;101:1150-6.

[52] Le Blanc S, Garrick MD, Arredondo M. Heme carrier protein 1 transports heme and is involved in heme-Fe metabolism. American Journal of Physiology-Cell Physiology. 2012;302:C1780-C5.

[53] Qiu A, Jansen M, Sakaris A, Min SH, Chattopadhyay S, Tsai E, et al. Identification of an intestinal folate transporter and the molecular basis for hereditary folate malabsorption. Cell. 2006;127:917-28.

[54] Nakai Y, Inoue K, Abe N, Hatakeyama M, Ohta K-y, Otagiri M, et al. Functional characterization of human proton-coupled folate transporter/heme carrier protein 1 heterologously expressed in mammalian cells as a folate transporter. Journal of Pharmacology and Experimental Therapeutics. 2007;322:469-76.

[55] Uc A, Stokes JB, Britigan BE. Heme transport exhibits polarity in Caco-2 cells: evidence for an active and membrane protein-mediated process. American Journal of Physiology-Gastrointestinal and Liver Physiology. 2004;287:G1150-G7.

[56] Shi H, Bencze KZ, Stemmler TL, Philpott CC. A cytosolic iron chaperone that delivers iron to ferritin. Science. 2008;320:1207-10.

[57] Nandal A, Ruiz JC, Subramanian P, Ghimire-Rijal S, Sinnamon RA, Stemmler TL, et al. Activation of the HIF prolyl hydroxylase by the iron chaperones PCBP1 and PCBP2. Cell Metabolism. 2011;14:647-57.

[58] Harrison PM, Arosio P. The ferritins: molecular properties, iron storage function and cellular regulation. Biochimica et Biophysica Acta (BBA)-Bioenergetics. 1996;1275:161-203.

[59] Chasteen ND, Harrison PM. Mineralization in ferritin: an efficient means of iron storage. Journal of Structural Biology. 1999;126:182-94.

[60] Theil EC. Iron, ferritin, and nutrition. Annual Review Nutrition. 2004;24:327-43.

[61] Hentze MW, Caughman SW, Rouault TA, Barriocanal JG, Dancis A, Harford JB, et al. Identification of the iron-responsive element for the translational regulation of human ferritin mRNA. Science. 1987;238:1570-4.

[62] Leibold EA, Munro HN. Cytoplasmic protein binds in vitro to a highly conserved sequence in the 5'untranslated region of ferritin heavy-and light-subunit mRNAs. Proceedings of the National Academy of Sciences. 1988;85:2171-5.

[63] Mancias JD, Wang X, Gygi SP, Harper JW, Kimmelman AC. Quantitative proteomics identifies NCOA4 as the cargo receptor mediating ferritinophagy. Nature. 2014;509:105-9.

[64] Bellelli R, Federico G, Colecchia D, Iolascon A, Chiariello M, Santoro M, et al. NCOA4 deficiency impairs systemic iron homeostasis. Cell Reports. 2016;14:411-21.

[65] Vanoaica L, Darshan D, Richman L, Schümann K, Kühn LC. Intestinal ferritin H is required for an accurate control of iron absorption. Cell Metabolism. 2010;12:273-82.

[66] Abboud S, Haile DJ. A novel mammalian iron-regulated protein involved in intracellular iron metabolism. Journal of Biological Chemistry. 2000;275:19906-12.

[67] Donovan A, Brownlie A, Zhou Y, Shepard J, Pratt SJ, Moynihan J, et al. Positional cloning of zebrafish ferroportin1 identifies a conserved vertebrate iron exporter. Nature. 2000;403:776-81.

[68] Nemeth E, Tuttle MS, Powelson J, Vaughn MB, Donovan A, Ward DM, et al. Hepcidin regulates cellular iron efflux by binding to ferroportin and inducing its internalization. Science. 2004;306:2090-3.

[69] Donovan A, Lima CA, Pinkus JL, Pinkus GS, Zon LI, Robine S, et al. The iron exporter ferroportin/Slc40a1 is essential for iron homeostasis. Cell Metabolism. 2005;1:191-200.

[70] Vulpe CD, Kuo Y-M, Murphy TL, Cowley L, Askwith C, Libina N, et al. Hephaestin, a ceruloplasmin homologue implicated in intestinal iron transport, is defective in the sla mouse. Nature Genetics. 1999;21:195-9.

[71] Chen H, Su T, Attieh ZK, Fox TC, McKie AT, Anderson GJ, et al. Systemic regulation of Hephaestin and Ireg1 revealed in studies of genetic and nutritional iron deficiency. Blood. 2003;102:1893-9.

[72] Chen H, Attieh ZK, Dang T, Huang G, van der Hee RM, Vulpe C. Decreased hephaestin expression and activity leads to decreased iron efflux from differentiated Caco2 cells. Journal of Cellular Biochemistry. 2009;107:803-8.

[73] Fuqua BK, Lu Y, Darshan D, Frazer DM, Wilkins SJ, Wolkow N, et al. The multicopper ferroxidase hephaestin enhances intestinal iron absorption in mice. PloS one. 2014;9:e98792.

[74] Krause A, Neitz S, Mägert H-J, Schulz A, Forssmann W-G, Schulz-Knappe P, et al. LEAP-1, a novel highly disulfide-bonded human peptide, exhibits antimicrobial activity. FEBS letters. 2000;480:147-50.

[75] Pigeon C, Ilyin G, Courselaud B, Leroyer P, Turlin B, Brissot P, et al. A new mouse liver-specific gene, encoding a protein homologous to human antimicrobial peptide hepcidin, is overexpressed during iron overload. Journal of Biological Chemistry. 2001;276:7811-9.

[76] Nemeth E, Valore EV, Territo M, Schiller G, Lichtenstein A, Ganz T. Hepcidin, a putative mediator of anemia of inflammation, is a type II acute-phase protein. Blood. 2003;101:2461-3.

[77] Nemeth E, Rivera S, Gabayan V, Keller C, Taudorf S, Pedersen BK, et al. IL-6 mediates hypoferremia of inflammation by inducing the synthesis of the iron regulatory hormone hepcidin. The Journal of Clinical Investigation. 2004;113:1271-6.

[78] Fairweather-Tait SJ, Wawer AA, Gillings R, Jennings A, Myint PK. Iron status in the elderly. Mechanisms of Ageing and Development. 2014;136:22-8.

[79] Park CH, Valore EV, Waring AJ, Ganz T. Hepcidin, a urinary antimicrobial peptide synthesized in the liver. Journal of Biological Chemistry. 2001;276:7806-10.

[80] Nicolas G, Bennoun M, Devaux I, Beaumont C, Grandchamp B, Kahn A, et al. Lack of hepcidin gene expression and severe tissue iron overload in upstream stimulatory factor 2 (USF2) knockout mice. Proceedings of the National Academy of Sciences. 2001;98:8780-5.

[81] Frazer DM, Wilkins SJ, Becker EM, Vulpe CD, McKie AT, Trinder D, et al. Hepcidin expression inversely correlates with the expression of duodenal iron transporters and iron absorption in rats. Gastroenterology. 2002;123:835-44.

[82] De Domenico I, Lo E, Ward DM, Kaplan J. Hepcidin-induced internalization of ferroportin requires binding and cooperative interaction with Jak2. Proceedings of the National Academy of Sciences. 2009;106:3800-5.

[83] Xia Y, Babitt JL, Sidis Y, Chung RT, Lin HY. Hemojuvelin regulates hepcidin expression via a selective subset of BMP ligands and receptors independently of neogenin. Blood. 2008;111:5195-204.

[84] Nai A, Rubio A, Campanella A, Gourbeyre O, Artuso I, Bordini J, et al. Limiting hepatic Bmp-Smad signaling by matriptase-2 is required for erythropoietin-mediated hepcidin suppression in mice. Blood. 2016;127:2327-36.

[85] Silvestri L, Pagani A, Nai A, De Domenico I, Kaplan J, Camaschella C. The serine protease matriptase-2 (TMPRSS6) inhibits hepcidin activation by cleaving membrane hemojuvelin. Cell Metabolism. 2008;8:502-11.

[86] Folgueras AR, de Lara FM, Pendás AM, Garabaya C, Rodríguez F, Astudillo A, et al. Membrane-bound serine protease matriptase-2 (Tmprss6) is an essential regulator of iron homeostasis. Blood. 2008;112:2539-45.

[87] Du X, She E, Gelbart T, Truksa J, Lee P, Xia Y, et al. The serine protease TMPRSS6 is required to sense iron deficiency. Science. 2008;320:1088-92.

[88] Finberg KE, Heeney MM, Campagna DR, Aydınok Y, Pearson HA, Hartman KR, et al. Mutations in TMPRSS6 cause iron-refractory iron deficiency anemia (IRIDA). Nature Genetics. 2008;40:569-71.

[89] Roetto A, Papanikolaou G, Politou M, Alberti F, Girelli D, Christakis J, et al. Mutant antimicrobial peptide hepcidin is associated with severe juvenile hemochromatosis. Nature Genetics. 2003;33:21.

[90] Kassebaum NJ, Jasrasaria R, Naghavi M, Wulf SK, Johns N, Lozano R, et al. A systematic analysis of global anemia burden from 1990 to 2010. Blood. 2014;123:615-24.

[91] McLean E, Cogswell M, Egli I, Wojdyla D, De Benoist B. Worldwide prevalence of anaemia, WHO vitamin and mineral nutrition information system, 1993–2005. Public Health Nutrition. 2009;12:444-54.

[92] Stevens GA, Finucane MM, De-Regil LM, Paciorek CJ, Flaxman SR, Branca F, et al. Global, regional, and national trends in haemoglobin concentration and prevalence of total and severe anaemia in children and pregnant and non-pregnant women for 1995–2011: a systematic analysis of population-representative data. The Lancet Global Health. 2013;1:e16-e25.

[93] Lozoff B, Jimenez E, Wolf AW. Long-term developmental outcome of infants with iron deficiency. New England Journal of Medicine. 1991;325:687-94.

[94] Lozoff B, Jimenez E, Hagen J, Mollen E, Wolf AW. Poorer behavioral and developmental outcome more than 10 years after treatment for iron deficiency in infancy. Pediatrics. 2000;105:e51-e.

[95] Beard J. Iron deficiency alters brain development and functioning. The Journal of Nutrition. 2003;133:1468S-72S.

[96] Horton S, Ross J. The economics of iron deficiency. Food Policy. 2003;28:51-75.

[97] World Health Organization. Iron deficiency anaemia: Assessment, prevention and control: A guide for programme managers. 2001.

[98] Pimentel D, Pimentel M. Sustainability of meat-based and plant-based diets and the environment. The American Journal of Clinical Nutrition. 2003;78:660S-3S.

[99] Fiala N. How meat contributes to global warming. Scientific American. 2009;4.

[100] Micha R, Wallace SK, Mozaffarian D. Red and processed meat consumption and risk of incident coronary heart disease, stroke, and diabetes mellitus. A systematic review and meta-analysis. Circulation. 2010.

[101] Monsen ER, Hallberg L, Layrisse M, Hegsted DM, Cook JD, Mertz W, et al. Estimation of available dietary iron. The American Journal of Clinical Nutrition. 1978;31:134-41.

[102] Hurrell RF, Reddy MB, Juillerat M, Cook JD. Meat protein fractions enhance nonheme iron absorption in humans. The Journal of Nutrition. 2006;136:2808-12.

[103] Hurrell R, Egli I. Iron bioavailability and dietary reference values. The American Journal of Clinical Nutrition. 2010;91:1461S-7S.

[104] Lopez A, Cacoub P, Macdougall IC, Peyrin-Biroulet L. Iron deficiency anaemia. The Lancet. 2016;387:907-16.

[105] Wienk KJH, Marx JJM, Beynen AC. The concept of iron bioavailability and its assessment. European Journal of Nutrition. 1999;38:51-75.

[106] West AR, Oates PS. Mechanisms of heme iron absorption: current questions and controversies. World Journal of Gastroenterology. 2008;14:4101.

[107] Hunt JR. Moving Toward a Plant-based Diet: Are Iron and Zinc at Risk? Nutrition reviews. 2002;60:127-34.

[108] Hallberg L. Bioavailability of dietary iron in man. Annual

Review of Nutrition. 1981;1:123-47.

[109] Fairweather-Tait S, Lynch S, Hotz C, Hurrell R, Abrahamse L, Beebe S, et al. The usefulness of in vitro models to predict the bioavailability of iron and zinc: a consensus statement from the HarvestPlus expert consultation. International Journal for Vitamin and Nutrition Research. 2005;75:371-4.

[110] Betesh AL, Santa Ana CA, Cole JA, Fordtran JS. Is achlorhydria a cause of iron deficiency anemia? The American Journal of Clinical Nutrition. 2015;102:9-19.

[111] Champagne ET. Low gastric hydrochloric acid secretion and mineral bioavailability. Mineral Absorption in the Monogastric GI Tract: Springer; 1989. p. 173-84.

[112] Siegenberg D, Baynes RD, Bothwell TH, Macfarlane BJ, Lamparelli RD, Car NG, et al. Ascorbic acid prevents the dose-dependent inhibitory effects of polyphenols and phytates on nonheme-iron absorption. The American Journal of Clinical Nutrition. 1991;53:537-41.

[113] Hallberg L, Brune M, Rossander L. Iron absorption in man: ascorbic acid and dose-dependent inhibition by phytate. The American Journal of Clinical Nutrition. 1989;49:140-4.

[114] Ma Q, Kim E-Y, Han O. Bioactive dietary polyphenols decrease heme iron absorption by decreasing basolateral iron release in human intestinal Caco-2 cells. The Journal of Nutrition. 2010;140:1117-21.

[115] Walczyk T, Muthayya S, Wegmüller R, Thankachan P, Sierksma A, Frenken LGJ, et al. Inhibition of iron absorption by calcium is modest in an iron-fortified, casein-and whey-based drink in Indian children and is easily compensated for by addition of ascorbic acid. The Journal of Nutrition. 2014;144:1703-9.

[116] World Health Organization, Allen LH, De Benoist B, Dary O, Hurrell R. Guidelines on food fortification with micronutrients. 2006.

[117] Hurrell RF, Egli I. Optimizing the bioavailability of iron compounds for food fortification. Nutritional Anemia. 2007:77.

[118] Gillooly M, Bothwell TH, Torrance JD, MacPhail AP, Derman DP, Bezwoda WR, et al. The effects of organic acids, phytates and polyphenols on the absorption of iron from vegetables. British Journal of Nutrition. 1983;49:331-42.

[119] Hunt JR, Gallagher SK, Johnson LK. Effect of ascorbic acid on apparent iron absorption by women with low iron stores. The American Journal of Clinical Nutrition. 1994;59:1381-5.

[120] Cook JD, Reddy MB. Effect of ascorbic acid intake on nonheme-iron absorption from a complete diet. The American Journal of Clinical Nutrition. 2001;73:93-8.

[121] Conrad ME, Schade SG. Ascorbic acid chelates in iron absorption: a role for hydrochloric acid and bile. Gastroenterology. 1968;55:35-45.

[122] Lynch SR, Cook JD. Interaction of vitamin C and iron. Annals of the New York Academy of Sciences. 1980;355:32-44.

[123] South PK, Miller DD. Iron binding by tannic acid: effects of selected ligands. Food Chemistry. 1998;63:167-72.

[124] Han O, Failla ML, Hill AD, Morris ER, Smith JC. Ascorbate offsets the inhibitory effect of inositol phosphates on iron uptake and transport by Caco-2 cells. Experimental Biology and Medicine. 1995;210:50-6.

[125] Luo X, Hill M, Johnson A, Latunde-Dada GO. Modulation of Dcytb (Cybrd 1) expression and function by iron, dehydroascorbate and Hif-2αin cultured cells. Biochim Biophys Acta 2014;1840:106-12.

[126] Scheers NM, Sandberg A-S. Ascorbic acid uptake affects ferritin, Dcytb and Nramp2 expression in Caco-2 cells. European Journal of Nutrition. 2008;47:401-8.

[127] Hurrell RF. Fortification: overcoming technical and practical barriers. Journal of Nutrition. 2002;132:806S-12S.

[128] Teucher, Olivares, Cori. Enhancers of iron absorption: ascorbic acid and other organic acids. International Journal for Vitamin and Nutrition Research. 2004;74:403-19.

[129] Hallberg L, Rossander-Hulthèn L, Brune M, Gleerup A. Inhibition of haem-iron absorption in man by calcium. British Journal of Nutrition. 1993;69:533-40.

[130] Hallberg L, Brune M, Erlandsson M, Sandberg A-S, Rossander-Hulten L. Calcium: effect of different amounts on nonheme-and heme-iron absorption in humans. The American Journal of Clinical Nutrition. 1991;53:112-9.

[131] Barton JC, Conrad ME, Parmley RT. Calcium inhibition of inorganic iron absorption in rats. Gastroenterology. 1983;84:90-101.

[132] Dawson-Hughes B, Seligson FH, Hughes VA. Effects of calcium carbonate and hydroxyapatite on zinc and iron retention in postmenopausal women. The American Journal of Clinical Nutrition. 1986;44:83-8.

[133] Cook JD, Dassenko SA, Whittaker P. Calcium supplementation: effect on iron absorption. The American Journal of Clinical Nutrition. 1991;53:106-11.

[134] Reddy MB, Cook JD. Effect of calcium intake on nonheme-iron absorption from a complete diet. The American Journal of Clinical Nutrition. 1997;65:1820-5.

[135] Minihane AM, Fairweather-Tait SJ. Effect of calcium supplementation on daily nonheme-iron absorption and long-term iron status. The American Journal of Clinical Nutrition. 1998;68:96-102.

[136] Abrams SA, Griffin IJ, Davila P, Liang L. Calcium fortification of breakfast cereal enhances calcium absorption in children without affecting iron absorption. The Journal of Pediatrics. 2001;139:522-6.

[137] Lönnerdal B. Calcium and iron absorption—mechanisms and public health relevance. International Journal for Vitamin and Nutrition Research. 2010;80:293.

[138] Shawki A, Mackenzie B. Interaction of calcium with the human divalent metal-ion transporter-1. Biochemical and Biophysical Research Communications. 2010;393:471-5.

[139] Thompson BA, Sharp PA, Elliott R, Fairweather-Tait SJ. Inhibitory effect of calcium on non-heme iron absorption may be related to translocation of DMT-1 at the apical membrane of enterocytes. Journal of Agriculture and Food Chemistry. 2010;58:8414-7.

[140] Gaitán DA, Flores S, Pizarro F, Olivares M, Suazo M, Arredondo M. The effect of calcium on non-heme iron uptake, efflux, and transport in intestinal-like epithelial cells (Caco-2 cells). Biological Trace Element Research. 2012;145:300-3.

[141] Lynch SR. The effect of calcium on iron absorption. Nutrition Research Reviews. 2000;13:141-58.

[142] Hurrell. Phytic acid degradation as a means of improving iron absorption. International Journal for Vitamin and Nutrition Research. 2004;74:445-52.

[143] Ravindran V, Ravindran G, Sivalogan S. Total and phytate phosphorus contents of various foods and feedstuffs of plant origin. Food Chemistry. 1994;50:133-6.

[144] Reddy NR, Sathe SK, Salunkhe DK. Phytates in legumes and cereals. Advances in Food Research. 1982;28:1-92.

[145] Brune M, Rossander-Hultén L, Hallberg L, Gleerup A, Sandberg AS. Iron absorption from bread in humans: inhibiting effects of cereal fiber, phytate and inositol phosphates with different numbers of phosphate groups. The Journal of Nutrition. 1992;122:442-9.

[146] Fairweather-Tait SJ. The effect of different levels of wheat bran on iron absorption in rats from bread containing similar amounts of phytate. British Journal of Nutrition. 1982;47:243-9.

[147] Hallberg L, Rossander L, Skånberg AB. Phytates and the inhibitory effect of bran on iron absorption in man. The American Journal of Clinical Nutrition. 1987;45:988-96.

[148] Frontela C, Ros G, Martínez C. Phytic acid content and “in vitro” iron, calcium and zinc bioavailability in bakery products: The effect of processing. Journal of Cereal Science. 2011;54:173-9.

[149] Eagling T, Wawer AA, Shewry PR, Zhao F-J, Fairweather-Tait SJ. Iron bioavailability in two commercial cultivars of wheat: comparison between wholegrain and white flour and the effects of nicotianamine and 2′-deoxymugineic acid on iron uptake into Caco-2 cells. Journal of Agricultural and Food Chemistry. 2014;62:10320-5.

[150] Scheers N, Rossander-Hulthen L, Torsdottir I, Sandberg A-S. Increased iron bioavailability from lactic-fermented vegetables is likely an effect of promoting the formation of ferric iron (Fe3+). European Journal of Nutrition. 2016;55:373-82.

[151] Rodriguez-Ramiro I, Brearley CA, Bruggraber SFA, Perfecto A, Shewry P, Fairweather-Tait S. Assessment of iron bioavailability from different bread making processes using an in vitro intestinal cell model. Food Chemistry. 2017;228:91-8.

[152] Frontela C, Scarino ML, Ferruzza S, Ros G, Martínez C. Effect of dephytinization on bioavailability of iron, calcium and zinc from infant cereals assessed in the Caco-2 cell model. World Journal of Gastroenterology. 2009;15:1977-84.

[153] Davidsson L, Galan P, Cherouvrier F, Kastenmayer P, Juillerat M-A, Hercberg S, et al. Bioavailability in infants of iron from infant cereals: effect of dephytinization. The American Journal of Clinical Nutrition. 1997;65:916-20.

[154] Schlemmer U, Frølich W, Prieto RM, Grases F. Phytate in foods and significance for humans: food sources, intake, processing, bioavailability, protective role and analysis. Molecular Nutrition & Food Research. 2009;53:S330-S75.

[155] Manach C, Scalbert A, Morand C, Rémésy C, Jiménez L. Polyphenols: food sources and bioavailability. The American Journal of Clinical Nutrition. 2004;79:727-47.

[156] Hurrell RF, Reddy M, Cook JD. Inhibition of non-haem iron absorption in man by polyphenolic-containing beverages. British Journal of Nutrition. 1999;81:289-95.

[157] Tuntawiroon M, Sritongkul N, Brune M, Rossander-Hulten L, Pleehachinda R, Suwanik R, et al. Dose-dependent inhibitory effect of phenolic compounds in foods on nonheme-iron absorption in men. The American Journal of Clinical Nutrition. 1991;53:554-7.

[158] Disler P, Lynch SR, Charlton RW, Torrance JD, Bothwell TH, Walker RB, et al. The effect of tea on iron absorption. Gut. 1975;16:193-200.

[159] Rossander L, Hallberg L, Björn-Rasmussen E. Absorption of iron from breakfast meals. The American Journal of Clinical Nutrition. 1979;32:2484-9.

[160] Morck TA, Lynch SR, Cook JD. Inhibition of food iron absorption by coffee. The American Journal of Clinical Nutrition. 1983;37:416-20.

[161] Disler PB, Lynch SR, Torrance JD, Sayers MH, Bothwell TH, Charlton RW. The mechanism of the inhibition of iron absorption by tea. The South African Journal of Medical Sciences. 1974;40:109-16.

[162] Kim E-Y, Ham S-K, Shigenaga MK, Han O. Bioactive dietary polyphenolic compounds reduce nonheme iron transport across human intestinal cell monolayers. The Journal of Nutrition. 2008;138:1647-51.

[163] Lesjak M, Hoque R, Balesaria S, Skinner V, Debnam ES, Srai SKS, et al. Quercetin inhibits intestinal iron absorption and ferroportin transporter expression in vivo and in vitro. PloS one. 2014;9:e102900.

[164] Auerbach M, Adamson JW. How we diagnose and treat iron deficiency anemia. American Journal of Hematology. 2016;91:31-8.

[165] Fairbanks VF, Beutler E. Iron metabolism. Williams Hematology 5th ed New York, NY: McGraw-Hill. 1995:369-80.

[166] Goddard AF, James MW, McIntyre AS, Scott BB. Guidelines for the management of iron deficiency anaemia. Gut. 2011:IV4-5.

[167] Roughead ZK, Hunt JR. Adaptation in iron absorption: iron supplementation reduces nonheme-iron but not heme-iron absorption from food. The American Journal of Clinical Nutrition. 2000;72:982-9.

[168] Santiago P. Ferrous versus ferric oral iron formulations for the treatment of iron deficiency: a clinical overview. The Scientific World Journal. 2012;2012:1-5.

[169] Davila-Hicks P, Theil EC, Lönnerdal B. Iron in ferritin or in salts (ferrous sulfate) is equally bioavailable in nonanemic women. The American Journal of Clinical Nutrition. 2004;80:936-40.

[170] Harrington M, Hotz C, Zeder C, Polvo GO, Villalpando S, Zimmermann MB, et al. A comparison of the bioavailability of ferrous fumarate and ferrous sulfate in non-anemic Mexican women and children consuming a sweetened maize and milk drink. European Journal of Clinical Nutrition. 2011;65:20-5.

[171] Cancelo-Hidalgo MJ, Castelo-Branco C, Palacios S, Haya-Palazuelos J, Ciria-Recasens M, Manasanch J, et al. Tolerability of different oral iron supplements: a systematic review. Current Medical Research and Opinion. 2013;29:291-303.

[172] Makrides M, Crowther CA, Gibson RA, Gibson RS, Skeaff CM. Efficacy and tolerability of low-dose iron supplements during pregnancy: a randomized controlled trial. The American Journal of Clinical Nutrition. 2003;78:145-53.

[173] Tolkien Z, Stecher L, Mander AP, Pereira DIA, Powell JJ. Ferrous sulfate supplementation causes significant gastrointestinal side-effects in adults: a systematic review and meta-analysis. PloS one. 2015;10:e0117383.

[174] Lund EK, Wharf SG, Fairweather-Tait SJ, Johnson IT. Oral ferrous sulfate supplements increase the free radical–generating capacity of feces from healthy volunteers. The American Journal of Clinical Nutrition. 1999;69:250-5.

[175] Seril DN, Liao J, Ho K-LK, Warsi A, Yang CS, Yang G-Y. Dietary iron supplementation enhances DSS-induced colitis and associated colorectal carcinoma development in mice. Digestive Diseases and Sciences. 2002;47:1266-78.

[176] Werner T, Wagner SJ, Martínez I, Walter J, Chang J-S, Clavel T, et al. Depletion of luminal iron alters the gut microbiota and prevents Crohn's disease-like ileitis. Gut. 2010:2010.216929.

[177] Zimmermann MB, Chassard C, Rohner F, N'Goran EK, Nindjin C, Dostal A, et al. The effects of iron fortification on the gut microbiota in African children: a randomized controlled trial in Cote d'Ivoire. The American Journal of Clinical Nutrition. 2010;92:1406-15.

[178] Bouis HE, Hotz C, McClafferty B, Meenakshi JV, Pfeiffer WH. Biofortification: a new tool to reduce micronutrient malnutrition. Food and Nutrition Bulletin. 2011;32:S31-S40.

[179] Rengel Z, Batten GD, Crowley DEd. Agronomic approaches for improving the micronutrient density in edible portions of field crops. Field Crops Research. 1999;60:27-40.

[180] Zhang Y, Shi R, Rezaul KM, Zhang F, Zou C. Iron and zinc concentrations in grain and flour of winter wheat as affected by foliar application. Journal of Agricultural and Food Chemistry. 2010;58:12268-74.

[181] Aciksoz SB, Yazici A, Ozturk L, Cakmak I. Biofortification of wheat with iron through soil and foliar application of nitrogen and iron fertilizers. Plant and Soil. 2011;349:215-25.

[182] Fawzi AFA, El-Fouly MM, Moubarak ZM. The need of grain legumes for iron, manganese, and zinc fertilization under Egyptian soil conditions: effect and uptake of metalosates. Journal of Plant Nutrition. 1993;16:813-23.

[183] Murgia I, Arosio P, Tarantino D, Soave C. Biofortification for combating ‘hidden hunger’for iron. Trends in Plant Science. 2012;17:47-55.

[184] Haas JD, Beard JL, Murray-Kolb LE, del Mundo AM, Felix A, Gregorio GB. Iron-biofortified rice improves the iron stores of nonanemic Filipino women. The Journal of Nutrition. 2005;135:2823-30.

[185] Trijatmiko KR, Dueñas C, Tsakirpaloglou N, Torrizo L, Arines FM, Adeva C, et al. Biofortified indica rice attains iron and zinc nutrition dietary targets in the field. Scientific Reports. 2016;6.

[186] Guttieri M, Bowen D, Dorsch JA, Raboy V, Souza E. Identification and characterization of a low phytic acid wheat. Crop Science. 2004;44:418-24.

[187] Zhao H-J, Liu Q-L, Fu H-W, Xu X-H, Wu D-X, Shu Q-Y. Effect of non-lethal low phytic acid mutations on grain yield and seed viability in rice. Field Crops Research. 2008;108:206-11.

[188] Petry N, Egli I, Campion B, Nielsen E, Hurrell R. Genetic reduction of phytate in common bean (Phaseolus vulgaris L.) seeds increases iron absorption in young women. The Journal of Nutrition. 2013;143:1219-24.

[189] Petry N, Rohner F, Gahutu JB, Campion B, Boy E, Tugirimana PL, et al. In Rwandese women with low iron status, iron absorption from low-phytic acid beans and biofortified beans is comparable, but low-phytic acid beans cause adverse gastrointestinal symptoms. The Journal of Nutrition. 2016;146:970-5.

[190] Haas JD, Luna SV, Lung'aho MG, Wenger MJ, Murray-Kolb LE, Beebe S, et al. Consuming iron biofortified beans increases iron status in Rwandan women after 128 days in a randomized controlled feeding trial. The Journal of Nutrition. 2016;146:1586-92.

[191] Lynch SR. The impact of iron fortification on nutritional anaemia. Best Pract Res Clin Haematol. 2005;18:333-46.

[192] Motzok I, Pennell M, Davies M, Ross H. Effect of particle size on the biological availability of reduced iron. Journal Association of Official Analytical Chemistry. 1975;58:99-103.

[193] Verma R, Motzok I, Chen S, Rasper J, Ross H. Effect of storage in flour and of particle size on the bioavailability of elemental iron powders for rats and humans. Journal-Association of Official Analytical Chemists. 1977;60:759-65.

[194] Harrison B, Pla G, Clark G, Fritz J. Selection of iron sources for cereal enrichment. Cereal Chem. 1976;53:78-84.

[195] Wegmüller R, Zimmermann MB, Moretti D, Arnold M, Langhans W, Hurrell RF. Particle size reduction and encapsulation affect the bioavailability of ferric pyrophosphate in rats. The Journal of Nutrition. 2004;134:3301-4.

[196] Fidler MC, Walczyk T, Davidsson L, Zeder C, Sakaguchi N, Juneja LR, et al. A micronised, dispersible ferric pyrophosphate with high relative bioavailability in man. British Journal of Nutrition. 2004;91:107-12.

[197] Moretti D, Zimmermann MB, Muthayya S, Thankachan P, Lee T-C, Kurpad AV, et al. Extruded rice fortified with micronized ground ferric pyrophosphate reduces iron deficiency in Indian schoolchildren: a double-blind randomized controlled trial. The American Journal of Clinical Nutrition. 2006;84:822-9.

[198] MacPhail AP, Patel RC, Bothwell TH, Lamparelli RD. EDTA and the absorption of iron from food. The American Journal of Clinical Nutrition. 1994;59:644-8.

[199] Hurrell R. How to ensure adequate iron absorption from iron-fortified food. Nutrition Reviews. 2002;60.

[200] Davidsson L, Dimitriou T, Boy E, Walczyk T, Hurrell RF. Iron bioavailability from iron-fortified Guatemalan meals based on corn tortillas and black bean paste. The American Journal of Clinical Nutrition. 2002;75:535-9.

[201] Viteri FE, Álvarez E, Batres R, Torun B, Pineda O, Mejía LA, et al. Fortification of sugar with iron sodium ethylenediaminotetraacetate (FeNaEDTA) improves iron status in semirural Guatemalan populations. The American Journal of Clinical Nutrition. 1995;61:1153-63.

[202] Van Thuy P, Berger J, Davidsson L, Khan NC, Lam NT, Cook JD, et al. Regular consumption of NaFeEDTA-fortified fish sauce improves iron status and reduces the prevalence of anemia in anemic Vietnamese women. The American Journal of Clinical Nutrition. 2003;78:284-90.

[203] Fidler MC, Davidsson L, Walczyk T, Hurrell RF. Iron absorption from fish sauce and soy sauce fortified with sodium iron EDTA. The American Journal of Clinical Nutrition. 2003;78:274-8.

[204] Hallberg L, Hulthén L. No advantage of using ferrous bisglycinate as an iron fortificant. The American Journal of Clinical Nutrition. 2000;72:1592-3.

[205] Hertrampf, Olivares. Iron amino acid chelates. International Journal for Vitamin and Nutrition Research. 2004;74:435-43.

[206] Bovell-Benjamin AC, Viteri FE, Allen LH. Iron absorption from ferrous bisglycinate and ferric trisglycinate in whole maize is regulated by iron status. The American Journal of Clinical Nutrition. 2000;71:1563-9.

[207] Layrisse M, García-Casal MN, Solano L, Barón MA, Arguello F, Llovera D, et al. Iron bioavailability in humans from breakfasts enriched with iron bis-glycine chelate, phytates and polyphenols. The Journal of Nutrition. 2000;130:2195-9.

[208] Reddy MB, Cook JD. Assessment of dietary determinants of nonheme-iron absorption in humans and rats. The American Journal of Clinical Nutrition. 1991;54:723-8.

[209] Hurrell RF. Bioavailability of iron. European Journal of Clinical Nutrition. 1997;51:S4-8.

[210] Kastenmayer P, Davidsson L, Galanz P, Cherouvrier F, Hercberg S, Hurrell RF. A double stable isotope technique for measuring iron absorption in infants. British Journal of Nutrition. 1994;71:411-24.

[211] Davidsson L, Galan P, Kastenmayer P, Cherouvrier F, Juillerat MA, Hercberg S, et al. Iron bioavailability studied in infants: the influence of phytic acid and ascorbic acid in infant formulas based on soy isolate. Pediatric Research. 1994;36:816-22.

[212] Hallberg L. Bioavailability of dietary iron in man. Annual Review of Nutrition. 1981;1:123-47.

[213] Glahn R, McClements D, Decker E. The use of Caco-2 cells in defining nutrient bioavailability: application to iron bioavailability of foods. Designing functional foods: measuring and controlling food structure breakdown and nutrient absorption. 2009:340-61.

[214] Miller DD, Schricker BR, Rasmussen RR, Van Campen D. An in vitro method for estimation of iron availability from meals. The American Journal of Clinical Nutrition. 1981;34:2248-56.

[215] Pynaert I, Armah C, Fairweather-Tait S, Kolsteren P, Van Camp J, De Henauw S. Iron solubility compared with in vitro digestion–Caco-2 cell culture method for the assessment of iron bioavailability in a processed and unprocessed complementary food for Tanzanian infants (6–12 months). British Journal of Nutrition. 2006;95:721-6.

[216] Garcia MN, Flowers C, Cook JD. The Caco-2 cell culture system can be used as a model to study food iron availability. The Journal of Nutrition. 1996;126:251-8.

[217] Gangloff MB, Glahn RP, Miller DD, Van Campen DR. Assessment of iron availability using combined in vitro digestion and Caco-2 cell culture. Nutrition Research. 1996;16:479-87.

[218] Glahn RP, Lee OA, Yeung A, Goldman MI, Miller DD. Caco-2 cell ferritin formation predicts nonradiolabeled food iron availability in an in vitro digestion/Caco-2 cell culture model. The Journal of Nutrition. 1998;128:1555-61.

[219] Fogh J, Fogh JM, Orfeo T. One hundred and twenty-seven cultured human tumor cell lines producing tumors in nude mice. Journal of the National Cancer Institute. 1977;59:221-6.

[220] Hidalgo IJ, Raub TJ, Borchardt RT. Characterization of the human colon carcinoma cell line (Caco-2) as a model system for intestinal epithelial permeability. Gastroenterology. 1989;96:736-49.

[221] Vachon PH, Beaulieu J-F. Transient mosaic patterns of morphological and functional differentiation in the Caco-2 cell line. Gastroenterology. 1992;103:414-23.

[222] Jumarie C, Malo C. Caco-2 cells cultured in serum-free medium as a model for the study of enterocytic differentiation in vitro. Journal of Cellular Physiology. 1991;149:24-33.

[223] Halleux C, Schneider Y-J. Iron absorption by intestinal epithelial cells: 1. CaCo2 cells cultivated in serum-free medium, on polyethyleneterephthalate microporous membranes, as an in vitro model. In Vitro Cellular & Developmental Biology-Animal. 1991;27:293-302.

[224] Sambuy Y, De Angelis I, Ranaldi G, Scarino ML, Stammati A, Zucco F. The Caco-2 cell line as a model of the intestinal barrier: influence of cell and culture-related factors on Caco-2 cell functional characteristics. Cell Biology and Toxicology. 2005;21:1-26.

[225] Briske-Anderson MJ, Finley JW, Newman SM. The influence of culture time and passage number on the morphological and physiological development of Caco-2 cells. Experimental Biology and Medicine. 1997;214:248-57.

[226] Alvarez-Hernandez X, Nichols GM, Glass J. Caco-2 cell line: a system for studying intestinal iron transport across epithelial cell monolayers. Biochimica et Biophysica Acta (BBA)-Biomembranes. 1991;1070:205-8.

[227] Gangloff MB, Lai C, Van Campen DR, Miller DD. Ferrous iron uptake but not transfer is down-regulated in Caco-2 cells grown in high iron serum-free medium. The Journal of Nutrition. 1996;126:3118.

[228] Han O, Failla ML, Hill AD, Morris ER, Smith Jr JC. Reduction of Fe (III) is required for uptake of nonheme iron by Caco-2 cells. The Journal of Nutrition. 1995;125:1291-9.

[229] Han O, Fleet JC, Wood RJ. Reciprocal regulation of HFE and Nramp2 gene expression by iron in human intestinal cells. The Journal of Nutrition. 1999;129:98-104.

[230] Sharp P, Tandy S, Yamaji S, Tennant J, Williams M, Singh Srai SK. Rapid regulation of divalent metal transporter (DMT1) protein but not mRNA expression by non-haem iron in human intestinal Caco-2 cells. FEBS letters. 2002;510:71-6.

[231] Martini LA, Tchack L, Wood RJ. Iron treatment downregulates DMT1 and IREG1 mRNA expression in Caco-2 cells. The Journal of Nutrition. 2002;132:693-6.

[232] Johnson DM, Yamaji S, Tennant J, Srai SK, Sharp PA. Regulation of divalent metal transporter expression in human intestinal epithelial cells following exposure to non-haem iron. FEBS letters. 2005;579:1923-9.

[233] Tandy S, Williams M, Leggett A, Lopez-Jimenez M, Dedes M, Ramesh B, et al. Nramp2 expression is associated with pH-dependent iron uptake across the apical membrane of human intestinal Caco-2 cells. Journal of Biological Chemistry. 2000;275:1023-9.

[234] Bannon DI, Abounader R, Lees PSJ, Bressler JP. Effect of DMT1 knockdown on iron, cadmium, and lead uptake in Caco-2 cells. American Journal of Physiology-Cell Physiology. 2003;284:C44-C50.

[235] Bannon DI, Abounader R, Lees PS, Bressler JP. Effect of DMT1 knockdown on iron, cadmium, and lead uptake in Caco-2 cells. American Journal of Physiology-Cell Physiology. 2003;284:C44-C50.

[236] Han O, Kim EY. Colocalization of ferroportin-1 with hephaestin on the basolateral membrane of human intestinal absorptive cells. Journal of Cellular Biochemistry. 2007;101:1000-10.

[237] Yamaji S, Sharp P, Ramesh B, Srai SK. Inhibition of iron transport across human intestinal epithelial cells by hepcidin. Blood. 2004;104:2178-80.

[238] Chung B, Chaston T, Marks J, Srai SK, Sharp PA. Hepcidin decreases iron transporter expression in vivo in mouse duodenum and spleen and in vitro in THP-1 macrophages and intestinal Caco-2 cells. The Journal of Nutrition. 2009;139:1457-62.

[239] Chaston T, Chung B, Mascarenhas M, Marks J, Patel B, Srai SK, et al. Evidence for differential effects of hepcidin in macrophages and intestinal epithelial cells. Gut. 2008;57:374-82.

[240] Mena NP, Esparza A, Tapia V, Valdés P, Nunez MT. Hepcidin inhibits apical iron uptake in intestinal cells. American Journal of Physiology-Gastrointestinal and Liver Physiology. 2008;294:G192-8.

[241] Brasse–Lagnel C, Karim Z, Letteron P, Bekri S, Bado A, Beaumont C. Intestinal DMT1 cotransporter is down-regulated by hepcidin via proteasome internalization and degradation. Gastroenterology. 2011;140:1261-71.

[242] Yun S, Habicht J-P, Miller DD, Glahn RP. An in vitro digestion/Caco-2 cell culture system accurately predicts the effects of ascorbic acid and polyphenolic compounds on iron bioavailability in humans. The Journal of Nutrition. 2004;134:2717-21.

[243] Björn-Rasmussen E, Hallberg L. Effect of animal proteins on the absorption of food iron in man. Annals of Nutrition and Metabolism. 1979;23:192-202.

[244] Cook JD, Monsen ER. Food iron absorption in human subjects. III. Comparison of the effect of animal proteins on nonheme iron absorption. The American Journal of Clinical Nutrition. 1976;29:859-67.

[245] Glahn RP, Wien EM, Van Campen DR, Miller DD. Caco-2 cell iron uptake from meat and casein digests parallels in vivo studies: use of a novel in vitro method for rapid estimation of iron bioavailability. The Journal of Nutrition. 1996;126:332-9.

[246] Glahn RP, Van Campen DR. Iron uptake is enhanced in Caco-2 cell monolayers by cysteine and reduced cysteinyl glycine. The Journal of Nutrition. 1997;127:642-7.

[247] Swain JH, Tabatabai LB, Reddy MB. Histidine content of low-molecular-weight beef proteins influences nonheme iron bioavailability in Caco-2 cells. The Journal of Nutrition. 2002;132:245-51.

[248] Glahn RP, Wortley GM, South PK, Miller DD. Inhibition of iron uptake by phytic acid, tannic acid, and ZnCl2: studies using an in vitro digestion/Caco-2 cell model. Journal of Agricultural and Food Chemistry. 2002;50:390-5.

[249] Engle-Stone R, Yeung A, Welch R, Glahn R. Meat and ascorbic acid can promote Fe availability from Fe– phytate but not from Fe– tannic acid complexes. Journal of Agricultural and Food Chemistry. 2005;53:10276-84.

[250] Boato F, Wortley GM, Liu RH, Glahn RP. Red grape juice inhibits iron availability: application of an in vitro digestion/Caco-2 cell model. Journal of Agricultural and Food Chemistry. 2002;50:6935-8.

[251] Hart JJ, Tako E, Kochian LV, Glahn RP. Identification of black bean (Phaseolus vulgaris L.) polyphenols that inhibit and promote iron uptake by Caco-2 cells. Journal of Agricultural and Food Chemistry. 2015;63:5950-6.

[252] Hu Y, Cheng Z, Heller LI, Krasnoff SB, Glahn RP, Welch RM. Kaempferol in red and pinto bean seed (Phaseolus vulgaris L.) coats inhibits iron bioavailability using an in vitro digestion/human Caco-2 cell model. Journal of Agricultural and Food Chemistry. 2006;54:9254-61.

[253] Glahn RP, Cheng Z, Welch RM, Gregorio GB. Comparison of iron bioavailability from 15 rice genotypes: studies using an in vitro digestion/Caco-2 cell culture model. Journal of Agricultural and Food Chemistry. 2002;50:3586-91.

[254] Oikeh SO, Menkir A, Maziya-Dixon B, Welch RM, Glahn RP. Assessment of iron bioavailability from twenty elite late-maturing tropical maize varieties using an in vitro digestion/Caco-2 cell model. Journal of the Science of Food and Agriculture. 2004;84:1202-6.

[255] Ariza-Nieto M, Blair MW, Welch RM, Glahn RP. Screening of iron bioavailability patterns in eight bean (Phaseolus vulgaris L.) genotypes using the Caco-2 cell in vitro model. Journal of Agricultural and Food Chemistry. 2007;55:7950-6.

[256] Tako E, Glahn RP. White beans provide more bioavailable iron than red beans: studies in poultry (Gallus gallus) and an in vitro digestion/Caco-2 model. International Journal for Vitamin and Nutrition Research. 2010;80:416-29.

[257] Drakakaki G, Marcel S, Glahn RP, Lund EK, Pariagh S, Fischer R, et al. Endosperm-specific co-expression of recombinant soybean ferritin and Aspergillus phytase in maize results in significant increases in the levels of bioavailable iron. Plant Molecular Biology. 2005;59:869-80.

[258] Tako E, Blair MW, Glahn RP. Biofortified red mottled beans (Phaseolus vulgaris L.) in a maize and bean diet provide more bioavailable iron than standard red mottled beans: Studies in poultry (Gallus gallus) and an in vitro digestion/Caco-2 model. Nutrition Journal. 2011;10:113.

[259] Glahn RP, Rassier M, Goldman MI, Lee OA, Cha J. A comparison of iron availability from commercial iron preparations using an in vitro digestion/Caco-2 cell culture model. The Journal of Nutritional Biochemistry. 2000;11:62-8.

[260] Zhu L, Glahn RP, Yeung CK, Miller DD. Iron uptake by Caco-2 cells from NaFeEDTA and FeSO4: Effects of ascorbic acid, pH, and a Fe (II) chelating agent. Journal of Agricultural and Food Chemistry. 2006;54:7924-8.

[261] García-Casal MN, Leets I, Layrisse M. Ethylenediaminetetraacetic acid (EDTA) does not increase iron uptake or ferritin synthesis by Caco-2 cells. The Journal of Nutritional Biochemistry. 2004;15:261-6.

[262] Yeung CK, Miller DD, Cheng Z, Glahn RE. Bioavailability of Elemental Iron Powders in Bread Assessed with an In vitro Digestion/Caco-2 Cell Culture Model. Journal of Food Science. 2005;70:S199-203.

[263] Wortley G, Leusner S, Good C, Gugger E, Glahn R. Iron availability of a fortified processed wheat cereal: a comparison of fourteen iron forms using an in vitro digestion/human colonic adenocarcinoma (CaCo-2) cell model. British Journal of Nutrition. 2005;93:65-71.

[264] Lynch, Bothwell, Campbell L. A comparison of physical properties, screening procedures and a human efficacy trial for predicting the bioavailability of commercial elemental iron powders used for food fortification. International Journal for Vitamin Nutrition Research. 2007;77:107-24.

[265] Swain JH, Newman SM, Hunt JR. Bioavailability of elemental iron powders to rats is less than bakery-grade ferrous sulfate and predicted by iron solubility and particle surface area. The Journal of Nutrition. 2003;133:3546-52.

[266] Arredondo M, Salvat V, Pizarro F, Olivares M. Smaller iron particle size improves bioavailability of hydrogen-reduced iron–fortified bread. Nutrition Research. 2006;26:235-9.

[267] He W-L, Feng Y, Li X-L, Yang X-E. Comparison of iron uptake from reduced iron powder and FeSO4 using the Caco-2 cell model: effects of ascorbic acid, phytic acid, and pH. Journal of Agricultural and Food Chemistry. 2008;56:2637-42.

[268] Au AP, Reddy MB. Caco-2 cells can be used to assess human iron bioavailability from a semipurified meal. The Journal of Nutrition. 2000;130:1329-34.

[269] Cook JD, Monsen ER. Food iron absorption. I. Use of semisynthetic diet to study absorption of nonheme iron. The American Journal of Clinical Nutrition. 1975;28:1289-95.

[270] Beiseigel JM, Hunt JR, Glahn RP, Welch RM, Menkir A, Maziya-Dixon BB. Iron bioavailability from maize and beans: a comparison of human measurements with Caco-2 cell and algorithm predictions. The American Journal of Clinical Nutrition. 2007;86:388-96.

[271] Minekus M, Alminger M, Alvito P, Ballance S, Bohn T, Bourlieu C, et al. A standardised static in vitro digestion method suitable for food–an international consensus. Food & Function. 2014;5:1113-24.

[272] Mahler GJ, Shuler ML, Glahn RP. Characterization of Caco-2 and HT29-MTX cocultures in an in vitro digestion/cell culture model used to predict iron bioavailability. The Journal of Nutritional Biochemistry. 2009;20:494-502.

[273] Lynch S. The precision of in vitro methods and algorithms for predicting the bioavailability of dietary iron. International Journal for Vitamin and Nutrition Research. 2005;75:436-45.

[274] Auffan M, Rose J, Bottero J-Y, Lowry GV, Jolivet J-P, Wiesner MR. Towards a definition of inorganic nanoparticles from an environmental, health and safety perspective. Nature Nanotechnology. 2009;4:634-41.

[275] Mädler L, Kammler H, Mueller R, Pratsinis S. Controlled synthesis of nanostructured particles by flame spray pyrolysis. Journal of Aerosol Science. 2002;33:369-89.

[276] Mueller R, Mädler L, Pratsinis SE. Nanoparticle synthesis at high production rates by flame spray pyrolysis. Chemical Engineering Science. 2003;58:1969-76.

[277] Jahn MR, Shukoor I, Tremel W, Wolfrum U, Kolb U, Nawroth T, et al. Hemin-coupled iron (III)-hydroxide nanoparticles show increased uptake in Caco-2 cells. Journal of Pharmacy and Pharmacology. 2011;63:1522-30.

[278] Bruggraber SF, FARIA NJR, Pereira DIA, Powell JJ. Ligand modified poly oxo-hydroxy metal ion materials, their uses and processes for their preparation. Google Patents; 2011.

[279] Hilty F, Teleki A, Krumeich F, Büchel R, Hurrell R, Pratsinis S, et al. Development and optimization of iron-and zinc-containing nanostructured powders for nutritional applications. Nanotechnology. 2009;20:475101.

[280] Jani P, Halbert GW, Langridge J, Florence AT. Nanoparticle uptake by the rat gastrointestinal mucosa: quantitation and particle size dependency. Journal of Pharmacy and Pharmacology. 1990;42:821-6.

[281] Powell JJ, Faria N, Thomas-McKay E, Pele LC. Origin and fate of dietary nanoparticles and microparticles in the gastrointestinal tract. Journal of Autoimmunity. 2010;34:J226-J33.

[282] Hussain N, Jaitley V, Florence AT. Recent advances in the understanding of uptake of microparticulates across the gastrointestinal lymphatics. Advanced Drug Delivery Reviews. 2001;50:107-42.

[283] Mahler GJ, Esch MB, Tako E, Southard TL, Archer SD, Glahn RP, et al. Oral exposure to polystyrene nanoparticles affects iron absorption. Nature Nanotechnology. 2012;7:264-71.

[284] des Rieux A, Ragnarsson EG, Gullberg E, Préat V, Schneider Y-J, Artursson P. Transport of nanoparticles across an in vitro model of the human intestinal follicle associated epithelium. European Journal of Pharmaceutical Sciences. 2005;25:455-65.

[285] Jahn MR, Nawroth T, Fütterer Sr, Wolfrum U, Kolb U, Langguth P. Iron oxide/hydroxide nanoparticles with negatively charged shells show increased uptake in Caco-2 cells. Molecular Pharmacology. 2012;9:1628-37.

[286] Pereira DI, Mergler BI, Faria N, Bruggraber SF, Aslam MF, Poots LK, et al. Caco-2 cell acquisition of dietary iron (III) invokes a nanoparticulate endocytic pathway. PLoS One. 2013;8:e81250.

[287] Pereira DIA, Bruggraber SFA, Faria N, Poots LK, Tagmount MA, Aslam MF, et al. Nanoparticulate iron (III) oxo-hydroxide delivers safe iron that is well absorbed and utilised in humans. Nanomedicine: Nanotechnology, Biology and Medicine. 2014;10:1877-86.

[288] Rohner F, Ernst FO, Arnold M, Hilbe M, Biebinger R, Ehrensperger F, et al. Synthesis, characterization, and bioavailability in rats of ferric phosphate nanoparticles. Journal of Nutrition. 2007;137:614-9.

[289] Hilty FM, Arnold M, Hilbe M, Teleki A, Knijnenburg JT, Ehrensperger F, et al. Iron from nanocompounds containing iron and zinc is highly bioavailable in rats without tissue accumulation. Nature Nanotechnology. 2010;5:374-80.

[290] Waldo GS, Wright E, Whang Z-H, Briat J-F, Theil EC, Sayers DE. Formation of the Ferritin Iron Mineral Occurs in Plastids (An X-Ray Absorption Spectroscopy Study. Plant Physiology. 1995;109:797-802.

[291] Theil EC. Ferritin: structure, gene regulation, and cellular function in animals, plants, and microorganisms. Annual Review of Biochemistry. 1987;56:289-315.

[292] Aisen P, Enns C, Wessling-Resnick M. Chemistry and biology of eukaryotic iron metabolism. The International Journal of Biochemistry & Cell Biology. 2001;33:940-59.

[293] Yang R, Zhou Z, Sun G, Gao Y, Xu J. Ferritin, a novel vehicle for iron supplementation and food nutritional factors encapsulation. Trends in Food Science & Technology. 2015;44:189-200.

[294] Lönnerdal B. Soybean ferritin: implications for iron status of vegetarians. The American Journal of Clinical Nutrition. 2009;89:1680S-5S.

[295] Lukac RJ, Aluru MR, Reddy MB. Quantification of ferritin from staple food crops. Journal of Agricultural and Food Chemistry. 2009;57:2155-61.

[296] Ambe S, Ambe F, Nozaki T. Mössbauer study of iron in soybean seeds. Journal of Agricultural and Food Chemistry. 1987;35:292-6.

[297] Marentes E, Grusak MA. Iron transport and storage within the seed coat and embryo of developing seeds of pea (Pisum sativum L.). Seed Science Research. 1998;8:367-75.

[298] Hoppler M, Schönbächler A, Meile L, Hurrell RF, Walczyk T. Ferritin-iron is released during boiling and in vitro gastric digestion. The Journal of Nutrition. 2008;138:878-84.

[299] Hoppler M, Egli I, Petry N, Gille D, Zeder C, Walczyk T, et al. Iron Speciation in Beans (Phaseolus vulgaris) Biofortified by Common Breeding. Journal of food science. 2014.

[300] Zhao G. Phytoferritin and its implications for human health and nutrition. Biochimica et Biophysica Acta (BBA)-General Subjects. 2010;1800:815-23.

[301] Zielińska-Dawidziak M. Plant ferritin—a source of iron to prevent its deficiency. Nutrients. 2015;7:1184-201.

[302] Drakakaki G, Christou P, Stöger E. Constitutive expression of soybean ferritin cDNA intransgenic wheat and rice results in increased iron levels in vegetative tissues but not in seeds. Transgenic Research. 2000;9:445-52.

[303] Masuda H, Ishimaru Y, Aung MS, Kobayashi T, Kakei Y, Takahashi M, et al. Iron biofortification in rice by the introduction of multiple genes involved in iron nutrition. Scientific Reports. 2012;2:543.

[304] Murray-Kolb LE, Welch R, Theil EC, Beard JL. Women with low iron stores absorb iron from soybeans. The American Journal of Clinical Nutrition. 2003;77:180-4.

[305] Lönnerdal B, Bryant A, Liu X, Theil EC. Iron absorption from soybean ferritin in nonanemic women. The American Journal of Clinical Nutrition. 2006;83:103-7.

[306] Hussain R, Walker RB, Lavrisse M, Clark P, Finch CA. Nutritive value of food iron. The American Journal of Clinical Nutrition. 1965;16:464-71.

[307] Layrisse M, MartInez-Torres C, Renzy M, Leets I. Ferritin iron absorption in man. Blood. 1975;45:689-98.

[308] Derman D, Bothwell T, Torrance J, Macphail A, Bezwoda W, Charlton R, et al. Iron absorption from ferritin and ferric hydroxide. Scandinavian Journal of Haematology. 1982;29:18-24.

[309] Skikne B, Fonzo D, Lynch S, Cook J. Bovine ferritin iron bioavailability in man. European Journal of Clinical Investigation. 1997;27:228-33.

[310] Martínez-Torres C, Leets I, Taylor P, Ramírez J, del Valle CM, Layrisse M. Heme, ferritin and vegetable iron absorption in humans from meals denatured of heme iron during the cooking of beef. The Journal of Nutrition. 1986;116:1720-5.

[311] Bejjani S, Pullakhandam R, Punjal R, Nair KM. Gastric digestion of pea ferritin and modulation of its iron bioavailability by ascorbic and phytic acids in Caco-2 cells. World Journal of Gastroenterology. 2007;13:2083.

[312] Jin F, Frohman C, Thannhauser TW, Welch RM, Glahn RP. Effects of ascorbic acid, phytic acid and tannic acid on iron bioavailability from reconstituted ferritin measured by an in vitro digestion-Caco-2 cell model. British Journal of Nutrition. 2009;101:972.

[313] Kalgaonkar S, Lönnerdal B. Effects of dietary factors on iron uptake from ferritin by Caco-2 cells. The Journal of nutritional biochemistry. 2008;19:33-9.

[314] Jin F, Welch R, Glahn R. Moving toward a more physiological model: application of mucin to refine the in vitro digestion/Caco-2 cell culture system. Journal of Agricultural and Food Chemistry. 2006;54:8962-7.

[315] Lv C, Zhao G, Lönnerdal B. Bioavailability of iron from plant and animal ferritins. The Journal of Nutritional Biochemistry. 2015;26:532-40.

[316] Kalgaonkar S, Lönnerdal B. Receptor-mediated uptake of ferritin-bound iron by human intestinal Caco-2 cells. Journal of Nutritional Biochemistry. 2009;20:304-11.

[317] San Martin CD, Garri C, Pizarro F, Walter T, Theil EC, Núñez MT. Caco-2 intestinal epithelial cells absorb soybean ferritin by μ2 (AP2)-dependent endocytosis. Journal of Nutrition. 2008;138:659-66.

[318] Owen DJ, Collins BM, Evans PR. Adaptors for clathrin coats: structure and function. Annu Rev Cell Dev Biol. 2004;20:153-91.

[319] Antileo E, Garri C, Tapia V, Muñoz JP, Chiong M, Nualart F, et al. Endocytic pathway of exogenous iron-loaded ferritin in intestinal epithelial (Caco-

2) cells. American Journal of Physiology-Gastrointestinal and Liver Physiology. 2013;304:G655-G61.

[320] Kidane TZ, Sauble E, Linder MC. Release of iron from ferritin requires lysosomal activity. American Journal of Physiology-Cell Physiology. 2006;291:C445-C55.

[321] Theil EC, Chen H, Miranda C, Janser H, Elsenhans B, Núñez MT, et al. Absorption of iron from ferritin is independent of heme iron and ferrous salts in women and rat intestinal segments. The Journal of Nutrition. 2012;142:478-83.

[322] Wang X, Ghio AJ, Yang F, Dolan KG, Garrick MD, Piantadosi CA. Iron uptake and Nramp2/DMT1/DCT1 in human bronchial epithelial cells. Am J Physiol Lung Cell Mol Physiol. 2002;282:L987-L95.

[323] Tulpule K, Robinson SR, Bishop GM, Dringen R. Uptake of ferrous iron by cultured rat astrocytes. J Neurosci Res. 2010;88:563-71.

[324] Strober W. Trypan blue exclusion test of cell viability. Current Protocols in Immunology. 2001:A3-B.

[325] Schmittgen TD, Livak KJ. Analyzing real-time PCR data by the comparative CT method. Nature Protocols. 2008;3:1101-8.

[326] Forbes AL, Arnaud M, Chichester C, Cook J, Harrison B, Hurrell R, et al. Comparison of in vitro, animal, and clinical determinations of iron bioavailability: International Nutritional Anemia Consultative Group Task Force report on iron bioavailability. The American Journal of Clinical Nutrition. 1989;49:225-38.

[327] Laulhere J-P, Laboure A-M, Briat J. Mechanism of the transition from plant ferritin to phytosiderin. Journal of Biological Chemistry. 1989;264:3629-35.

[328] Perfecto A, Elgy C, Valsami-Jones E, Sharp P, Hilty F, Fairweather-Tait S. Mechanisms of Iron Uptake from Ferric Phosphate Nanoparticles in Human Intestinal Caco-2 Cells. Nutrients. 2017;9:359.

[329] Latunde-Dada GO, Pereira DI, Tempest B, Ilyas H, Flynn AC, Aslam MF, et al. A nanoparticulate ferritin-core mimetic is well taken up by hutu 80 duodenal cells and its absorption in mice is regulated by body iron. J Nutr. 2014;144:1896-902.

[330] Arredondo M, Kloosterman J, Núñez S, Segovia F, Candia V, Flores S, et al. Heme iron uptake by Caco-2 cells is a saturable, temperature sensitive and modulated by extracellular pH and potassium. Biological Trace Element Research. 2008;125:109-19.

[331] Bourseau-Guilmain E, Griveau A, Benoit J-P, Garcion E. The importance of the stem cell marker prominin-1/CD133 in the uptake of transferrin and in iron metabolism in human colon cancer Caco-2 cells. PLoS One. 2011;6:e25515.

[332] Krieger SE, Kim C, Zhang L, Marjomaki V, Bergelson JM. Echovirus 1 entry into polarized Caco-2 cells depends on dynamin, cholesterol, and cellular factors associated with macropinocytosis. Journal of Virology. 2013;87:8884-95.

[333] Livak KJ, Schmittgen TD. Analysis of relative gene expression data using real-time quantitative PCR and the 2−(Delta Delta C(T)) method. Methods. 2001;25:402-8.

[334] Bihari P, Vippola M, Schultes S, Praetner M, Khandoga AG, Reichel CA, et al. Optimized dispersion of nanoparticles for biological in vitro and in vivo studies. Particle and Fibre Toxicology. 2008;5:14.

[335] Maiorano G, Sabella S, Sorce B, Brunetti V, Malvindi MA, Cingolani R, et al. Effects of cell culture media on the dynamic formation of protein− nanoparticle complexes and influence on the cellular response. ACS Nano. 2010;4:7481-91.

[336] Sager TM, Porter DW, Robinson VA, Lindsley WG, Schwegler-Berry DE, Castranova V. Improved method to disperse nanoparticles for in vitro and in vivo investigation of toxicity. Nanotoxicology. 2007;1:118-29.

[337] Guggenheim EJ, Khan A, Pike J, Chang L, Lynch I, Rappoport JZ. Comparison of Confocal and Super-Resolution Reflectance Imaging of Metal Oxide Nanoparticles. PloS one. 2016;11:e0159980.

[338] Nel A, Xia T, Mädler L, Li N. Toxic potential of materials at the nanolevel. Science. 2006;311:622-7.

[339] Abbott LC, Maynard AD. Exposure assessment approaches for engineered nanomaterials. Risk Analysis. 2010;30:1634-44.

[340] Fröhlich E. The role of surface charge in cellular uptake and cytotoxicity of medical nanoparticles. International Journal of Nanomedicine. 2012;7:5577-91.

[341] Gerloff K, Pereira DI, Faria N, Boots AW, Kolling J, Förster I, et al. Influence of simulated gastrointestinal conditions on particle-induced cytotoxicity and interleukin-8 regulation in differentiated and undifferentiated Caco-2 cells. Nanotoxicology. 2013;7:353-66.

[342] Wawer AA, Sharp PA, Perez-Moral N, Fairweather-Tait SJ. Evidence for an enhancing effect of alginate on iron availability in Caco-2 cells. J Agric Food Chem. 2012;60:11318-22.

[343] Dutta D, Sundaram SK, Teeguarden JG, Riley BJ, Fifield LS, Jacobs JM, et al. Adsorbed proteins influence the biological activity and molecular targeting of nanomaterials. Toxicological Sciences. 2007;100:303-15.

[344] Conrad ME, Umbreit JN. Iron absorption and transport—an update. American Journal of Hematology. 2000;64:287-98.

[345] Kararli TT. Comparison of the gastrointestinal anatomy, physiology, and biochemistry of humans and commonly used laboratory animals. Biopharmaceutics & Drug Disposition. 1995;16:351-80.

[346] McConnell EL, Basit AW, Murdan S. Measurements of rat and mouse gastrointestinal pH, fluid and lymphoid tissue, and implications for in-vivo experiments. Journal of Pharmacy and Pharmacology. 2008;60:63-70.

[347] des Rieux A, Fievez V, Théate I, Mast J, Préat V, Schneider Y-J. An improved in vitro model of human intestinal follicle-associated epithelium to study nanoparticle transport by M cells. European Journal of Pharmaceutical Sciences. 2007;30:380-91.

[348] Hunt JR. Moving toward a plant-based diet: are iron and zinc at risk? Nutrition Reviews. 2002;60:127-34.

[349] Rodríguez-Ramiro I, Ramos S, Bravo L, Goya L, Martín MÁ. Procyanidin B2 and a cocoa polyphenolic extract inhibit acrylamide-induced apoptosis in human Caco-2 cells by preventing oxidative stress and activation of JNK pathway. The Journal of Nutritional Biochemistry. 2011;22:1186-94.

[350] Bienfait H, Van den Briel M. Rapid mobilization of ferritin iron by ascorbate in the presence of oxygen. Biochimica et Biophysica Acta (BBA)-General Subjects. 1980;631:507-10.

[351] Laulhere J-P, Briat J-Fo. Iron release and uptake by plant ferritin: effects of pH, reduction and chelation. Biochemical Journal. 1993;290:693-9.

[352] Deng J, Cheng J, Liao X, Zhang T, Leng X, Zhao G. Comparative study on iron release from soybean (Glycine max) seed ferritin induced by anthocyanins and ascorbate. Journal of Agricultural and Food Chemistry. 2009;58:635-41.

[353] Kalgaonkar S, Lönnerdal B. Effects of dietary factors on iron uptake from ferritin by Caco-2 cells. Journal of Nutritional Biochemistry. 2008;19:33-9.

[354] Pourvali K, Matak P, Latunde-Dada GO, Solomou S, Mastrogiannaki M, Peyssonnaux C, et al. Basal expression of copper transporter 1 in intestinal epithelial cells is regulated by hypoxia-inducible factor 2α. FEBS letters. 2012;586:2423-7.

[355] Pasricha S-R, Drakesmith H, Black J, Hipgrave D, Biggs B-A. Control of iron deficiency anemia in low-and middle-income countries. Blood. 2013;121:2607-17.

[356] Troesch B, Egli I, Zeder C, Hurrell RF, De Pee S, Zimmermann MB. Optimization of a phytase-containing micronutrient powder with low amounts of highly bioavailable iron for in-home fortification of complementary foods. The American Journal of Clinical Nutrition. 2009;89:539-44.

[357] Troesch B, van Stujivenberg ME, Smuts CM, Kruger HS, Biebinger R, Hurrell RF, et al. A micronutrient powder with low doses of highly absorbable iron and zinc reduces iron and zinc deficiency and improves weight-for-age Z-scores in South African children. The Journal of Nutrition. 2011;141:237-42.

[358] Geerligs P, Brabin, Fairweather T. Iron contents of Malawian foods when prepared in iron cooking pots. International Journal for Vitamin and Nutrition Research. 2004;74:21-6.

[359] Kollipara UK, Brittin HC. Increased iron content of some Indian foods due to cookware. Journal of the Academy of Nutrition and Dietetics. 1996;96:508.

[360] Fairweather-Tait SJ, Fox TE, Mallillin A. Balti curries and iron. BMJ. 1995;310:1368.

[361] Park J, Brittin HC. Increased iron content of food due to stainless steel cookware. Journal of the American Dietetic Association. 1997;97:659-61.

[362] Liu D-Y, Chen Z-G, Lei H-Q, Lu M-Q, Li R, Li L-X. Investigation of the amount of dissolved iron in food cooked in Chinese iron pots and estimation of daily iron intake. Biomedical and environmental sciences: BES. 1990;3:276-80.

[363] Kröger-Ohlsen MV, Trugvason T, Skibsted LH, Michaelsen KF. Release of iron into foods cooked in an iron pot: effect of pH, salt, and organic acids. Journal of Food Science. 2002;67:3301-3.

[364] Martinez FE, Vannucchi H. Bioavailability of iron added to the diet by cooking food in an iron pot. Nutrition Research. 1986;6:421-8.

[365] Geerligs P, Brabin B, Mkumbwa A, Broadhead R, Cuevas L. The effect on haemoglobin of the use of iron cooking pots in rural Malawian households in an area with high malaria prevalence: a randomized trial. Tropical Medicine & International Health. 2003;8:310-5.

[366] Adish AA, Esrey SA, Gyorkos TW, Jean-Baptiste J, Rojhani A. Effect of consumption of food cooked in iron pots on iron status and growth of young children: a randomised trial. The Lancet. 1999;353:712-6.

[367] Borigato EVM, Martinez FE. Iron nutritional status is improved in Brazilian preterm infants fed food cooked in iron pots. The Journal of Nutrition. 1998;128:855-9.

[368] Tripp K, MacKeith N, Woodruff BA, Talley L, Mselle L, Mirghani Z, et al. Acceptability and use of iron and iron-alloy cooking pots: implications for anaemia control programmes. Public Health Nutrition. 2010;13:123-30.

[369] Geerligs PP, Brabin B, Mkumbwa A, Broadhead R, Cuevas LE. Acceptability of the use of iron cooking pots to reduce anaemia in developing countries. Public Health Nutrition. 2002;5:619-24.

[370] Charles CV, Dewey CE, Daniell WE, Summerlee AJS. Iron-deficiency anaemia in rural Cambodia: community trial of a novel iron supplementation technique. The European Journal of Public Health. 2010:ckp237.

[371] Charles CV, Dewey CE, Hall A, Hak C, Channary S, Summerlee AJ. A Randomized Control Trial Using a Fish-Shaped Iron Ingot for the Amelioration of Iron Deficiency Anemia in Rural Cambodian Women. Tropical Medicine & Surgery. 2015;3.

[372] Armstrong GR, Dewey CE, Summerlee AJS. Iron release from the Lucky Iron Fish™: safety considerations.

[373] Cook JD, Minnich V, Moore CV, Rasmussen A, Bradley WB, Finch CA. Absorption of fortification iron in bread. The American Journal of Clinical Nutrition. 1973;26:861-72.

[374] Hallberg L, Brune M, Rossander L. Low bioavailability of carbonyl iron in man: studies on iron fortification of wheat flour. The American Journal of Clinical Nutrition. 1986;43:59-67.

[375] Lynch SR, Beard JL, Dassenko SA, Cook JD. Iron absorption from legumes in humans. The American Journal of Clinical Nutrition. 1984;40:42-7.

[376] Sandberg A-S. Bioavailability of minerals in legumes. British Journal of Nutrition. 2002;88:S281-S5.

[377] Bangar P, Glahn RP, Liu Y, Arganosa GC, Whiting S, Warkentin TD. Iron Bioavailability in Field Pea Seeds: Correlations with Iron, Phytate, and Carotenoids. Crop Science. 2017;57:891-902.

[378] Davidsson L. Approaches to improve iron bioavailability from complementary foods. The Journal of Nutrition. 2003;133:1560S-2S.

[379] Frias J, Vidal-Valverde C, Kozlowska H, Gorecki R, Honke J, Hedley CL. Evolution of soluble carbohydrates during the development of pea, faba bean and lupin seeds. Zeitschrift für Lebensmitteluntersuchung und-Forschung A. 1996;203:27-32.

[380] Pollack S, Kaufman RM, Crosby WH. Iron absorption: effects of sugars and reducing agents. Blood. 1964;24:577-81.

[381] Charley PJ, Sarkar B, Stitt CF, Saltman P. Chelation of iron by sugars. Biochimica et biophysica acta. 1963;69:313-21.

[382] O'Dell BL. Fructose and mineral metabolism. The American Journal of Clinical Nutrition. 1993;58:771S-8S.

[383] Christides T, Sharp P. Sugars increase non-heme iron bioavailability in human epithelial intestinal and liver cells. PloS one. 2013;8:e83031.

[384] Brune M, Rossander L, Hallberg L. Iron absorption and phenolic compounds: importance of different phenolic structures. European Journal of Clinical Nutrition. 1989;43:547-57.

[385] von Moos L, Trantakis I, Rast P, Hilty-Vancura F, Zimmermann M, Pratsinis S, et al. In vitro exposure of human intestinal cells to iron phosphate nanoparticles indicate no direct cytotoxicity. Toxicology Letters. 2013:S242.

8. Appendices

Appendix A Optimisation of Caco-2 transfection

The optimal levels of transfection reagent (Lipofectamine® 3000) were determined in Caco-2 cells seeded at different days in culture. Caco-2 cells were seeded in 96-well plates and transfected according to manufacturer's instructions. Briefly, 0.1 µg GPF plasmid (donated by the Rushworth lab, UEA) was mixed with either 0.35 or 0.5 µg TR. Transfections were carried out 4, 7, and 10 days post seeding and analysed for GFP integrated into cells (using fluorescence microscopy) after 48 hrs.

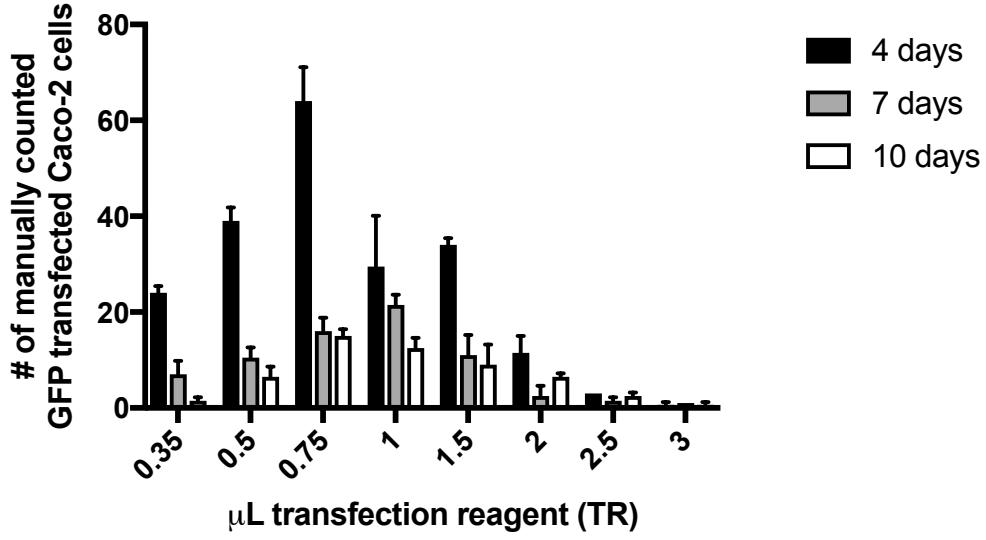

As shown in the graph, transfection efficiency was highest in cells after 4 days post seeding. This was to be expected as cell transfections are usually conducted in pre-confluent cells. Evidence of cellular toxicity occurred with 2 µL TR. The best transfection efficiency occurred with either 0.75 or 1 µL TR. Since all cell culture experiments were conducted at 12 days post confluence, conditions for siRNA treatments were 0.75 µL TR at 10 days post-seeding (scaled up appropriately for 12 well plates).

Appendix B TEM of Caco-2 cell monolayer

Representative TEM images depicting the apical layer of Caco-2 cells (with microvilli) are shown below.

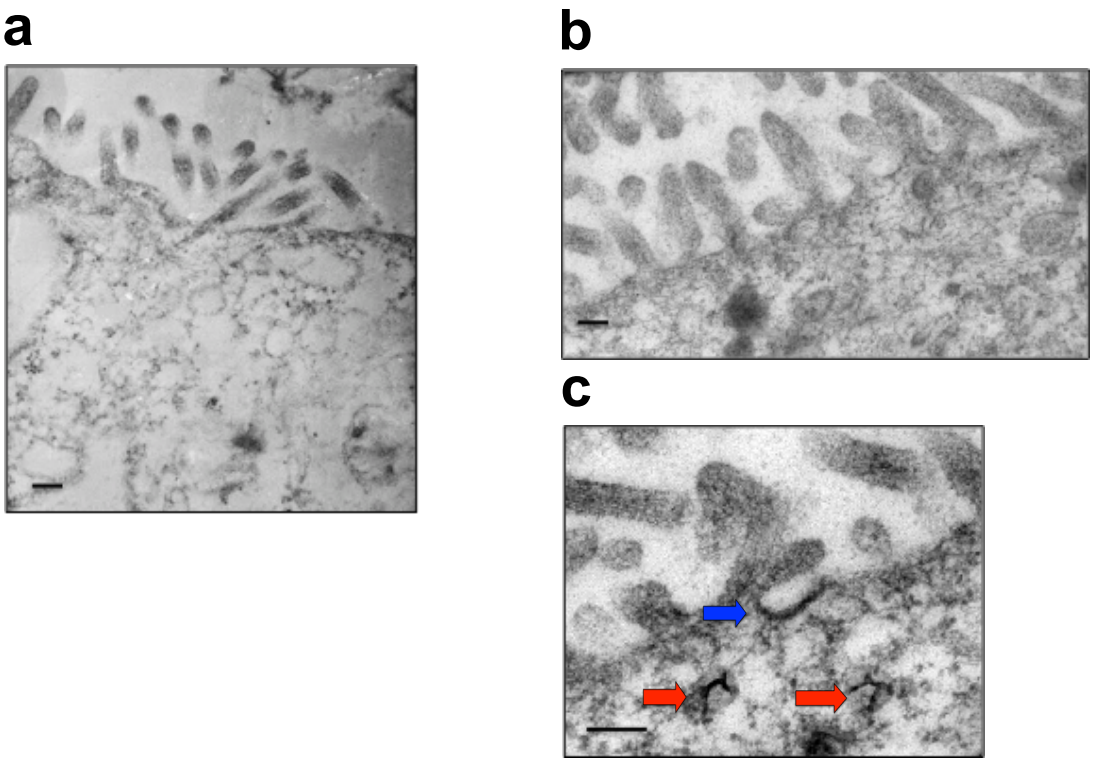

As shown in the images, cells were either left (a) untreated or (b, c) treated with sonicated NP-$FePO_4$ (200). There is evidence of NP uptake in Figure c, signified with blue arrows. The blue arrow is possible evidence of clathrin coat formation and particle internailsation. The red arrows indicate particles within clathrin-coated vesicles. Scale bars represent 200 nm.

Appendix C Presentations/Conferences/Awards

- **Perfecto, Antonio P.** "Pea ferritin uptake in Caco-2 cells."

  Diet and Health Tea Club, UEA, Norwich UK, October 2016. Oral Presentation.

- **Perfecto, Antonio P.** "Pea ferritin uptake in Caco-2 cells."

  The Rank Prize Funds: Mini-symposium on The Role of Crops in Providing Micronutrients (Fe, Zn, Se) for Human Health, Grasmere UK, May 2016. Oral presentation.

- **Perfecto, Antonio P.** "Size characterizations of food fortificant grade ferric phosphate nanoparticles during simulated in vitro digestion and its absorption in a Caco-2 cell model."

  1st FENAC Academic Workshop: Biological and Environmental Impacts of Nanomaterials, University of Birmingham, Birmingham UK, March 2016. Oral presentation.

- **Perfecto, Antonio P.**, Rodriguez-Ramiro, I., Rodriguez-Celma, J**.,** Balk, S., Shewry, P., Fairweather-Tait, S. "The availability of iron in peas."

  Diet and Health Research Industry Club (DRINC), Oxford UK, September 2015. Poster Presentation.

- **Perfecto, Antonio P.** "Uptake and in vitro digestion of pea ferritin in Caco-2 cells."

  FMH Postgraduate Research Student Conference, UEA, Norwich UK, March 2015. Oral Presentation

- **Perfecto, Antonio P.** "Uptake and in vitro digestion of pea ferritin in Caco-2 cells."

  Diet and Health Tea Club, UEA, Norwich UK, June 2014. Oral Presentation.

- Facility for Environmental Nanoscience Analysis and Characterisation (FENAC) Award Recipient 2014-2015. Award amount: £ 9000. Project Title: Imaging of iron nanocompounds in Caco-2 cells using confocal and TEM.
- Facility for Environmental Nanoscience Analysis and Characterisation (FENAC) Award Recipient 2014-2015. Award amount: £ 10000. Project Title: Size characterization of iron nanocompounds during an in vitro digestion.
- Harvest Plus (CIAT/IFPRI) Challenge Award Recipient (2013-2016). Project code R22850. Award amount: $ 31241. Project Title: Mechanisms of uptake of different forms of iron using a Caco-2 cell model.
- International Studentship Award Recipient, University of East Anglia (2013-2016).